



AN INVESTIGATION OF ALTERNATIVE SEPARATION STRATEGIES FOR  
COMMON CHEMICAL MIXTURES BY MEANS OF HOST-GUEST  
CHEMISTRY PROTOCOLS WITH HOST COMPOUNDS *N,N'*-BIS(5-  
PHENYL-5- DIBENZO[A,D]CYCLOHEPTENYL)ETHYLENEDIAMINE  
AND *N,N'*-BIS(5-PHENYL-10,11-DIHYDRO-5-  
DIBENZO[A,D]CYCLOHEPTENYL)ETHYLENEDIAMINE



DANICA B. TROLLIP  
217468225

An investigation of alternative separation strategies for common chemical mixtures by means of host-guest chemistry protocols with host compounds *N,N'*-bis(5-phenyl-5-dibenzo[a,d]cycloheptenyl)-ethylenediamine and *N,N'*-bis(5-phenyl-10,11-dihydro-5-dibenzo[a,d]cycloheptenyl)ethylenediamine

D.B. Trollip

Submitted in fulfilment of the requirements for the degree of Magister Scientiae (Chemistry)  
to be awarded at the Nelson Mandela University

April 2023

Supervisor: Prof Benita Barton

**NELSON MANDELA**  
UNIVERSITY

**DECLARATION BY CANDIDATE**

**NAME:** Danica Trollip

**STUDENT NUMBER:** 217468225

**QUALIFICATION:** MSc (Chemistry)

**TITLE OF PROJECT:** An investigation of alternative separation strategies for common chemical mixtures by means of host-guest chemistry protocols with host compounds *N,N'*-bis(5-phenyl-5-dibenzo[a,d]cycloheptenyl)ethylenediamine and *N,N'*-bis(5-phenyl-10,11-dihydro-5-dibenzo[a,d]cycloheptenyl)ethylenediamine

---

**DECLARATION:**

In accordance with Rule G5.11.4, I hereby declare that the above-mentioned treatise/ dissertation/ thesis is my own work and that it has not previously been submitted for assessment to another University or for another qualification.

**SIGNATURE:**  \_\_\_\_\_

**DATE:** 02/12/2022

## Contents

Acknowledgements.....	i
Publication details.....	ii
Abbreviations.....	iii
Abstract.....	iv
1. Introduction.....	1
1.1 Supramolecular and host-guest chemistry.....	1
1.2 The preparation of host-guest complexes.....	4
1.3 Interaction types between host and guest species to form complexes.....	6
1.3.1 van der Waals forces.....	6
1.3.2 Hydrogen bonds.....	7
1.3.3 $\pi\cdots\pi$ stacking interactions.....	8
1.3.4 Dipole $\cdots$ dipole interactions.....	8
1.3.5 Ion $\cdots$ dipole interactions.....	9
1.4 Applications of host-guest chemistry.....	9
1.5 Analysis of host-guest complexes.....	16
1.5.1 Proton nuclear magnetic resonance spectroscopy.....	16
1.5.2 Gas chromatography.....	16
1.5.3 Single crystal X-ray diffraction analyses.....	16
1.5.4 Thermal analyses.....	17
1.5.5 Powder diffraction.....	18
1.6 Well-established host compounds.....	18
1.6.1 Cavitands.....	19
1.6.1.1 Crown ethers.....	19
1.6.1.2 Cryptands.....	20
1.6.1.3 Spherands and hemi-spherands.....	21

1.6.1.4 Cyclodextrins.....	23
1.6.1.5 Calixarenes.....	24
1.6.1.6 Carcerands and hemi-carcerands .....	26
1.6.2 Clathrands.....	28
1.6.2.1 $\alpha,\alpha',\alpha',\alpha'$ -Tetraaryl-1,3-dioxolane-4,5-dimethanols .....	28
1.6.2.2 (+)-(2R,3R)-1,1,4,4-Tetraphenylbutane-1,2,3,4-tetraol.....	29
1.6.2.3 Roof-shaped host compounds.....	30
1.6.2.4 Tricyclic-fused host systems .....	32
1.6.2.5 Urea and thiourea.....	34
1.7 The present investigation.....	35
1.8 Aim and objectives.....	37
2. Methods.....	39
2.1 General.....	39
2.2 Synthesis of host compounds <b>H1</b> and <b>H2</b> .....	42
2.2.1 5-Hydroxy-5-phenyldibenzo[a,d]cycloheptene ( <b>2</b> ) .....	43
2.2.2 <i>N,N'</i> -Bis(5-phenyl-5-dibenzo[a,d]cycloheptenyl)ethylenediamine ( <b>H1</b> ).....	44
2.2.3 5 Hydroxy-5-phenyl-10,11-dihydrodibenzo[a,d]cycloheptene ( <b>5</b> ).....	44
2.2.4 <i>N,N'</i> -Bis(5-phenyl-10,11-dihydro-5-dibenzo[a,d]cycloheptenyl)ethylenediamine ( <b>H2</b> ) .....	45
2.3 Single solvent recrystallization experiments.....	46
2.4 Recrystallization experiments involving equimolar mixed guests.....	46
2.5 Recrystallization experiments involving binary guest mixtures in varying ratios.....	47
2.6 Computational methods .....	48
3. Molecular modelling.....	49
3.1 Computational analysis of <b>H1</b> and <b>H2</b> .....	49
3.2 Crystal structure of host compound <b>H2</b> .....	51

4. Selectivity of <b>H1</b> and <b>H2</b> in isomeric xylene and ethylbenzene mixtures.....	55
4.1 Introduction.....	55
4.2 Results and discussion.....	56
4.2.1 Assessment of the host potential of <b>H1</b> and <b>H2</b> for Xy and EB in single solvent recrystallization experiments .....	56
4.2.2 Assessment of the selectivity behaviour of <b>H1</b> and <b>H2</b> in equimolar mixed guests .....	57
4.2.3 Assessment of the selectivity behaviour of <b>H1</b> and <b>H2</b> in binary mixtures of Xy/EB where the $G_A:G_B$ molar ratios were sequentially varied .....	59
4.2.4 Single crystal X-ray diffraction experiments.....	65
4.2.5 Thermal analysis .....	70
4.3 Conclusion .....	72
5. Selectivity of <b>H1</b> and <b>H2</b> in pyridine and methylpyridine isomers .....	73
5.1 Introduction.....	73
5.2 Results and discussion.....	74
5.2.1 Assessment of the host potential of <b>H1</b> and <b>H2</b> for PYR and 2MP/3MP/4MP in single solvent recrystallization experiments .....	74
5.2.2 Assessment of the selectivity behaviour of <b>H1</b> and <b>H2</b> in equimolar mixed guests .....	75
5.2.3 Assessment of the selectivity behaviour of <b>H1</b> and <b>H2</b> in binary mixtures of PYR/MP where the $G_A:G_B$ molar ratios were sequentially varied .....	78
5.2.4 Single crystal X-ray diffraction experiments.....	85
5.2.5 Thermal analysis .....	96
5.3 Conclusion .....	101
6. Selectivity of host compounds <b>H1</b> and <b>H2</b> in anisole and isomeric methylanisole mixtures .....	102
6.1 Introduction.....	102

6.2 Results and discussion.....	103
6.2.1 Assessment of the host potential of <b>H1</b> and <b>H2</b> for ANI/2MA/3MA/4MA in single solvent recrystallization experiments .....	103
6.2.2 Assessment of the selectivity behaviour of <b>H1</b> and <b>H2</b> in equimolar mixed guests .....	104
6.2.3 Assessment of the selectivity behaviour of <b>H1</b> in binary mixtures containing ANI, 2MA, 3MA and 4MA where the $G_A:G_B$ molar ratios were sequentially varied .....	105
6.2.4 Single crystal X-ray diffraction experiments.....	108
6.2.5 Thermal analysis .....	115
6.3 Conclusion .....	120
7. Final remarks.....	122
8. Future work.....	125
References .....	130
Supplementary Information .....	140

## Acknowledgements

I wish to give my sincere thanks to:

- Professor Benita Barton for all her help (no matter the time of day), attention to detail, direction (the green brick), support, encouragement and humour throughout the whole project
- The lab technicians for their help
- Dr Hosten and Professor Caira for SCXRD analyses
- My friends and family for their constant support and love
- Nelson Mandela University (NMU) for their facilities and PGRS for the funding
- This work is based on the research supported in part by the National Research Foundation of South Africa (Grant number 144918)
- Almighty God for his unending love and without whom this would not have been possible



## Publication details

Chapter 4 of this dissertation has been published: Barton, B.; Trollip, D. B.; Hosten, E. C. Selected Tricyclic Fused Systems: Host Behavior in the Presence of Mixed Xylenes and Ethylbenzene. *Cryst. Growth Des.* **2022**, *22* (11), 6726–6734.

## Abbreviations

NMR	Nuclear Magnetic Resonance
GC	Gas Chromatography
GC-MS	Gas Chromatography-Mass Spectroscopy
SCXRD	Single Crystal X-Ray Diffraction
PXRD	Powder X-Ray diffraction
TGA	Thermogravimetric Analysis
DTG	Derivative of the Thermogravimetric Experiment
DSC	Differential Scanning Calorimetry
<b>H1</b>	<i>N,N'</i> -Bis(5-phenyl-5-dibenzo[a,d]cycloheptenyl)ethylenediamine
<b>H2</b>	<i>N,N'</i> -Bis(5-phenyl-10,11-dihydro-5-dibenzo[a,d]cycloheptenyl)ethylenediamine
H:G	Host:Guest ratio
o-Xy	<i>ortho</i> -Xylene
m-Xy	<i>meta</i> -Xylene
p-Xy	<i>para</i> -Xylene
EB	Ethylbenzene
PYR	Pyridine
2MP	2-Methylpyridine
3MP	3-Methylpyridine
4MP	4-Methylpyridine
ANI	Anisole
2MA	2-Methylanisole
3MA	3-Methylanisole
4MA	4-Methylanisole
IR	Infrared

## Abstract

In this work, the selectivity behaviour of two host compounds, namely *N,N'*-bis(5-phenyl-5-dibenzo[a,d]cycloheptenyl)ethylenediamine (**H1**) and *N,N'*-bis(5-phenyl-10,11-dihydro-5-dibenzo[a,d]cycloheptenyl)ethylenediamine (**H2**), was assessed in mixtures of difficult-to-separate compounds, including the xylenes and ethylbenzene, pyridine and methylpyridines, and anisole and methylanisoles.

These host compounds were synthesized using Grignard addition reactions with phenylmagnesium bromide on dibenzo[a,d]cyclohepten-5-one and 10,11-dihydrodibenzo[a,d]cyclohepten-5-one, respectively. The resultant alcohols were treated with perchloric acid to form the corresponding perchlorate salts, which were then reacted with ethylenediamine to afford the required **H1** and **H2** host compounds. Yields were 95 and 52% for this final step in each case.

An investigation of the conformations, both from experiment (using single crystal X-ray diffractometry (SCXRD) on the apohost compound) and computational calculations was undertaken. Unfortunately, **H1** always crystallized out as a powder unless this host compound formed a complex with a guest species, and so could not be subjected to SCXRD analysis as apohost alone. However, a single crystal structure for apohost **H2** was successfully obtained and compared with computational data from a previous investigation. It was observed that the conformation of apohost **H2** compared favourably with that of the lowest energy conformer from that work.

In single solvent recrystallization experiments with *o*-, *m*-, *p*-xylene (*o*-Xy, *m*-Xy, *p*-Xy) and ethylbenzene (EB), both **H1** and **H2** formed complexes with only one of the four guest species, namely *p*-Xy and *o*-Xy, respectively. The host:guest (H:G) ratios were 1:1 for both of these complexes. In the equimolar guest/guest competition experiments, inclusion complexes only formed when *p*-Xy or *o*-Xy, respectively, were present in the mixtures; if *p*-Xy (for experiments with **H1**) or *o*-Xy (**H2**) was absent from these mixtures, only apohost was recovered from the glass vessels. Three selectivity profiles were constructed for each of these host compounds,

in which each one was recrystallized from binary mixed guests in various proportions. These demonstrated an overwhelming preference of **H1** for *p*-Xy and **H2** for *o*-Xy, which concurred with the results from the equimolar experiments. Thermal analysis using **H1**·*p*-Xy revealed that this complex was unstable at ambient conditions, while SCXRD explained this observation: this complex may be defined as a true clathrate since no host-guest interactions were identified at all, and the guest was retained in the complex by means of steric factors alone. Furthermore, the guest molecules resided in wide open channels that may have facilitated the guest release process. **H2**·*o*-Xy, on the other hand, was stable at room temperature, and the guest release event only commenced at 69.7 °C ( $T_{on}$ ). This too was explained by SCXRD analyses in that interactions between host and guest species were observed in this case. Additionally, the guest molecules were housed in discrete cages, which made their escape more challenging compared with *p*-Xy in **H1**·*p*-Xy. It was concluded that, in this guest series, both of the host compounds would be effective as separatory tools employing host-guest chemistry protocols due to their remarkable selectivities for *p*-Xy (**H1**) and *o*-Xy (**H2**).

In the guest series comprising pyridine (PYR) and its methylated derivatives (2MP, 3MP and 4MP), it was observed that **H2** was significantly more selective than **H1**: this host compound (**H1**) formed complexes with each of the four guest solvents, and equimolar binary guest/guest competition experiments showed that 2MP was most preferred when the other guest species present was PYR, 3MP or 4MP (selectivities were then 91.2, 88.8 and 63.5 %, respectively). Contrastingly, **H2** only formed inclusion compounds with each of PYR and 4MP (2MP and 3MP were not complexed). Remarkably, the **H2** selectivity towards PYR was near-complete in equimolar binary solutions when the other guest was 2MP or 3MP (98.2 and 97.9 %). However, it was also noted that in the presence of 4MP, the selectivity for PYR declined, though this remained in favour of PYR. The constructed selectivity profiles demonstrated a preference for 2MP in 2MP/PYR (except at low concentrations of 2MP) and 2MP/3MP mixtures for **H1**, while PYR was the most favoured by **H2** in PYR/2MP and PYR/3MP solutions, with selectivities greater than 95% in these mixtures. **H2** was therefore shown to be an ideal candidate for the extraction of PYR from such mixtures. SCXRD analyses revealed that the complexes of **H1** and **H2** with PYR were isostructural in a non-conventional way (along different unit cell axes). Furthermore, from thermoanalytical experiments, both **H1**·2(2MP)

and **H2**·2(PYR) (containing their preferred guests) were the most thermally stable ( $T_{on}$  values were the highest in these cases) compared with the guest release onset temperatures for the remaining complexes of each of **H1** and **H2**, respectively. These observations were explained by SCXRD analyses, and the guest compound in each of the two complexes experienced the shortest classical H-bond with the host compound relative to the H-bonds in the other complexes. In this investigation, therefore, it was concluded that **H2** would be a more effective separatory tool compared to **H1** when using host-guest chemistry strategies.

In the guest series anisole (ANI) and the methylanisole isomers (2MA, 3MA and 4MA), **H1** formed inclusion complexes, in single solvent recrystallization experiments, with 2MA, 3MA and 4MA (H:G ratios were 2:1, 1:1 and 1:1). **H2**, on the other hand, only included ANI (H:G 2:3). However, the recrystallization process of **H2** from any of these guest mixtures was impractical, requiring months before crystals were formed, and hence **H2** as a separation agent for such mixtures was not investigated. However, employing **H1** in such mixed solvent experiments was more feasible, and competition experiments showed that this host compound favoured 4MA unwaveringly (in the binary experiments, selectivities of 80% and more were calculated in favour of 4MA). When 4MA was absent from any of these experiments, then only apohost was recovered in all cases. Selectivity profiles constructed from binary experiments where 4MA was present showed this guest to be significantly favoured with the exception of the 4MA/3MA profile, where data points suggested low host selectivities. From SCXRD data, it was shown that the complexes containing 3MA and 4MA shared an isostructural host packing. However, the 4MA-containing crystal possessed a higher density, smaller voids in which the guests were accommodated and shorter hydrogen bonding between host and guest molecules relative to the 3MA-containing complex. These observations explained the preference of **H1** for 4MP. The thermal analyses added credence to the selectivity behaviour of **H1** in that the complex with 4MA possessed the greater thermal stability ( $T_{on}$  104.9 °C) compared with that of 3MA (70.5 °C). **H1** was thus shown to be an excellent host candidate for many of the mixtures with which it was presented.

## 1. Introduction

### 1.1 Supramolecular and host-guest chemistry

Supramolecular chemistry was defined as the “chemistry beyond the molecule” by Jean-Marie Lehn in 1987.<sup>1</sup> This type of chemistry deals with interactions between molecules that are non-covalent in nature and include hydrogen bonding (both classical and non-classical), C–H··· $\pi$  and aromatic stacking interactions, amongst others.<sup>2,3</sup>

Host-guest chemistry is a subcategory of supramolecular chemistry and involves the formation of complexes between host and guest molecules. Donald Cram defined these host-guest complexes as follows:<sup>4</sup>

*“Complexes are composed of two or more molecules or ions held together in unique structural relationships by electrostatic forces other than those of full covalent bonds ... molecular complexes are usually held together by hydrogen bonding, by ion pairing, by  $\pi$ -acid to  $\pi$ -base interactions, by metal-to-ligand binding, by van der Waals attractive forces, by solvent reorganising, and by partially made and broken covalent bonds (transition states)... High structural organisation is usually produced only through multiple binding sites... A highly structured molecular complex is composed of at least one host and one guest component... A host–guest relationship involves a complementary stereo-electronic arrangement of binding sites in host and guest... The host component is defined as an organic molecule or ion whose binding sites converge in the complex... The guest component is defined as any molecule or ion whose binding sites diverge in the complex...”*

From the description above, it should be noted that the “organic molecule”<sup>5,6</sup> that was used to describe the host component may be generalized, as subsequent work carried out since 1977 (when the definition was first written) revealed that inorganic host compounds, such as zeolites and polyoxometallates, or mixed metal–organic coordination compounds, exist.<sup>2</sup>

In the presence of the guest species, the host molecules (clathrands) either pack in such a way that interstitial voids are formed into which the guest molecules then fit forming a special complex also known as a clathrate, or the host molecule (cavitand) itself possesses an intrinsic permanent cavity that houses the guest molecules (the complex formed here may also be referred to as a cavitare in this case) (Figure 1.1).<sup>2,7</sup>

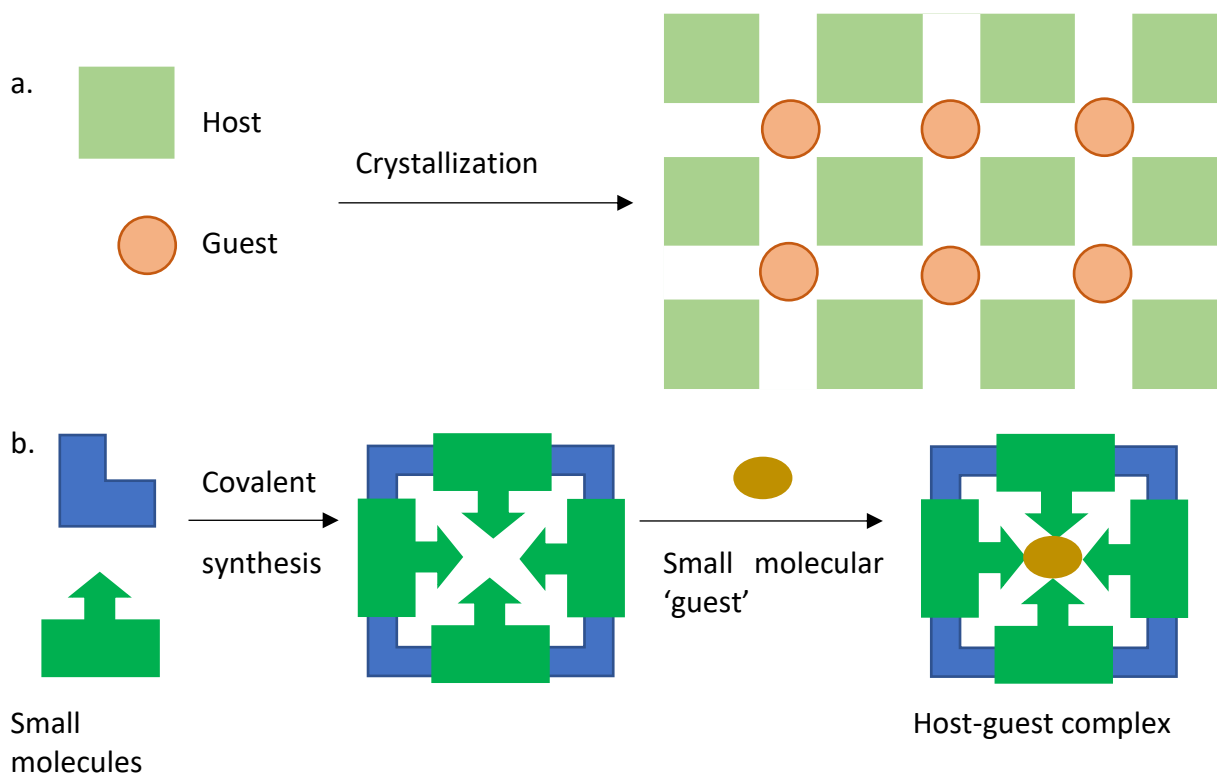


**Figure 1.1:** Formation of a. clathrates and b. cavitates<sup>2</sup>

Of importance to this field of chemistry are the concepts of *complementarity* and *preorganization*. Donald Cram provided statements on the *principles of complementarity* and *preorganization* that exist between host and guest molecules:

*“The principle of complementarity states that “to complex, hosts must have binding sites which can simultaneously contact and attract the binding sites of the guests without generating internal strains or strong nonbonded repulsions.” The principle of preorganization states that “the more highly hosts and guests are organized for binding and low solvation prior to their complexation, the more stable will be their complexes.”*<sup>8,9</sup>

Cram further explained how flexible host compounds are not preorganized due to them possessing weak and few guest binding sites. In order to understand preorganization, a podand and a spherand may be compared, as in Figure 1.2. In these examples, the podand has no detectable specificity (the  $K_a$  values for  $\text{Na}^+$  and  $\text{Li}^+$  ions are similar, both being  $< 2.5 \times 10^4 \text{ M}^{-1}$ ), and it possesses an extremely low affinity<sup>10</sup> ( $K_a$  is the binding affinity and it describes the tendency for a receptor-ligand pair to be in the bound state).<sup>11</sup> The spherand, on the other hand, displays very high affinity and specificity since the  $K_a$  values differ significantly for the various cations ( $\text{Li}^+ > 7.5 \times 10^{16} \text{ M}^{-1}$ ,  $\text{Na}^+ > 1.4 \times 10^{14} \text{ M}^{-1}$ , and  $\text{K}^+ > 2.5 \times 10^4 \text{ M}^{-1}$ ). These observations are as a result of the podand being more flexible and thus less preorganized than the spherand.<sup>10</sup>

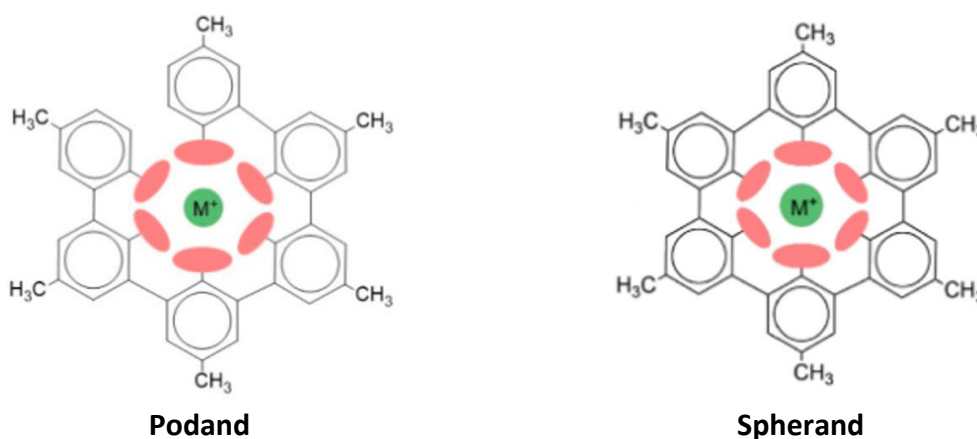


**Figure 1.2:** Contrast between a podand and spherand<sup>10</sup>

Table 1.1 summarizes the various examples of complementarity and preorganization.

**Table 1.1:** Examples of the characteristics of host and guest species for effective complementarity and preorganization<sup>8</sup>

Complementarity	Preorganization
<ul style="list-style-type: none"> <li>• Lock-and-key versus induced fit</li> <li>• Hydrogen bonds</li> <li>• Electrostatic interactions</li> <li>• Size and shape</li> <li>• van der Waals forces</li> <li>• Spatial complementarity</li> </ul>	<ul style="list-style-type: none"> <li>• Macrocyclic preorganization</li> <li>• Acyclic preorganization</li> </ul>



Figure 1.3 is a schematic illustration showing the various species that are involved in host-guest chemistry. Here, first is synthesized a host compound through usual molecular chemistry followed by the entrapment of a guest species in its cavity (this figure is, once more, displaying a complex that is defined as a cavitate, owing to the permanent cavity of the host compound).

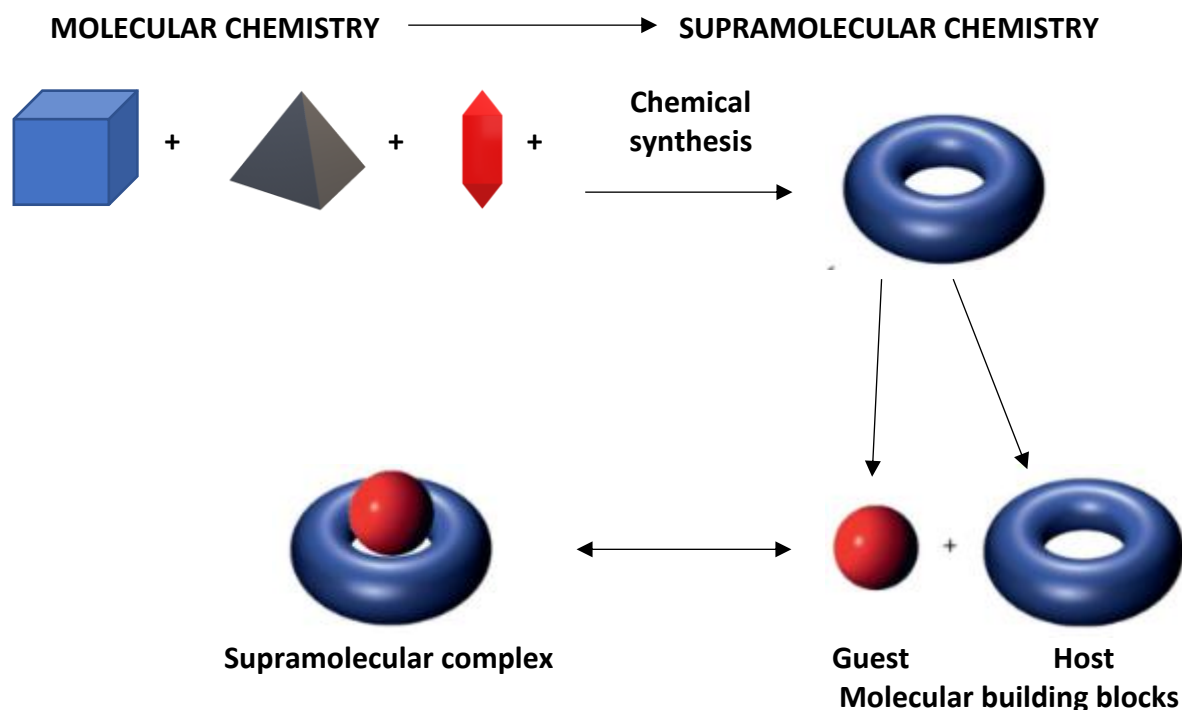


**Figure 1.3:** Schematic representation of the various components involved in host-guest complex formation<sup>2</sup>

## 1.2 The preparation of host-guest complexes

Solid state host-guest complexes are formed by dissolving the host species (which is normally a solid) in an excess molar amount of the guest compound, often a liquid (Figure 1.4),<sup>12-14</sup> but which may also be in the solid or gas phase. When the guest is a solid, a solvent that is not enclathrated by the host compound is required in order to furnish a solution containing both host and guest species. Once the host compound is dissolved in the guest, the vessel containing the solution may be kept open to the ambient conditions to allow for sufficient guest/solvent to evaporate off which facilitates crystallization of the complex from the solution.<sup>12,13</sup> Alternatively, the vessel may be capped and stored in a refrigerator to hasten the crystallization process by reducing the solubility of the complex in the solution due to the

colder temperatures.<sup>12</sup> The crystals that form in this way are collected, crushed, and washed with a suitable solvent to remove any guest that may be present on the crystal surfaces. The crystals are then analysed by appropriate analytical techniques (to be discussed later). In order to assess the selectivity of the host species for any particular guest compound, competition experiments are conducted in which the host is recrystallized from guest mixtures, these being present either in equimolar or varying known proportions. Here, the vessels must be closed and refrigerated to retain the guest:guest ratios that were initially prepared. Crystals that form from these solutions are treated in the same way as before, and applicable analytical techniques provide information on how much of each guest is present in the crystals; these data may then be compared to the amount of each guest in the solution initially prepared, thus identifying any favoured guest species.

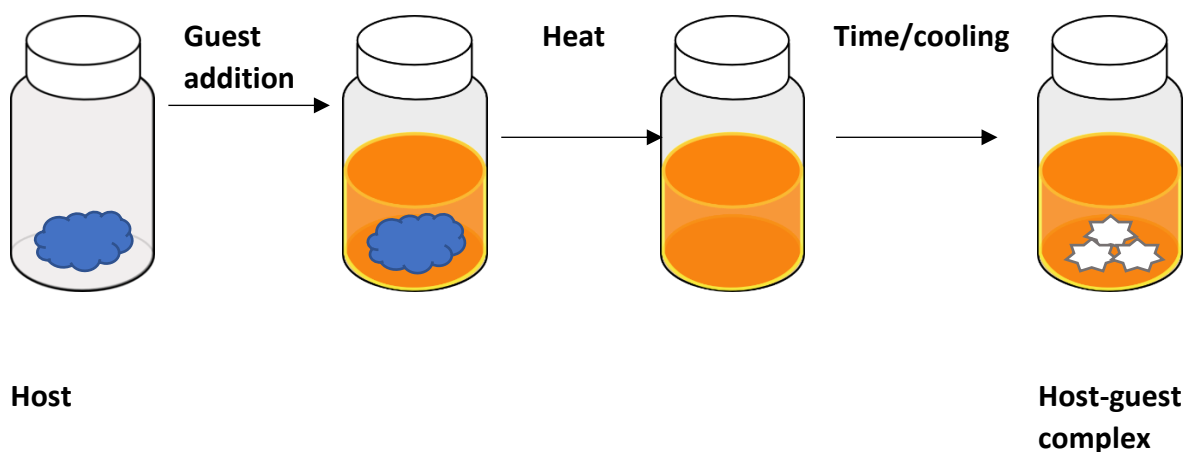


**Figure 1.4:** Experimental procedure for the formation of complexes by means of solid host and liquid guest species

For vapour inclusions,<sup>15</sup> pure host compound is suspended above the liquid-phase guest (or guests) in some or other way, and the vessel closed (Figure 1.5). In this way, some of the guest species vapourizes, ensuring the host compound is then subjected to this vapour. The host compound may then enclathrate the guest (or guests) from the gas phase, which is to be revealed by an apt analytical tool after treatment of the crystals in the same fashion as before.

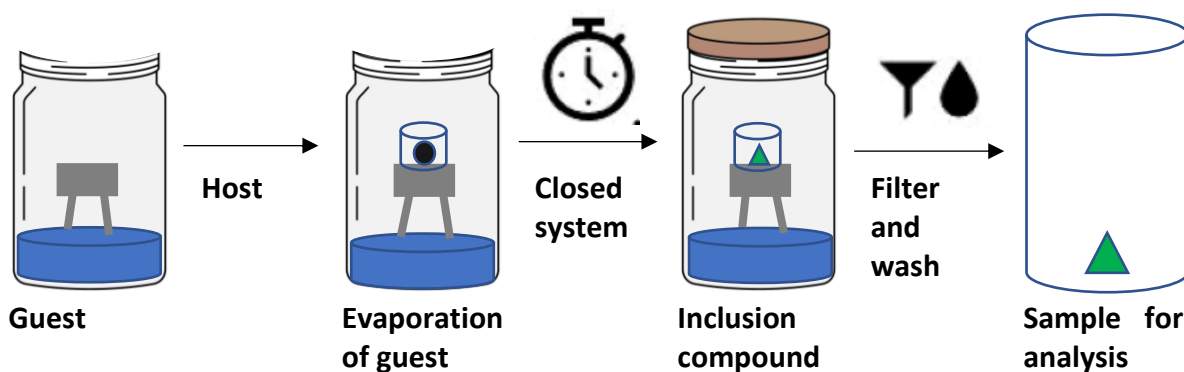


**Figure 1.5:** Experimental procedure for the formation of complexes through vapour inclusion<sup>15</sup>

### 1.3 Interaction types between host and guest species to form complexes

#### 1.3.1 van der Waals forces

van der Waals (vdW) interactions arise when there is a weak electrostatic attraction present between species, which occurs due to an electron cloud becoming polarised as a result of a positively charged nucleus being in close proximity.<sup>16</sup> These interactions play an important role in the formation of inclusion compounds. Figure 1.6 illustrates an example of the inclusion of an organic guest molecule (toluene) into a molecule with a permanent cavity (*p*-*tert*-butylcalix[4]arene).

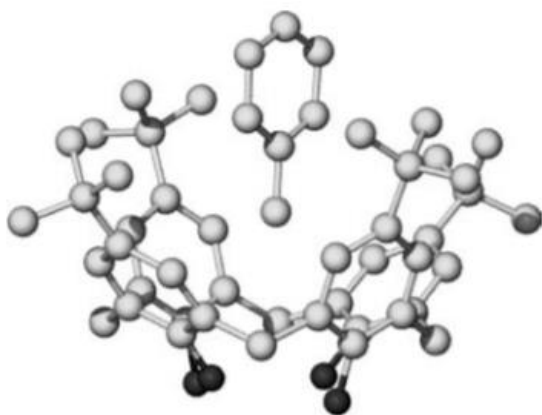


**Figure 1.6:** An X-ray crystal structure of the vdW inclusion complex *p*-*tert*-butylcalix[4]arene·toluene<sup>2</sup>

### 1.3.2 Hydrogen bonds

A classical hydrogen bond is regarded as a type of dipole...dipole interaction that occurs between a hydrogen atom, bonded traditionally to an electron-withdrawing nitrogen, oxygen or fluorine atom, and a neighbouring nitrogen, oxygen, or fluorine atom on an adjacent molecule/functional group.<sup>17,18</sup> An example of these hydrogen bonding interactions is demonstrated in Figure 1.7 using molecules with the carboxylic acid functionality.

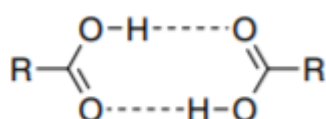


**Figure 1.7:** Hydrogen bonding between two carboxylic acid molecules to form a carboxylic acid dimer<sup>2</sup>

Hydrogen bonds may also be non-classical in nature. These occur between weak donors, such as C–H, and atoms that have lone pairs, such as oxygen and nitrogen, giving rise to C–H...N and C–H...O non-classical hydrogen bonds, as examples.<sup>17</sup> These interactions are by definition weak. Figure 1.8 is an example of this interaction type between a crown ether and nitromethane.<sup>2</sup>

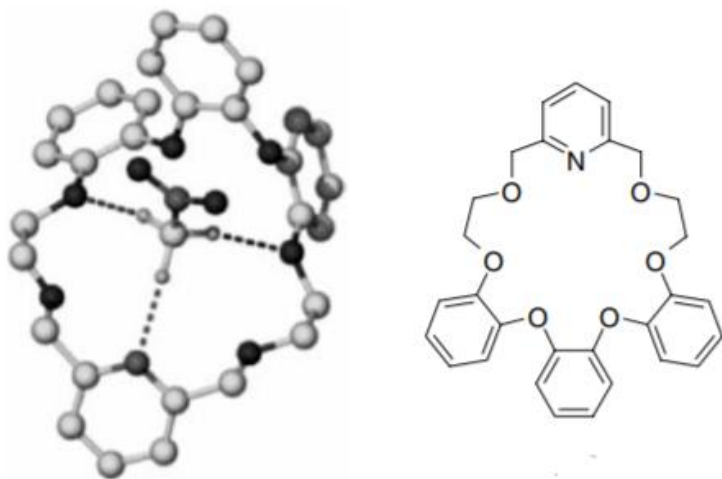


**Figure 1.8:** An X-ray crystal structure (left) that shows the C–H...N and C–H...O hydrogen bonds between a crown ether and nitromethane,<sup>1</sup> and the crown ether alone (right) for clarity<sup>2</sup>

### 1.3.3 $\pi\cdots\pi$ stacking interactions

Interactions of the  $\pi\cdots\pi$  stacking type occur between aromatic rings, especially when there are electron rich and electron poor sites on these rings.<sup>19,20</sup> Two common types of  $\pi\cdots\pi$  stacking interactions exist, namely face-to-face and edge-to-face contacts, illustrated in Figure 1.9.

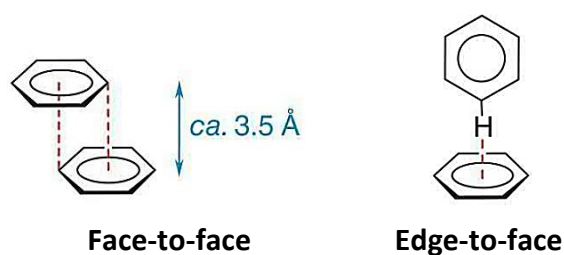


**Figure 1.9:** Face-to-face (left) and edge-to-face (right)  $\pi\cdots\pi$  stacking interactions that may exist between aromatic rings<sup>2</sup>

The face-to-face  $\pi\cdots\pi$  interactions are responsible for the slippery feel of, for example, graphite, and these interactions provide lubricant properties to various commodities.<sup>2</sup> Edge-to-face interactions, on the other hand, are often described as weak forms of hydrogen bonds that occur between an electron rich  $\pi$ -cloud of an aromatic ring and a slightly electron deficient hydrogen atom of another aromatic ring.<sup>21</sup>

### 1.3.4 Dipole $\cdots$ dipole interactions

There are two types of dipole $\cdots$ dipole interactions that exist (Figure 1.10). Type I interactions occur as a result of the attraction of the partial positive charge of one dipole to the partial negative charge of another dipole.<sup>2,22</sup> Type II interactions involve opposing alignments of one dipole with the other.<sup>2</sup>

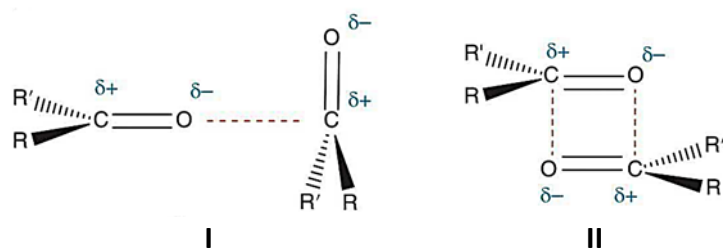
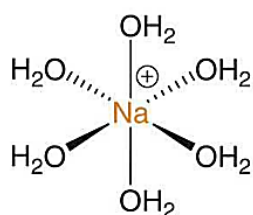


**Figure 1.10:** Examples of Type I and Type II dipole $\cdots$ dipole interactions<sup>2</sup>

### 1.3.5 Ion···dipole interactions

Ion···dipole interactions occur when an ion interacts with molecules that contain a dipole.<sup>22</sup> As an example, these interaction types are observed when alkali metal cations coordinate with macrocyclic ethers, such as the crown ethers (Figure 1.11). The crown ether oxygen atoms behave similarly to polar water molecules, where the lone pairs on these oxygens are attracted to the positive charge of the cation.<sup>2</sup>



Hydrated Na<sup>+</sup>



Na<sup>+</sup> crown ether complex

**Figure 1.11:** Crown ethers (right) behave similarly to polar water molecules in the presence of Na<sup>+</sup> (left) to form ion···dipole interactions<sup>2</sup>

Non-covalent interaction strengths are much weaker than those of covalent bonds, and these relative strengths may be observed in Table 1.2.

**Table 1.2:** The relative strengths of covalent bonds and supramolecular interactions<sup>23</sup>

Interaction	Strength (kJ·mol <sup>-1</sup> )
Covalent bonds	200–400
van der Waals	< 5 (variable depending on surface area)
Hydrogen bonding	4–120
$\pi$ ··· $\pi$ stacking	0–50
Dipole···dipole	5–50
Ion···dipole	50–200

### 1.4 Applications of host-guest chemistry

There are many applications of host-guest chemistry, and these are in, amongst others, the biomedical, biological and chemical fields.<sup>24</sup> The relatively weak non-covalent interactions required to form host-guest complexes implies that there exists a facile approach towards building supramolecular structures; these supramolecules are even able to form through

intrinsic self-assembly and can dissociate and reconstruct at low energy cost owing to these weak and dynamic interactions.<sup>25</sup>

In biomedicine, host-guest chemistry finds application in drug and gene delivery, bioimaging and photodynamic therapy. The cyclodextrins (to be discussed in more detail later) are extremely suitable host compounds to deliver drug actives into the body through host-guest chemistry owing to their non-toxic nature and superior complexation ability. Furthermore, drug actives can also be introduced in the form of supramolecular nanocarriers and hydrogels. Gene delivery employs supramolecular nanoparticles, rotaxanes/polyrotaxanes and other host-guest gene delivery systems to achieve gene transport.<sup>25</sup> Figure 1.12 is an illustration of this.

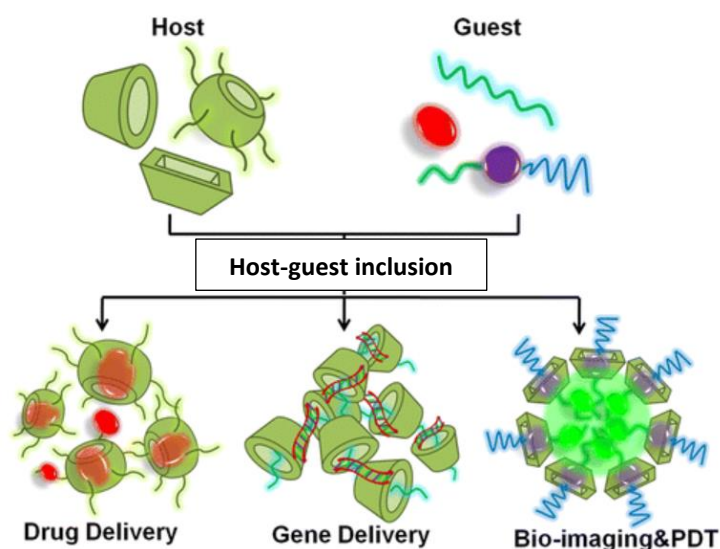


**Figure 1.12:** Gene delivery employing supramolecular systems that are based on host-guest chemistry<sup>25</sup>

Some biological applications of host-guest chemistry include fluorescence-based sensing of biological substances, tandem assays for enzymatic activity, screening for enzyme inhibitors, and detoxification of hazardous substances.<sup>26</sup> Figure 1.13 illustrates the fluorescent-sensing systems: when an analyte is added to, for example, a dye-host complex, the dye is displaced and the biological system fluoresces.

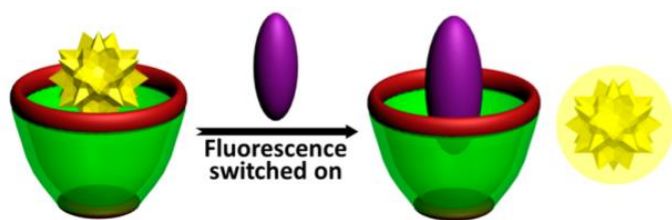


**Figure 1.13:** Analyte sensing by dye displacement employing host-guest chemistry principles<sup>26</sup>

*p*-Sulfonatocalix[*n*]arenes (SCnAs, Figure 1.14) are a family of water-soluble calixarene derivatives that have a strong ability to bind guests in their cavities when they are in aqueous media. These SCnAs are useful in both the biological and pharmaceutical fields:<sup>27,28</sup> SCnAs, due to their preorganized conical shapes and their cavities having binding abilities, serve in fluorescent sensing and enzymatic reaction monitoring, drug delivery via supramolecular binary vesicles that are formed by calixarene-induced aggregation, and pesticide detoxification.<sup>26–29</sup>

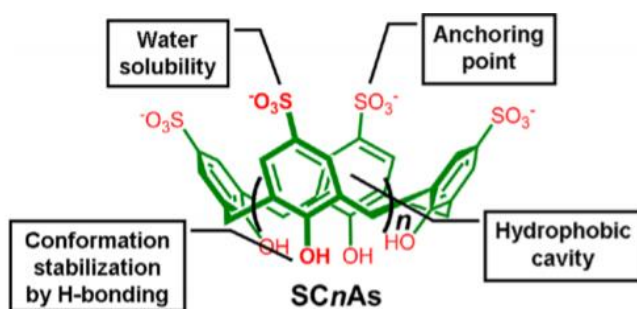


**Figure 1.14:** The structure of *p*-sulfonatocalix[*n*]arenes (SCnAs,  $n = 4–8$ )<sup>26</sup>

A chemical application of host-guest chemistry is that it may serve as a separatory tool for mixtures that are difficult to separate, such as isomers. Isomers are compounds that have the same molecular formula, but their structures differ due to the placement of the atoms.<sup>30</sup> In particular, positional isomers are those isomers that possess identical carbon skeletons and functional groups, but the location of these groups differ. An example of these types of isomers is provided in Figure 1.15 for an amine with molecular formula  $C_3H_9N$ .

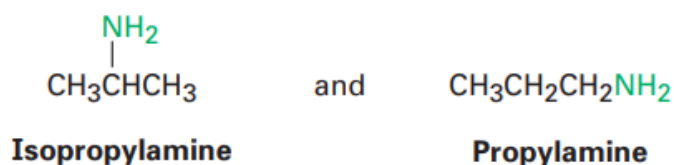


**Figure 1.15:** The positional isomers of an amine with molecular formula  $C_3H_9N$ <sup>30</sup>



Positional isomers such as the xylenes and ethylbenzene (Figure 1.16), the methylanisoles, the methylpyridines, dihydroxybenzenes and hydroxytoluenes are often difficult to separate from one another after recovery from coal tar (or other sources) owing to their very similar physical properties. For example, the boiling points of *ortho*-xylene, *meta*-xylene, *para*-xylene and ethylbenzene are 144 °C, 139 °C, 138 °C and 136 °C, respectively,<sup>31</sup> rendering them challenging to separate by means of fractional distillation (or fractional crystallization in the case of similar melting points). These techniques, at best, afford isomers that have a low purity, too low for their employment in many subsequent applications. As an example, *para*-xylene is required to be pure when used in the production of polyethylene terephthalate. In order to isolate pure *para*-xylene by fractional distillation, many theoretical plates are required, and these processes become extremely energy-consuming with respect to the (limited) fossil fuels required. These processes are also particularly time-consuming, yet another shortcoming of a fractional distillation in this case.<sup>32</sup>

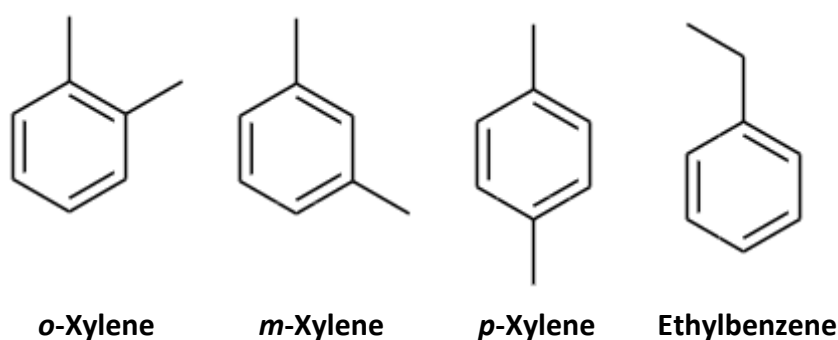


**Figure 1.16:** Positional isomers of the C<sub>8</sub>H<sub>10</sub> fraction of coal tar

Host-guest chemistry, however, may serve as an alternative separation strategy for such isomers if the host compound possesses selectivity for one particular guest species in the isomeric mixture. Therefore, when the host compound is presented with the isomeric mixture, if indeed it possesses selectivity, it will complex with only one particular isomer and crystallize out of the solution. A simple filtration of the solid complex effectively separates the preferred guest species from the remaining isomers. The favoured guest is then recovered from the complex by means of simple distillation or chromatographic techniques. Advantageously, the host compound may then be recycled in this process a multitude of times.

It is not only positional isomers that have similar boiling points; for example, mixtures of aniline (ANI), *N*-methylaniline (NMA) and *N,N*-dimethylaniline (DMA) boil in a narrow 184–196 °C range, and fractional distillations are also challenging to effect their separation. These anilines do exist as mixtures because both of the alkylated derivatives are synthesized from ANI by means of methylation processes.<sup>33</sup> Host-guest chemistry may play a role here too in their separation. In fact, *trans*-*N,N'*-bis(9-phenyl-9-xanthenyl)cyclohexane-1,2-diamine (1,2-DAX) and *trans*-*N,N'*-bis(9-phenyl-9-thioxanthenyl)cyclohexane-1,2-diamine (1,2-DAT) have demonstrated, in solutions containing equimolar amounts of aniline (ANI), *N*-methylaniline (NMA) and *N,N*-dimethylaniline (DMA) (Figure 1.17), increased selectivities for DMA (> 80%) in recrystallization experiments. However, in binary mixtures where the amount of each guest was varied, 1,2-DAX always favoured DMA across the entire concentration range, while the behaviour of 1,2-DAT depended upon the concentration of the two guest species present. The average *K* (the selectivity coefficient, a measure of the host selectivity) values for 1,2-DAX in DMA/ANI was significant (14.2). Nassimbeni et al.<sup>34</sup> reported that effective separations are possible when *K* is 10 or greater.

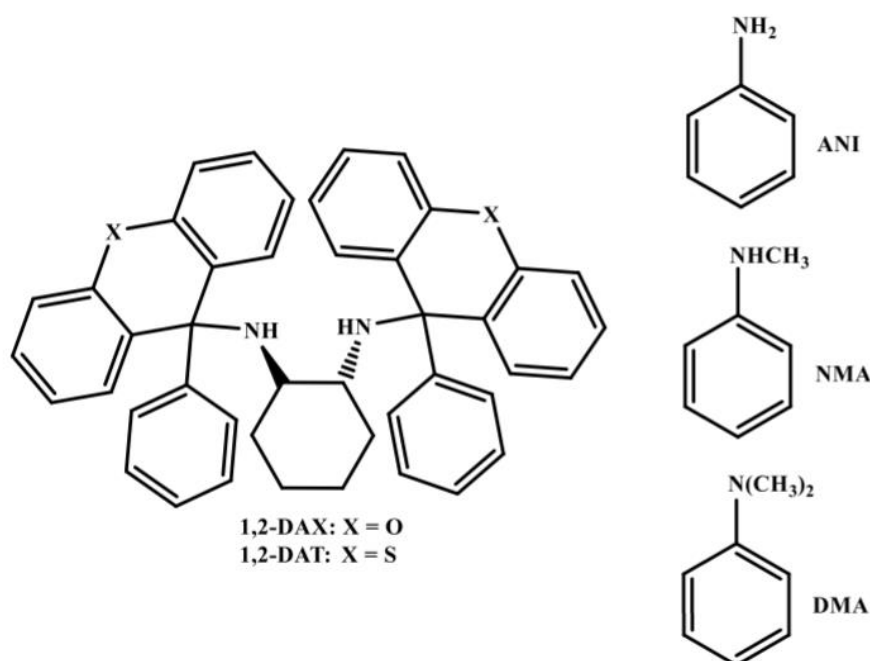


**Figure 1.17:** Structures of host compounds 1,2-DAX and 1,2-DAT, and guest compounds ANI, NMA and DMA<sup>33</sup>

Other methods that may be utilized for the separation of isomers and related compounds involve zeolites and metal-organic frameworks (MOFs), amongst others. However, these methods are oftentimes inefficient and extremely costly.<sup>15</sup> Zeolites are solids with complex rigid structures<sup>35,36</sup> that contain silica and alumina which are connected by oxygen anions to form infinite strands of inorganic polymers. The channel/pore openings of zeolites range from 3 to 8 Å.

One example of a zeolite is Ba-X which has been employed to separate *para*-xylene from *meta*-xylene, *ortho*-xylene, and ethylbenzene (Figure 1.18).

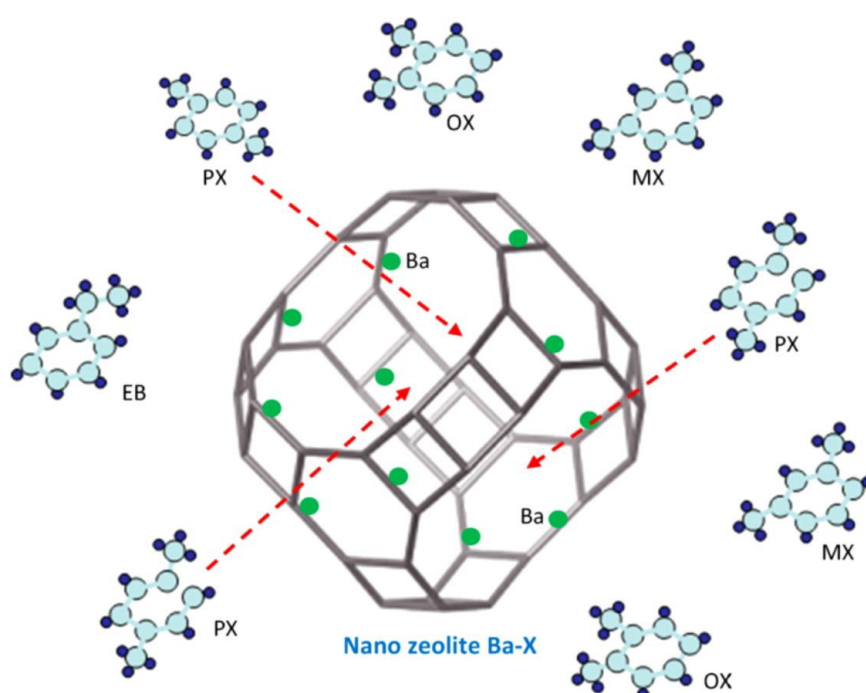


**Figure 1.18:** Graphical representation of the nano zeolite Ba-X<sup>37</sup>

The framework for Ba-X comprises sodalite cages linked through double six-rings, which create a large “supercage” within the structure which can be accessed by a three dimensional 12-ring pore system.<sup>37</sup> Ba-X possesses the ability to adsorb *para*-xylene selectively from a mixture of the C<sub>8</sub> aromatic isomers.

Na-BETA zeolites have also been shown to be selective for *para*-xylene.<sup>38</sup> The adsorptions of the xylene/ethylbenzene isomers were investigated using this zeolite at 15, 25 and 35 °C, and the saturation adsorption capacities were in the order *para*-xylene (143 mg/g) > ethylbenzene (105 mg/g) > *meta*-xylene (83 mg/g) > *ortho*-xylene (68 mg/g) at a temperature of 25 °C.

MOFs are nanoporous crystalline materials with characteristic coordination bonds between the organic linker molecules and metal nodes.<sup>39–41</sup> Examples of MOFs include MOF-48, which is *para*-xylene selective, and MIL-47, which is *ortho*-xylene selective.<sup>42</sup> MOF-48 displayed improved *para*-xylene selectivities compared with the Ba-X zeolite. Zn-MOF (Figure 1.19), which contains hexagonal nanotubular channels, has a preferential affinity for benzene and also for *para*-xylene over the other C<sub>8</sub> isomers.<sup>43</sup> The adsorption amounts, determined at room temperature, were *para*-xylene (1.79 mg/g) > benzene (1.08 mg/g) > *meta*-xylene (1.04 mg/g). When the temperature was altered from room temperature to 40 °C, the adsorption amount for *para*-xylene increased from 1.79 mg/g to 4.14 mg/g.

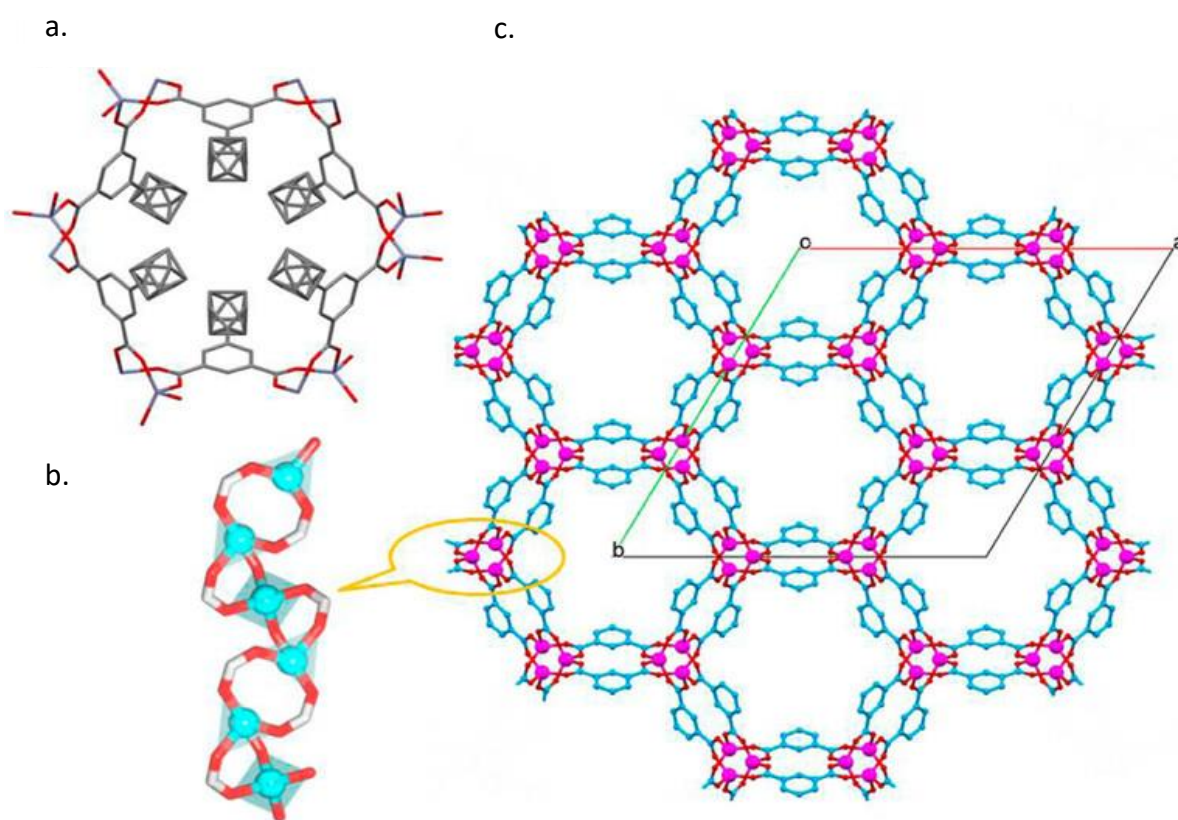


**Figure 1.19:** a. A Zn-MOF hexagonal nanotube in which disordered phenyl rings reside. b. A fragment view of a one-dimensional helical strand of the zinc centre. c. Three-dimensional tubular metal-organic framework with the disordered phenyl groups omitted for clarity. Zinc is purple, carbon cyan and oxygen red<sup>43</sup>

## 1.5 Analysis of host-guest complexes

Several analytical techniques are applicable for the analysis of host-guest complexes, and the more important of these will be discussed now.

### 1.5.1 Proton nuclear magnetic resonance spectroscopy

Proton nuclear magnetic resonance ( $^1\text{H}$  NMR) spectroscopy is widely used for the analysis of host-guest compounds. This type of spectroscopy is employed to, firstly, characterize a newly synthesized host compound (together with  $^{13}\text{C}$  NMR) and to subsequently determine if a potential guest species has been enclathrated successfully by the host compound after the recrystallization experiment. In this case, the proton NMR spectrum will have resonance signals for both the host and guest species. A comparison of the areas under the selected host and guest resonance signals then provides the host:guest (H:G) ratio.<sup>44</sup>

### 1.5.2 Gas chromatography

Gas chromatography (GC) is used to quantify the guest components in host-guest complexes when the host compound is presented with more than one guest concomitantly, and where the host and/or guest proton signals overlap on the  $^1\text{H}$  NMR spectrum.<sup>5</sup> A suitable dissolution solvent is used to dissolve the complex, and this injected into the instrument.

### 1.5.3 Single crystal X-ray diffraction analyses

Single crystal X-ray diffraction (SCXRD) is used to determine the crystal structures of the host compound and the host-guest inclusion complexes if their crystal quality is suitable. When these compounds crystallize with stable repeating molecular motifs in three dimensions, SCXRD analyses can reveal the unit cell of the crystal (which is the smallest repeating unit of the packing diagram), the space group and the crystal system. Furthermore, the inter-atomic distances and angles of the non-covalent interactions present may also be investigated, together with the type of non-covalent interaction at play. An in-depth analysis of these often

reveals the reasons for any observed guest preferences of the host compound. By removing the guests from the packing calculation and calculating the remaining voids, the crystal structures can also assist in determining the nature of the guest accommodation, that is, whether guests are housed in discrete cages or in endless channels.<sup>45</sup>

#### 1.5.4 Thermal analyses

Thermal analysis (TA) is a technique that measures the changes in the physical properties of the inclusion compound as a function of temperature.<sup>46</sup> There are two experiments that can be conducted thermoanalytically, namely thermogravimetry (TG and its derivative, the DTG) and differential scanning calorimetry (DSC). Figure 1.20 is an illustration of typical overlaid TG, DTG and DSC traces obtained for the complex of *N,N'*-bis(9-phenyl-9-thioxanthenyl)ethylenediamine with THF. In this figure, the blue trace represents the TG, while the red trace is the DTG; the green trace is the DSC.<sup>47</sup>

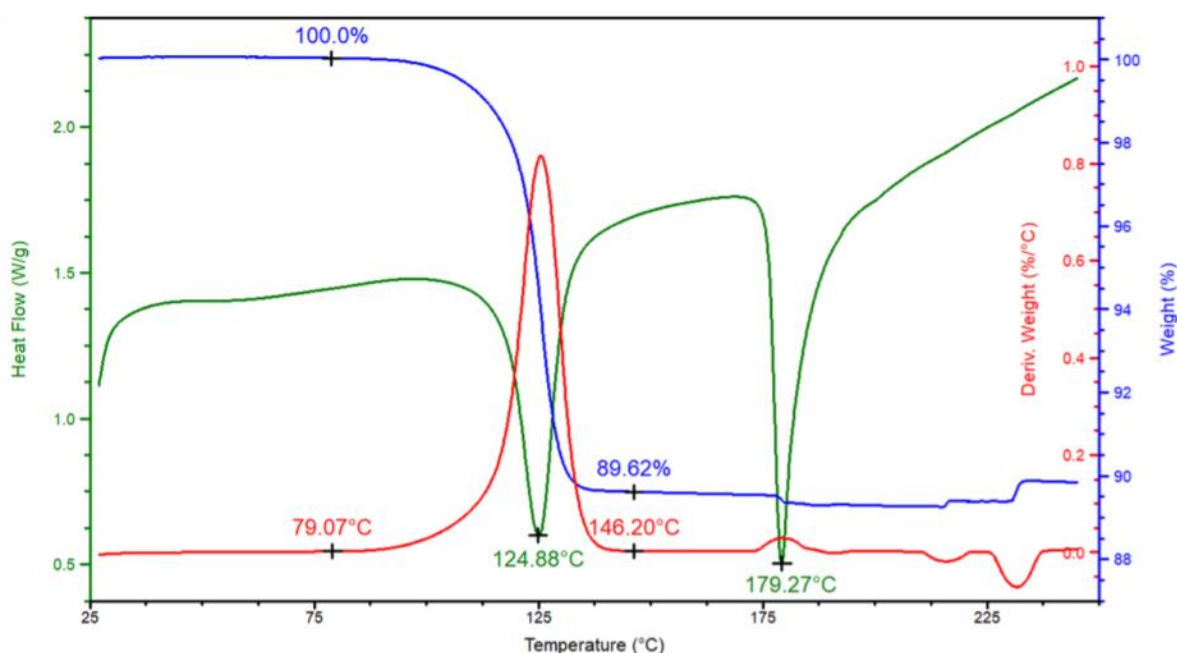


**Figure 1.20:** Example of a thermogram showing the overlaid TG (blue), DTG (red) and DSC (green) traces obtained after heating a complex of *N,N'*-bis(9-phenyl-9-thioxanthenyl)ethylenediamine with THF under thermoanalytical conditions<sup>47</sup>

Important information may be obtained from these TG, DTG and DSC traces. Considering the example as supplied in Figure 1.20, the TG shows a mass change from 100.0% to 89.6% during

the heating process which represents the guest escaping from the crystals; this may be used to calculate the H:G ratio since the molecular structures of both host and guest species are known. The area beneath the DSC peak for the guest release event corresponds to the enthalpy change for this process.<sup>48</sup> Also clear in this particular example is that the guest release initiates at 79.1 °C (this is the onset temperature for the guest release process,  $T_{on}$ , estimated from the DTG and is a measure of the thermal stability of the complex), and is most rapid at 124.9 °C (as obtained from the DSC). The host melt corresponds to the endotherm with a peak temperature of 179.3 °C (at which the melting of the host compound is most rapid). It is clear from this discussion that TA provides a wealth of information when analysing host-guest complexes.

#### 1.5.5 Powder diffraction

Since SCXRD analysis employs only one crystal from the solid in the experiment, an experimental powder X-ray diffraction (PXRD) pattern may be used to confirm that this singular crystal is representative of the bulk.<sup>49</sup> If so, the calculated powder pattern from the SCXRD experiment (obtained using appropriate crystal analysis software) will concur with that of the PXRD experiment. Furthermore, powder patterns can provide information on polymorphism and crystallinity of the solid material.

#### 1.6 Well-established host compounds

The number of journal articles published annually on the topic of host-chemistry is overwhelming and, as such, to select and describe the more important host compounds in this field is an onerous task. However, just such an attempt shall be made here. As described earlier, two broad categories of host compounds exist, namely cavitands and clathrands, and these two host types will be discussed separately.

## 1.6.1 Cavitands

### 1.6.1.1 Crown ethers

Crown ethers are described as heterocyclic macrocycles, and in their simplest forms they have at least three  $\text{CH}_2\text{CH}_2\text{O}$  repeating units.<sup>50</sup> Figure 1.21 is an illustration of some of the various crown ethers that exist (note that dioxane only contains two  $\text{CH}_2\text{CH}_2\text{O}$  units and is thus not named as a crown ether).

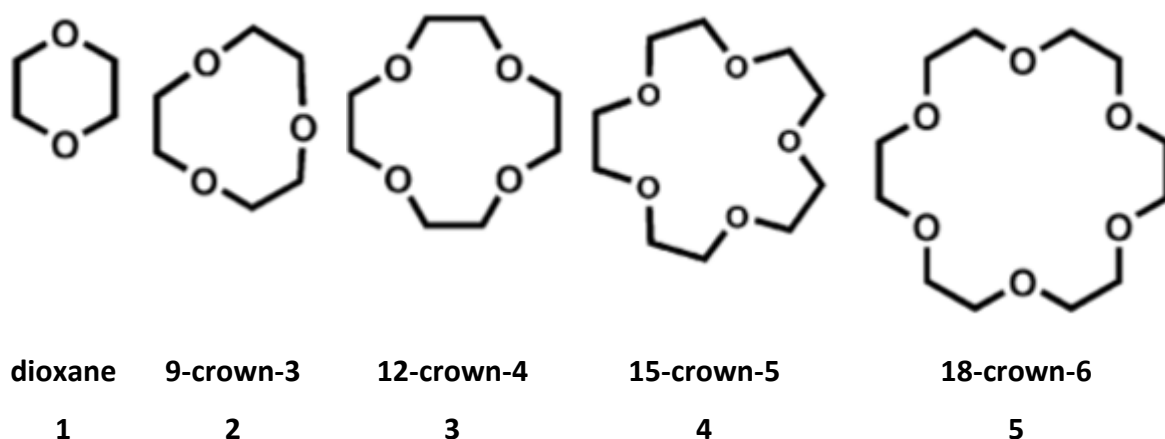


**Figure 1.21:** Dioxane (**1**) and crown ethers **2–5**<sup>50</sup>

Crown ethers have the ability to encapsulate alkali and alkaline earth metal cations in their central cavities by means of an electrostatic attraction between this cation and the lone pairs on the oxygen atoms.<sup>51</sup> The diameter of the central cavity determines which metal cations can be accommodated; clearly, 9-crown-3 cannot complex with large metal cations due to the small space in its interior, compared with 18-crown-6 which can form an inclusion complex with larger cations.

Interestingly, dibenzo-18-crown-6 (**6**, Figure 1.22) was the first crown ether ever identified, and its discovery was made by Pedersen.<sup>51</sup>



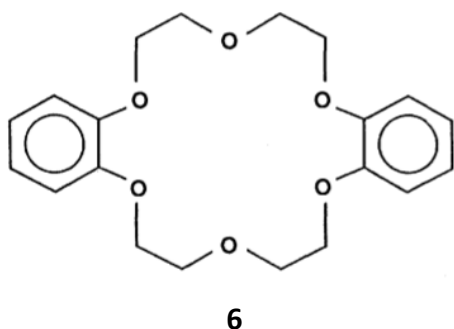


**Figure 1.22:** Dibenzo-18-crown-6 (2,3,11,12-dibenzo-1,4,7,10,13,16-hexaoxacyclooctadeca-2,11-diene)<sup>52</sup> (**6**)

The oxygen atoms present in crown ethers may be substituted by nitrogen (N), sulfur (S), phosphorous (P) and selenium (Se) atoms instead, these also possessing the ability to behave as donor atoms in the ring structures.<sup>52</sup> When some of the O donor atoms of a crown ether are replaced with N, NH or NR, the molecules are referred to as azacrown ethers, while the presence of some sulfur atoms afford what are called thiacrown ethers; if each of O, S and N are present simultaneously, the compound is an azathiacrown ether.

#### 1.6.1.2 Cryptands

Cryptands are derivatives of crown ethers and thus have the same properties that crown ethers have, with the exception that they additionally possess a three-dimensional spatial structure and higher association constants.<sup>53</sup> (As mentioned before, an association constant is the interaction affinity between the host and guest species.) In fact, the association constants of the cryptands are  $10^3$ – $10^4$  times higher than those of crown ethers as the cryptands have additional binding sites and a highly preorganized structure.<sup>54</sup> The non-covalent interactions that exist between the cryptands and their guest components are hydrogen bonds, charge transfer,  $\pi \cdots \pi$  stacking and C–H $\cdots\pi$  interactions. Some prototypical cryptands (**7–9**) are provided in Figure 1.23.<sup>54</sup>

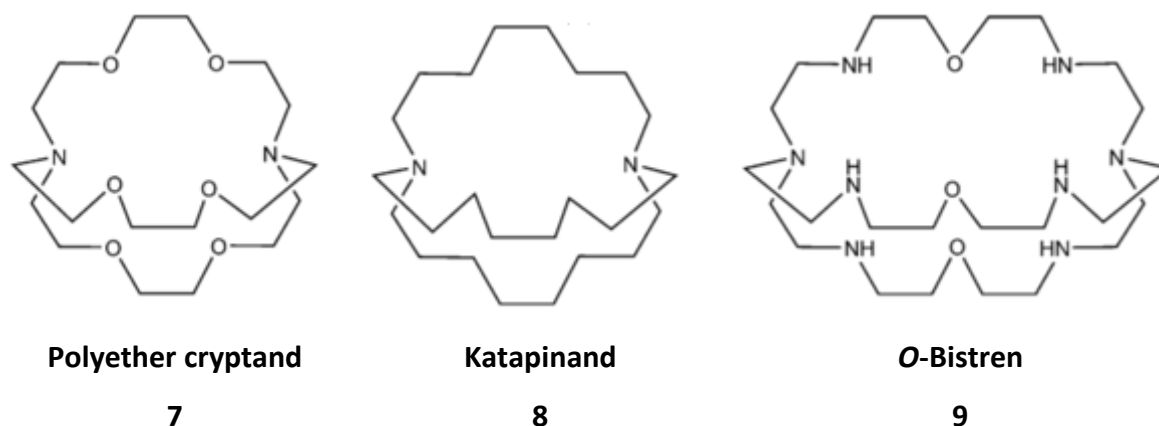


**Figure 1.23:** The early cryptands<sup>53</sup>

The first cryptand was discovered by Parks and Simmons who referred to it as a diazabicyclic “katapinand” (**8**) (Figure 1.23). The “katapinands” were later renamed “cryptands” by Lehn and co-workers due to their crypt-like shapes. They also rather described these compounds as azabicyclic ligands.<sup>55</sup>

#### 1.6.1.3 Spherands and hemi-spherands

The family of host compounds known as the spherands was first reported by Donald J. Cram in 1987.<sup>56</sup> The synthesis of these compound types followed that of the crown ethers and cryptands, and their binding affinity with their guest species is in the order of their discovery, that is, crown ethers < cryptands < spherands.<sup>2</sup> Figure 1.24 shows the progression from a simple crown ether (**10**) through to the spherand (**16**) by successively replacing the aliphatic ether group with rigid anisole units. Spherands are molecules that have rigid cavities with donor sites, that are usually oxygen atoms, which are directed inwards for complexation with usually spherically-shaped guests.<sup>57</sup>

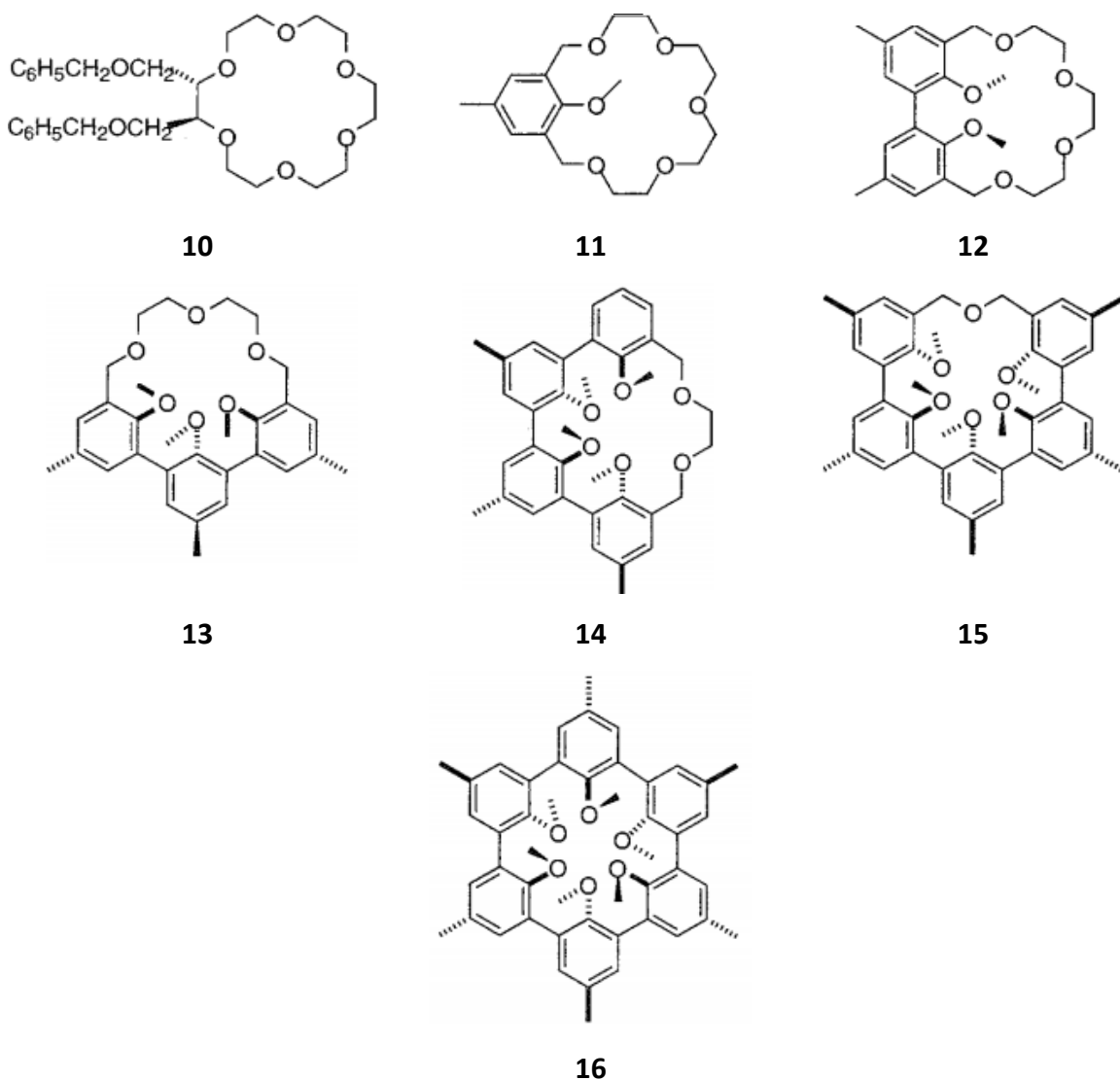


**Figure 1.24:** Progression from the simple crown ether (10) to the spherand (16) by the successive replacement of the aliphatic ether group with anisole units<sup>9</sup>

Hemi-spherands consist of half preorganized ligands, and compound 17 in Figure 1.25 is an example. This class of compounds binds strongest with the alkali metals, more specifically with  $\text{Na}^+$  and  $\text{K}^+$  ions.<sup>58</sup>

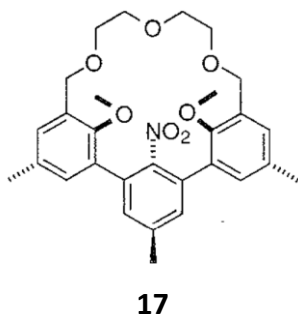


**Figure 1.25:** A hemi-spherand with a nitro functional group<sup>9</sup>

Cryptahemi-spherands (**18**) and calix-spherands (**19**) (Figure 1.26) are host compounds with permanent cavities that comprise, in the former case, half cryptand and half spherand units and, in the latter, a spherand unit that is capped with a calixarene.<sup>9</sup>

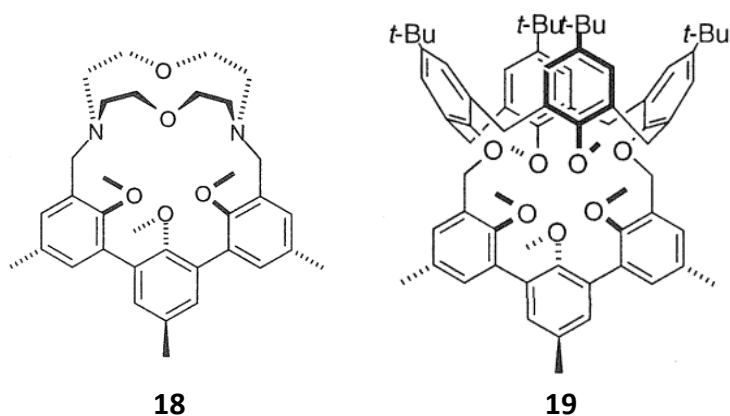


**Figure 1.26:** A cryptahemi-spherand (**18**) and a calix-spherand (**19**)<sup>9</sup>

#### 1.6.1.4 Cyclodextrins

Cyclodextrins are cyclic oligosaccharides in which each saccharide unit is linked end-to-end via  $\alpha$ -1,4 glycosidic bonds. These compounds are formed when starch is degraded by glucosyltransferase enzyme. The first known record of cyclodextrins was published by A. Villiers, a French scientist, in 1891.<sup>59</sup> In his work, he described the isolation of 3 g of a crystalline substance from the bacterial digest of 1000 g of starch. Figure 1.27 illustrates the three more important cyclodextrins comprising six, seven and eight glucose units to furnish  $\alpha$ -,  $\beta$ - and  $\gamma$ -cyclodextrin (**20–22**), respectively.<sup>60</sup>

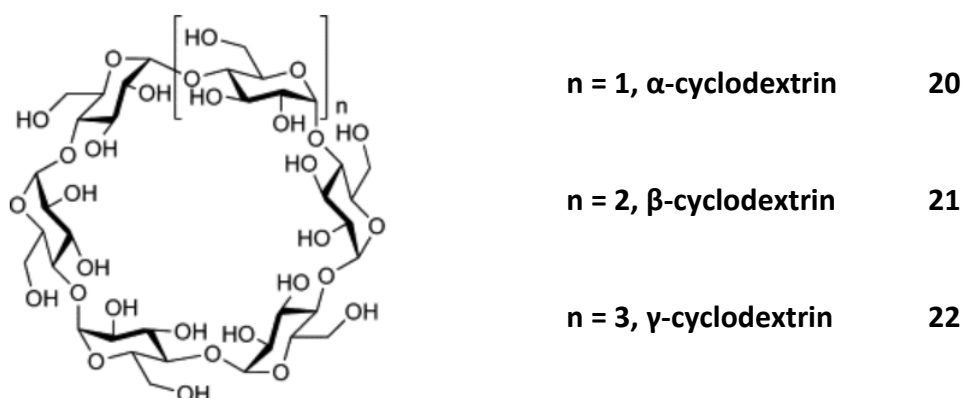


**Figure 1.27:** The structure of cyclodextrins ( $n = 1$ ,  $\alpha$ -cyclodextrin;  $n = 2$ ,  $\beta$ -cyclodextrin;  $n = 3$ ,  $\gamma$ -cyclodextrin)<sup>60</sup>

Cyclodextrins have a cone-shaped structure which possesses a hydrophobic centre and hydrophilic exterior (Figure 1.28). The interior is hydrophobic owing to the presence of the skeletal carbons and ethereal oxygens of the glucose residues, while the hydrophilic exterior is as a result of the hydroxyl groups.<sup>61,62</sup> Consequently, cyclodextrins are able to accommodate hydrophobic guest compounds in their cavities and, since the exterior is hydrophilic, the resulting complex is water soluble which assists immensely in the transport of these guests in the human body if they were, for example, drug actives.

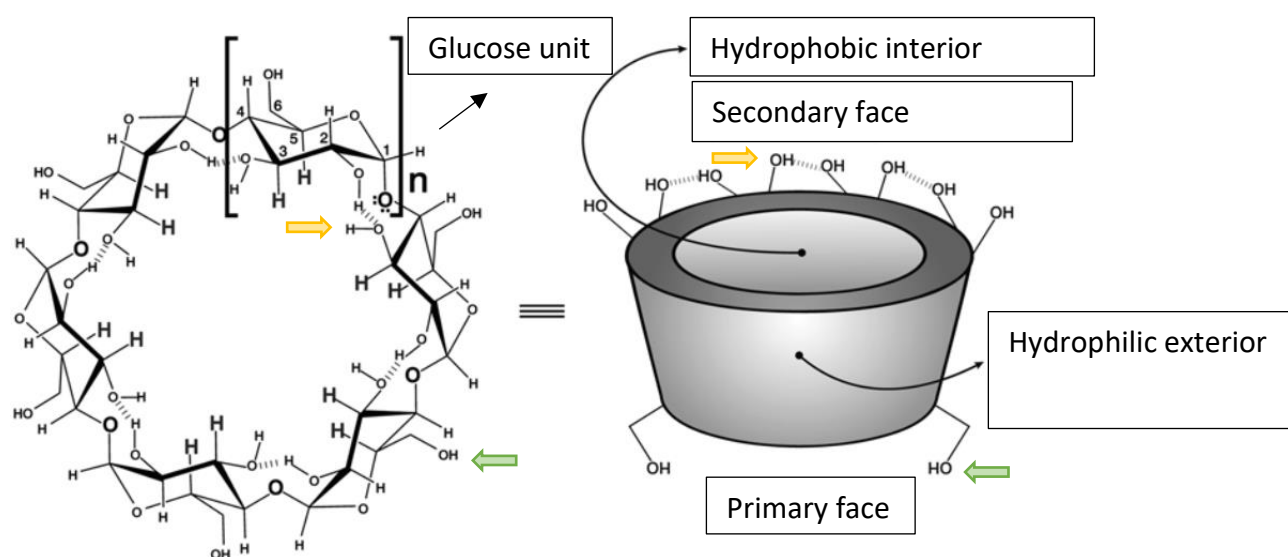


**Figure 1.28:** Schematic representation of a cyclodextrin<sup>62</sup>

#### 1.6.1.5 Calixarenes

In 1872, the first synthesis of a calixarene was carried out by Adolph von Baeyer, but this compound remained uncharacterised for nearly 70 years due to limitations in analysing products in those days.<sup>63</sup> In the 1940's, scientists Zinke and Ziegler assigned cyclic tetrameric structures (**23**) to the substances that were obtained from the reaction of *para*-substituted phenols with formaldehyde (Figure 1.29); the reaction was base-induced.<sup>64</sup> Furthermore, Niederl and Vogel carried out the acid-catalyzed reaction of resorcinol with aldehydes to furnish cyclic products (**24**),<sup>65</sup> also provided in this figure.

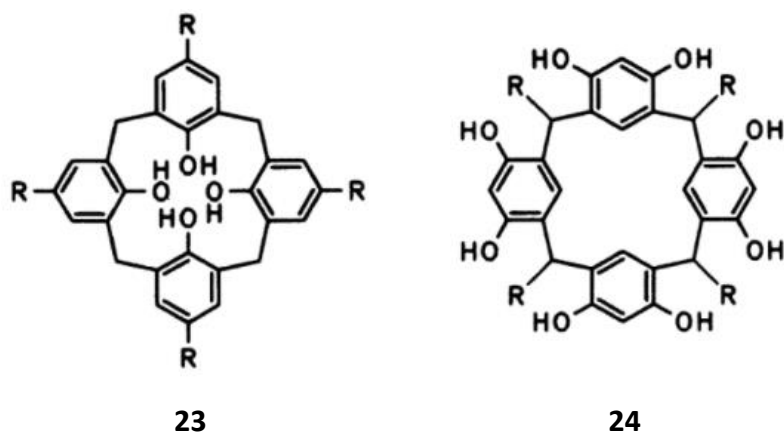


**Figure 1.29:** The cyclic tetrameric structures obtained by Zinke and Ziegler (**23**, left), and the compounds synthesized by Niederl and Vogel (**24**, right)<sup>66</sup>

More recent work by Gutsche and Högberg offered insights into these base- and acid-induced reactions.<sup>67–70</sup> They reported that both reactions allowed for the facile synthesis of calixarenes. The phenol-derived calixarenes may be obtained by means of base-induced processes, while calixresorcinarenes (resorcinol-derived calixarenes) are prepared after acid-catalyzed reactions.

The name “calixarene” was used to describe the cone geometry of these cyclic tetramers. To differentiate between the various calixarenes, a bracketed number is inserted between “calix” and “arene” to indicate the number of aromatic rings present. In more systematic applications of calixarene nomenclature, the substituents are all indicated in their specified positions and the basic ‘calix[n]arene’ is retained. Figure 1.30 indicates these more systematic approaches, namely for 25,26,27,28-tetrahydroxycalix[4]arene (**25**) and 49,50,51,52,53,54,55,56-octahydroxycalix[8]arene (**26**).

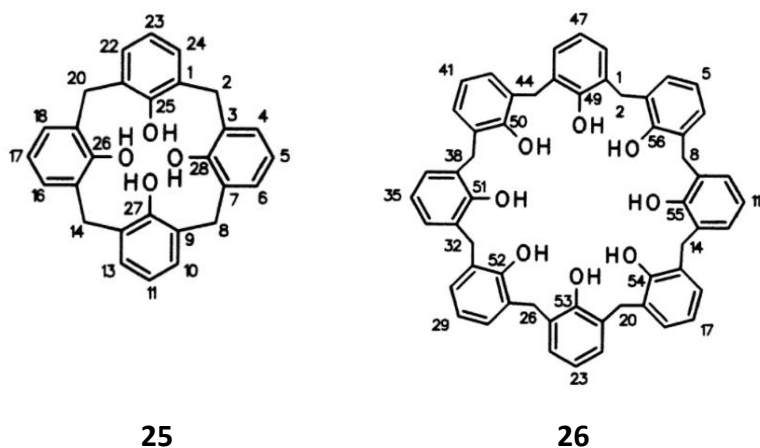


**Figure 1.30:** Structures of calix[4]arene (**25**, left) and calix[8]arene (**26**, right)<sup>66</sup>

#### 1.6.1.6 Carcerands and hemi-carcerands

Carcerands and hemi-carcerands were developed in the mid-1980s by Donald J. Cram.<sup>71,72</sup> These molecules were the first container molecules with the ability to permanently or semi-permanently encapsulate simple organic molecules as guests.<sup>73</sup> These molecules are spherical and hollow and are built from two cup-shaped cavitands (**27** and **28**, Figure 1.31) to create a smaller inner cavity which can accommodate these guest species<sup>72</sup> (**29**, referred to as a carceplex).

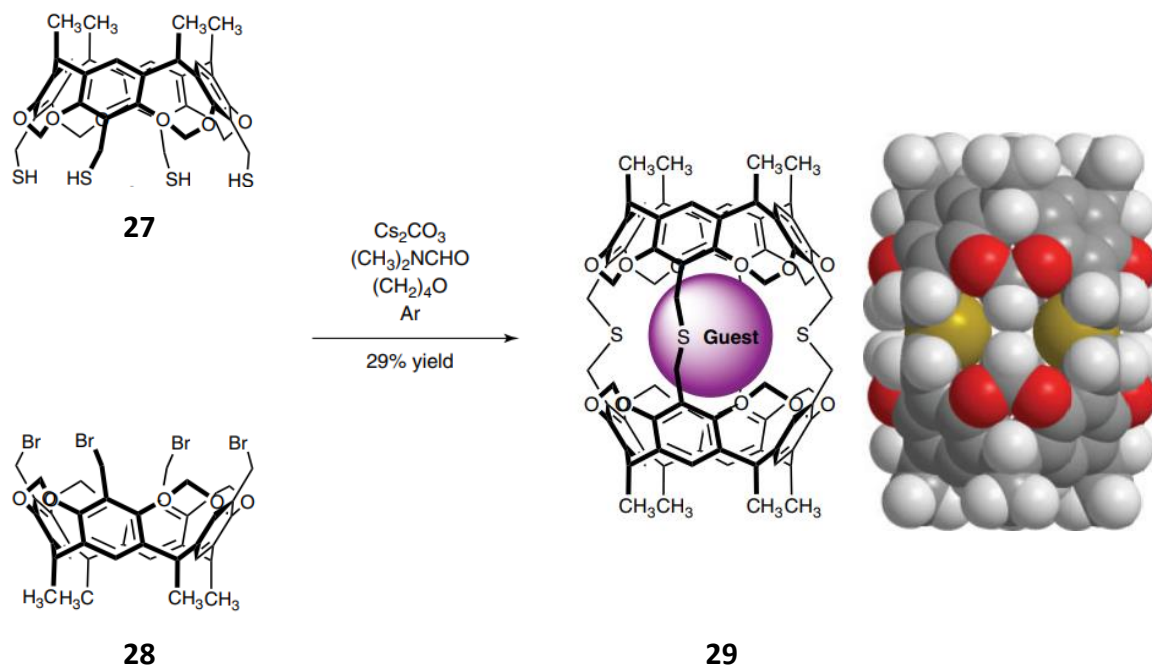


**Figure 1.31:** Synthesis of a carceplex (**29**) from two cup-shaped cavitands (**27**, **28**) with an encapsulated guest molecule (left); a space-filling model is also provided on the right<sup>74</sup>

The term carcerand is derived from the Latin word “carcer”, which means “prison”. Carcerands form stable complexes with guest compounds: once the guest is included in the cavity, it becomes incredibly difficult to remove it, even at elevated temperatures, and hence the name of these host-guest complexes.

Hemi-carcerands, on the other hand, form stable hemi-carceplexes at ambient temperatures, but it is possible for these guests to be released or exchanged at elevated temperatures. Therefore, after isolation and characterization of the formed complex, heat may be applied in order to overcome the energy barriers that retain the guest molecules in the cavities.<sup>75</sup> Figure 1.32 illustrates some of the hemi-carcerands (**30–33**) that were synthesized by Cram and his co-workers.<sup>72</sup>

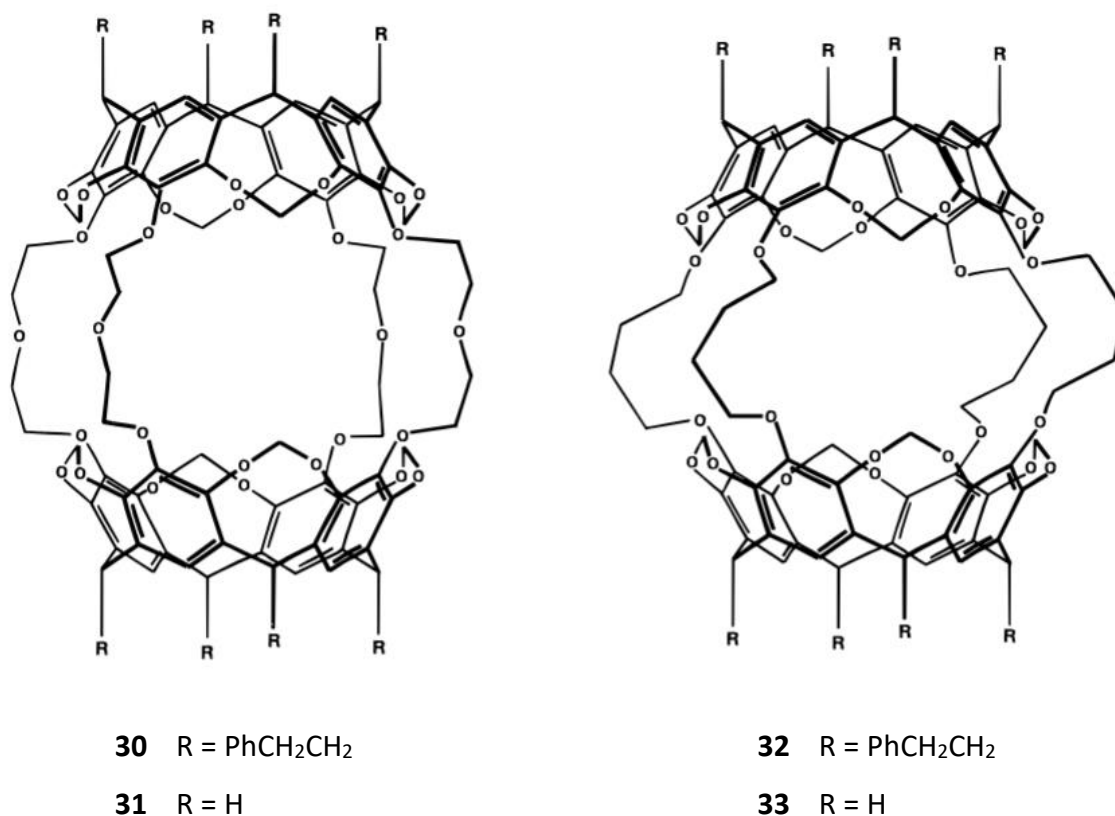


**Figure 1.32:** Some of the hemi-carcerands (**30–33**)<sup>75</sup> that were synthesized by Cram and co-workers



## 1.6.2 Clathrands

### 1.6.2.1 $\alpha,\alpha',\alpha',\alpha'$ -Tetraaryl-1,3-dioxolane-4,5-dimethanols

$\alpha,\alpha',\alpha',\alpha'$ -Tetraaryl-1,3-dioxolane-4,5-dimethanols (**36**, TADDOLs) are made from the diester of naturally-occurring (+)-tartaric acid by employing the synthetic route provided in Figure 1.33<sup>76</sup>:

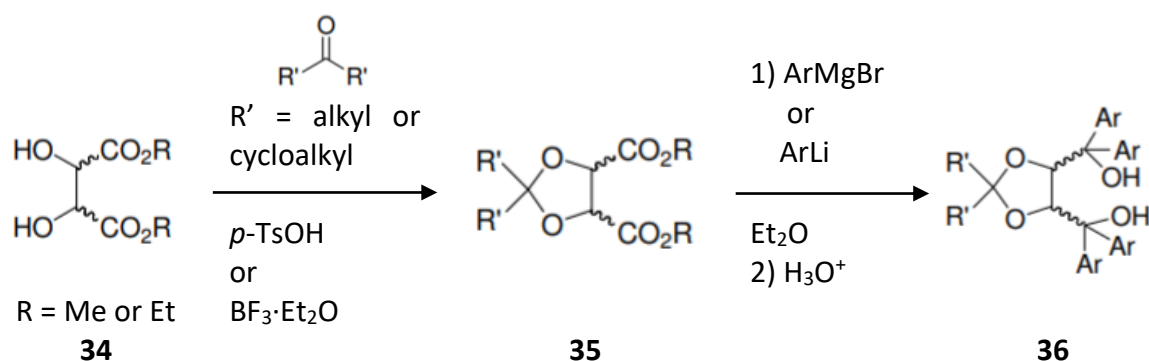


**Figure 1.33:** The general synthetic pathway towards TADDOLs<sup>76</sup>

Therefore, in order to prepare TADDOLs, the methyl or ethyl ester of tartaric acid (**34**) is reacted with an acyclic or cyclic ketone in the presence of *p*-toluenesulfonic acid (*p*-TsOH) or boron trifluoride etherate ( $\text{BF}_3 \cdot \text{Et}_2\text{O}$ ) to furnish a ketal (**35**). The ketal is then reacted with Grignard reagents or similar lithium derivatives to afford the TADDOL (**36**). These molecules can be readily derivatized (**37**, Figure 1.34) by varying the  $R'$  alkyl groups, the aromatic functionalities and also by substituting the hydroxyl groups of **36** with other groups.<sup>51</sup>

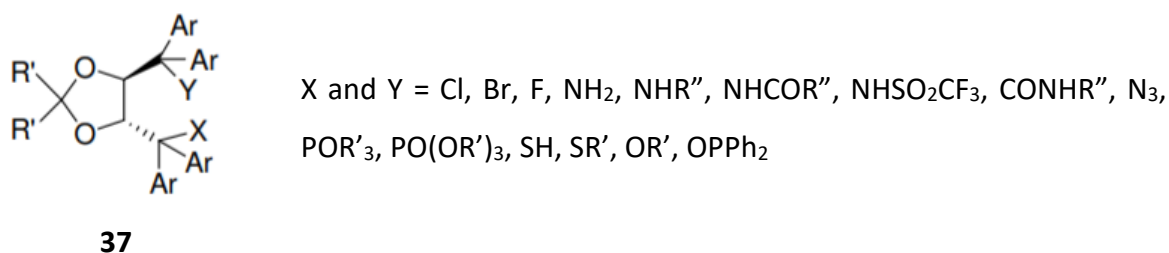


**Figure 1.34:** The general structure of TADDOL and derivatives<sup>76</sup>

Unmodified TADDOL ( $\text{Ar} = \text{Ph}$ ,  $\text{R} = \text{Me}$ ), **36**, exists in optically pure and racemic forms. Goldberg and colleagues<sup>77</sup> demonstrated that when the compound is optically pure it forms inclusion

complexes with secondary alkylamines, whereas in its racemic form it has a preference for primary and secondary amines.

Seebach and colleagues discovered that optically pure TADDOLs may be employed for the separation of a myriad enantiomeric mixtures owing to its chiral cavities.<sup>78</sup> Furthermore, TADDOLs have functioned as stationary phases for chromatographic applications, and also as chiral auxiliaries in enantiomeric transformations.

TADDOLs (**36**) are relatively small organic molecules, but larger derivatives have been synthesized by Tanaka and co-workers<sup>79</sup> (**38**, **39**, Figure 1.35).

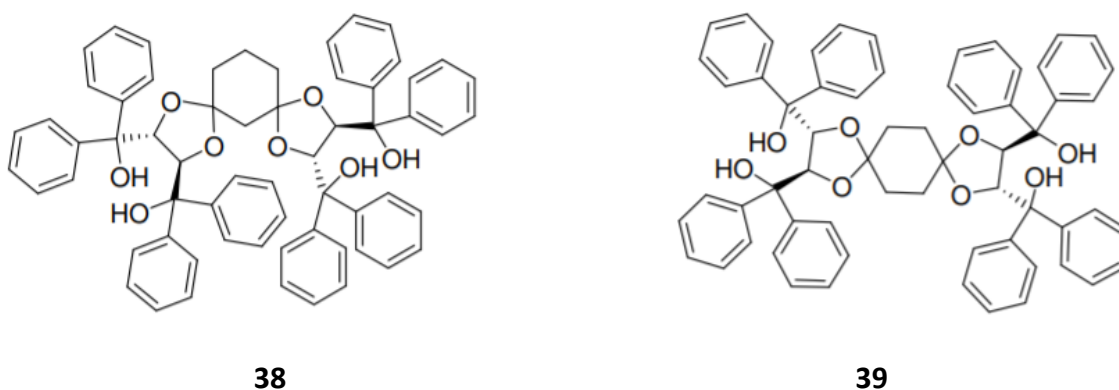


**Figure 1.35:** Larger TADDOL host molecules (**38** and **39**) synthesized using 1,3- and 1,4-cyclohexanedione, respectively<sup>79</sup>

TADDOL **38** was able to optically resolve racemic cyanohydrins, while **39** possessed enhanced molecular recognition properties for chiral alcohols such as but-3-yn-2-ol, 2-hexanol and 2-methyl-1-butanol.

#### 1.6.2.2 (+)-(2*R*,3*R*)-1,1,4,4-Tetraphenylbutane-1,2,3,4-tetraol

(+)-(2*R*,3*R*)-1,1,4,4-Tetraphenylbutane-1,2,3,4-tetraol (TETROL, **40**, Figure 1.36) is a compound with similar structural features to TADDOL and, like TADDOL, is also synthesized from tartaric acid diester followed by a Grignard reaction with phenylmagnesium bromide.<sup>80</sup> The geometry of each TETROL molecule is stabilized by a pair of 1,3-intramolecular hydrogen bonds, and this ability to form hydrogen bonds allows TETROL to behave as a highly efficient

host compound. TETROL thus forms complexes with a wide variety of guest species, including the alkylated aromatics toluene, ethylbenzene and cumene, and the aminated aromatics aniline, *N*-methylaniline and *N,N*-dimethylaniline, amongst numerous others. A derivative of TETROL, 2,3-dimethoxy-1,1,4,4-tetraphenylbutane-1,4-diol (DMT, **41**, Figure 1.36), formed by deprotonation and subsequent methylation of the internal hydroxyl groups, was also extremely successful as a host compound, and formed inclusion complexes with the different isomeric xylenes and ethylbenzene, and a wide variety of other guest compounds.

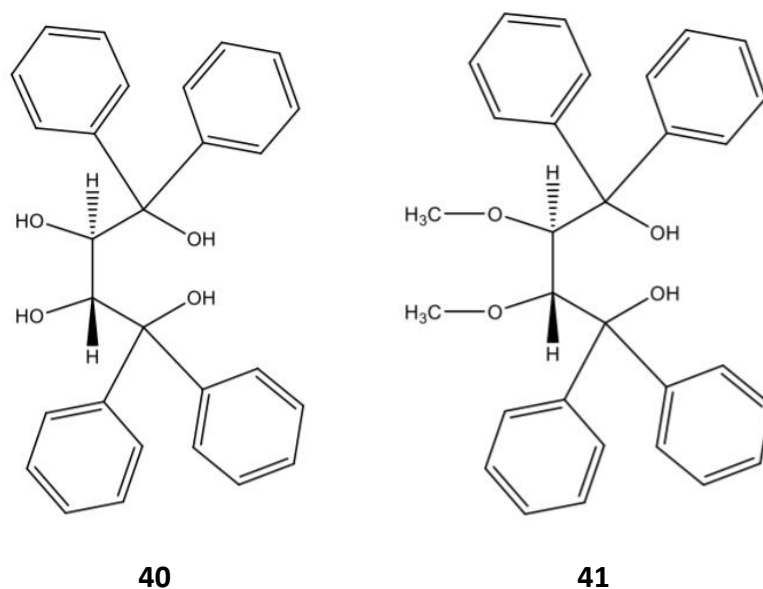


**Figure 1.36:** The structures of TETROL (**40**) and DMT (**41**)<sup>80</sup>

### 1.6.2.3 Roof-shaped host compounds

A new host design was investigated by Weber and co-workers in 1996, which involved the characteristic roof-shaped basic skeleton of 9,10-dihydro-9,10-ethanoanthracene with appended diarylmethanol clathratogenic groups (Figure 1.37, **42a–e** and **43a–e**).<sup>81</sup>



**Table 1.3:** Crystalline inclusion compounds of **42** and **43**, and their H:G ratios<sup>81</sup>

Guest solvent	Host compound									
	42a	42b	42c	42d	42e	43a	43b	43c	43d <sup>a</sup>	43e
PrNH <sub>2</sub>	3:2	–	3:2	–	1:1	1:2	1:1	1:1		1:1
BuNH <sub>2</sub>	–	1:1	–	–	1:1	1:2	1:1	1:1		1:1
Piperidine	1:2	–	1:2	–		1:2	1:2	1:2		1:2
DMSO	1:1	–	–	–	1:1	1:2	1:2	1:2		1:2
Benzene	–	–	–	1:1	1:1	2:1	1:1	1:1		1:1
Toluene	–	–	–	1:1	1:1	3:1	1:1	1:1		1:1

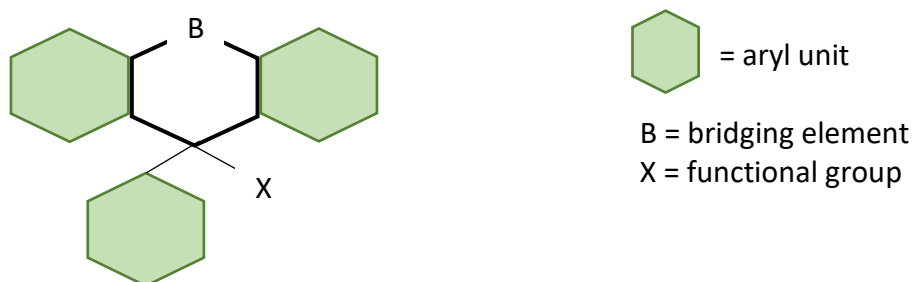
– no enclathration took place

<sup>a</sup> no information was available for **43d**

As observed from this table, H:G ratios varied between 1:1, 1:2, 2:1, 3:1 and 3:2. Other guests were reported to be included with H:G ratios as high as 4:1. These compounds are clearly highly efficient host species for a broad variety of organic guest molecules.

#### 1.6.2.4 Tricyclic-fused host systems

Weber and co-workers reported a novel family of host molecules based on singly-bridged triarylmethanol and triarylacetic acid frameworks (Figure 1.39).<sup>82</sup>

**Figure 1.39:** Representation of the tricyclic-fused host systems<sup>82</sup>

These singly-bridged triarylmethanols and analogues are an excellent source of many efficient host compounds, and are simple in constitution, facilely synthesized, and readily modified structurally. Furthermore, their complexes often possess adequate crystal quality for SCXRD

analyses. The SCXRD analyses for three inclusion compounds with fluorene-based host compounds **46** and **47** (Figure 1.40) have been reported by Weber et al.

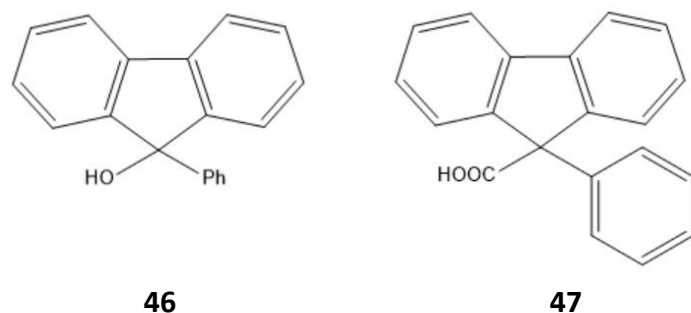


**Figure 1.40:** Fluorene-based host compounds with a hydroxyl (**46**) and carboxylic acid (**47**)<sup>82</sup> moiety

From benzene, **46** formed a complex with a H:G ratio of 8:3, where the benzene molecules were entrapped by H-bonded tetramer clusters within the crystals. When the same host compound was recrystallized from dioxane, the H:G ratio was 4:3, and these crystals were made up of H-bonded 2:1 H:G complexes with additional interstitial molecules of dioxane. Host compound **47**, on the other hand, formed a 1:1 H:G complex with ethanol, and here the crystals comprised 2:2 host-guest clusters through a twelve-membered H-bonded ring.

de Jager and colleagues prepared two closely related xanthenyl-derived host compounds,<sup>15</sup> namely *N,N'*-bis(9-phenyl-9-xanthenyl)ethylenediamine (**48**) and *N,N'*-bis(9-phenyl-9-thioxanthenyl)-ethylenediamine (**49**) as provided in Figure 1.41.

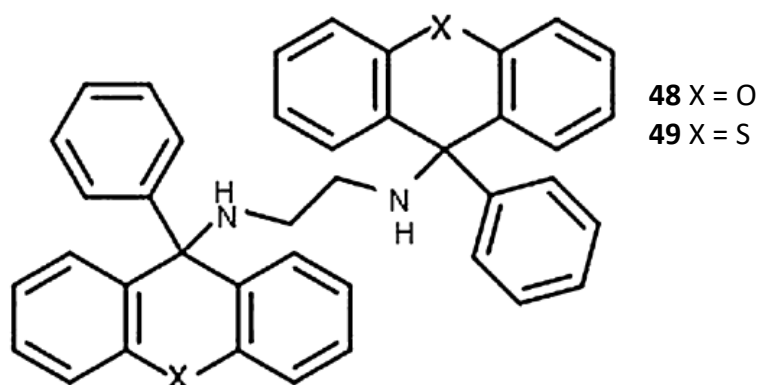


**Figure 1.41:** Structures of *N,N'*-bis(9-phenyl-9-xanthenyl)ethylenediamine (**48**) and *N,N'*-bis(9-phenyl-9-thioxanthenyl)ethylenediamine (**49**) prepared by de Jager and co-workers<sup>15</sup>

Compounds **48** and **49** were highly efficient host species and formed very many inclusion complexes with a great variety of different guest molecules. As an example, **48** included dichloromethane (DCM), dibromomethane (DBM) and diiodomethane (DIM) with 1:1 H:G ratios from the vapour phase, while inclusion complexes of **49** with these guests had H:G ratios of 1:2 for DIM, but 1:1 for the remaining two dihalomethanes.<sup>15</sup> Furthermore, both of these host compounds were selective for DBM when presented with all three dihaloalkanes in a mixture. Besides the dihaloalkanes, **49** also formed complexes with each of *o*-xylene, *p*-xylene and ethylbenzene, but did not form an inclusion compound with *m*-xylene. H:G ratios were 1:2 in each instance. Interestingly, **48** did not include any of these C<sub>8</sub>H<sub>10</sub> isomers.<sup>83</sup> The equimolar quaternary mixture experiment with **49** showed this host compound to possess an enhanced affinity for *p*-Xy (the mixed complex contained 2.5%/4.1%/68.3%/25.1% *o*-Xy/*m*-Xy/*p*-Xy/EB). When gas phase experiments were conducted with these guests, only *p*-Xy was enclathrated and only after one day of exposure to the vapour.

#### 1.6.2.5 Urea and thiourea

Urea inclusion compounds were discovered by Bengen in the 1940s.<sup>84</sup> This discovery was serendipitous when octanol was found to form a crystalline adduct with urea. The crystal structure for the inclusion complex showed the urea molecules to be involved in an extensive hydrogen-bonded arrangement forming linear, parallel tunnels into which the guest molecules were densely packed. Figure 1.42 shows the crystal structure of urea with hexadecane.<sup>85</sup>

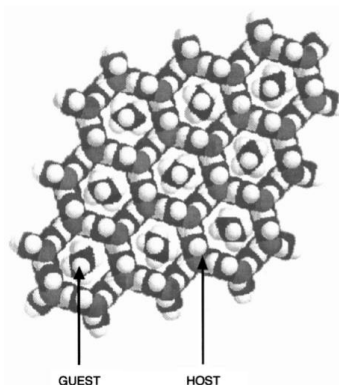


**Figure 1.42:** The urea·hexadecane inclusion compound showing complete tunnels in which the guest molecules are packed<sup>85</sup>

Clearly, urea has the ability to form inclusion compounds with long alkyl chain guest molecules. It was reported that, for inclusion to be successful, these chains should have only a restricted degree of substitution<sup>85</sup> in order to fit in the tunnels. After removal of the guest from the complex, the tunnels collapsed and pure  $\alpha$ -phase urea crystallized out which possessed no tunnels or other voids.

Host-guest complexes with thiourea as the host compound were first described by Hermann<sup>86</sup> and Lenné<sup>87</sup> when they discovered an inclusion complex with hexagonal channels with a 6.1 Å diameter (Figure 1.43).<sup>88</sup> The guest compound here was cyclohexane.



**Figure 1.43:** Thiourea-cyclohexane inclusion complex at ambient temperature; ten complete tunnels can be seen in which the cyclohexane molecules reside<sup>84</sup>

The unit cells of the thiourea inclusion compounds may be rhombohedral or monoclinic,<sup>84</sup> and the guest compounds that thiourea included in infinite channels were cyclohexane, ferrocene and other organometallic compounds, as well as aromatic molecules.

## 1.7 The present investigation

In the continuing search for alternative host compounds with improved selectivities for a particular guest species in a mixture, the present work reports on the host potential and selectivity behaviour of two compounds, namely *N,N'*-bis(5-phenyl-5-dibenzo[a,d]cycloheptenyl)ethylenediamine (**H1**) and *N,N'*-bis(5-phenyl-10,11-dihydro-5-dibenzo[a,d]cycloheptenyl)ethylenediamine (**H2**), when presented with various chemical industry-applicable organic mixtures (Figure 1.44). While these compounds are not novel, their employment as



host compounds for the separation of difficult-to-separate isomers and related compounds using host-guest chemistry protocols is, which is the focus of the present work.

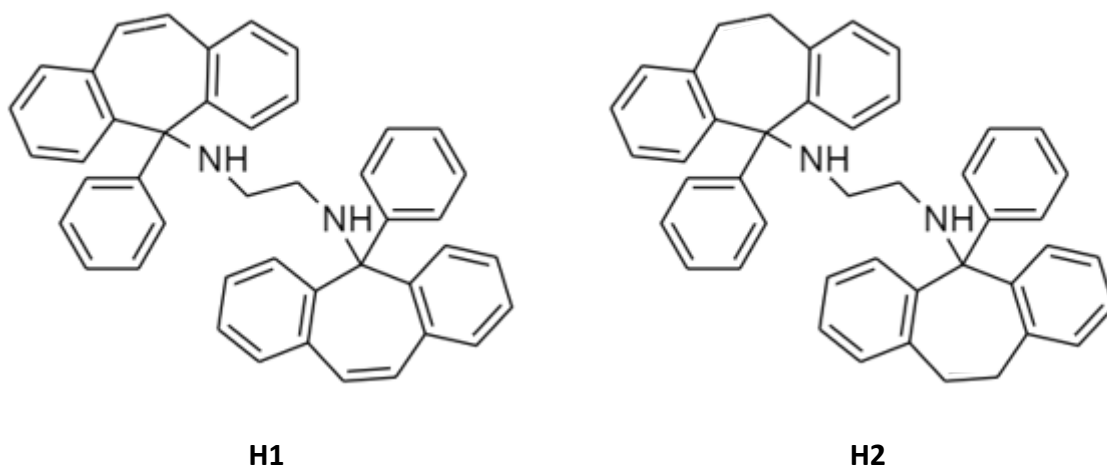


**Figure 1.44:** Structures of host compounds *N,N'*-bis(5-phenyl-5-dibenzo[a,d]cycloheptenyl)-ethylenediamine (**H1**) and *N,N'*-bis(5-phenyl-10,11-dihydro-5-dibenzo[a,d]cycloheptenyl)-ethylenediamine

In this work, each host compound will be dissolved in an excess of the guest compound; a co-solvent (that does not form a complex with the host) will be employed in cases where the host does not dissolve in the guest or if the guest is a solid. The vessels of these experiments will be left open to the ambient conditions<sup>89</sup> in order to facilitate the evaporation of some guest/solvent. The solids so-formed will be collected under vacuum and washed with petroleum ether (40–60 °C) and then dried by suction filtration. <sup>1</sup>H NMR spectroscopy will serve as an appropriate analytical tool to analyse these solids and thus determine whether inclusion occurred. If so, the H:G ratios will be obtained by comparing the integrals of selected host and guest signals.

After assessment of their host behaviour in single solvents, **H1** and **H2** will be investigated for any selectivity they may possess when presented with mixed guests and, more especially, guest mixtures that are challenging to separate by the more usual fractional distillations and crystallizations owing to similar physical properties. In this way, each host compound will be dissolved in every combination of equimolar guest mixtures from each guest series; low heat will be used to facilitate host dissolution. The appropriate guest series include pyridine and the methylpyridines (picolines), xylene isomers and ethylbenzene, and anisole and the

methylanisoles. The vessels of these experiments will be closed and stored at 4 °C in order to retain the equimolar conditions. Any crystals formed in this way will be treated as before and analysed by either  $^1\text{H}$  NMR spectroscopy,  $^{13}\text{C}$  NMR spectroscopy, or GC in order to quantify each of the guests present in the so-formed mixed complexes.  $^1\text{H}$  NMR spectroscopy will also provide information on the overall H:G ratios. Not only will equimolar guest mixtures be considered, but also binary guest mixtures from each guest series in which the G:G ratios are varied in order to observe how the two host compounds behave in such conditions.

Appropriate analyses will be carried out on all successfully-formed single solvent complexes, including  $^1\text{H}$  NMR spectroscopy, SCXRD and also thermal analyses (TG, DTG and, in some instances, DSC). The latter two methods will assist in understanding details of the mode of guest retention and the relative thermal stabilities of the complexes.

## 1.8 Aim and objectives

The aim of the present investigation is to determine whether host compounds **H1** and **H2** possess the ability to separate common chemical mixtures that are, more usually, difficult to separate by ordinary means (owing to physical property similarities) using host-guest chemistry strategies as an alternative separatory tool.

In order to achieve this aim, the following objectives will be actioned:

- a) Assessment of the host ability of **H1** and **H2** in the presence of applicable guest compounds by means of single solvent recrystallization experiments ( $^1\text{H}$  NMR analyses will be appropriate here);
- b) Preparation of applicable mixed guest solutions where guests are present in equimolar proportions, and recrystallization experiments of each host compound from the guest mixture in order to determine if these host compounds possess selectivity for any particular guest compound in such conditions (GC and/or  $^1\text{H}$  NMR and/or  $^{13}\text{C}$  NMR analyses will be applicable here);
- c) Preparation of binary guest mixtures in non-equimolar proportions, and recrystallization experiments of each host compound from these mixtures in order to determine how the

behaviour of the host varies with G:G ratio changes (GC and/or  $^1\text{H}$  NMR and/or  $^{13}\text{C}$  NMR analyses are applicable here);

d) The carrying out of SCXRD experiments on suitable crystals of the single solvent complexes to understand details of the mode of guest encapsulation; and

e) The carrying out of thermal analyses (TG, DTG and DSC, as appropriate) on all single solvent complexes to ascertain their relative thermal stabilities.

## 2. Methods

### 2.1 General

The starting and guest materials were purchased from Sigma-Aldrich, South Africa, and these were used without further purification.

The  $^1\text{H}$  and  $^{13}\text{C}$  NMR experiments were conducted by means of a Bruker Ultrashield Plus 400 MHz spectrometer with  $\text{CDCl}_3$  as the deuterated solvent, and the data were analysed by means of MNOVA software.  $^1\text{H}$  NMR spectroscopy was used in the following cases:

- To characterize the host compounds (in conjunction with  $^{13}\text{C}$  NMR and melting points)
- To determine whether inclusion had occurred successfully in the single solvent recrystallization experiments
- To determine H:G ratios for the single solvent recrystallization experiments
- To determine the overall H:G ratios of mixed complexes

The melting points of the host compounds were recorded on a TA SDT Q600/STA6000 Simultaneous Thermal Analyser or a Stuart SMP10 melting point apparatus.

The infrared spectra were obtained by means of a Bruker Tensor 27 Fourier Transform infrared spectrophotometer and the data were analysed using OPUS software.

The thermoanalytical experiments were carried out on all of the single solvent complexes prepared in this work. For these analyses, after recovery of the solids from the glass vials by means of vacuum filtration and washing with petroleum ether (40–60 °C) (washing is carried out to remove all superficial solvent from the crystal; by doing so, some guest release may occur and is an indication of whether the complex is stable or not), the crystals were patted dry in folded filter paper and then analysed directly without further manipulation. The instrumentation used was either a TA SDT Q600 (with the data analysed using TA Universal Analysis 2000 software) or a Perkin Elmer STA6000 Simultaneous Thermal Analyser (with the data analysed by means of Perkin Elmer Pyris 13 Thermal Analysis software). The samples

were placed in open ceramic pans while an empty ceramic pan functioned as the reference. The purge gas was high purity nitrogen. The samples were heated from approximately 40 to 400 °C (for the TA SDT Q600 module system) and from 40 to 340 °C (for the Pyris system) with a heating rate of 10 °C·min<sup>-1</sup>.

The gas chromatograph (GC) methods used to quantify the guests in the mixed complexes produced in this work are as follows, in chapter order in this dissertation (note that dichloromethane was the dissolution solvent in every case):

- Chapter 4 (xylenes/ethylbenzene): the mixed complexes were analysed by means of a Young Lin YL6500 GC equipped with an Agilent J&W Cyclosil-B column (30 m × 250 μm × 0.25 μm, calibrated) coupled to a flame ionization detector. The method involved an initial 1 min hold time at 50 °C. A ramp rate of 10 °C·min<sup>-1</sup> was then initiated until a final temperature of 90 °C was reached, and this held there for 3 min. The flow rate used was 1.5 mL·min<sup>-1</sup> and the split ratio 1:50. Due to instrument availability, an Agilent 7890A GC-Agilent 5975C VL mass spectrometer (GC-MS) equipped with the same column (as stated before) was also used at times. This method involved an initial hold time of 1 min at 50 °C after which the sample was heated until 52 °C was reached by means of a ramp rate of 10 °C·min<sup>-1</sup>, following which a rate of 0.3 °C·min<sup>-1</sup> was applied until a final temperature of 54 °C was attained. The flow rate was 1.5 mL·min<sup>-1</sup> and the split ratio 1:80.<sup>90</sup>
- Chapter 5 (pyridine/methylpyridines): once again, the same two GC instruments were employed, and the column remained the same. In the case of the Young Lin YL6500 GC instrument, the method involved an initial 2 min hold time followed by a heating rate of 30 °C·min<sup>-1</sup> to a temperature of 100 °C, which was then subsequently heated at a rate of 1.5 °C·min<sup>-1</sup> until 102 °C was attained. Finally, the temperature was increased to 103 °C at 0.5 °C·min<sup>-1</sup>. The flow rate was 1.8 mL·min<sup>-1</sup> and the split ratio 1:80. For the Agilent Technologies 7890A GC instrument, the method commenced with a temperature of 50 °C that was held there for 5 min and then ramped at 10 °C·min<sup>-1</sup> until 100 °C was reached. The flow rate was 1.5 mL·min<sup>-1</sup> and the split ratio 1:80.
- Chapter 6 (anisole/methylanisoles): Three GC instruments were used for this guest series, but the column remained as before. The Young Lin YL6500 GC method involved an initial temperature hold time for a minute at 50 °C, which was then heated at a rate of 10 °C·min<sup>-1</sup> until a final temperature of 110 °C was reached; this was held there for 4 min.

The split ratio and flow rate were altered from 1:80 to 1:20 and 1.5 to 1.7 and then back to 1.5 mL·min<sup>-1</sup>, respectively (the split ratio was altered from the previous method to increase the intensity of the peaks on the chromatogram, while the flow rate was changed in order to improve separations between the peaks). The method employing the Agilent Technologies 7890A GC instrument commenced with an initial temperature of 50 °C that was held for 1 min, followed by a heating rate of 10 °C·min<sup>-1</sup> until 110 °C was reached; this temperature was maintained for 3 min. The flow rate of the column had fluctuations between 1 and 1.5 mL·min<sup>-1</sup> due to the column pressure changing at times. The split ratio was 1:80. The third method used an Agilent Technologies 6890N GC instrument. An initial temperature of 50 °C was held for 1 min, followed by a heating rate of 10 °C·min<sup>-1</sup> until 110 °C was reached, and this temperature was maintained for 2 min. The flow rate and split ratio were 1.5 mL·min<sup>-1</sup> and 1:80, respectively.

Once suitable crystals of successfully formed complexes had formed during the single solvent recrystallization experiments, they were analysed by means of single crystal X-ray diffraction (SCXRD) experiments by making use of a Bruker Kappa Apex II diffractometer with graphite-monochromated MoK $\alpha$  radiation ( $\lambda = 0.71073 \text{ \AA}$ ). The data were collected using APEXII, whereas cell refinement and data reduction were achieved by employing SAINT; numerical absorption corrections were carried out with SADABS.<sup>91</sup> The structures were solved with SHELXT-2018/2 and refined by means of SHELXL-2018/3<sup>92</sup> (using least-squares procedures) together with SHELXLE<sup>93</sup> as the graphical interface. All non-hydrogen atoms were refined anisotropically, while the carbon- and oxygen-bound hydrogen atoms were inserted in idealized geometrical positions in a riding model; nitrogen-bound hydrogens were found on the difference map and were then allowed to refine freely. These analyses were conducted at different temperatures dependent on the state of the cryo unit of the Bruker instrument. In chapter order, these temperatures are as follows:

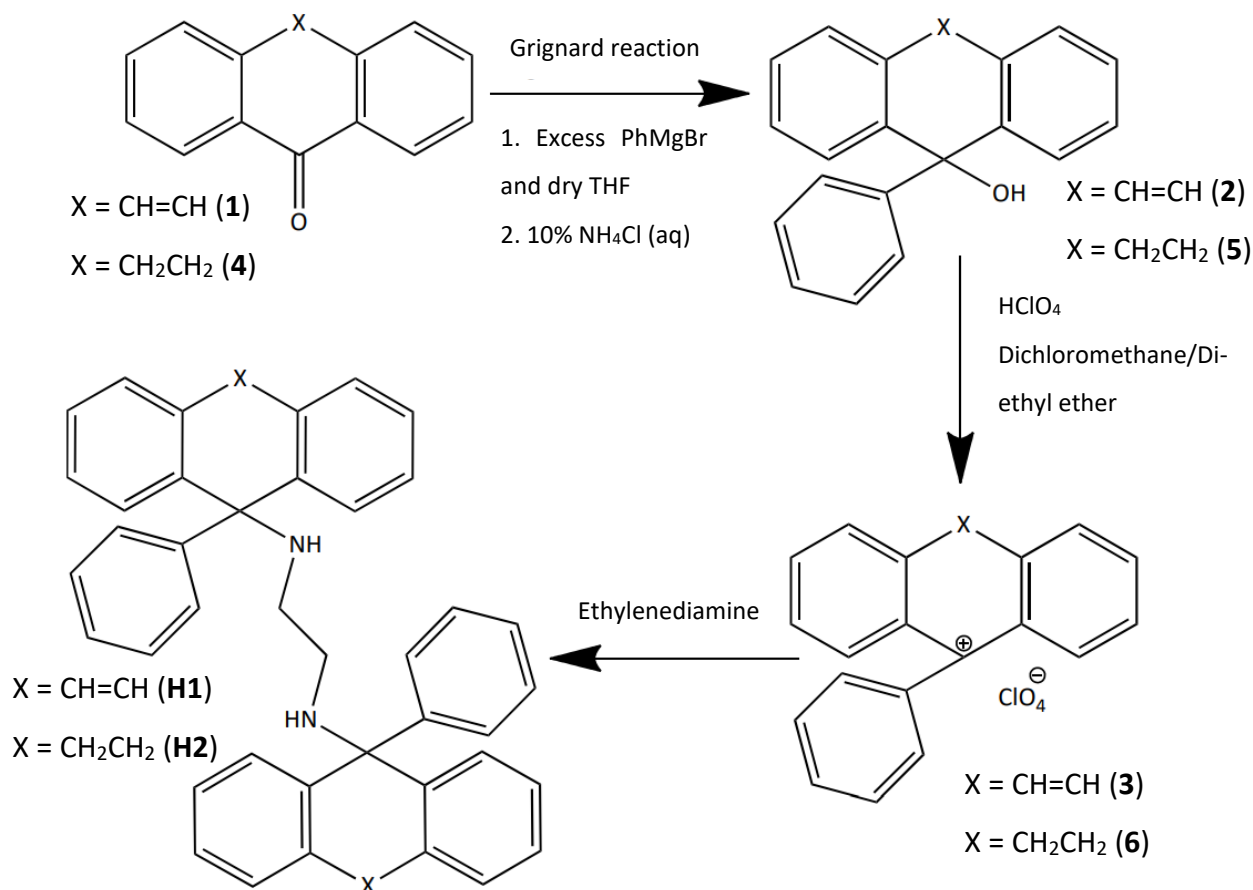
- Chapter 4 (xylenes/ethylbenzene): 200(2) and 296(2) K for **H1** with *p*-Xy and **H2** with *o*-Xy, respectively.
- Chapter 5 (pyridine/methylpyridines): 200(2) and 296(2) K for **H1** with 2MP and 4MP, and 296(2) and 200(2) K for **H2** with PYR and 4MP, correspondingly.
- Chapter 6 (anisole/methylanisoles): 296(2) and 200(2) K for **H1** when guests were 3MA and 4MA, respectively, and 296(2) K for **H2** with ANI.

An alternative diffractometer was utilized for the complex of **H1** with PYR. Intensity data were collected on a Bruker D8 VENTURE single crystal X-ray diffractometer using graphite-monochromated MoK $\alpha$ -radiation, with the crystal specimen cooled to 173(2) K with nitrogen vapour from a cryostream (Oxford Cryosystems). Data collection, performed with  $\omega$ - and  $\phi$ -scans of width 1.0 $^\circ$ , was controlled using APEX3/v2019.1-0 (Bruker) software and refinement of the unit cell and data-reduction were performed with program SAINT v8.40A (Bruker).<sup>94</sup> Absorption corrections were applied using the multi-scan method (program SADABS (2016/2)).<sup>95</sup> The structure was solved by direct methods and refined by full-matrix least-squares (programs in the SHELX suite).<sup>96</sup> As a graphical user interface (GUI), version 4.0 of X-Seed (a program for supramolecular crystallography) was employed.<sup>97</sup> In the final cycles of refinement all non-hydrogen atoms were treated anisotropically, while H atoms were added in idealised positions in a riding model following their unequivocal location in successive difference Fourier maps.

The PXRD for 2(**H2**)-4MP was carried out on a Bruker D2 with Cu radiation with the scan ranging from 5 to 50 2theta at 0.02 deg/steps and 0.5 sec/step.

## 2.2 Synthesis of host compounds **H1** and **H2**

The two host compounds **H1** and **H2** were synthesized according to the synthetic route provided in Scheme 1. This involved the addition of PhMgBr to dibenzo[a,d]cyclohepten-5-one (**1**) or dibenzo[a,d]cyclohepten-5-one (**4**) to afford the tertiary alcohols **2** and **5**, respectively. These alcohols were reacted with perchloric acid to form the perchlorate salts **3** and **6** after which treatment with ethylenediamine furnished the required host compounds **H1** and **H2**.



**Scheme 1:** Synthetic route towards the two host compounds **H1** and **H2**

### 2.2.1 5-Hydroxy-5-phenyldibenzo[a,d]cycloheptene (**2**)

This compound was synthesized by means of a Grignard addition reaction according to a published procedure.<sup>98</sup> Therefore, bromobenzene (4.60 g, 29.3 mmol), magnesium turnings (0.83 g, 34.2 mmol) and dibenzo[a,d]cyclohepten-5-one (**1**) (5.16 g, 25.0 mmol) afforded a crude product that was recrystallized from petroleum ether and a small amount of dichloromethane to afford 5-hydroxy-5-phenyldibenzo[a,d]cycloheptene (**2**) (6.70 g, 23.6 mmol, 97%), mp 149–150 °C (lit.,<sup>99</sup> mp 150–151 °C);  $\nu_{max}(\text{solid})/\text{cm}^{-1}$  3537 (sharp, free OH), 3475 (br, H-bonded OH) and 1596 (Ar);  $\delta_H(\text{CDCl}_3)/\text{ppm}$  2.30 (1H, s, OH), 6.61–6.77 (4H, m, CH=CH and Ar), 7.06–7.22 (3H, m, Ar), 7.25–7.41 (4H, m, Ar), 7.45–7.59 (2H, m, Ar) and 8.22 (2H, d,  $J$  8.2, Ar);  $\delta_C(\text{CDCl}_3)/\text{ppm}$  78.77 (COH), 124.60 (Ar), 126.69 (Ar), 127.69 (Ar), 128.11 (Ar), 128.72 (CH=CH), 131.30 (Ar), 133.29 (quaternary Ar), 142.39 (quaternary Ar) and 145.95 (quaternary Ar).



The  $^1\text{H}$  NMR,  $^{13}\text{C}$  NMR and IR spectra for 5-hydroxy-5-phenyldibenzo[a,d]cycloheptene (**2**) are provided in the Supplementary Information (SI), Figure S1.

### 2.2.2 *N,N'*-Bis(5-phenyl-5-dibenzo[a,d]cycloheptenyl)ethylenediamine (**H1**)

5-Hydroxy-5-phenyldibenzo[a,d]cycloheptene (**2**) (3.00 g, 10.6 mmol) was dissolved in acetic anhydride (30 mL), and 70% perchloric acid (4 mL) was added dropwise to the solution to afford a solid ruby-red perchlorate salt (**3**) (2.79 g, 7.61 mmol, 72%), mp 210–212 °C (lit.,<sup>99</sup> mp 211–213 °C);  $\nu_{\max}(\text{CHCl}_3)/\text{cm}^{-1}$  1605 (Ar);  $\delta_{\text{H}}(\text{CDCl}_3)/\text{ppm}$  6.60–9.57 (15H, multiplets, Ar and  $\text{CH}=\text{CH}$ ). The perchlorate salt (**3**) (2.00 g, 5.45 mmol) was dissolved in dichloromethane (40 mL), and this solution added to a mixture of ethylenediamine (0.66 g, 10.9 mmol) in dichloromethane (20 mL). The resultant solution was stirred for 10 min after which water (100 mL) was added to it. The lower organic layer was separated and dried with anhydrous  $\text{Na}_2\text{SO}_4$ . The solids were removed by vacuum filtration, and the solvent of the filtrate removed on a rotary evaporator to afford the crude solid product which was recrystallized from dichloromethane to furnish *N,N'*-bis(5-phenyl-5-dibenzo[a,d]cycloheptenyl)ethylenediamine (**H1**) (1.53 g, 2.77 mmol, 95%), mp 250–252 °C (decomp.) (lit.,<sup>99</sup> mp 255 °C (decomp.));  $\nu_{\max}(\text{solid})/\text{cm}^{-1}$  3287 (weak, NH) and 1595 (Ar);  $\delta_{\text{H}}(\text{CDCl}_3)/\text{ppm}$  2.11 (2H, br s,  $\text{NH}$ ), 2.43 (4H, s,  $\text{CH}_2$ ), 6.45–6.65 (4H, m, Ar), 6.72 (4H, s,  $\text{CH}=\text{CH}$ ), 6.94–7.19 (6H, m, Ar), 7.20–7.43 (8H, m, Ar), 7.41–7.7.65 (4H, m, Ar) and 8.17 (4H, d,  $J$  8.0 Hz, Ar);  $\delta_{\text{C}}(\text{CDCl}_3)/\text{ppm}$  44.36 ( $\text{CH}_2$ ), 67.42 ( $\text{PhCH}_2$ ), 124.80 (Ar), 125.88 (Ar), 126.66 (Ar), 127.20 (Ar), 128.06 (Ar), 128.91 ( $\text{CH}=\text{CH}$ ), 131.28 (Ar), 134.43 (quaternary Ar), 141.80 (quaternary Ar) and 144.58 (quaternary Ar).

The  $^1\text{H}$  NMR,  $^{13}\text{C}$  NMR and IR spectra for *N,N'*-bis(5-phenyl-5-dibenzo[a,d]cycloheptenyl)-ethylenediamine (**H1**) are in the SI (Figure S2).

### 2.2.3 5-Hydroxy-5-phenyl-10,11-dihydrodibenzo[a,d]cycloheptene (**5**)

This compound was synthesized by means of a Grignard addition reaction according to a previous literature report.<sup>1</sup> Bromobenzene (15.10 g, 96.2 mmol), magnesium turnings (2.41 g, 98.8 mmol) and 10,11-dihydrodibenzo[a,d]cyclohepten-5-one (**4**) (10.12 g, 48.6 mmol)

furnished the crude product which was recrystallized from petroleum ether/dichloromethane to afford 5-hydroxy-5-phenyl-10,11-dihydrodibenzo[a,d]cycloheptene (**5**) as a white solid (12.56 g, 43.9 mmol, 91%), mp 148–151 °C (lit.,<sup>99</sup> mp 153 °C);  $\nu_{max}(\text{solid})/\text{cm}^{-1}$  3541 (sharp, free OH), 3453 (br, H-bonded OH) and 1595 (Ar);  $\delta_H(\text{CDCl}_3)/\text{ppm}$  2.38 (1H, s, OH), 2.65–2.99 (4H, m, CH<sub>2</sub>), 6.93–7.75 (11H, m, Ar) and 8.09 (2H, d, *J* 8.1, Ar);  $\delta_C(\text{CDCl}_3)/\text{ppm}$  32.44 (CH<sub>2</sub>), 79.40 (COH), 125.57 (Ar), 125.90 (Ar), 126.61 (Ar), 127.17 (Ar), 127.60 (Ar), 128.68 (Ar), 130.55 (Ar), 137.79 (quaternary Ar), 143.54 (quaternary Ar) and 148.55 (quaternary Ar)

The <sup>1</sup>H NMR, <sup>13</sup>C NMR and IR spectra for 5-hydroxy-5-phenyl-10,11-dihydrodibenzo[a,d]cycloheptene (**5**) are provided in the SI (Figure S3).

#### 2.2.4 *N,N'*-Bis(5-phenyl-10,11-dihydro-5-dibenzo[a,d]cycloheptenyl)ethylenediamine (**H2**)

A solid orange perchlorate salt (**6**) (3.74 g, 10.1 mmol, 97 %), mp 97–99 °C (decomp.) (lit.,<sup>99</sup> 97–98 °C (decomp.)) was obtained when 5-hydroxy-5-phenyl-10,11-dihydrodibenzo[a,d]cycloheptene (**5**) (2.99 g, 10.5 mmol) was dissolved in acetic anhydride (30 mL), and then to this solution was added, dropwise, 70% perchloric acid (4 mL);  $\nu_{max}(\text{CHCl}_3)/\text{cm}^{-1}$  1595 (Ar);  $\delta_H(\text{CDCl}_3)$  2.70–3.12 (4H, m, CH<sub>2</sub>CH<sub>2</sub>) and 6.60–9.57 (13H, m, Ar). The perchlorate salt (**6**) (1.96 g, 5.31 mmol) was dissolved in dichloromethane (40 mL), and this solution was then added to a solution of ethylenediamine (0.65 g, 10.8 mmol) in dichloromethane (20 mL). After stirring for 10 min, water (100 mL) was added to the mixture. The lower organic layer was separated and dried with anhydrous Na<sub>2</sub>SO<sub>4</sub>, and the solids filtered off by vacuum filtration. The filtrate was then distilled on the rotary evaporator and the remaining solid residue recrystallized from dichloromethane to afford *N,N'*-bis(5-phenyl-10,11-dihydro-5-dibenzo[a,d]cycloheptenyl)-ethylenediamine (**H2**) (0.86 g, 1.40 mmol, 52 %), mp 180–183 °C (lit.,<sup>99</sup> mp 186–187 °C);  $\nu_{max}(\text{solid})/\text{cm}^{-1}$  3300 (weak, NH) and 1597 (Ar);  $\delta_H(\text{CDCl}_3)/\text{ppm}$  2.11 (2H, br s, NH), 2.43 (4H, s, NCH<sub>2</sub>CH<sub>2</sub>N), 2.77–3.07 (8H, m, CCH<sub>2</sub>CH<sub>2</sub>C), 6.94–7.40 (22H, m, Ar) and 7.64–7.94 (4H, m, Ar);  $\delta_C(\text{CDCl}_3)/\text{ppm}$  33.92 (CCH<sub>2</sub>CH<sub>2</sub>C), 44.10 (NCH<sub>2</sub>CH<sub>2</sub>N), 69.50 (PhCNH), 126.11 (Ar), 126.73 (Ar), 127.36 (Ar), 127.80 (Ar), 127.94 (Ar), 130.75 (Ar), 139.44 (quaternary Ar), 144.36 (quaternary Ar) and 147.42 (quaternary Ar).

The  $^1\text{H}$  NMR,  $^{13}\text{C}$  NMR and IR spectra for *N,N'*-bis(5-phenyl-10,11-dihydro-5-dibenzo[a,d])-ethylenediamine (**H2**) are in the SI (Figure S4).

### 2.3 Single solvent recrystallization experiments

The host compounds were recrystallized from each of the solvents in the three guest series, namely anisole and the methylated isomers, pyridine and its methylated isomers, and the isomeric xylenes and ethylbenzene, in order to determine their host enclathration abilities for these organic solvents. As such, **H1** (0.05 g, 0.08 mmol) was dissolved in an excess of each of the pyridines (5 mmol) and anisoles (10 mmol); the remaining guest series required less **H1** (0.04 g, 0.07 mmol) which was dissolved in 10 mmol of each of xylenes/ethylbenzene. When employing **H2**, 0.04 g (0.07 mmol) was dissolved in an excess of the guest compounds (5mmol for the pyridines, 10 mmol anisoles and 5 mmol xylenes/ethylbenzene). The glass vials in which these experiments were conducted were then closed and placed in the cold room (4 °C) which facilitated crystallization. The crystals were collected by means of vacuum filtration, crushed and washed with petroleum ether (40–60 °C), and then analysed by means of  $^1\text{H}$  NMR spectroscopy. This analytical technique assisted in determining if complexation had occurred and, if so, the host:guest (H:G) ratio of each complex was calculated through comparisons of the integrals of relevant host and guest resonance signals.

### 2.4 Recrystallization experiments involving equimolar mixed guests

The selectivity behaviour of the host compounds was evaluated by recrystallizing **H1** (0.05 g, 0.08 mmol) from equimolar mixtures of guests from each guest series (5 mmol combined amount for the pyridines and 7mmol for the anisoles; in the anisoles, an additional 10 drops of benzene were added to facilitate host dissolution). In xylenes/ethylbenzene (10 mmol combined amount), 0.04 g (0.07 mmol) of **H1** was more appropriate. The selectivity behaviour of **H2** (0.04 g, 0.07 mmol) was also evaluated by means of recrystallization experiments from equimolar mixed pyridines (5mmol combined amount), anisoles (10 mmol) and xylenes/ethylbenzene (5 mmol). All possible guest combinations were considered, and thus binary, ternary and quaternary mixed solvent host recrystallization experiments were carried

out. Once the host compound was dissolved in the different mixtures, the vials were closed and stored in the cold room (4 °C), and the crystals that formed in this way were collected by suction filtration, washed with petroleum ether (40–60 °C) or methanol (when no petroleum ether was available), and analysed by means of GC-MS to obtain the guest ratios in the mixed complexes.

## 2.5 Recrystallization experiments involving binary guest mixtures in varying ratios

The selectivity behaviour of each host compound was assessed in binary guest mixtures where the guest:guest (G:G) molar ratios were varied between approximately 80:20, 60:40, 40:60 and 20:80 (and on occasion, 50:50), for guests A ( $G_A$ ) and B ( $G_B$ ), respectively. The host compound **H1** (0.05 g, 0.08 mmol) was dissolved in these solutions (combined amount of 5 mmol for pyridines and 7 mmol for anisoles, with an added 20 drops of benzene in the latter case). For **H1** in xylenes/ethylbenzene, 0.04 g (0.07 mmol) was more appropriate, and the combined guest amounts were 10 and 5 mmol, respectively. For **H2**, 0.04 g (0.07 mmol) was dissolved in equimolar mixed pyridines (5 mmol combined amount), anisoles (10 mmol) and xylenes/ethylbenzene (5 mmol). In each case, the vials were closed and stored in the cold room (4 °C). Upon crystallization in these conditions, the crystals were recovered and treated as in the equimolar experiments, and the G:G ratios in each of the so-formed crystals ( $Z$ ) quantified by means of GC-MS to determine the  $G_A:G_B$  molar ratios in this phase. Selectivity profiles were then constructed by plotting  $Z$  for  $G_A$  (or  $G_B$ ) against  $X$  for  $G_A$  (or  $G_B$ ) (where  $X$  is the amount of  $G_A$  (or  $G_B$ ) in the original solution). These profiles allowed a visual depiction of the host selectivity behaviour as the guest concentrations varied. The selectivity coefficient,  $K_{G_A:G_B}$ , which was obtained by using the equation  $K_{G_A:G_B} = Z_{G_A}/Z_{G_B} \times X_{G_B}/X_{G_A}$ , where  $X_{G_A} + X_{G_B} = 1$ , served as a measure of the selectivity of each host compound in these conditions. Figure 2.1 represents the three types of selectivity profiles that are possible here: profile a) is one in which the host compound has no definitive selectivity for either guest species present, b) occurs when  $G_A$  is preferentially enclathrated across the entire guest concentration range, and c) is obtained when the selectivity of the host compound is guest concentration-dependent.<sup>100</sup>

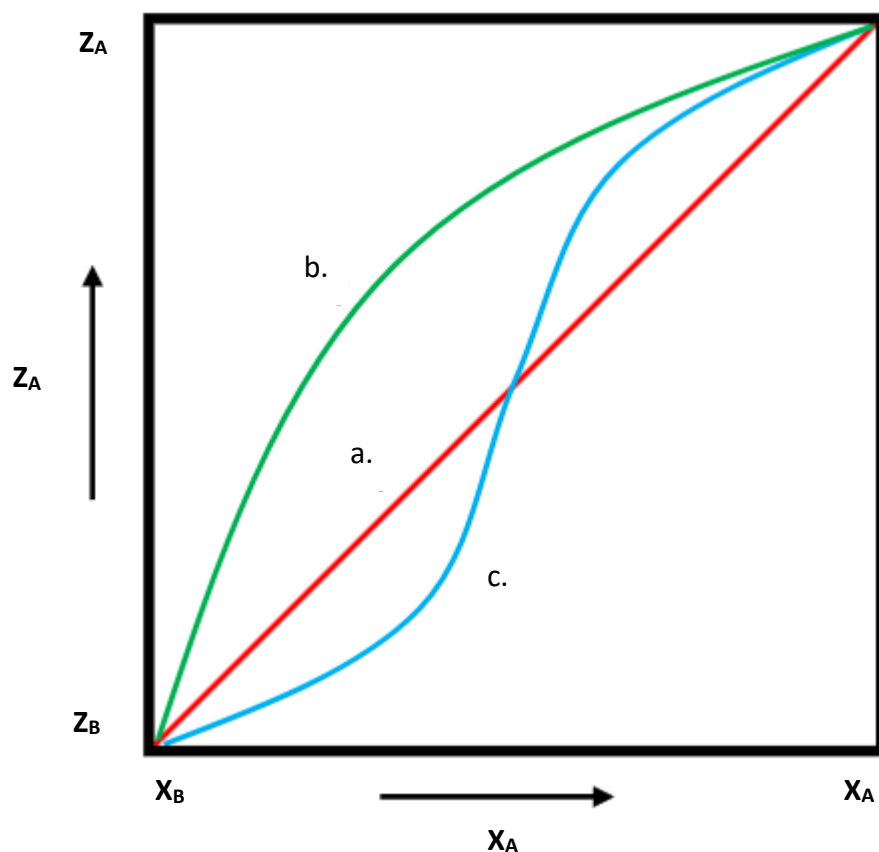


**Figure 2.1:** General selectivity profiles representing host compounds with a. no selectivity, b. a consistent preference for one guest, and c. a selectivity that is guest concentration-dependent<sup>100</sup>

## 2.6 Computational methods

Spartan 10 software (supplied by Wavefunction Inc, for Windows, 1.1.0 Build)<sup>101</sup> was used to perform the computational calculations. Comprehensive conformational searches were carried out using the MMFF molecular mechanics approach by starting with the geometries of experimentally-obtained molecular structures of **H1** and **H2**. (These molecular structures were extracted from crystal structure .cif files of the two host compounds in complexes with dihalomethanes.<sup>98</sup>) In the single point calculations, the hydrogen atom locations were allowed to optimize whereas the heavy atom positions were constrained. Refinement of the resultant structures at the DFT (B3LYP/6-31G\*) level was then performed.

### 3. Molecular modelling

#### 3.1 Computational analysis of **H1** and **H2**<sup>98</sup>

The calculated geometries of **H1** and **H2** have been reported by Barton et al.<sup>98</sup> In that work, the conformations of the two host compounds were compared from experimentally-obtained molecular structures (in complexes with dihalomethanes) and from computational methods. These calculations were carried out using the MMFF molecular mechanics approach which was later followed by refinement of the two structures at a DFT (B3LYP/6-31G\*) level. In the present work, the structure of apohost **H2** will also be compared with results from these calculations. (Note that **H1** simply complexed with the solvent from which it was recrystallized, or the crystal quality was too poor for SCXRD analysis and, as such, no structure of this apohost could be investigated here.) These findings will be briefly highlighted now.

The bonds in **H1** and **H2** are labelled as in Figure 3.1.

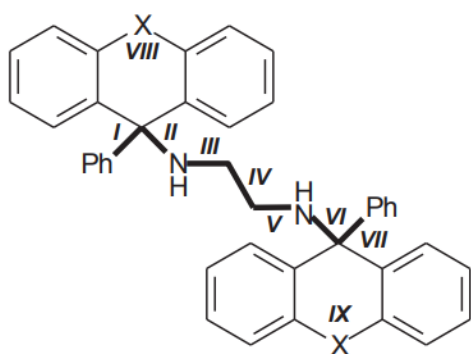


**Figure 3.1:** Bonds I–VIII assigned to **H1** and **H2**<sup>98</sup>

The lowest computed energy conformer for **H1** (**H1-i**, 8.6 kJ·mol<sup>-1</sup>) has successive torsion angles of bonds II–VI of the ethylenediamine linker alternating between the synclinal (*gauche*) and antiperiplanar conformations. It was observed also that the conformer with a slightly higher energy (**H1-ii**, 20.4 kJ·mol<sup>-1</sup>) has the dibenzocycloheptenyl system bonded pseudo-axially to the linking chain, but the phenyl moiety then shifted to reduce interference from the *peri* hydrogens. Interestingly, the next conformer (**H1-iii**, 24.7 kJ·mol<sup>-1</sup>) has one dibenzocycloheptenyl moiety that is planar compared to the other tricyclic fused system and

those in the first two conformers, where their geometries were more bent. These three low energy conformers are provided in Figure 3.2.

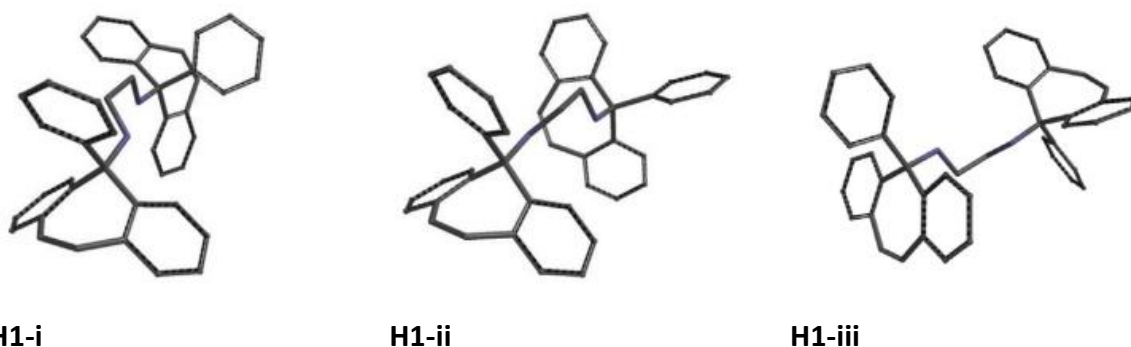


**Figure 3.2:** DFT-computed geometries for the three lowest energy conformers of *N,N'*-bis(5-phenyl-5-dibenzo[*a,d*]cycloheptenyl)ethylenediamine **H1**<sup>98</sup>

Figure 3.3 illustrates the geometries of the three lowest energy conformers computed for **H2**, labelled **H2-i**, **H2-ii** and **H2-iii**. The lowest of these (**H2-i**,  $7.5 \text{ kJ} \cdot \text{mol}^{-1}$ ) has successive torsion angles of bonds *II–VI* with (–)synclinal, antiperiplanar, synclinal, antiperiplanar and antiperiplanar geometries, respectively. In this conformer, the one ethano bridge is borderline synclinal/anticlinal whereas the other ethano bridge is synperiplanar (with torsion angles of  $86^\circ$  and  $-11^\circ$ , respectively). One 10,11-dihydro-5-dibenzo[*a,d*]cycloheptenyl moiety is propeller-shaped and the other is folded like a boat. The next conformer, **H2-ii** ( $8.3 \text{ kJ} \cdot \text{mol}^{-1}$ ), has both tricyclic fused systems adopting the propeller-shaped conformation. **H2-iii** ( $8.9 \text{ kJ} \cdot \text{mol}^{-1}$ ), on the other hand, has staggered conformations along bonds *III*, *IV* and *V* ( $170^\circ$ ,  $-178^\circ$  and  $178^\circ$ ), while the C–C–C–C ethano bridges *VIII* and *IX* have geometries that are both gauche ( $87^\circ$  and  $-87^\circ$ ).

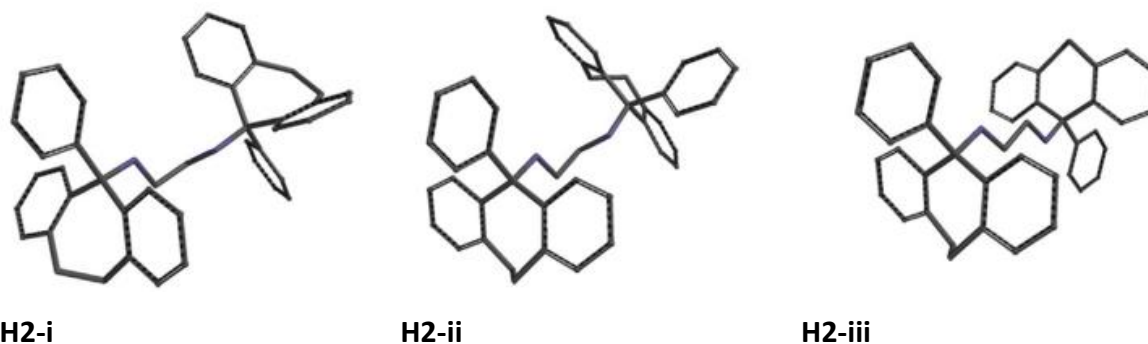


**Figure 3.3:** DFT-computed geometries for the three lowest energy conformers of *N,N'*-bis(5-phenyl-10,11-dihydro-5-dibenzo[*a,d*]cycloheptenyl)ethylenediamine **H2**<sup>98</sup>

## 3.2 Crystal structure of host compound H2

SCXRD analysis was carried out on apohost compound **H2** in the present work after it was recrystallized from 2-methylpyridine (2MP), a solvent which it did not enclathrate. The relevant crystallographic data and refinement parameters are provided in Table 3.1.

**Table 3.1:** Crystallographic data for apohost compound **H2**

	<b>H2</b>
Chemical formula	C <sub>44</sub> H <sub>40</sub> N <sub>2</sub>
Formula weight	596.78
Crystal system	Monoclinic
Space group	<i>P2<sub>1</sub>/c</i>
$\mu$ (Mo-K $\alpha$ )/mm <sup>-1</sup>	0.070
a/Å	13.6296 (6)
b/Å	19.2775 (8)
c/Å	12.4717 (6)
alpha/°	90
beta/°	94.326 (2)
gamma/°	90
V/Å <sup>3</sup>	3267.5 (3)
Z	4
D(calc)/g.cm <sup>-3</sup>	1.213
F(000)	1272
Temp./K	296
Restraints	0
Nref	8153
Npar	421
R	0.0467
wR2	0.1257
S	1.03
$\theta$ min–max/°	1.5, 28.3
Tot. data	46688
Unique data	8153
Observed data [ $I > 2.0 \sigma(I)$ ]	5931
R <sub>int</sub>	0.027
Completeness	1.000
Min. resd. dens. (e/Å <sup>3</sup> )	–0.17
Max. resd. dens. (e/Å <sup>3</sup> )	0.22



**H2** crystallized in the monoclinic crystal system and space group  $P2_1/c$ , and no disorder was noted in this molecule. The C–C–C–C ethano bridge torsion angles are illustrated in Figure 3.4 for both of the seven-membered rings of each of the four host molecules in the unit cell. Notably, the torsion angles alternate between negative and positive values, and each host molecule has one ethano bridge gauche ( $-87.35$  or  $87.35^\circ$ ) and the other synperiplanar ( $-16.83$  or  $16.83^\circ$ ). The torsion angles of these ethano bridges in the crystals appear to correspond most closely with those of the lowest energy DFT conformer, **H2-i** ( $87.35$  and  $86^\circ$ , and  $-16.83$  and  $-11^\circ$ ).

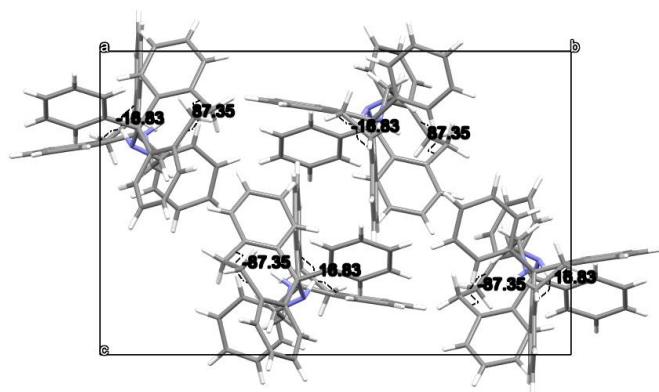


**Figure 3.4:** Torsion angles of the ethano bridges in each of the four **H2** molecules in the unit cell

The similarities and differences in the geometry of **H2** in the crystal and its calculated lowest energy conformer **H2-i** is evident in the overlay of these two molecules as illustrated in Figure 3.5. Here, the molecule with a blue hue represents **H2** from the crystals.

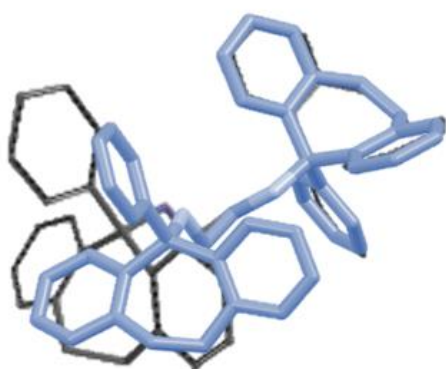


**Figure 3.5:** Overlaid structures of **H2** (blue hue) from the crystal with the calculated lowest energy conformer **H2-i**

The host packing diagram for **H2** in the crystal is illustrated in Figure 3.6.

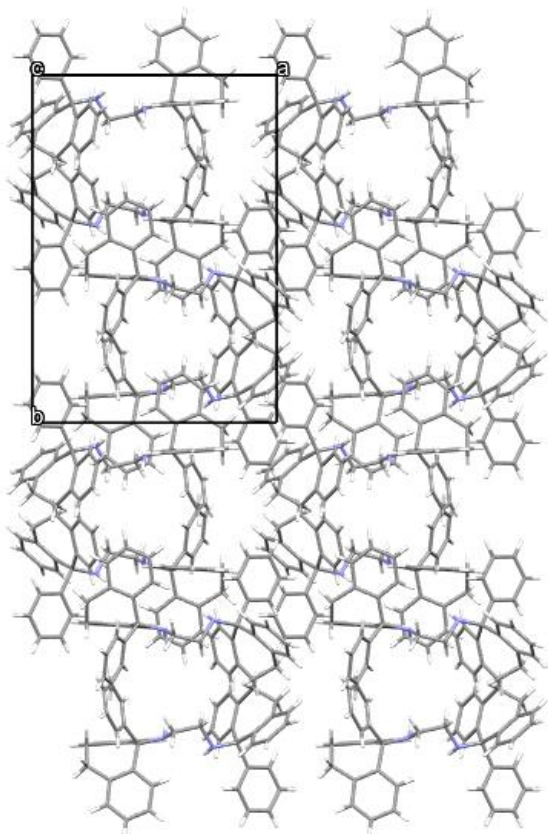


**Figure 3.6:** Host packing [along 001] of **H2** in the crystal

Surprisingly, given the numerous aromatic moieties, **H2** did not experience any significant  $\pi\cdots\pi$  interactions (distances were too long, 4.506 Å–5.898 Å). However, two intramolecular C–H $\cdots\pi$  interactions were observed and these are illustrated in Figure 3.7a and measured 2.91 and 2.87 Å (H $\cdots\pi$ ), with angles 128 and 138°, respectively. Furthermore, **H2** also experienced several intramolecular C–H $\cdots$ N interactions (2.33–2.40 Å, H $\cdots$ N, 103–106°) and two of these are displayed in Figure 3.7b.

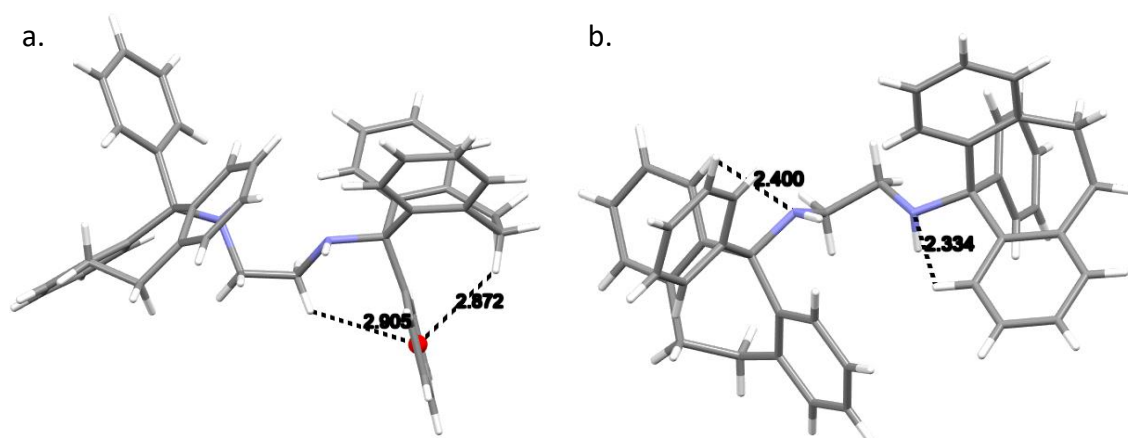


**Figure 3.7:** Examples of intramolecular a. (host)C–H··· $\pi$ (host) and b. (host)C–H···N(host) interactions present in the crystal of **H2**

In this section, therefore, the computed and experimentally obtained geometries of **H2** have been scrutinized and compared. The geometry of the molecule in the crystal concurred most closely with that of the calculated lowest energy conformer, although some differences were evident. Additionally, the host molecule geometry was stabilized by a number of non-covalent intramolecular host···host interactions.

## 4. Selectivity of **H1** and **H2** in isomeric xylene and ethylbenzene mixtures

### 4.1 Introduction

The BTEX fraction (benzene (B), toluene (T), ethylbenzene (EB) and xylenes (Xy)) are by-products that are formed in the catalytic reforming of crude oils.<sup>102,103</sup> Therefore, the xylene isomers can either be isolated as a mixture from this catalytic reforming process or they may be prepared by means of alternative naphtha-reforming catalytic processes.<sup>83</sup> The benzene and toluene by-products from this fraction are readily isolated owing to their distinctive boiling points (80.1 and 110.6 °C, respectively), but EB and the xylene isomers, *o*-, *m*- and *p*-xylene (*o*-Xy, *m*-Xy and *p*-Xy) (the C<sub>8</sub> aromatic fraction of crude oil) have boiling points that are nearly identical (136.2, 144, 139.3 and 138.4 °C respectively)<sup>104</sup> and, as such, result in fractional distillation processes that are incredibly challenging and also uneconomical.<sup>105</sup> Therefore, there is a need for an inexpensive and facile separation technique that can be used to isolate each component from these EB/Xy mixtures. Different methods to effect these separations have been reported, but are oftentimes expensive or non-recyclable. Examples include simulated moving bed (SMB) adsorptive separation technologies (which rely on the affinities of the C<sub>8</sub> aromatics towards an adsorbent),<sup>105</sup> zeolites<sup>106</sup> and metal-organic frameworks (MOFs).<sup>107</sup> The separation of these isomers is of immense importance since ethylbenzene and the xylene isomers each have unique applications in the chemical industry. For example, pure *p*-Xy is the isomer in highest demand.<sup>108</sup> Mixed isomers are used as solvents (in the paint industry), whereas *o*-, *m*- and *p*-Xy have exclusive uses which involve their oxidation to terephthalic acid, isophthalic acid and phthalic anhydride, respectively. EB undergoes a dehydrogenation process in order to form styrene,<sup>109</sup> and styrene can be further used in the production of polystyrene resins, plastics and synthetic rubber.<sup>110</sup>

Compounds **H1** and **H2** were subsequently assessed for their selectivity behaviour in these mixed EB/Xy solvents (Figure 4.1) to determine whether one or both may serve as separation agents for these solvents by means of host-guest chemistry strategies. This concept would provide an alternative method for their separation compared to tedious distillations. The findings of this investigation are provided herein.

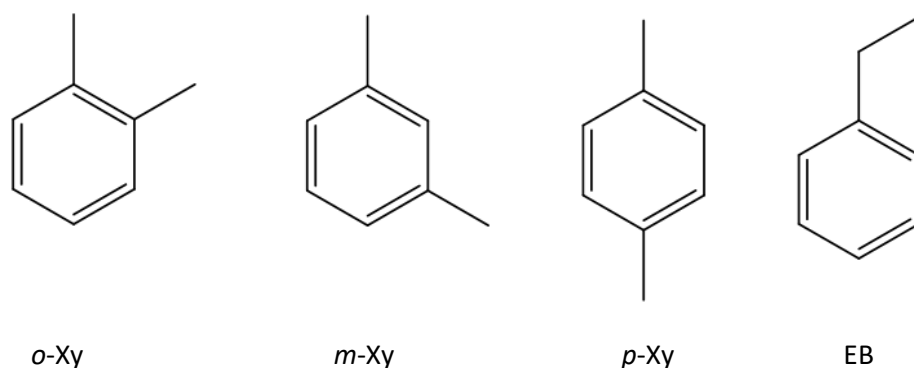


**Figure 4.1:** Structures of the potential guest compounds *o*-xylene (*o*-Xy), *m*-xylene (*m*-Xy), *p*-xylene (*p*-Xy) and ethylbenzene (EB)

## 4.2 Results and discussion

### 4.2.1 Assessment of the host potential of **H1** and **H2** for Xy and EB in single solvent recrystallization experiments

Table 4.1 contains the data obtained when host compounds **H1** and **H2** were recrystallized from each of the xylene isomers and also EB.

**Table 4.1:** Recrystallization experiments of **H1** and **H2** from each of *p*-Xy, *o*-Xy, *m*-Xy and EB<sup>90</sup>

Guest	<b>H1</b> :G <sup>a</sup>	<b>H2</b> :G <sup>a</sup>
<i>p</i> -Xy	1:1	1:0
<i>o</i> -Xy	1:0	1:1
<i>m</i> -Xy	1:0	1:0
EB	1:0	1:0

<sup>a</sup> Host:guest (H:G) ratios were determined using <sup>1</sup>H-NMR spectroscopy

These single solvent experiments revealed remarkable affinities with respect to both host compounds since each of **H1** and **H2** only enclathrated one of the four guest solvents in the series: **H1** formed a complex with only *p*-Xy (with a H:G ratio of 1:1) and **H2** enclathrated only *o*-Xy (also with a 1:1 H:G ratio). The <sup>1</sup>H NMR spectra for these complexes are provided in Figure S5 for **H1** and Figure S13 for **H2** in the SI.

#### 4.2.2 Assessment of the selectivity behaviour of H1 and H2 in equimolar mixed guests

Tables 4.2 and 4.3 summarize the results obtained from competition experiments when host compounds **H1** and **H2** were recrystallized from equimolar mixtures of *o*-Xy, *m*-Xy, *p*-Xy and EB. The preferred guest is indicated in bold black text for each individual competition experiment, and the percentage estimated standard deviations (%e.s.d.s) are provided in parentheses, calculated as a result of the fact that each experiment was conducted in duplicate.

**Table 4.2:** Complexes formed by **H1** in equimolar mixed guests<sup>a,b 90</sup>

<i>o</i> -Xy	<i>m</i> -Xy	<i>p</i> -Xy	EB	Guest ratios (%e.s.d.s)	Overall H:G ratio
X	X			<sup>c</sup>	1:0
X		<b>X</b>		11.3: <b>88.7</b> (0.3)	1:1
X			X	<sup>c</sup>	1:0
	X	<b>X</b>		12.8: <b>87.2</b> (1.2)	1:1
	X		X	<sup>c</sup>	1:0
		<b>X</b>	X	<b>87.4</b> :12.6 (2.1)	1:1
X	X	<b>X</b>		9.8:9.9: <b>80.3</b> (0.5:0.0:0.5)	1:1
X	X		X	<sup>c</sup>	1:0
X		<b>X</b>	X	9.5: <b>83.2</b> :7.3 (1.1:0.5:1.5)	1:1
	X	<b>X</b>	X	10.2: <b>83.6</b> :6.2 (0.5:0.3:0.7)	1:1
X	X	<b>X</b>	X	8.3:8.8: <b>76.7</b> :6.2 (0.8:0.4:1.0:0.2)	1:1

<sup>a</sup> GC-MS and <sup>1</sup>H NMR spectroscopy were used to obtain the G:G and overall H:G ratios, respectively

<sup>b</sup> The competition experiments were conducted in duplicate; the %e.s.d.s are provided in parentheses

<sup>c</sup> No inclusion occurred and only apohost was recovered from the experiment

Host compound **H1** only formed crystalline inclusion complexes when the solutions contained *p*-Xy. In its absence, apohost was recovered from the glass vessels. Owing to only including *p*-Xy in the single solvent experiments (Table 4.1), it was somewhat anticipated that **H1** would

favour this guest solvent in mixtures, and the selectivities for *p*-Xy in the binary equimolar solutions were 88.7, 87.2 and 87.4 % when the other guest compounds were *o*-Xy, *m*-Xy and EB, respectively. Based on these data, host compound **H1** may be employed as an efficient separatory tool for equimolar binary mixtures of these guests when *p*-Xy is present in the solution. The ternary mixture experiments also revealed remarkable selectivities for *p*-Xy ranging from 80.3–83.6 %, while this was 76.7% when the quaternary solution was employed in the experiment. In all successful enclathrating experiments, the overall H:G was consistently 1:1.

In a similar fashion, host compound **H2** (Table 4.3) also formed inclusion complexes only in the presence of *o*-Xy, the sole solvent that was enclathrated in the single solvent experiments; the remaining experiments furnished apohost. Furthermore, excellent selectivities towards *o*-Xy were noted in many cases: in the binary solutions, these measured 73.7, 91.3 and 88.1% when the other guest species was *m*-Xy, *p*-Xy and EB, respectively. Clearly *m*-Xy competes more effectively with *o*-Xy than *p*-Xy or EB. Equimolar ternary solutions containing both *o*-Xy and *m*-Xy also afforded crystals with only a moderately higher amount of *o*-Xy (70.6 and 69.1%), while in the absence of *m*-Xy, the amount of *o*-Xy in the solid was an enhanced 83.7%. Finally, the quaternary mixture experiment still demonstrated a favourable selectivity for *o*-Xy, 61.4 %.

Here, overall H:G ratios ranged between being 1:1 and 2:1.

**Table 4.3:** Complexes formed by **H2** in equimolar mixed guests<sup>a,b,90</sup>

<i>o</i> -Xy	<i>m</i> -Xy	<i>p</i> -Xy	EB	Guest ratios <sup>b</sup> (%e.s.d.s)	Overall H:G ratio
<b>X</b>	X			<b>73.7:26.3</b> (0.1)	1:1
<b>X</b>		X		<b>91.3:8.7</b> (0.4)	1:1
<b>X</b>			X	<b>88.1:11.9</b> (1.1)	1:1
	X	X		<sup>c</sup>	1:0
	X		X	<sup>c</sup>	1:0
		X	X	<sup>c</sup>	1:0
<b>X</b>	X	X		<b>70.6:23.9:5.5</b> (0.3:0.4:0.2)	2:1
<b>X</b>	X		X	<b>69.1:20.8:10.1</b> (0.6:0.1:0.5)	1:1
<b>X</b>		X	X	<b>83.7:6.5:9.8</b> (1.5:0.8:0.7)	2:1
	X	X	X	<sup>c</sup>	1:0
<b>X</b>	X	X	X	<b>61.4:17.7:6.5:14.4</b> (1.3:0.8:1.1:1.0)	2:1

<sup>a</sup> The competition experiments were conducted in duplicate; %e.s.d.s are provided in parentheses

<sup>b</sup> GC-MS and <sup>1</sup>H NMR spectroscopy were used to obtain the guest and overall H:G ratios

<sup>c</sup> No inclusion occurred and only apohost was recovered from the experiment

The <sup>1</sup>H NMR spectra and GC-MS traces for all of these competition experiments for **H1** and **H2** are provided in the SI (Figure S6 to Figure S9 for **H1** and Figure S14 to Figure S17 for **H2**).

#### 4.2.3 Assessment of the selectivity behaviour of **H1** and **H2** in binary mixtures of Xy/EB where the G<sub>A</sub>:G<sub>B</sub> molar ratios were sequentially varied

The selectivity profiles were obtained by using the original solution G<sub>A</sub>:G<sub>B</sub> ratios that were measured and GC data from the crystals, which are shown in Figures 4.2a–c (**H1**) and 4.3a–c (**H2**) in the selectivity coefficient calculation. Note that all binary mixtures in which *p*-Xy (for **H1**) and *o*-Xy (for **H2**) were absent failed to form inclusion complexes, mixed or otherwise, and hence these profiles could not be constructed here.



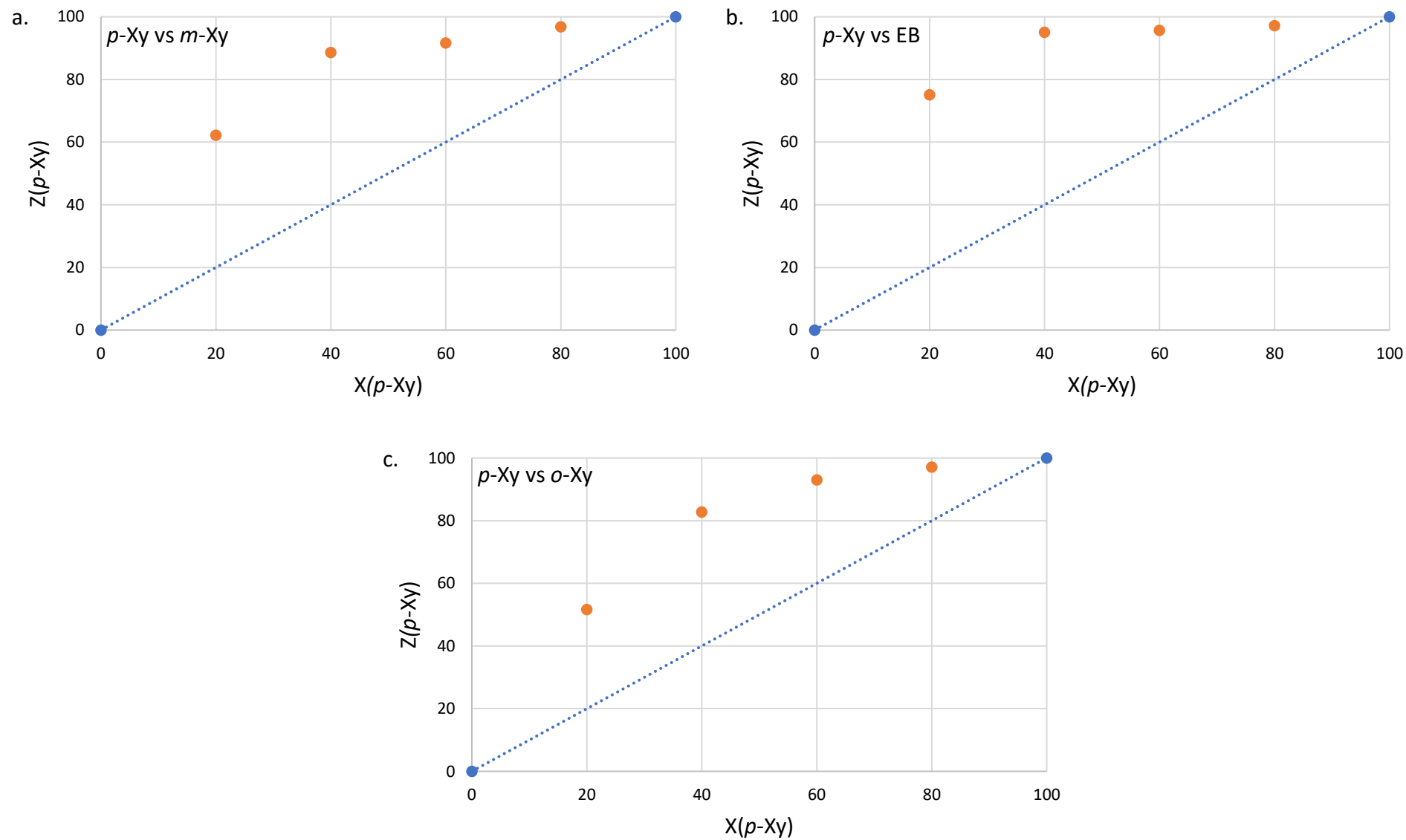


**Figure 4.2:** Selectivity profiles of **H1** in a.  $p\text{-Xy}/m\text{-Xy}$ , b.  $p\text{-Xy}/\text{EB}$  and c.  $p\text{-Xy}/o\text{-Xy}$  binary solutions<sup>90</sup>

From the profiles in Figure 4.2, it is clear that even when the  $G_A:G_B$  ratios were varied, the overwhelming preference of **H1** for *p*-Xy remained, and this was unwavering across the concentration range in each of *p*-Xy/*m*-Xy (Figure 4.2a), *p*-Xy/EB (Figure 4.2b) and *p*-Xy/*o*-Xy (Figure 4.2c). This observation was not unexpected given the fact that **H1** only included *p*-Xy in the single solvent recrystallization experiments (Table 4.1). Unsurprisingly, **H2** also always selected for *o*-Xy in all of these binary experiments (Figures 4.3a–c) with one exception: in *o*-Xy/EB, low concentrations of *o*-Xy (20%) furnished crystals with a somewhat higher selectivity for EB (83.3%).

A comparison of the selectivity behaviour of **H1** (Figure 4.2) and **H2** (Figure 4.3) suggests that the former host compound possesses a greater preference for *p*-Xy than the latter does for *o*-Xy. In order to confirm this observation, the K values (where K is the selectivity coefficient) were calculated and are summarized in Table 4.4.

**Table 4.4:**  $K_{ave}$  values for the binary guest competition experiments with **H1** and **H2**<sup>90</sup>

<b>H1</b>		<b>H2</b>	
Binary mixture	$K_{ave}$	Binary mixture	$K_{ave}$
<i>p</i> -Xy/ <i>m</i> -Xy	8.3	<i>o</i> -Xy/ <i>p</i> -Xy	11.3
<i>p</i> -Xy/EB	16.2	<i>o</i> -Xy/ <i>m</i> -Xy	2.6
<i>p</i> -Xy/ <i>o</i> -Xy	7.2	<i>o</i> -Xy/EB	7.3 <sup>a</sup>

<sup>a</sup>This averaged K value disregards the data point where the amount of *o*-Xy present in *o*-Xy/EB was 20% since this experiment then favoured EB to a small extent

From these data (Table 4.4), the selectivity of **H1** for *p*-Xy is greatest in *p*-Xy/EB mixtures ( $K_{ave}$  16.2) while **H2** performed optimally in mixtures comprising *o*-Xy/*p*-Xy, where  $K_{ave}$  was calculated to be 11.3 in favour of *o*-Xy. The selectivity coefficient, K, is a measure of the host affinity for a particular guest species and is 1 for a host compound that possesses no selectivity for either guest species present.<sup>34</sup> Nassimbeni and coworkers<sup>34</sup> reported that when  $K \geq 10$  then, for all intents and purposes, the host compound is able to separate such binary mixtures in a practical setting. These data (Table 4.4) also concur with a prior suggestion, and the selectivity of **H1** for *p*-Xy is, more usually, greater than that of **H2** for *o*-Xy.

A discussion now follows on each of the profiles in Figures 4.2 and 4.3.

In *p*-Xy/*m*-Xy mixtures (Figure 4.2a), when *p*-Xy was present in the solution in concentrations of 40% and greater, the recovered crystals were prodigiously enriched with this guest, and 88.6, 91.7 and 96.8% *p*-Xy, respectively, were measured in each of the three complexes. This host would therefore be efficient in purifying/separating mixtures of *p*-Xy and *m*-Xy, especially when these contain 40% or more *p*-Xy. The average selectivity coefficient for this set of experiments was determined to be 8.3 (Table 4.4), while the highest K value (the greatest selectivity) was obtained when the concentration of *p*-Xy in the solution was 40% (K = 11.7).

The selectivity profile that was obtained for **H1** in *p*-Xy/EB mixtures (Figure 4.2b) revealed the host compound to, once again, favour *p*-Xy in each of these experiments, even at low concentrations of *p*-Xy (20%) in the solution; at this concentration, 75.1% *p*-Xy was already present in the crystals. The average K value for these experiments was significantly higher than in the *p*-Xy/*m*-Xy experiments and measured 16.2 (Table 4.4). Interestingly, the highest K value, 29.1, was obtained for the experiment where a lower concentration, 40%, of *p*-Xy was present. Once again, **H1** is an effective host compound for separating *p*-Xy/EB mixtures and is most effective when the quantity of *p*-Xy present is 40% or greater.

In *p*-Xy/*o*-Xy mixtures (Figure 4.2c), the average K value for this set of experiments was the lowest of the three, with 7.2 (Table 4.4) being calculated in favour of *p*-Xy. However, the crystals became significantly enriched with this guest (93.0 and 97.1%) when the solutions contained 60 and 80% *p*-Xy. The highest K value was 8.9 and was calculated in the 60:40 *p*-Xy/*o*-Xy experiment. These experiments have, therefore, demonstrated that **H1** would be an effective separatory host compound for *p*-Xy/*o*-Xy mixtures when the concentration of *p*-Xy in the solution is approximately 60% or higher.

In *o*-Xy/*p*-Xy mixtures (Figure 4.3a), **H2** preferred *o*-Xy, even at low concentrations of this guest species: when the solution contained 20% *o*-Xy, the crystals already contained 78.8% of this guest solvent. The average K value for these experiments was 11.3 (Table 4.4), and therefore separations are feasible with this host compound and more especially when the mixture has 60% or more *o*-Xy. The greatest K value was 14.9 and this was calculated for the experiment that had 20% *o*-Xy in the solution; the crystals then contained 78.8% *o*-Xy.

When the solutions were made up of *o*-Xy and *m*-Xy, *o*-Xy remained preferred throughout (Figure 4.3b), but not as notably as in the *o*-Xy/*p*-Xy mixtures (Figure 4.3a). The average K value here was only 2.6 (Table 4.4) with the greatest K value being 2.8 for the 40:60 and 60:40 solutions; 65.3 and 80.8% of *o*-Xy were then measured in the crystals.

Figure 4.3c, constructed from data obtained from the *o*-Xy/EB experiments, revealed that the host selectivity was dependent upon the relative concentrations of the guests present and, as mentioned before, EB was moderately preferred when the solution contained only 20% *o*-Xy. At higher *o*-Xy concentrations, this guest was then preferred, and solutions comprising 40, 60 and 80% *o*-Xy furnished crystals with 84.1, 91.9 and 96.3% *o*-Xy, respectively. The average K value was 7.3 with the greatest K value obtained for the 40:60 *o*-Xy/EB experiment (7.9).

The GC results that allowed for the construction of Figures 4.2 and 4.3 are provided in the SI (Figures S10–S12 for **H1** and Figures S18–S20 for **H2**).

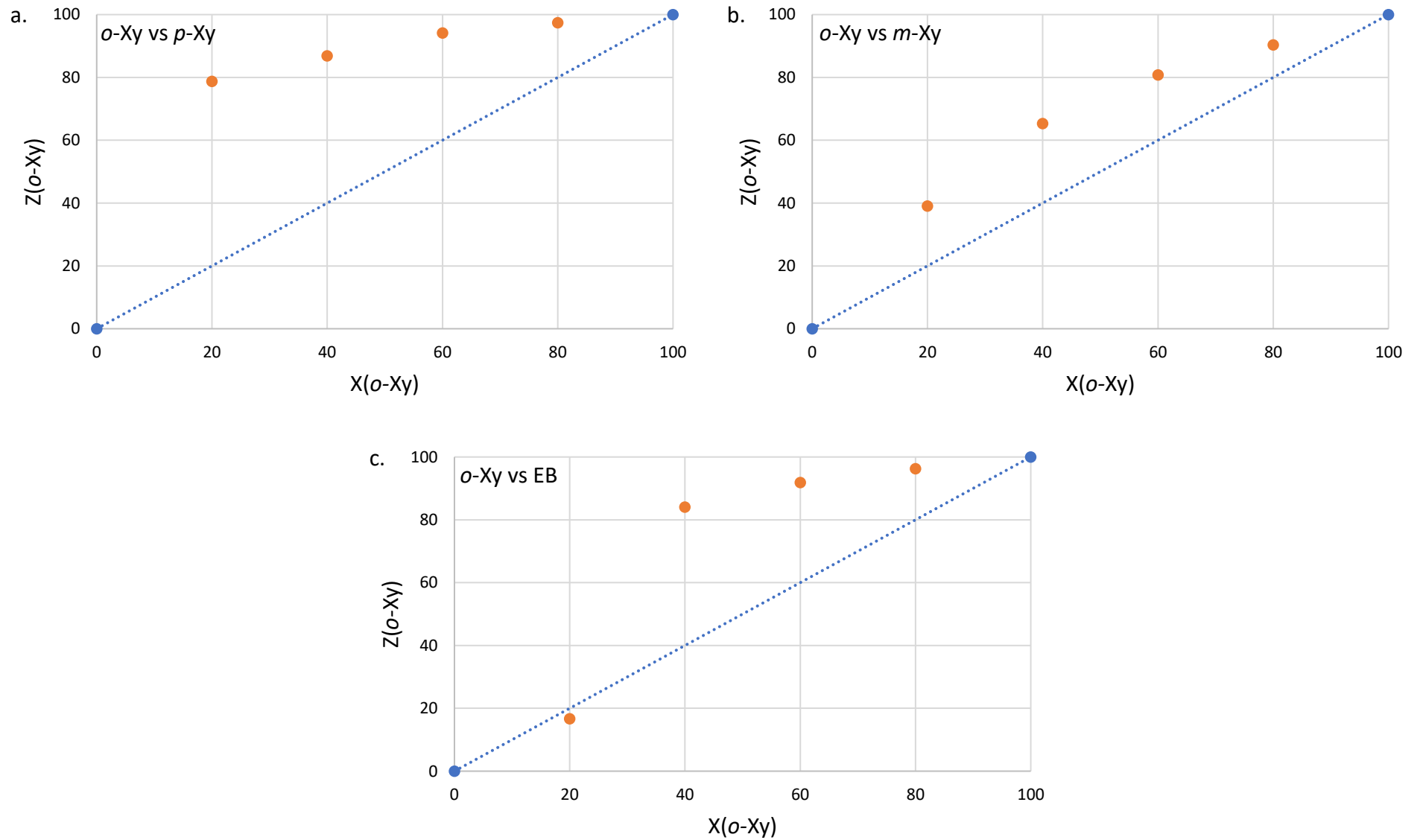


**Figure 4.3:** Selectivity profiles of **H2** in a.  $o\text{-Xy}/p\text{-Xy}$ , b.  $o\text{-Xy}/m\text{-Xy}$  and c.  $o\text{-Xy}/\text{EB}$  binary solutions<sup>90</sup>

#### 4.2.4 Single crystal X-ray diffraction experiments

The novel **H1** · *p*-Xy and **H2** · *o*-Xy inclusion compounds with suitable quality crystals for SCXRD analyses were obtained by a slow recrystallization process. These analyses revealed that *p*-Xy, in its complex with **H1**, was disordered around an inversion centre, while *o*-Xy in **H2** · *o*-Xy was extensively disordered. Only three of the *o*-Xy disorder orientations were thus modelled, and their site occupancy factors (s.o.f.s) were 0.568(3), 0.334(3) and 0.098(2).

The relevant crystallographic data for these SCXRD experiments are provided in Table 4.5. Both **H1** · *p*-Xy and **H2** · *o*-Xy crystallized in the triclinic crystal system and space group  $P\bar{1}$ , but markedly different unit cell dimensions and angles confirmed that the host packing differed in each one.

**Table 4.5:** Crystallographic data for the **H1** · *p*-Xy and **H2** · *o*-Xy complexes<sup>90</sup>

	<b>H1</b> · <i>p</i> -Xy	<b>H2</b> · <i>o</i> -Xy
Chemical formula	C <sub>44</sub> H <sub>36</sub> N <sub>2</sub> · C <sub>8</sub> H <sub>10</sub>	C <sub>44</sub> H <sub>40</sub> N <sub>2</sub> · C <sub>8</sub> H <sub>10</sub>
Formula weight	698.91	702.94
Crystal system	Triclinic	Triclinic
Space group	$P\bar{1}$	$P\bar{1}$
$\mu$ (Mo-K $\alpha$ )/mm <sup>-1</sup>	0.068	0.068
<i>a</i> /Å	8.7756(4)	12.4192(9)
<i>b</i> /Å	10.3113(5)	13.0572(9)
<i>c</i> /Å	11.4752(6)	14.7198(10)
alpha/°	96.537(2)	109.219(2)
beta/°	102.397(2)	94.472(3)
gamma/°	102.809(2)	114.813(2)
<i>V</i> /Å <sup>3</sup>	974.61(8)	1979.8(2)
<i>Z</i>	1	2
<i>D</i> (calc)/g · cm <sup>-1</sup>	1.191	1.179
<i>F</i> (000)	372	752
Temp./K	200(2)	296(2)
Restraints	55	373
<i>N</i> <sub>ref</sub>	4844	9793
<i>N</i> <sub>par</sub>	275	606
<i>R</i>	0.0398	0.0512
<i>wR</i> <sub>2</sub>	0.1093	0.1526
<i>S</i>	1.05	1.04
$\theta$ min–max/°	1.8, 28.3	1.9, 28.3
Tot. data	28789	54652
Unique data	4844	9793
Observed data [ <i>I</i> > 2.0 sigma( <i>I</i> )]	4045	7178
<i>R</i> <sub>int</sub>	0.019	0.017
Completeness	1.000	0.997
Min. resd. dens. (e/Å <sup>3</sup> )	–0.18	–0.29
Max. resd. dens. (e/Å <sup>3</sup> )	0.32	0.32

The unit cells of **H1** · *p*-Xy (along [100]) and **H2** · *o*-Xy (along [001]) are depicted on the left-hand side of Figures 4.4a and b, respectively, and these were prepared using Mercury software;<sup>111</sup> the void (yellow) diagrams are also provided here on the right-hand side (the probe radius and approximate grid spacing, for the void calculations, remained the same throughout, with values of 1.2 and 0.7 Å, respectively).

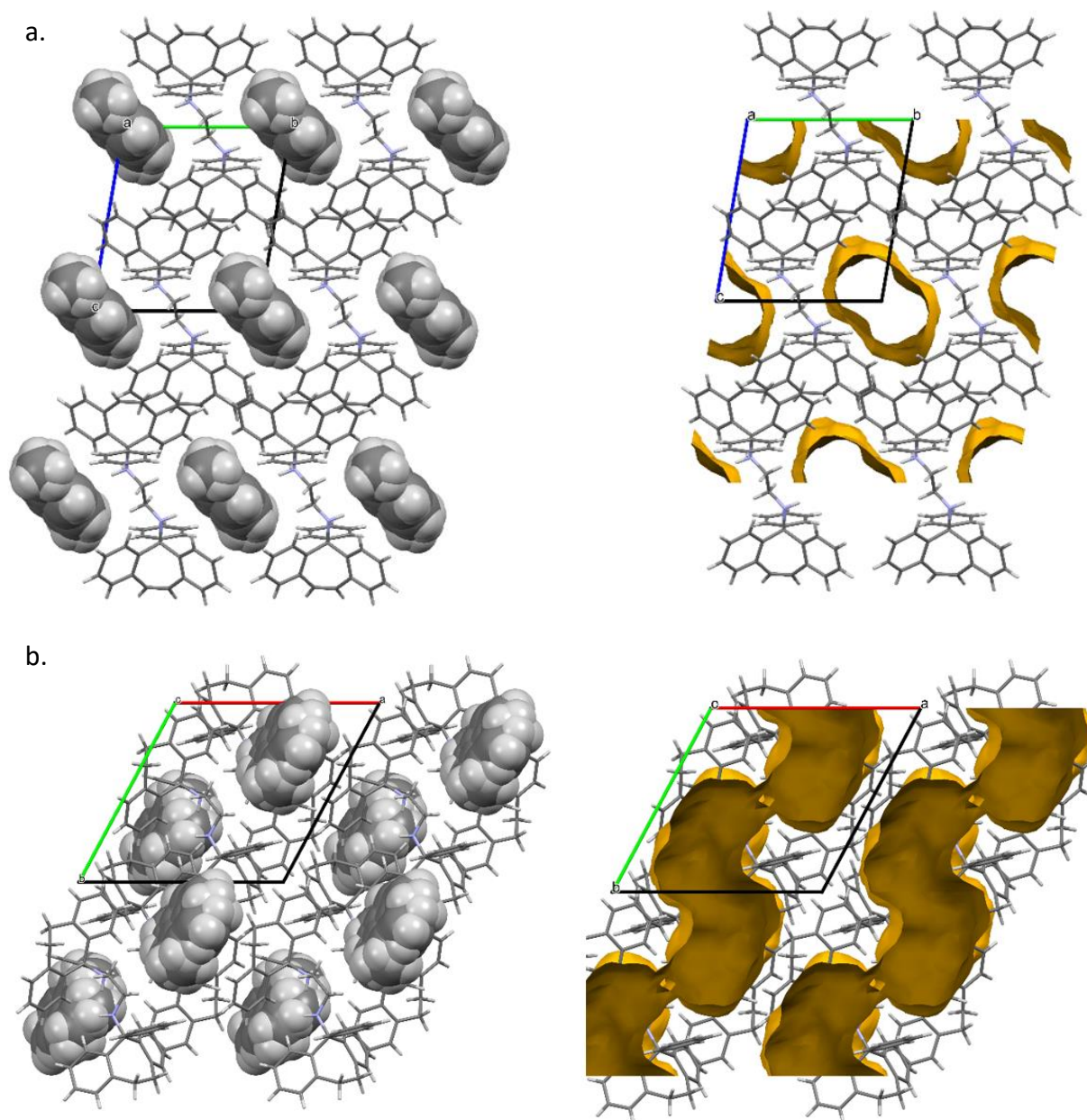


**Figure 4.4** Unit cells (left) and void diagrams (right) for a.  $\mathbf{H1} \cdot p\text{-Xy}$  and b.  $\mathbf{H2} \cdot o\text{-Xy}$ <sup>90</sup>

From Figure 4.4a, the *p*-Xy guest species in crystals of  $\mathbf{H1} \cdot p\text{-Xy}$  were accommodated in wide open and infinite channels parallel to the a-axis while, on the other hand, the guest molecules in  $\mathbf{H2} \cdot o\text{-Xy}$  (Figure 4.4b) were housed in highly constricted channels along the b-axis, the characteristics of which approached that of isolated cages, with two guest molecules in each “cage”.

Subsequently, the non-covalent interactions in the two complexes prepared in this work were investigated. Interestingly, in  $\mathbf{H1} \cdot p\text{-Xy}$ , completely absent were any short stabilizing



interactions between host and guest molecules, and the complex therefore approached that of a *true clathrate* as defined by Weber et al.,<sup>112</sup> where the guest molecules were held in the crystal by means of steric factors alone. The only significant interaction in this complex was an intermolecular (host) $\pi\cdots\pi$ (host) contact that occurred between two fused aromatic ring systems of two distinct host molecules, and which stabilized the host packing arrangement in the crystal, a stereoview of which is provided in Figure 4.5.

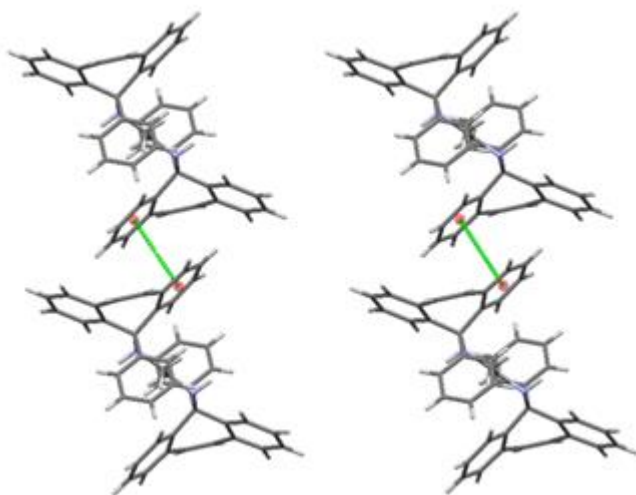


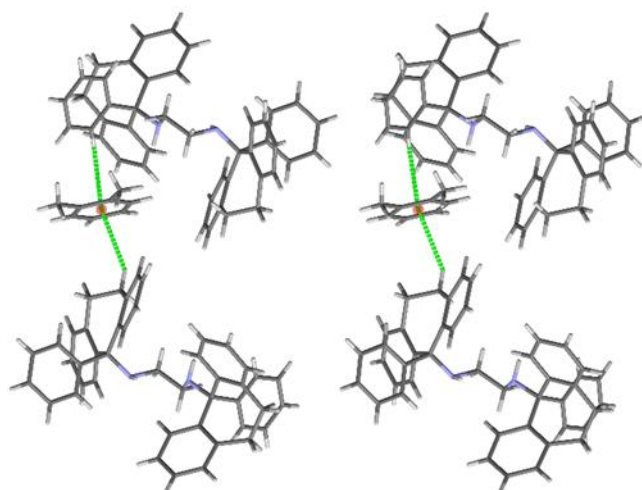
**Figure 4.5:** Stereoview of the intermolecular (host) $\pi\cdots\pi$ (host) interaction in **H1**·*p*-Xy (stabilizing the host packing arrangement), the only significant contact between molecular species in this clathrate<sup>90</sup>

However, a consideration of the non-covalent interactions in the **H2**·*o*-Xy complex revealed that there were two types of interactions between host and guest species, namely (host)C–H $\cdots\pi$ (guest) (the stereoview in Figure 4.6) and (guest)C–H $\cdots\pi$ (host) close contacts, and the distances and angles of each of these are summarized in Table 4.6, measuring between 2.95–2.99 Å (137–155°) and 2.80 Å (156°), respectively.

**Table 4.6:** Characteristics of the intermolecular C–H $\cdots$  $\pi$  interactions in **H2**·*o*-Xy<sup>a 90</sup>

Interaction	H $\cdots$ $\pi$ /Å	C–H $\cdots$ $\pi$ /°
(host)C–H $\cdots$ $\pi$ (guest 1)	2.99	149
(host)C–H $\cdots$ $\pi$ (guest 2)	2.95	155
(host)C–H $\cdots$ $\pi$ (guest 1)	2.95	138
(host)C–H $\cdots$ $\pi$ (guest 2)	2.96	137
(guest 2)C–H $\cdots$ $\pi$ (host)	2.80	156

<sup>a</sup> Guest 1 and guest 2 refer to two of the three disordered guest components that were modelled.

**Figure 4.6:** Stereoview of two of the (host)C–H $\cdots$  $\pi$ (guest) interactions, as examples, in **H2**·*o*-Xy<sup>90</sup>

The geometry of the host molecules in **H1**·*p*-Xy and **H2**·*o*-Xy are not similar: in **H1**, the N–C–C–N torsion angle adopts a more antiperiplanar arrangement ( $-153.87^\circ$ ) while in **H2** this conformation is more gauche ( $-62.66^\circ$ ). These observations may suggest that the more linear antiperiplanar arrangements favour channels in which the guests reside while the skewed gauche conformers prefer to pack so that guest compounds experience near-discrete cavity occupation. A previous report<sup>98</sup> confirmed this supposition. In that work, **H1** and **H2** were found to form complexes with dihaloalkanes and, in each instance, the geometry of the N–C–C–N linker was antiperiplanar when the guest accommodation was in channels and gauche when in cavities.

#### 4.2.5 Thermal analysis

The thermogravimetric (TG), its derivative (DTG), and differential scanning calorimetric (DSC) traces are provided (overlaid) in Figures 4.7a and b for the **H1** · *p*-Xy and **H2** · *o*-Xy complexes, respectively, while the more important thermal data obtained from these are summarised in Table 4.6.

**Table 4.6:** Thermal data for the **H1** · *p*-Xy and **H2** · *o*-Xy complexes<sup>90</sup>

Complex	T <sub>on</sub> /°C <sup>a</sup>	Calculated mass loss/%	Experimental mass loss/%
<b>H1</b> · <i>p</i> -Xy	<sup>b</sup>	15.2	<sup>b</sup>
<b>H2</b> · <i>o</i> -Xy	69.7	15.1	14.8

<sup>a</sup> T<sub>on</sub> is the onset temperature for the guest release process and serves as a measure of the thermal stability of the complex and was estimated from the DTG/TG

<sup>b</sup> The onset of guest release commenced during sample preparation, and T<sub>on</sub> and the experimental mass loss could thus not be measured

The mass loss for the **H1** · *p*-Xy complex (1:1 H:G ratio) was expected to be 15.2 % (Table 4.6) whereas the actual mass loss measured was only 10.3 % (TG, Figure 4.7a). This lower-than-expected mass loss suggested that the complex was unstable at room temperature and that some guest release occurred during the sample preparation phase of this experiment. From the TG, some mass loss is indeed visible just before 40 °C which correlates with this supposition. This observation is not unexpected given the nature of the guest accommodation in wide open and endless channels in this complex and that there were no non-covalent host···guest interactions whatsoever, ensuring facile escape of the guest molecules from the crystal owing to its reduced thermal stability.<sup>113</sup> However, in the case of the 1:1 H:G **H2** · *o*-Xy complex, the calculated and experimental mass losses were congruent (15.1 and 14.8 %, respectively, Figure 4.7b and Table 4.6) which suggested an enhanced thermal stability for this complex. Here, the guest release onset temperature was a significant 69.7 °C and is as a result of the guest molecules being tightly bound in near-discrete cages (with two guest molecules in each cage) and the non-covalent interactions present between host and guest species.

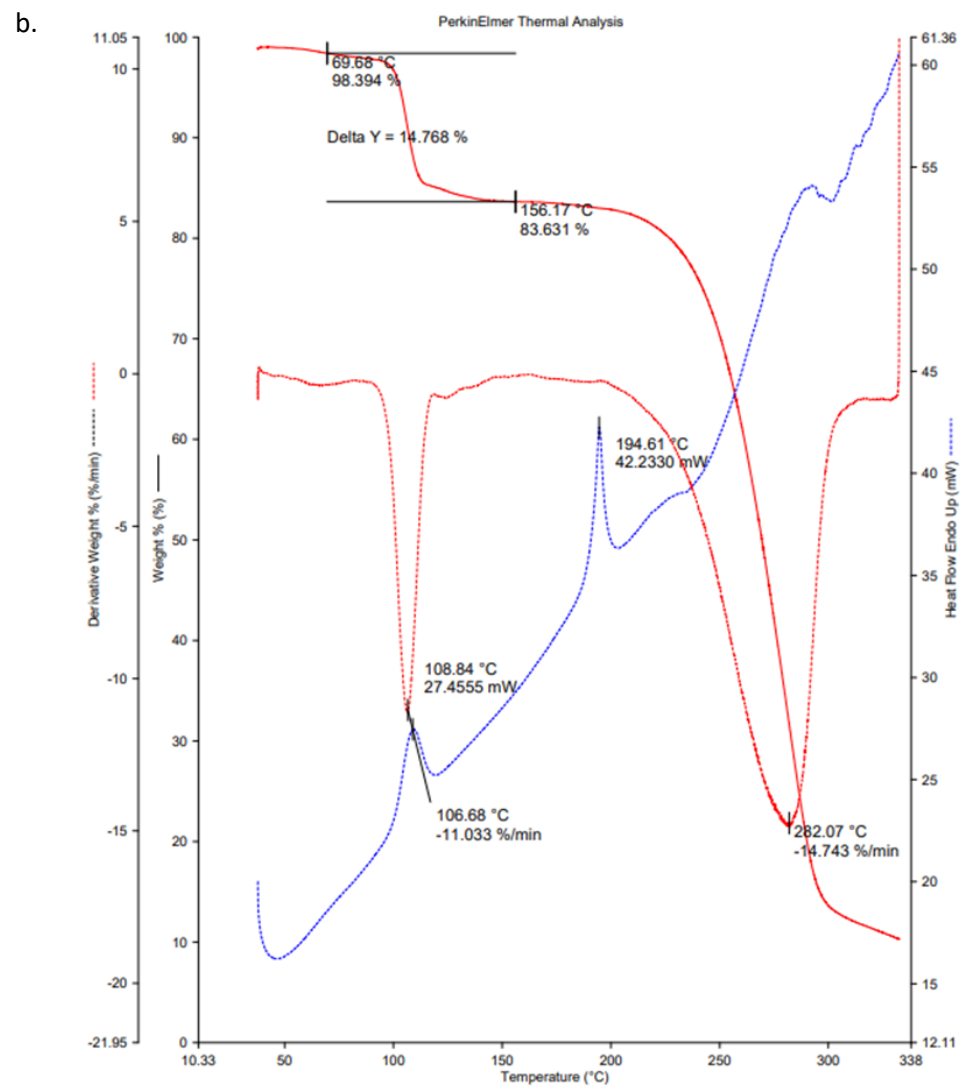
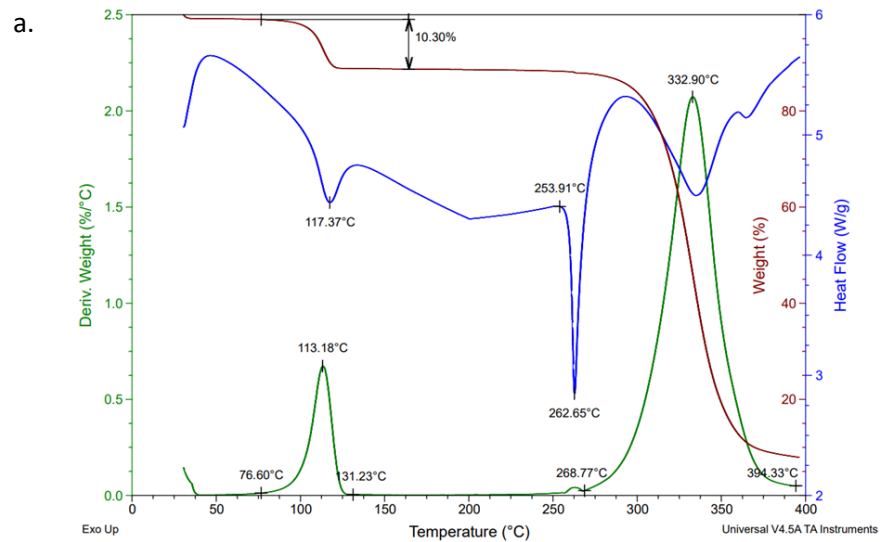


Figure 4.7: Overlaid TG, DTG and DSC Traces for a.  $H1 \cdot p\text{-Xy}$  and b.  $H2 \cdot o\text{-Xy}$ <sup>90</sup>

### 4.3 Conclusion

In this work, **H1** and **H2** were both demonstrated to possess significant selectivities for *p*-Xy and *o*-Xy, respectively, when crystals of each were grown from equimolar mixtures of the xylene isomers (*o*-Xy, *m*-Xy and *p*-Xy) and ethylbenzene (EB). The single solvent experiments revealed that **H1** only formed a complex with *p*-Xy while **H2** enclathrated only *o*-Xy. In all guest/guest competition experiments in which *p*-Xy (for **H1**) and *o*-Xy (for **H2**) were absent, only apohost was recovered from the glass vessels. Data from constructed selectivity profiles were in excellent agreement with observations made in the equimolar experiments. Thermal analyses showed that the thermal stability of the **H2** · *o*-Xy complex was significant, with  $T_{on} = 69.7$  °C, compared with **H1** · *p*-Xy where the guest species was released from the crystals even at ambient conditions. These observations were explained by SCXRD analyses: the guest species in **H1** · *p*-Xy were accommodated in wide open endless channels and experienced no non-covalent contacts with the host molecules, resulting in the observed low thermal stability for this complex; on the other hand, in **H2** · *o*-Xy, the guest molecules were bound tightly in near-discrete cavities and also experienced interactions with the host species, rendering this complex more thermally stable than **H1** · *p*-Xy. Finally, this investigation has shown that both **H1** and **H2** possess the ability to separate or purify very many of these difficult-to-separate-by-fractional-distillation C<sub>8</sub>H<sub>10</sub> mixtures described in this work. Advantageously, the host compound is not destroyed in this manner, and may be recrystallized continuously in this process.

## 5. Selectivity of **H1** and **H2** in pyridine and methylpyridine isomers

### 5.1 Introduction

Pyridine (PYR) is a six-membered heterocyclic aromatic compound with five carbon atoms and one nitrogen atom in the ring, and has the molecular formula  $C_5H_5N$ .<sup>114</sup> The molecular structure of this compound and its 2-, 3- and 4-methyl-substituted analogues (2MP, 3MP, 4MP, also known as the picolines and pyridine bases) are provided in Figure 5.1. They serve as important building blocks in the chemical industry, and are used widely in the synthesis of pesticides, herbicides, pharmaceuticals, dyes and adhesives.<sup>115,116</sup> Additionally, they are employed as solvents and bases in chemical reactions.<sup>117</sup>

These pyridine compounds are recovered from the coke oven after coking coal at extremely high temperatures. Once the elevated temperature has been reached, the non-condensed gases are passed through a saturator that contains sulfuric acid and ammonia, which then furnishes a solution of ammonium and pyridinium sulfates. Pyridine (70%) is recovered from the pyridine bases which are formed when the pyridinium sulfates are further treated with ammonia.<sup>117</sup> A volatilization process then takes place, and the condensed portion contains the pyridine bases and 2,6-lutidine, which can be separated by making use of extractions and fractional distillation. The pyridines may also be synthesized on an industrial scale by means of the Chichibabin synthesis.<sup>115,117</sup> This synthetic procedure depends on the condensation between formaldehyde, acetaldehyde and ammonia, which affords a mixture of pyridine and mono- and dimethylated pyridines.<sup>117</sup> The unmodified Chichibabin method provides low yields of these pyridines (20%), and therefore still requires multi-stage separation processes to ultimately afford pure compounds. The MP isomers are extremely challenging to separate owing to their narrow boiling point range (2MP boils at 129 °C, 3MP at 144 °C and 4MP at 145 °C), while the boiling point of PYR is much lower (116°C), and so is readily recovered from the pyridine bases through distillation.<sup>118–120</sup>

Host compounds **H1** and **H2** were subsequently assessed for their selectivity behaviour in these mixed PYR and MP solvents to determine whether one or both may serve as separation

agents for these mixed solvents by means of host-guest chemistry protocols. This strategy would provide an alternative method for their separation compared to energy- and cost-intensive fractional distillations. The findings of this investigation will be discussed now.

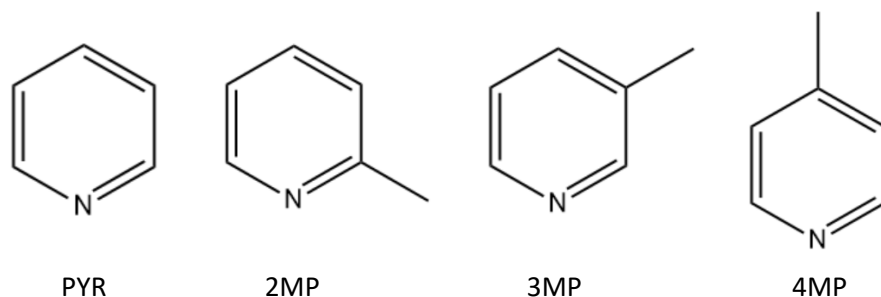


**Figure 5.1:** Structures of the potential guest compounds pyridine (PYR), 2-methylpyridine (2MP), 3-methylpyridine (3MP) and 4-methylpyridine (4MP)

## 5.2 Results and discussion

### 5.2.1 Assessment of the host potential of **H1** and **H2** for PYR and 2MP/3MP/4MP in single solvent recrystallization experiments

Table 5.1 contains the data obtained when host compounds **H1** and **H2** were recrystallized from pyridine and each of the methylpyridine isomers.

**Table 5.1:** Recrystallization experiments of **H1** and **H2** from each of PYR, 2MP, 3MP and 4MP<sup>a</sup>

Guest	<b>H1</b> :G	<b>H2</b> :G
PYR	1:2	1:2
2MP	1:2	1:0
3MP	1:1	1:0
4MP	1:2	2:1

<sup>a</sup> Host:guest (H:G) ratios were determined using <sup>1</sup>H NMR spectroscopy

These single solvent experiments demonstrated that **H1** possessed the ability to complex with all four of the guest solvents in this series (Table 5.1). H:G ratios were 1:2, 1:2, 1:1 and 1:2 for solvents PYR, 2MP, 3MP and 4MP, respectively. **H2**, on the other hand, did not include 2MP

and 3MP, and only apohost compound was recovered from these recrystallization experiments. However, PYR and 4MP were enclathrated: the H:G ratio for the pyridine-containing complex was 1:2, while 4MP was included with a 2:1 ratio.

All  $^1\text{H}$  NMR spectra for these single solvent complexes are provided in Figures S21 (**H1**) and S32 (**H2**) in the SI.

### 5.2.2 Assessment of the selectivity behaviour of **H1** and **H2** in equimolar mixed guests

Tables 5.2 and 5.3 summarize the results obtained from competition experiments when host compounds **H1** and **H2** were recrystallized from equimolar mixtures of PYR, 2MP, 3MP and 4MP. The preferred guest is indicated in bold black text in each case, and the percentage estimated standard deviations (%e.s.d.s) are provided in parentheses since experiments were carried out in duplicate.

After GC analyses of the solids obtained from these equimolar guest mixtures, it was observed that 2MP was the guest most favoured by **H1** (Table 5.2) when binary solutions were employed: the amount of 2MP present in these complexes was 91.2, 88.8 and 63.5% when the other guest present was PYR, 3MP and 4MP, respectively. In the absence of 2MP in these binary solutions, the host compound displayed very modest to no tangible selectivity for either guest present: PYR/3MP, PYR/4MP and 3MP/4MP mixtures furnished crystals with only 50.5, 56.9 and 52.4% PYR, 4MP and 3MP, correspondingly. Furthermore, if 2MP was absent in the ternary experiment (PYR/3MP/4MP), then **H1** also possessed essentially no selectivity (35.3/32.4/32.3%) for any of the guest solvents. From the remaining ternary experiments, it appeared as though the presence of both 2MP and 4MP resulted in poor **H1** selectivities, in favour of PYR (56.8%, PYR/2MP/4MP) and 2MP (43.4%, 2MP/3MP/4MP). Only the PYR/2MP/3MP experiment produced exceptional results, and the mixed complex resulting from this equimolar solution already contained 84.4% 2MP. Finally, in the quaternary experiment, 2MP remained preferred but the host selectivity for this guest species was low (32.1%). Here, the host selectivity was thus in the order 2MP (32.1%) > PYR (27.0%) > 4MP (23.2%) > 3MP (17.7%). Therefore, **H1** may be a likely candidate for the separation of



equimolar 2MP/PYR, 2MP/3MP and PYR/2MP/3MP mixtures, extracting significant amounts of 2MP from these solutions in host-guest chemistry experiments.

The overall H:G ratios in these experiments varied widely.

**Table 5.2:** Complexes formed by **H1** in equimolar mixed pyridine guests<sup>a,b</sup>

PYR	2MP	3MP	4MP	Guest ratios (%e.s.d.s)	Overall H:G ratio
X	X			8.8: <b>91.2</b> (0)	1:2
X		X		<b>50.5</b> :49.5(3.2)	3:1
X			X	43.1: <b>56.9</b> (2.1)	1:2
	X	X		<b>88.8</b> :11.2(0.8)	1:3
	X		X	<b>63.5</b> :36.5(0.3)	2:3
		X	X	<b>52.4</b> :47.6(0.2)	4:1
X	X	X		7.3: <b>84.4</b> :8.3(1.0:3.5:2.5)	1:2
X	X		X	<b>56.8</b> :2.2:41.0(2.2:0.4:1.9)	1:2
X		X	X	<b>35.3</b> :32.4:32.3(0.1:1.0:1.0)	2:3
	X	X	X	<b>43.4</b> :35.1:21.5(1:1.9:0.9)	1:2
X	X	X	X	27.0: <b>32.1</b> :17.7:23.2(0.2:0.4:0.4:0.2)	5:1

<sup>a</sup> GC-MS and <sup>1</sup>H NMR spectroscopy were used to obtain the G:G and overall H:G ratios, respectively

<sup>b</sup> The competition experiments were conducted in duplicate; the %e.s.d.s are provided in parentheses

Contrastingly, the selectivity of **H2** was always in favour of PYR in these equimolar experiments (Table 5.3) when this guest solvent was present. In fact, the selectivity for PYR was overwhelming when 4MP was absent in the binary and ternary solutions: PYR/2MP, PYR/3MP and PYR/2MP/3MP furnished mixed complexes with a near-complete selectivity for PYR (97.9–98.2%). The presence of PYR and 4MP in any of these mixtures, including the quaternary solution, resulted in a significant decline in the affinity of **H2** for PYR, though the selectivity remained in favour of PYR: PYR/4MP, PYR/2MP/4MP, PYR/3MP/4MP and PYR/2MP/3MP/4MP solutions afforded mixed complexes with only between 50.5 and 57.5%

PYR. In the absence of PYR, 4MP was usually moderately favoured, and crystals from 2MP/4MP and 3MP/4MP contained 76.1 and 71.1% 4MP. An exception was noted when the three MP isomers were mixed: here, 2MP was selected, but the amount of 2MP in the complex was low (44.7%). Interestingly, only apohost compound was recovered from the binary 2MP/3MP mixture. Therefore, the host selectivity (from the quaternary experiment) may be noted as in the order PYR (57.5%) > 4MP (40.7%) > 3MP (1.2%)  $\approx$  2MP (0.6%).

The overall H:G ratios in these experiments also varied widely, as was the case in analogous experiments with **H1** (Table 5.2).

**Table 5.3:** Complexes formed by **H2** in equimolar mixed pyridine guests<sup>a,b</sup>

PYR	2MP	3MP	4MP	Guest ratios (%e.s.d.s)	Overall H:G ratio
<b>X</b>	<b>X</b>			<b>98.2:1.8(1.9)</b>	2:3
<b>X</b>		<b>X</b>		<b>97.9:2.1(2.1)</b>	2:3
<b>X</b>			<b>X</b>	<b>50.5:49.5(2.3)</b>	3:4
	<b>X</b>	<b>X</b>		<sup>c</sup>	<sup>c</sup>
	<b>X</b>		<b>X</b>	23.9: <b>76.1(0.7)</b>	3:4
		<b>X</b>	<b>X</b>	28.9: <b>71.1(1.2)</b>	1:2
<b>X</b>	<b>X</b>	<b>X</b>		<b>97.9:0.8:1.3(2.2:0.8:1.4)</b>	1:2
<b>X</b>	<b>X</b>		<b>X</b>	<b>53.5:1.0:45.5(0:1:1)</b>	2:3
<b>X</b>		<b>X</b>	<b>X</b>	<b>55.4:2.2:42.4(0.7:2.3:1.6)</b>	1:2
	<b>X</b>	<b>X</b>	<b>X</b>	<b>44.7:28.0:27.3 (1.5:1.3:2.8)</b>	1:2
<b>X</b>	<b>X</b>	<b>X</b>	<b>X</b>	<b>57.5:0.6:1.2:40.7(1.8:0.7:1.2:0.1)</b>	1:2

<sup>a</sup> These experiments were conducted in duplicate; %e.s.d.s are provided in parentheses

<sup>b</sup> GC-MS and <sup>1</sup>H NMR spectroscopy were used to obtain the guest and overall H:G ratios

<sup>c</sup> No inclusion occurred and only apohost was recovered from the experiment

All <sup>1</sup>H NMR spectra and GC-MS traces for these equimolar competition experiments for **H1** and **H2** are provided in the SI (Figures S22–S25 for **H1** and Figures S33–S36 for **H2**).

### 5.2.3 Assessment of the selectivity behaviour of **H1** and **H2** in binary mixtures of PYR/MP where the $G_A:G_B$ molar ratios were sequentially varied

The selectivity profiles that were obtained after GC analysis of the crystals that formed from binary mixtures in which the molar ratio of each guest was sequentially varied, and plotting Z against X, are provided in Figures 5.2a–c (in the presence of PYR) and 5.3a–c (in the absence of PYR) for **H1**, and Figures 5.4a–c (in the presence of PYR) and 5.5a and b (in the absence of PYR) for **H2**. (Note that 2MP/3MP mixtures, in the case of **H2**, furnished only apohost compound, and therefore no selectivity profile could be constructed in this instance.)

When **H1** was presented with binary mixtures containing PYR (Figures 5.2a–c), PYR remained largely disfavoured by the host compound.

When 2MP/PYR mixtures contained 40, 60 and 80% 2MP, the recovered crystals were significantly enriched with 2MP, and 88.7, 92.8 and 95.8% of this guest were measured in the isolated solids, respectively (Figure 5.2a). The average selectivity coefficient ( $K_{ave}$ ) for the experiments in favour of 2MP was 8.7, while the highest K value (11.8) was calculated for the mixture that contained 40% 2MP. According to Nassimbeni and co-workers,<sup>34</sup> **H1** may therefore serve as an excellent host compound for the separation of this particular mixture, since K at this point was greater than 10. Only when the solution contained low amounts of PYR (20%) was 2MP disfavoured, and the complex contained only 6.2% 2MP.

The selectivity of **H1** in 3MP/PYR and 4MP/PYR mixtures (Figures 5.2b and c), however, was not noteworthy, and all of the data points lie close to the line of no selectivity where  $K = 1$ . The average K values (in favour of 3MP and 4MP, respectively) was only 1.6 and 1.9, and host-guest chemistry strategies here would not be an effective method for the separations of such mixtures.

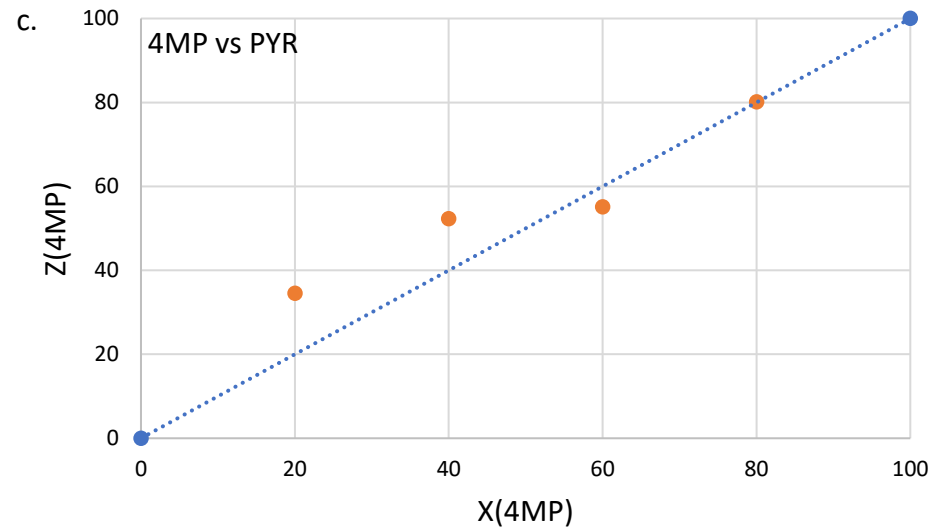
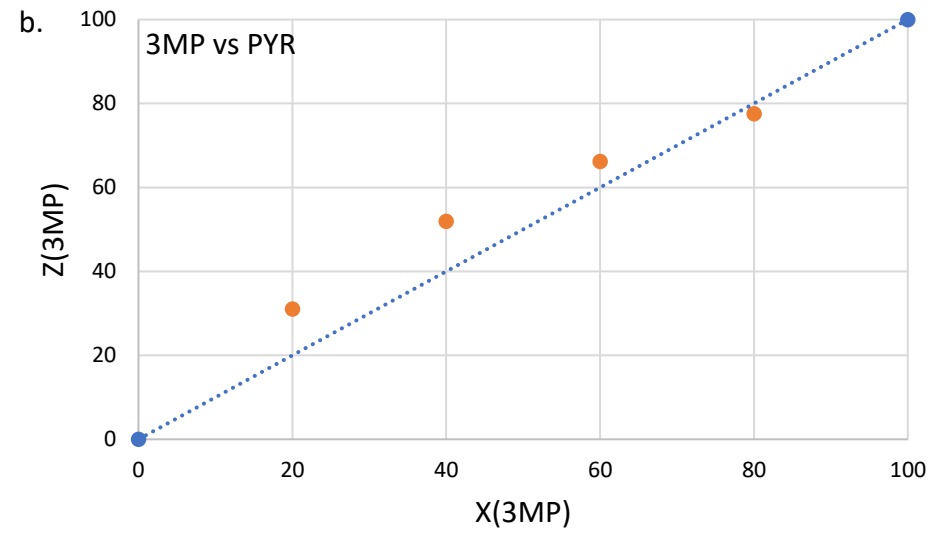
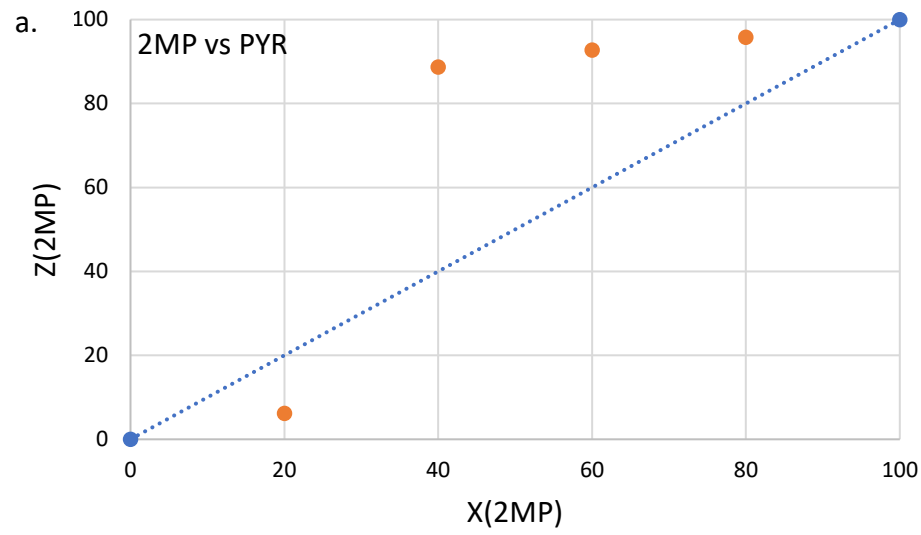
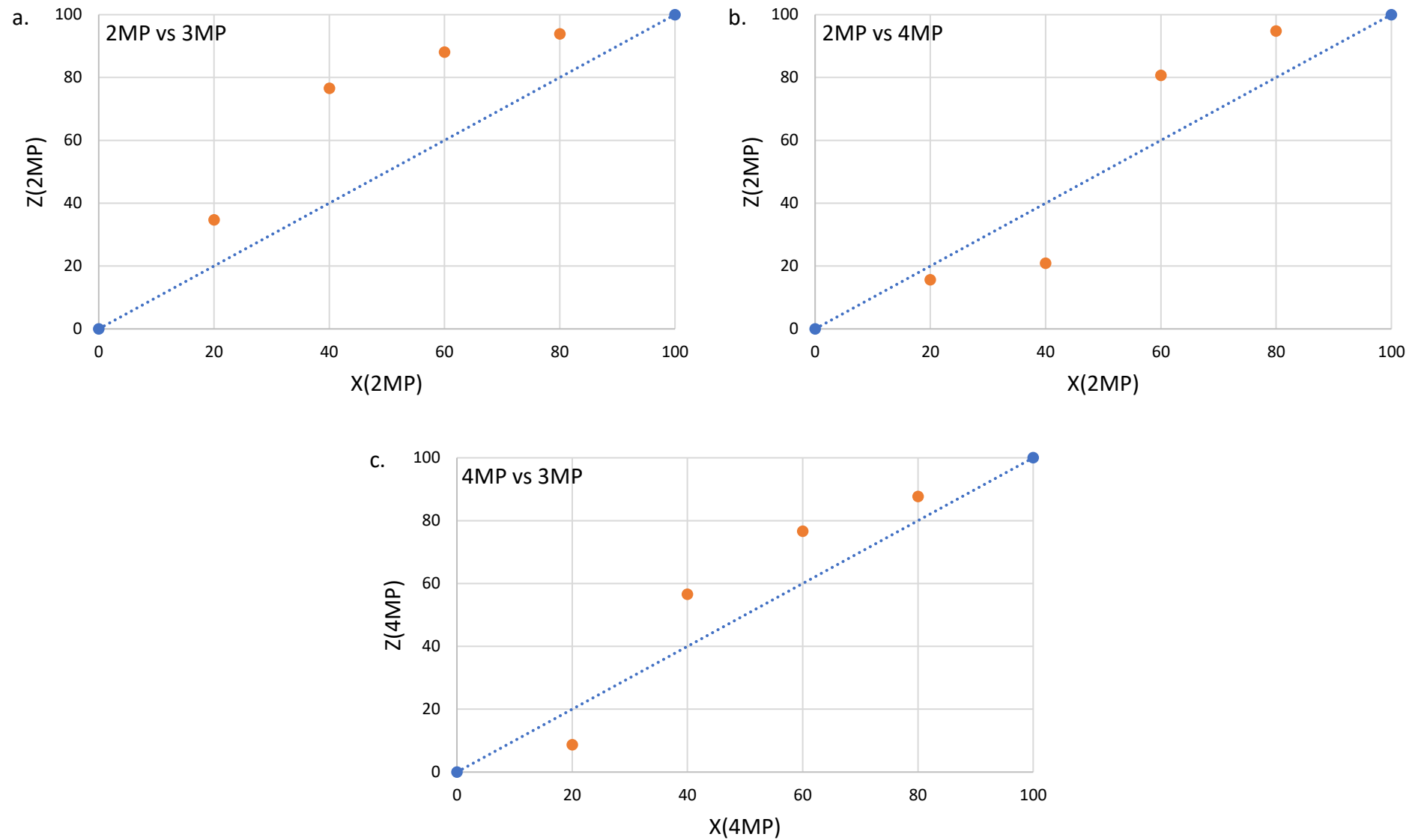


Figure 5.2: Selectivity profiles of H1 in a. 2MP/PYR, b. 3MP/PYR and c. 4MP/PYR binary solutions



**Figure 5.3:** Selectivity profiles of H1 in a. 2MP/3MP, b. 2MP/4MP and c. 4MP/3MP binary solutions

The selectivity profile that was obtained for **H1** in 2MP/3MP mixtures (Figure 5.3a) demonstrates that this host compound was consistently selective for 2MP even at low concentrations of this guest solvent.  $K_{ave}$  was modest (4.0), while the greatest K value was calculated in both the 40 and 60% 2MP binary mixtures (4.9). Since these values are significantly less than 10, **H1** cannot serve as an effective separatory tool for these mixtures.

Figure 5.3b demonstrates that the preferential behaviour of **H1** in 2MP/4MP mixtures was dependent upon the relative amounts of each guest present in the solution. When the mixture contained 60 and 80% 2MP, 80.7 and 94.8% 2MP were measured in the mixed complex. On the other hand, solutions enriched with 4MP (60 and 80%) afforded complexes with greater amounts of 4MP (79.1 and 84.3%). Experiments in favour of 2MP provided an average K value of 3.7 (the highest K value, 4.6, was calculated in the mixture comprising 80% 2MP). In experiments that favoured 4MP, on the other hand, K was only 1.9 and 2.5 (the latter value was calculated for the mixture that contained 60% 4MP). These K values are too low for efficient separations of these solutions.

As was the case in 2MP/4MP mixtures, when the solutions comprised 3MP and 4MP (Figure 5.3c), the host selectivity behaviour fluctuated, once more, according to the relative guest amounts present. 3MP was moderately preferred when the solution contained only 20% 4MP; the crystals then contained only 8.7% 4MP. However, at higher concentrations of 4MP (40, 60 and 80%), 4MP was then selected preferentially, and the mixed complexes contained 56.6, 76.6 and 87.7% 4MP, respectively.  $K_{ave}$ , excluding the point in favour of 3MP, was only 2.0, and successful separations of these mixtures with **H1** as the host compound is thus not viable.

In the case of **H2** in solutions containing PYR and 2MP (Figure 5.4a) and PYR and 3MP (Figure 5.4b), remarkable selectivities were observed in favour of PYR, and this was unwavering across the concentration range. All of these experiments, extraordinarily, resulted in complexes with at least 95.0% PYR, even in solutions with low concentrations (20%) of this guest solvent. The average K values were 76.9 and 17.2 for PYR/2MP and PYR/3MP, respectively. (Note that in these calculations, K values could not be obtained when 100% PYR was found in the crystals, according to the mathematical expression for K.) The greatest K

value in PYR/2MP mixtures was an astounding 186.5 (the solution contained only 20% PYR), and that in PYR/3MP mixtures was 28.5 (when 40% PYR was present). Clearly, **H2** is an excellent candidate to use to separate all mixtures of PYR/2MP and PYR/3MP when these contain 20% or more PYR. However, it is acknowledged that distillations would achieve similar results since PYR does boil at significantly lower temperatures than 2MP and 3MP.

The selectivity profiles provided in both Figures 5.4c (PYR/4MP) and 5.5b (4MP/3MP) revealed **H2** to be largely unselective for either guest species present since data points lie close to the  $K = 1$  line for no selectivity. In these solutions, **H2** would not be successful for any separations.

In Figure 5.5a (2MP/4MP), the host behaviour changed depending on the concentrations of the two guest species present. At low concentrations of 2MP (20 and 40%), 4MP was favoured (the crystals contained only 18.6 and 23.5% 2MP), while 2MP was significantly preferred when 60 and 80% of this guest was present in the solution: the crystals that were isolated then contained 92.8 and 100.0% 2MP. The  $K$  value recorded for the mixture that contained 60% 2MP was 8.6 (this value could not be calculated in the solution containing 80% 2MP since the amount of 2MP in the crystals was 100.0%, and the selectivity coefficient expression does not allow for such a calculation). Those experiments favouring 4MP had a  $K_{ave}$  value of only 1.6, with the highest  $K$  value recorded being 2.2 when 60% of 4MP was present. **H2** would thus only be successful as a separatory tool if mixtures contained 80% or more 2MP.

The GC results that allowed for the construction of Figures 5.2 to 5.5 are provided in the SI, Figures S26–S31 (**H1**) and S37–S41 (**H2**).

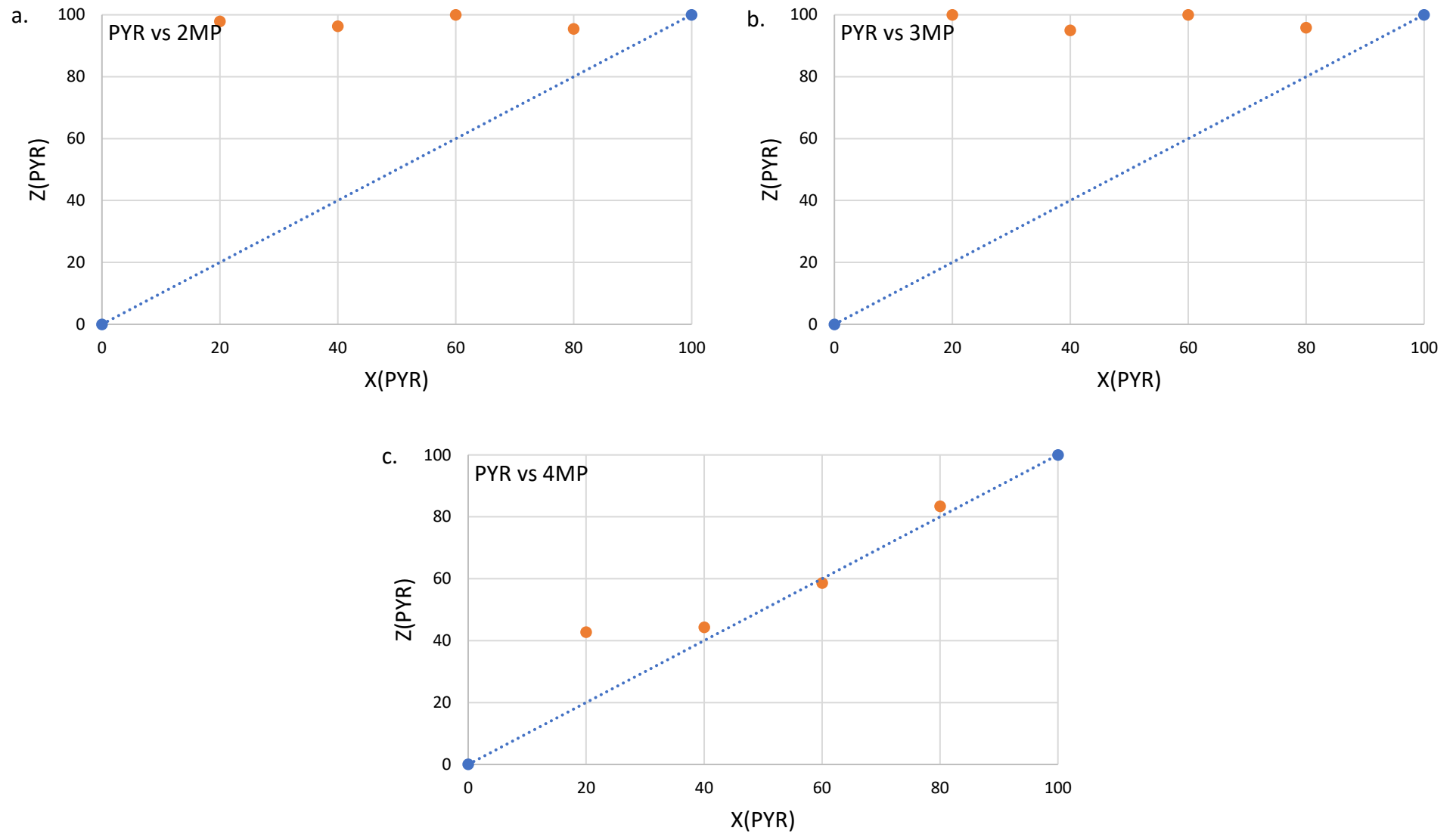


**Figure 5.4:** Selectivity profiles of **H2** in a. PYR/2MP, b. PYR/3MP and c. PYR/4MP binary solutions



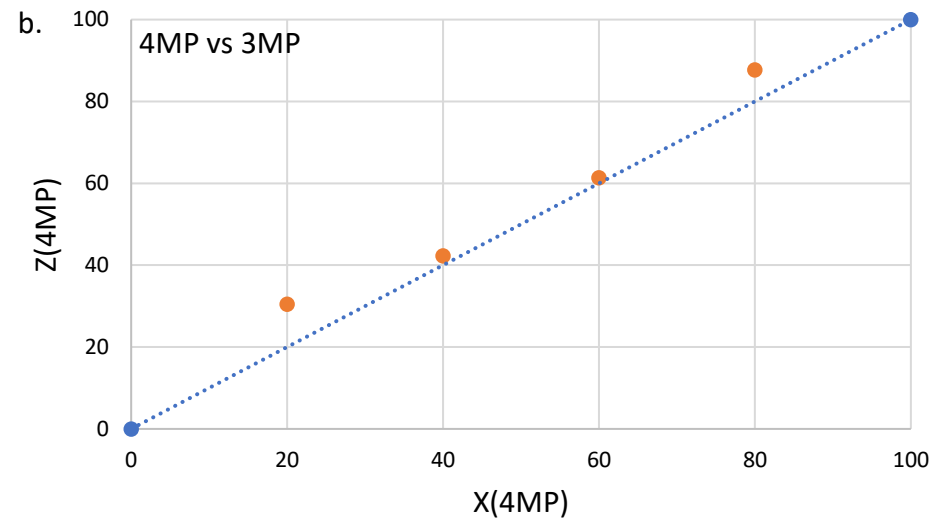
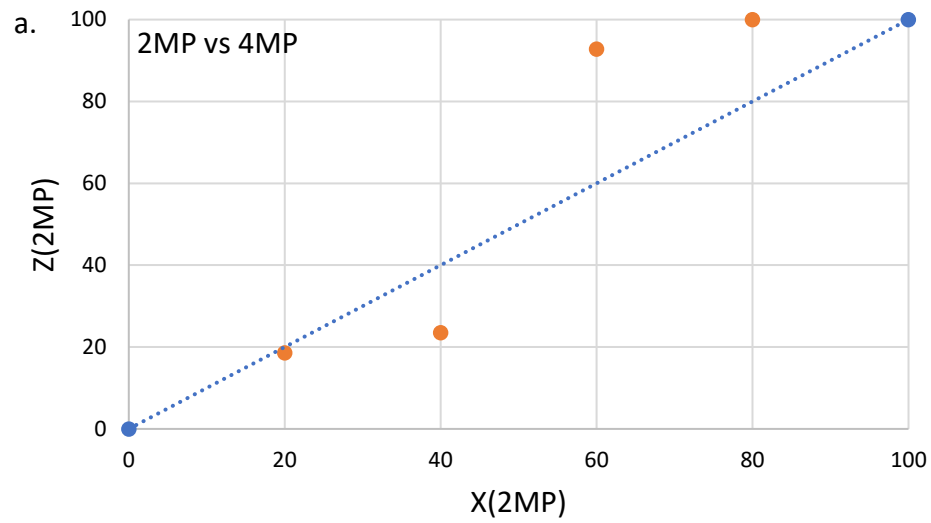


**Figure 5.5:** Selectivity profiles of **H2** in a. 2MP/4MP and b. 4MP/3MP solutions; 2MP/3MP mixtures furnished only apohost and so the selectivity profile for these experiments could not be constructed for this reason

#### 5.2.4 Single crystal X-ray diffraction experiments

All novel inclusion compounds with suitable quality crystals were analysed by means of SCXRD experiments. The only complex that could not be analysed in this way was **H1**·3MP; the crystals in this case were too small despite numerous recrystallization attempts at various temperatures and crystallization rates. Note that in the case of the inclusion complex of **H2** with 4MP, the H:G ratio of the crystal that was selected for the SCXRD experiment was 2:3, and thus differed from the single solvent recrystallization experiment (H:G 2:1, ascertained through  $^1\text{H}$  NMR spectroscopy, a bulk analytical method; this was confirmed (see later) by thermal analysis, also a bulk analytical technique). Clearly the selected crystal did not represent the bulk. In order to provide experimental data to confirm this statement, an experimental powder pattern was obtained for the 2(**H1**)·4MP complex and this pattern compared with the Mercury-generated powder pattern for the single crystal. These two patterns are provided in Figures 5.6, experimental (yellow) and computed (brown) and, from these, it is clear that the single crystal does not represent the bulk since these patterns differ; the unit cell dimensions from both are similar but due to the drastic intensity differences the composition of the material must be different (e.g., same host but different guest amounts with, e.g., different orientations, positions, etc.). However, the aim of this work is to determine whether the two host compounds are able to facilitate the separation of these difficult-to-separate compounds, and thus this anomaly does not detract from the results that are provided here.

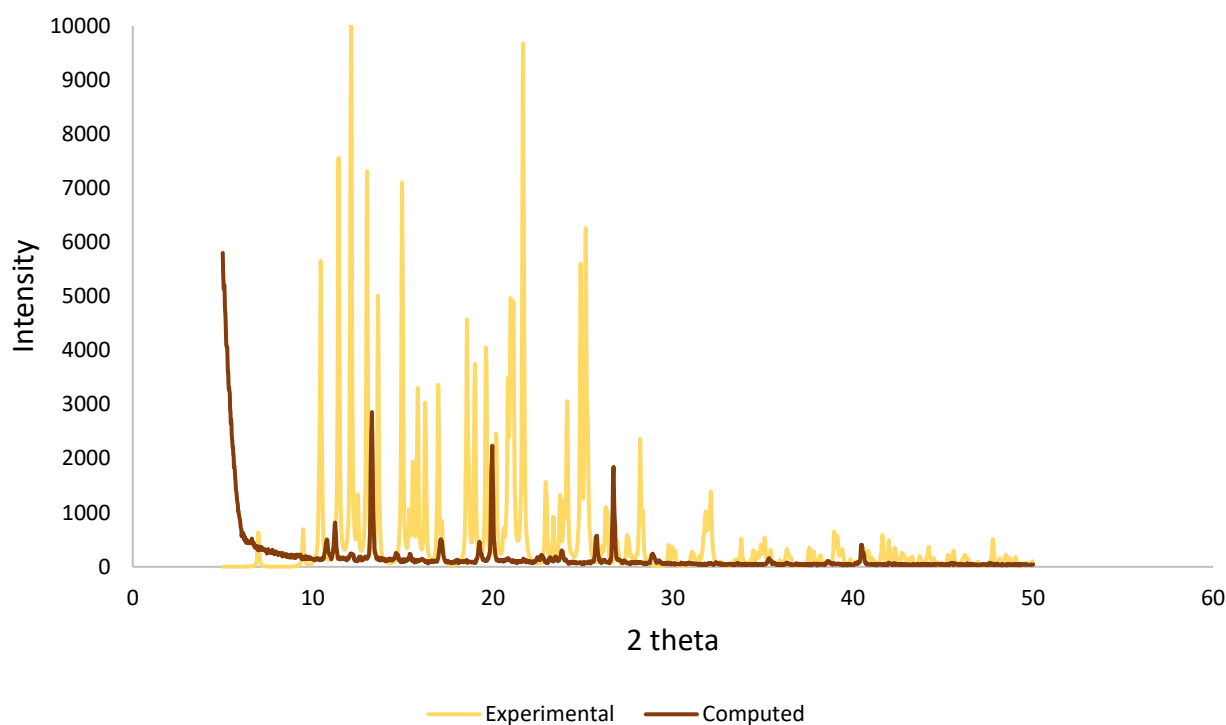


**Figure 5.6:** Experimental (yellow) and computed powder (brown) patterns for the complex of **H2** with 4MP, suggesting the single crystal employed for SCXRD analysis does not represent the bulk material

Complexes **H1**·2(PYR) and **H2**·2(PYR) displayed no disorder while the guest molecules in **H1**·2(2MP) were disordered over two orientations. In **H1**·2(4MP), both host and guest compounds displayed some disorder too, and guest molecules in 2(**H2**)·3(4MP) experienced disorder around an inversion point.

The relevant crystallographic data for these SCXRD experiments are provided in Table 5.4. All complexes, except 2(**H2**)·3(4MP) which crystallized in the monoclinic crystal system and space group  $P2_1/c$ , were found to crystallize in the triclinic crystal system and space group  $P\bar{1}$ .

The unit cells of **H1**·2(PYR) (along [100]), **H1**·2(2MP) ([100]) and **H1**·2(4MP) ([100]), and **H2**·2(PYR) ([010]) and 2(**H2**)·3(4MP) ([100]), are depicted on the left-hand side in Figures 5.7 (**H1**) and 5.8 (**H2**), respectively; these were prepared using Mercury software;<sup>111</sup> the void (yellow) diagrams are also provided here (right-hand side) which were calculated after deleting the guest molecules from the packing calculations and examining the remaining spaces that could accommodate a probe of 1.2 Å diameter. Note that two views of the voids are provided in each of Figures 5.7a and c, and Figure 5.8a, for clarity.

**Table 5.4:** Crystallographic data for the **H1·2(PYR)**, **H1·2(2MP)**, **H1·2(4MP)**, **H2·2(PYR)** and **2(H2)·3(4MP)** complexes

	<b>H1·2(PYR)</b>	<b>H1·2(2MP)</b>	<b>H1·2(4MP)</b>	<b>H2·2(PYR)</b>	<b>2(H2)·3(4MP)</b>
Chemical formula	C <sub>44</sub> H <sub>36</sub> N <sub>2</sub> ·2(C <sub>5</sub> H <sub>5</sub> N)	C <sub>44</sub> H <sub>36</sub> N <sub>2</sub> ·2(C <sub>6</sub> H <sub>7</sub> N)	C <sub>44</sub> H <sub>36</sub> N <sub>2</sub> ·2(C <sub>6</sub> H <sub>7</sub> N)	C <sub>44</sub> H <sub>40</sub> N <sub>2</sub> ·2(C <sub>5</sub> H <sub>5</sub> N)	2(C <sub>44</sub> H <sub>40</sub> N <sub>2</sub> )·3(C <sub>5</sub> H <sub>5</sub> N)
Formula weight	750.95	779.00	779.00	754.98	1472.94
Crystal system	Triclinic	Triclinic	Triclinic	Triclinic	Monoclinic
Space group	<i>P</i> $\bar{1}$	<i>P</i> $\bar{1}$	<i>P</i> $\bar{1}$	<i>P</i> $\bar{1}$	<i>P</i> 2 <sub>1</sub> / <i>c</i>
$\mu$ (Mo-K $\alpha$ )/mm <sup>-1</sup>	0.074	0.071	0.069	0.072	0.071
<i>a</i> /Å	9.0392(4)	8.7173(6)	8.9471(10)	8.9716(5)	9.0013(3)
<i>b</i> /Å	9.0518(3)	11.2718(8)	9.9740(11)	9.2886(5)	26.7346(9)
<i>c</i> /Å	13.7313(6)	12.6826(9)	13.4375(14)	13.8221(8)	9.0416(3)
alpha/°	76.202(1)	108.163(3)	73.488(4)	75.212(3)	90
beta/°	74.883(1)	105.764(2)	75.543(4)	76.005(3)	114.066(2)
gamma/°	67.225(1)	104.337(2)	74.301(4)	66.684(3)	90
<i>V</i> /Å <sup>3</sup>	988.05(7)	1061.65(13)	2(2)	1009.80(10)	1986.70(12)
<i>Z</i>	1	1	1	1	1
<i>D</i> (calc)/g·cm <sup>-1</sup>	1.262	1.219	1.190	1.242	1.231
<i>F</i> (000)	398	414	414	402	786
Temp./K	173	200	296	296	200
Restraints	0	105	178	0	105
<i>N</i> <sub>ref</sub>	6435	5285	5369	5002	4910
<i>N</i> <sub>par</sub>	266	342	346	268	318
<i>R</i>	0.0476	0.0392	0.0614	0.0406	0.0499
<i>wR</i> <sub>2</sub>	0.1300	0.1095	0.1912	0.0974	0.1362
<i>S</i>	1.08	1.03	1.05	1.05	1.02
$\theta$ min–max/°	2.5, 31.7	1.8, 28.4	2.2, 28.3	2.4, 28.4	2.5, 28.3
Tot. data	57670	33628	39159	5002	47566
Unique data	6435	5285	5369	5002	4910
Observed data [ <i>I</i> > 2.0 $\sigma$ ( <i>I</i> )]	4672	4470	4428	4112	3894
<i>R</i> <sub>int</sub>	0.060	0.022	0.015	0.0000	0.024
Completeness	0.994	0.998	0.999	0.995	1.000
Min. resd. dens. (e/Å <sup>3</sup> )	–0.27	–0.19	–0.45	–0.19	–0.40
Max. resd. dens. (e/Å <sup>3</sup> )	0.33	0.30	0.40	0.23	0.38

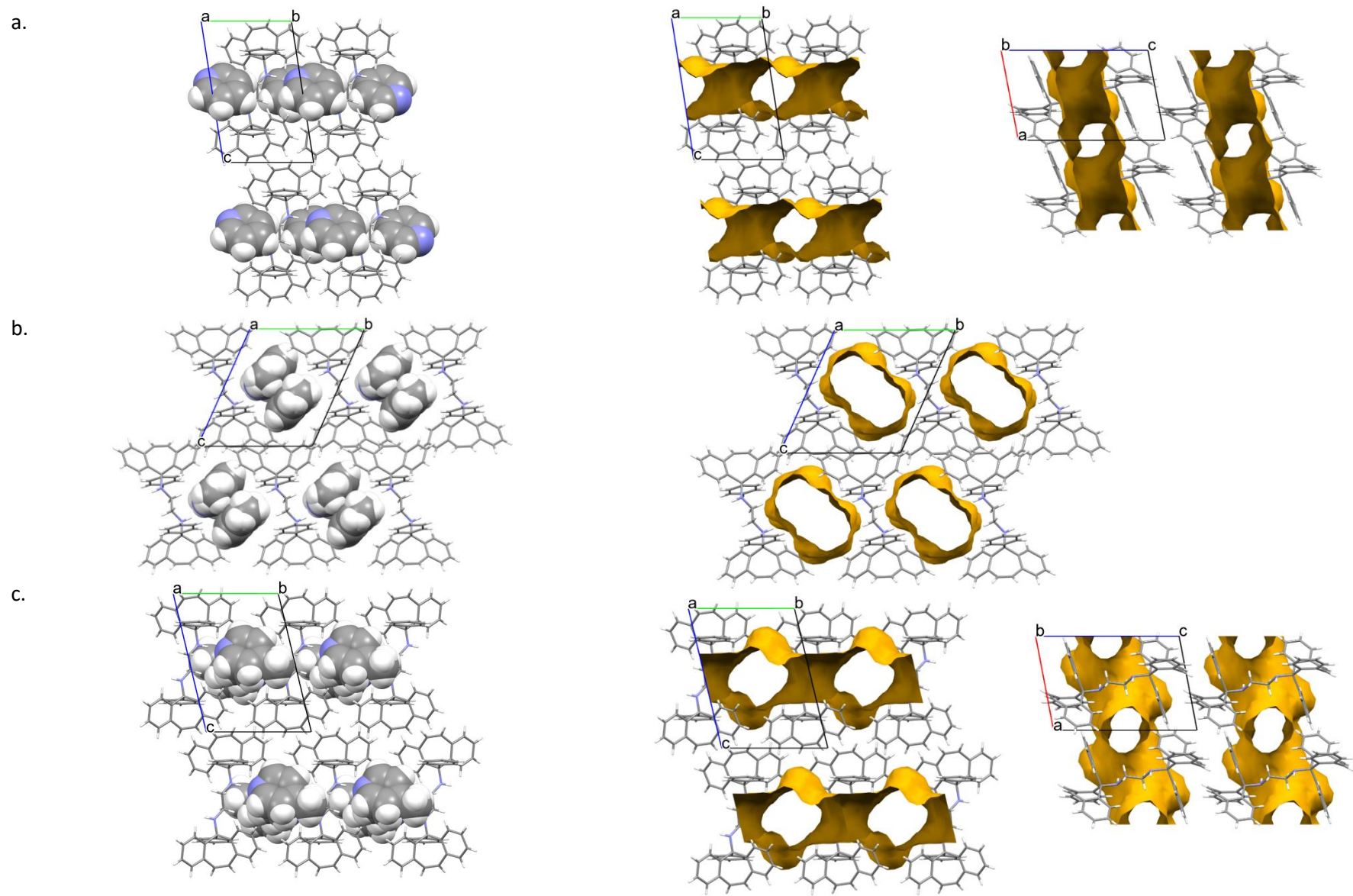


**Figure 5.7:** Unit cells (left) and void diagrams (right) for a.  $\text{H1}\cdot\text{2(PYR)}$ , b.  $\text{H1}\cdot\text{2(2MP)}$  and c.  $\text{H1}\cdot\text{2(4MP)}$

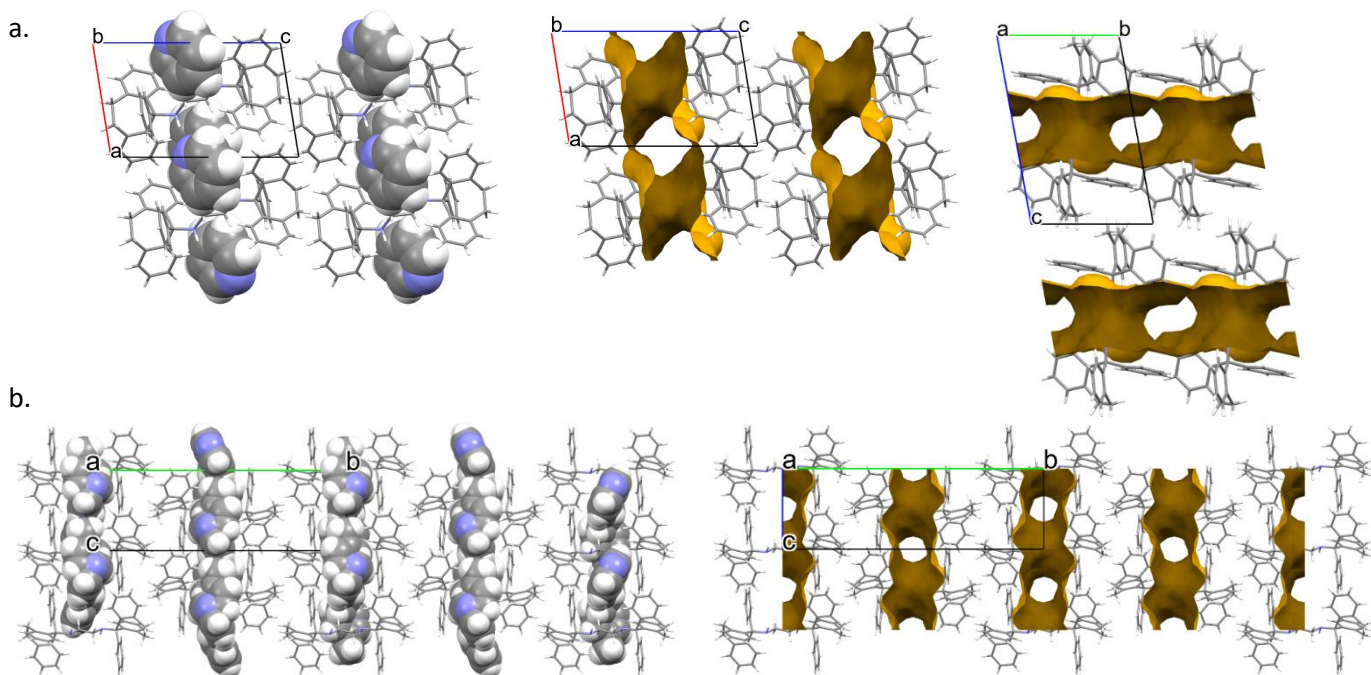


**Figure 5.8:** Unit cells (left) and void diagrams (right) for a. **H<sub>2</sub>·2(PYR)** and b. **2(H<sub>2</sub>)·3(4MP)**

Interestingly, both PYR-containing complexes (for **H1** and **H2**) have very similar unit cell dimensions (Table 5.4) and the host packing is therefore isostructural in each. However, this similarity in host packing is along two different axes as is witnessed in Figures 5.7a and 5.8a (the structures are isostructural if you use a non-conventional unit cell by swapping the a and b axes in one of these complexes). Also clear from these figures is that the guest molecules in **H1**·2(PYR) (Figure 5.7a) and **H1**·2(4MP) (Figure 5.7c) were accommodated in multidirectional channels, while 2MP in **H1**·2(2MP) (Figure 5.7b) were found to reside in wide open channels that were parallel to the a-axis. In fact, The PYR molecules in **H1**·2(PYR) are arranged in close pairs and the distance between such pairs is relatively small, with the result that there is a continuity of guest molecules in three linear directions. In a similar fashion, PYR and 4MP were also housed in endless channels that assumed more than one direction in the crystals of the respective complexes with **H2** (Figures 5.8a and b).

The non-covalent interactions present in the five complexes produced in this work were subsequently investigated. All of those involving atom···atom contacts are summarised in Table 5.5. In **H1**·2(PYR) was observed a classical (host)N–H···N–C(guest) hydrogen bond. This is illustrated by means of two stereoviews in Figure 5.9 (in both stick (top) and spacefill

(bottom) representation) and measured 2.39(2) (173.4(13)°). Despite all of the aromatic moieties present, no significant inter- or intramolecular (host) $\pi\cdots\pi$ (host) or (host) $\pi\cdots\pi$ (guest) contacts could be identified in this complex. However, two (host)C–H $\cdots\pi$ (guest) close contacts were observed, and these are illustrated, also by means of a stereoview, in Figure 5.10 (in this figure is also shown the H-bonds that were mentioned earlier). These interactions measured 2.95 Å (145°) and 2.70 (163°). This complex also experienced two intramolecular non-classical hydrogen bonds, and distances were 2.40 and 2.39 Å and associated angles 103 and 104°. These were of the (host)C–H $\cdots$ N(host) type. Five other short contacts were additionally identified here, with distances that ranged between 2.38 and 2.86 Å (122–151°)(Table 5.5).

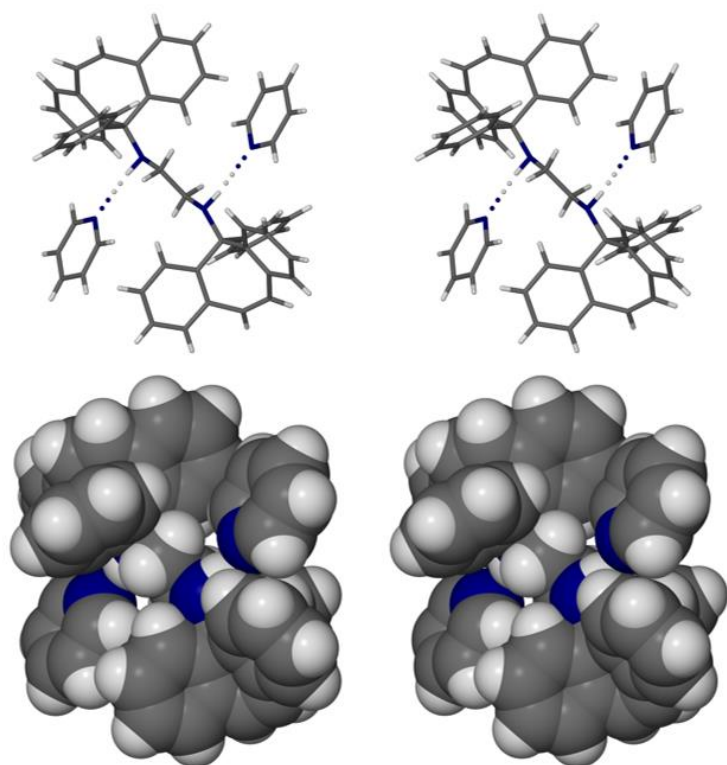


**Figure 5.9:** Stereoview of the **H1·2(PYR)** complex unit showing host $\cdots$ guest hydrogen bonding, with atoms in stick representation (top) and space-filling mode (bottom)

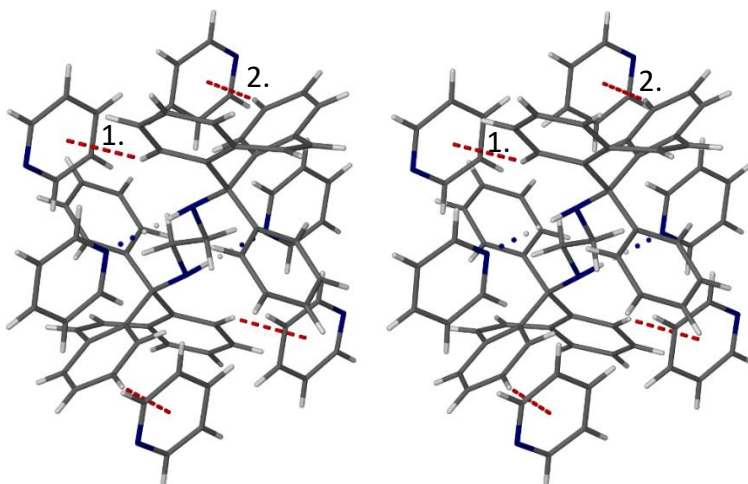


**Figure 5.10:** Stereoview showing host···guest H-bonds (blue dotted lines) and the two unique C–H··· $\pi$  interactions (red dashed lines) between the host molecule and symmetry-generated pyridine molecules in the **H1·2(PYR)** complex

In Figure 5.11 is shown two significant short stabilizing  $\pi$ ··· $\pi$  interactions in the **H1·2(2MP)** complex involving two distinct host (Figure 5.11a) and guest (Figure 5.11b) molecules. The distances between the centroids were 3.624(1) and 3.958(4) Å, respectively, with slippages of 0.854 and 1.789 Å. One of each of guest···host and host···host C–H··· $\pi$  contacts were also identified (2.702 Å, 151° and 2.755 Å, 150°) and are illustrated in Figure 5.12. Once more, classical (host)N–H···N–C(guest) hydrogen bonds were observed as well: each of the two guest molecules interacted with the host molecule in this way, and respective distances and angles measured 2.28(2) Å and 2.31(3) Å, and 158.1(12) and 156.1(13)°. Additionally, as summarised in Table 5.5, four other short contacts were also observed (2.28–2.86 Å, 119–174 °C). Finally, as was the case in **H1·2(PYR)**, two comparable intramolecular (host)C–H···N(host) interactions were also identified and these measured 2.40 and 2.37 Å; the respective angles were 104 and 103°.



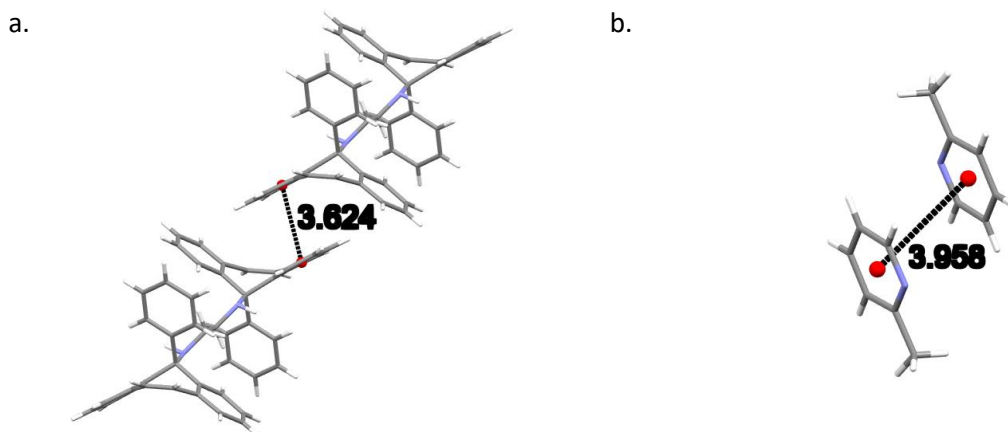


**Figure 5.11:** Illustration of the two intermolecular a. (host) $\pi\cdots\pi$ (host) and b. (guest) $\pi\cdots\pi$ (guest) interactions in **H1·2(2MP)**

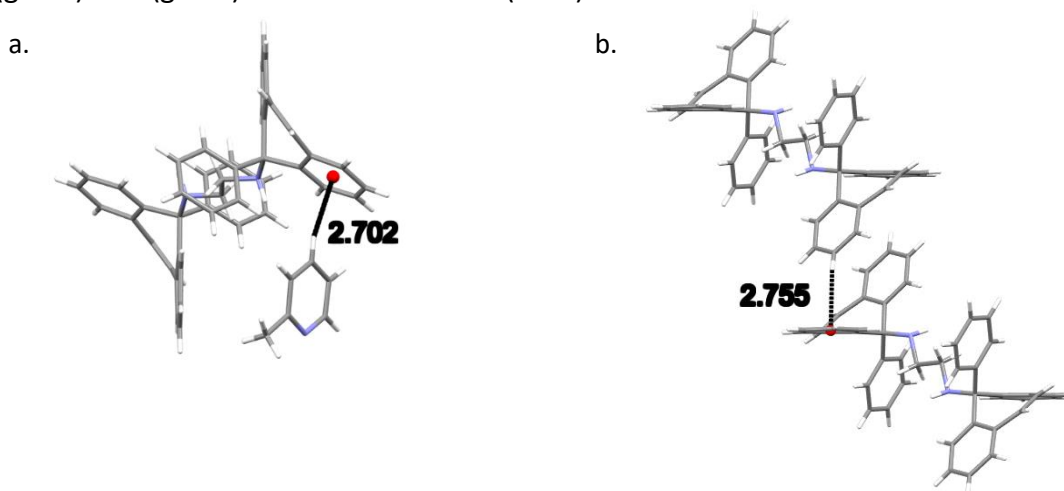


**Figure 5.12:** The a. (guest)C–H $\cdots\pi$ (host) and b. (host)C–H $\cdots\pi$ (host) intermolecular interactions in complex **H1·2(2MP)**

A subsequent analysis of the non-covalent interactions present in the **H1·2(4MP)** complex revealed that there were no significant guest $\cdots$ guest, guest $\cdots$ host or host $\cdots$ host  $\pi\cdots\pi$  interactions present since all of these measurements were greater than 4.0 Å. However, as in the previous two complexes, classical (host)N–H $\cdots$ N–C(guest) contacts were experienced by both guest molecules (2.49(2) and 2.34(2) Å, 177.4(19) and 176.8(19)°). It is notable that the preferred guest compound of **H1** (2MP), despite the N–H $\cdots$ N angles being somewhat smaller in that complex compared with in **H1·2(PYR)** and **H1·2(4MP)**, experienced the shorter H $\cdots$ N distances (2.28(2) and 2.31(3) Å relative to 2.39(2) (**H1·2(PYR)**), and 2.49(2) and 2.34(2) (**H1·2(4MP)**)). Perhaps this observation plays some role in the preferential behaviour of **H1** for 2MP. As was the case in the first two complexes, two intramolecular contacts were also identified in **H1·2(4MP)**, of the (host)C–H $\cdots$ N(host) type, and distances for both were 2.40 Å

and angles  $104^\circ$ . Finally, another five other short interactions were also observed (2.26–2.87 Å,  $110$ – $148^\circ$ ), the details of which are provided in Table 5.5.

For complexes involving **H2**, no significant  $\pi\cdots\pi$  interactions were, once more, observed. In the **H2**·2(PYR) complex, however, two C–H $\cdots\pi$  contacts were noted, one between two host molecules and one between the host and guest species; measurements were 2.760 Å ( $140^\circ$ ) and 2.703 Å ( $167^\circ$ ), respectively, and Figure 5.13 illustrates these. A stereoview was also prepared in order to clarify the (host)N–H $\cdots$ N–C(guest) interaction that is present in this complex; this classical H-bond between host and guest molecules measured 2.380(2) Å ( $171.8(15)^\circ$ ) (Figure 5.14). Two further short contacts were also observed between host and guest species; these were of the (host)C–H $\cdots$ H–C(guest) and (host)C–H $\cdots$ C–C(guest) types (2.39, 2.89 Å and  $122$ ,  $133^\circ$ ) together with the now common two intramolecular (host)C–H $\cdots$ N(host) interactions (2.39, 2.33 Å and  $105$ ,  $106^\circ$ ).

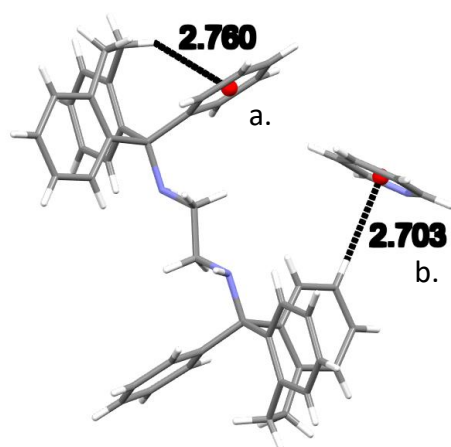


**Figure 5.13:** C–H $\cdots\pi$  interactions between a. host and host (intramolecular), and b. host and guest molecules in **H2**·2(PYR)

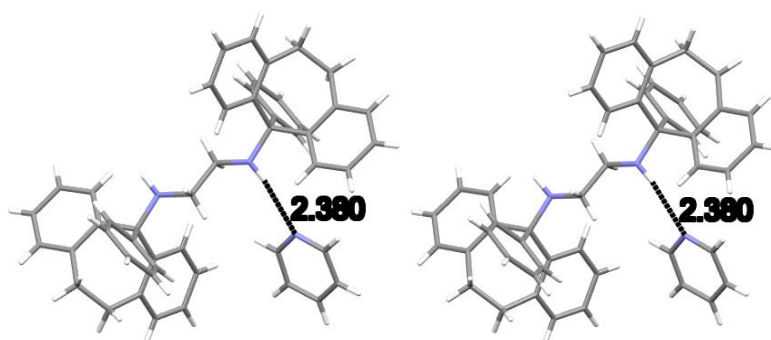


**Figure 5.14.** Stereoview of the **H2**·2(PYR) host $\cdots$ guest hydrogen bonding interaction

Four C–H··· $\pi$  interactions were observed in the 4MP-containing complex with **H2**. Figures 5.15a and b are illustrations of three of these, one an intramolecular (host)C–H··· $\pi$ (host) interaction, another a (guest)C–H··· $\pi$ (host) contact, and finally, a (host)C–H··· $\pi$ (guest) interaction. These measured 2.679, 2.892 and 2.935 Å, and associated angles were 143, 140 and 141°, respectively).

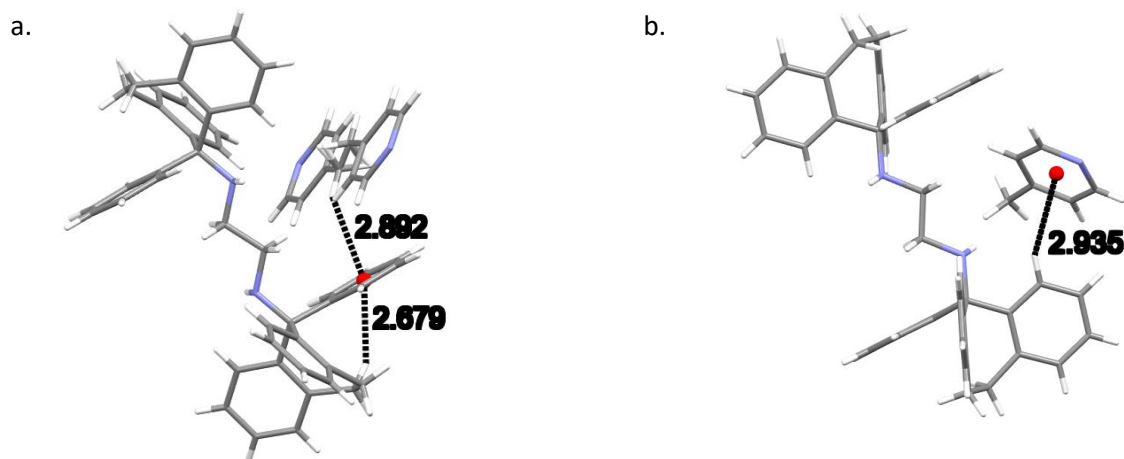


**Figure 5.15:** a. Intramolecular (host)C–H··· $\pi$ (host) and intermolecular (guest)C–H··· $\pi$ (host), and b. intermolecular (host)C–H··· $\pi$ (guest) interactions in 2(**H2**)·3(4MP)

Once more, the guest was bound in the crystals by means of a classical hydrogen bond ((host)N–H···N–C(guest)) that measured 2.40(2) Å with a corresponding angle of 169.2(16)°. These hydrogen bond dimensions for the complex containing the preferred PYR guest species are shorter (2.38(2) Å) and more linear (171.8(15)°) than in the present instance, and plausibly explains the affinity of **H2** for PYR. Again present in the 2(**H2**)·3(4MP) complex are the ubiquitous intramolecular (host)C–H···N(host) non-classical hydrogen bonding interactions (2.37, 2.36 Å and 104, 106°) as well as a number of other short contacts (2.19–2.79 Å, 109–166°, Table 5.5).

**Table 5.5:** Various short interactions present in the pyridine complexes formed with host compounds **H1** and **H2**<sup>a</sup>

	H1·2(PYR)	H1·2(2MP)	H1·2(4MP)	H2·2(PYR)	2(H2)·3(4MP)
(host)C–H···C–C(host)	2.85 Å, 135°, <	None	2.87 Å, 140°, < (guest 1)	None	2.79 Å, 161°, < (guest 1)
(host)C–C···H–C(host)	None	None	None	None	2.79 Å, 109°, < (guest 1)
(host)C–H···N–C(guest)	2.86 Å, 151°, <	None	None	None	None
(host)C–H···H–C(guest)	2.38 Å, 122°, <	2.39 Å, 156°, < (guest 1)	2.26 Å, 129°, < (guest 2)	2.39 Å, 122°, <	None
(host)C–H···C–C(guest)	2.84 Å, 134°, <	None	2.84 Å, 148°, < (guest 2)	2.89 Å, 133°, <	None
(host)C–H···C–H(guest)	None	None	None	None	2.78 Å, 156°, < (guest 1)
(host)C–C···H–C(guest)	2.83 Å, 125°, <	None	2.75 Å, 110°, < (guest 1)	None	None
(guest)C–H···H–C (host)	None	None	2.38 Å, 140°, < (guest 2)	None	None
(guest)C–H···H–C (guest)	None	2.28 Å, 119°, < (guest 1)	None	None	2.26 Å, 166°, < (guest 1) 2.22 Å, 166°, < (guest 1) 2.37 Å, 138°, < (guest 1 interacting with guest 2) 2.19 Å, 144°, << (guest 1 interacting with guest 2)
(guest)C–H···C–C (guest)	None	2.73 Å, 160°, < (guest 2 interacting with guest 2) 2.86 Å, 174°, < (guest 2 interacting with guest 1)	None	None	None
(host)N–H···N–C(guest)	2.39(2) Å, 173.4(13)°, <<	2.28(2) Å, 158.1(12)°, << (guest 1) 2.31(3) Å, 156.1(13)°, << (guest 2)	2.49(2) Å, 177.4(19)°, << (guest 1) 2.34 (2) Å, 176.8(19)°, << (guest 2)	2.38(2) Å, 171.8(15)°, <<	2.40(2) Å, 169.2(16)°, << (guest 1)
(guest)N–C···H–C(host)	None	None	2.88 Å, 105°, < (guest 2)	None	None
Intra (host)C–H···N(host)	2.40 Å, 103° 2.39 Å, 104°	2.40 Å, 104° 2.37 Å, 103°	2.40 Å, 104° 2.40 Å, 104°	2.39 Å, 105° 2.33 Å, 106°	2.37 Å, 104° 2.36 Å, 106°

<sup>a</sup> < denotes contacts less than the sum of the van der Waals radii and << contacts less than this sum minus 0.2 Å

### 5.2.5 Thermal analysis

The thermogravimetric (TG), its derivative (DTG), and differential scanning calorimetric (DSC) traces after thermal analyses of the five pyridine-containing complexes are provided (overlaid) in Figures 5.16a–d (**H1**) and 5.17a and b (**H2**), while the more important thermal data obtained from these are summarised in Table 5.6.

**Table 5.6:** Thermal data for the pyridine complexes with **H1** and **H2**

Complex	T <sub>on</sub> /°C <sup>a</sup>	Calculated mass loss/%	Experimental mass loss/%
<b>H1</b> ·2(PYR)	54.6	21.1	21.5
<b>H1</b> ·2(2MP)	63.2	23.9	23.2
<b>H1</b> ·3MP	<i>b</i>	13.6	<i>b</i>
<b>H1</b> ·2(4MP)	<i>b</i>	23.9	<i>b</i>
<b>H2</b> ·2(PYR)	76.5	21.0	19.8
2( <b>H2</b> )·4MP	68.2	7.2	6.5

<sup>a</sup> T<sub>on</sub> is the onset temperature for the guest release process and serves as a measure of the thermal stability of the complex and was estimated from the DTG/TG

<sup>b</sup> The onset of guest release commenced during sample preparation, and T<sub>on</sub> and the experimental mass loss could thus not be measured

The mass losses experienced by the **H1**·2(PYR) (Figure 5.16a) and **H1**·2(2MP) (Figure 5.16b) complexes, where both H:G ratios were 1:2, were in close accordance with the expected mass losses (21.5 and 23.2% was measured while 21.1, 23.9% was calculated, Table 5.6). However, in the case of both **H1**·3MP and **H1**·2(4MP) (Figures 5.16c and d), the mass losses that were expected (13.6 and 23.9%) were significantly higher than the measurements made in these experiments (10.1 and 7.0%). A plausible reason for this is that some guest may have escaped from the crystals during sample preparation, indicating that these two complexes were unstable at room temperature. While PYR was released in a multi-stepped manner, the escape was in a simple single step for the 2MP-containing complex (in the latter case, the small inflection below 50 °C is attributed to the low boiling petroleum ether that was used to wash the crystals). Here, since the onset temperature (T<sub>on</sub>) for the guest release process was the highest for **H1**·2(2MP) (63.2 compared with 54.6 °C for the PYR-containing complex, with the remaining two complexes being unstable at ambient conditions (3MP and 4MP)), this

complex thus possessed the greatest thermal stability of the four, which agrees with the guest/guest competition experiments, where 2MP was demonstrated to be favoured by **H1**. This may be as a result of the shorter H-bond between host and guest molecules as observed from SCXRD data. Note that the guest release events for all four complexes were followed by host melt and/or decomposition process as can be discerned by both the DSC and TG traces.

In the case of the **H2**·2(PYR) (Figure 5.17a) and 2(**H2**)·4MP (Figure 5.17b) complexes, expected (21.0 and 7.2%) mass losses were in close agreement with the experimentally-obtained measurements (19.8 and 6.5%). In the first of these, guest release occurred in two distinct steps while 4MP escaped as a singular event. Once more, and as was the case with the four complexes of **H1**, the preferred guest species of **H2** (PYR) was bound tighter in the complex than 4MP, as was demonstrated by the greater  $T_{on}$  for **H2**·2(PYR) (76.5 °C) compared with 2(**H2**)·4MP (68.2 °C). Therefore, the complex containing the favoured PYR guest species formed the more stable complex, and this again was predicted by the guest/guest competition experiments (which favoured PYR) and was explained by SCXRD data (the host and guest molecules in this case experienced shorter and more linear classical H-bonds). Finally, both TG traces demonstrated that host decomposition events followed that of the guest release processes.

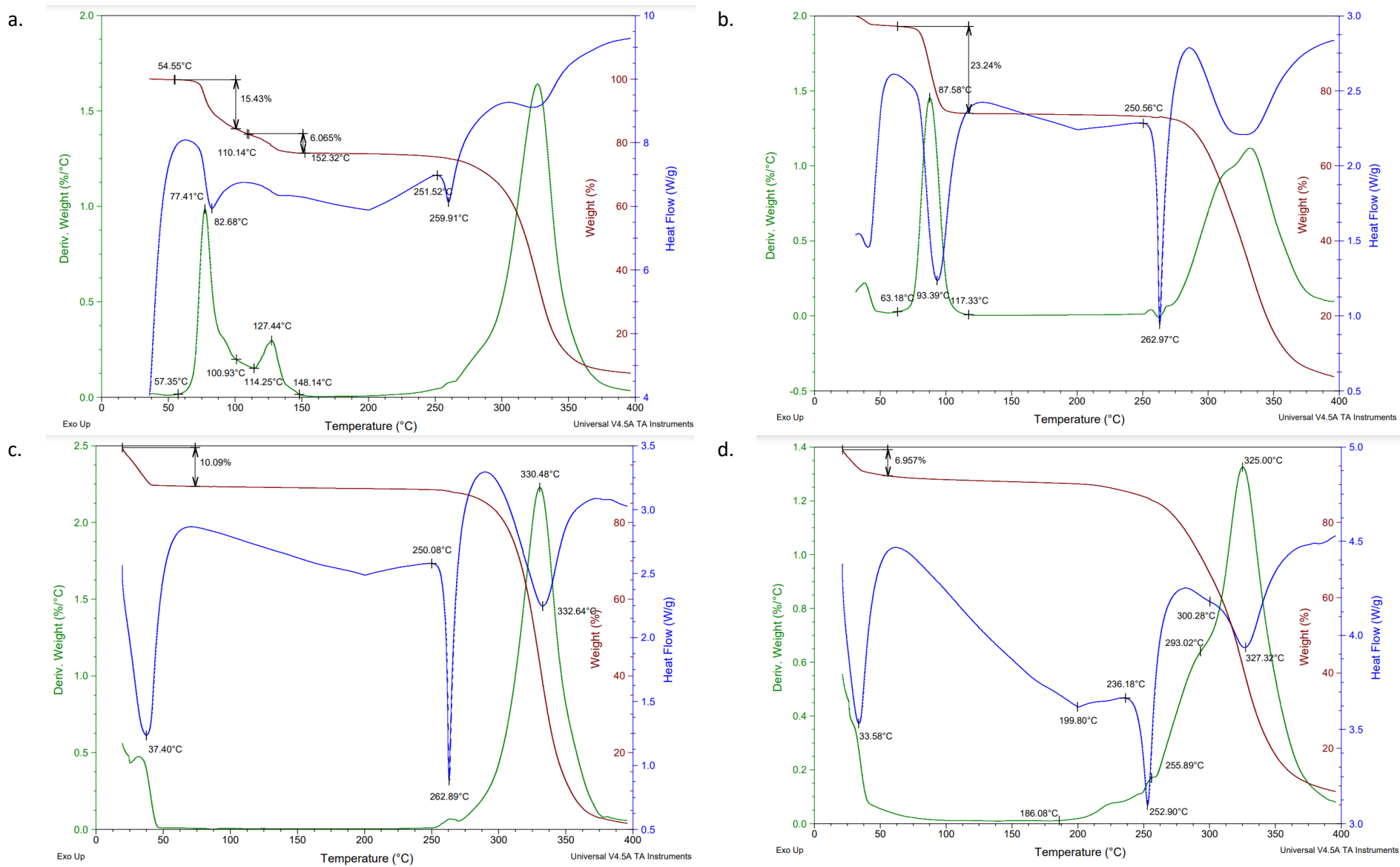
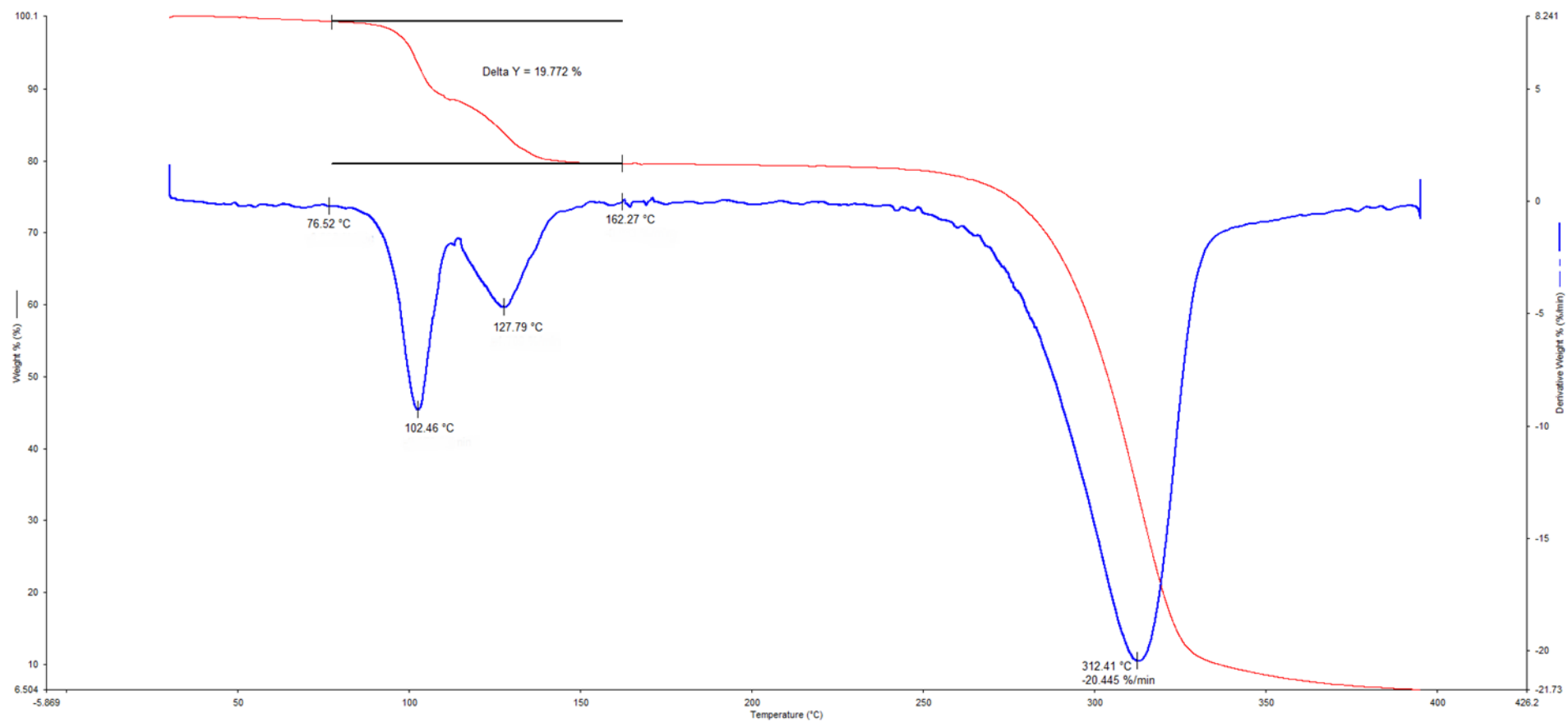


**Figure 5.16:** Overlaid TG, DTG and DSC traces for a. H1·2(PYR), b. H1·2(2MP), H1·3MP, and H1·2(4MP)

a.





b.

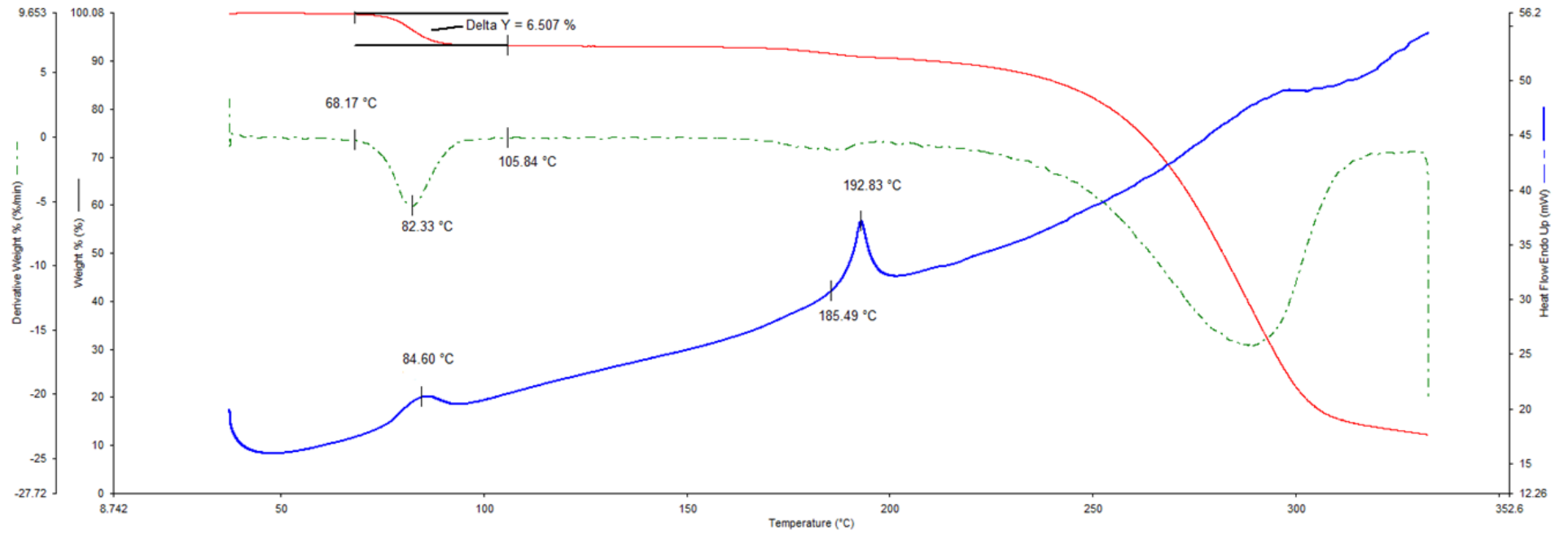


Figure 5.17: Overlaid thermal traces for a. H<sub>2</sub>·2(PYR) and b. 2(H<sub>2</sub>)·4MP

### 5.3 Conclusion

From this investigation, it was revealed that **H2** is a more selective host compound compared with **H1** in pyridine and methylpyridine guest solvents. In the single solvent experiments, **H1** enclathrated all four guest pyridines, with a 1:2 H:G ratio being predominant (one exception was the **H1**·3MP complex where this ratio was 1:1). **H2**, on the other hand, only enclathrated two guest species of the four, namely PYR and 4MP. The H:G ratio of the former was also 1:2, while the 4MP guest produced a complex that <sup>1</sup>H NMR suggested had a 2:1 H:G ratio; however, the single crystal selected for SCXRD analyses alluded to a 2:3 H:G ratio. (PXRD then confirmed that the single crystal did not represent the bulk.) In the equimolar binary guest experiments for **H1**, 2MP remained the most favoured guest compound, while **H2** demonstrated a preference for PYR. The results from equimolar ternary and quaternary guest competition experiments for both host compounds largely agreed with the results from these binary experiments. Selectivity profiles constructed with **H1** as the host compound demonstrated that it has the ability to separate mixtures of 2MP/PYR when these mixtures contained 40% 2MP (K was then 11.8). On the other hand, **H2** was revealed to have excellent separatory potential for PYR/2MP and PYR/3MP mixtures even when the amount of PYR present in these was low (20%). Numerous non-covalent interactions were identified by SCXRD analyses. The most significant of these were the shorter hydrogen bonding contacts in both **H1**·2(2MP) and **H2**·2(PYR), thus plausibly explaining the affinities of these host compounds for 2MP and PYR, respectively. Furthermore, thermal analyses demonstrated also that these favoured guest compounds formed complexes with **H1** and **H2** that possessed the greater thermal stabilities, where the guest release onset temperatures ( $T_{on}$ ) were highest for **H1**·2(2MP) (63.2 °C) and **H2**·2(PYR) (76.5 °C) compared with the other complexes for each host compound. Therefore, both **H1** and **H2** do indeed have the ability, in certain conditions, to serve as candidates for the separation of various of these pyridine mixtures through host-guest chemistry strategies, as demonstrated by the results obtained in these investigations.

## 6. Selectivity of host compounds **H1** and **H2** in anisole and isomeric methylanisole mixtures

### 6.1 Introduction

Anisole (ANI)<sup>121</sup> and its *C*-methylated derivatives (methylanisoles 2MA, 3MA and 4MA) (Figure 6.1) have a broad range of applications, and examples include their employment as building blocks in the preparation of pharmaceutical products, pheromones and perfumes.<sup>122</sup> Additionally, ANI and 4MA can be found in trace amounts in certain natural products and crop oils.<sup>123</sup> Alkylation using methanol is one of the more common methods used to transform phenol to ANI, and the different *o*-, *m*- and *p*-cresols to the MAs.<sup>122,124</sup> In the case of the synthesis of the MAs, phenol may be subjected to *O*-alkylation to form ANI following which ANI then reacts through *C*-alkylation to form the MA compound.<sup>125</sup> However, these reactions oftentimes lead to a mixture of ANI and isomeric MA products. While ANI may readily be removed from the mixture through distillation processes owing to its different boiling point (153.8 °C), the MAs are not as readily separated into their pure constituents as a result of their very similar boiling points (171.0, 175.5 and 175.5 °C for 2MA, 3MA and 4MA, respectively).<sup>127</sup> As such, fractional distillations and/or crystallizations present a challenge and, therefore, there exists a need to discover separation techniques that are more facile and efficient, and less costly than these more conventional means.

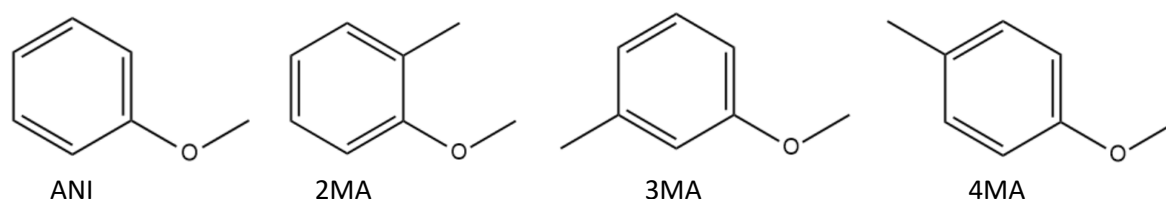


**Figure 6.1:** Molecular structures of anisole (ANI), 2-methylanisole (2MA), 3-methylanisole (3MA) and 4-methylanisole (4MA)

As such, **H1** and **H2** were assessed for the ability to separate such mixtures in the present investigation.

## 6.2 Results and discussion

### 6.2.1 Assessment of the host potential of **H1** and **H2** for ANI/2MA/3MA/4MA in single solvent recrystallization experiments

Table 6.1 contains the data obtained when host compounds **H1** and **H2** were recrystallized from each of the anisole isomers and anisole.

**Table 6.1:** Recrystallization experiments of **H1** and **H2** from each of ANI, 2MA, 3MA and 4MA

Guest	<b>H1</b> :G <sup>a</sup>	<b>H2</b> :G <sup>a</sup>
ANI	1:0	2:3
2MA	2:1	<i>b</i>
3MA	1:0 (RT <sup>c</sup> )	<i>b</i>
	1:1 (4 °C)	
4MA	1:1	<i>b</i>

<sup>a</sup> Host:guest (H:G) ratios were determined using <sup>1</sup>H-NMR spectroscopy

<sup>b</sup> No crystallization occurred

<sup>c</sup> Room temperature

All of the experiments with **H1** were conducted at both 4 °C and at ambient temperature. These changes in temperature affected solely the experiment in 3MA and it was noted that **H1** included 3MA only at low temperatures (4 °C, H:G 1:1) and not at ambient conditions (Table 6.1). The remaining recrystallization experiments with **H1** were unaffected by temperature variances, and this host compound was observed to consistently also include 2MA and 4MA with H:G ratios of 2:1 and 1:1, respectively. **H1** did not form a complex with ANI in these conditions. **H2**, on the other hand, presented significant challenges: only ANI was enclathrated (H:G 2:3), while crystallization did not occur in any of the MA isomers and gels remained in the glass vessels. The <sup>1</sup>H NMR spectra for these single solvent complexes are provided in the SI in Figure S42 (**H1**) and Figure S50 (**H2**).

## 6.2.2 Assessment of the selectivity behaviour of H1 and H2 in equimolar mixed guests

Table 6.2 summarizes the results obtained from competition experiments when host compound H1 was recrystallized from equimolar binary, ternary and quaternary mixtures of ANI, 2MA, 3MA and 4MA. (Owing to the challenges associated with the recrystallization of H2 from such mixtures and extraordinarily slow recrystallization times (months), comparable equimolar experiments with this host compound were not feasible in this case.) Here, the preferred guest is indicated in bold black text for each individual competition experiment, and the percentage estimated standard deviations (%e.s.d.s) are provided in parentheses, calculated as a result of the fact that each experiment was conducted in duplicate.

**Table 6.2:** Complexes formed by H1 in equimolar mixed anisole guests<sup>a,b</sup>

ANI	2MA	3MA	4MA	Guest ratios (%e.s.d.s)	Overall H:G ratio
X	X			<sup>c</sup>	<sup>c</sup>
X		X		<sup>c</sup>	<sup>c</sup>
X			<b>X</b>	8.3: <b>91.7</b> (0.6)	1:1
	X	X		<sup>c</sup>	<sup>c</sup>
	X		<b>X</b>	10.7: <b>89.3</b> (1.4)	1:1
		X	<b>X</b>	15.6: <b>84.4</b> (1.4)	1:1
X	X	X		<sup>c</sup>	<sup>c</sup>
X	X		<b>X</b>	19.0:14.7: <b>66.3</b> (2.6:2.0:4.6)	1:1
X		X	<b>X</b>	9.4:15.6: <b>75.0</b> (2.1:0.4:1.7)	1:1
	X	X	<b>X</b>	9.1:15.0: <b>75.9</b> (2.2:1.4:3.5)	1:1
X	X	X	<b>X</b>	8.5:8.5:14.1: <b>68.9</b> (2.3:1.8:0.9:3.2)	1:2

<sup>a</sup> GC-MS and <sup>1</sup>H NMR spectroscopy were used to obtain the G:G and overall H:G ratios, respectively

<sup>b</sup> The competition experiments were conducted in duplicate; the %e.s.d.s are provided in parentheses

<sup>c</sup> No inclusion occurred and only apohost was recovered from the experiment

From the table (Table 6.2), it is clear that no inclusion occurred in the binary experiments ANI/2MA, ANI/3MA and 2MA/3MA, and only apohost was recovered from the glass vials in these instances. In fact, only when the solutions contained 4MA was complexation with **H1** successful. The binary experiments ANI/4MA, 2MA/4MA and 3MA/4MA afforded crystals with significant amounts of 4MA (91.7, 89.3 and 84.4 %, respectively), and this guest was thus undoubtedly overwhelmingly preferred in these guest/guest competition experiments.

The ternary equimolar experiments comprising ANI/2MA/4MA, ANI/3MA/4MA and 2MA/3MA/4MA revealed that the host affinity for 4MA persisted in these conditions, and recovered crystals contained 66.3, 75.0 and 75.9 % 4MA, respectively. As alluded to earlier, the ternary equimolar solution where 4MA was absent, ANI/2MA/3MA, furnished only apohost compound. Finally, the equimolar experiment in which all four guest solvents were present resulted in a mixed complex with an elevated quantity of 4MA once more (68.9%). From this particular experiment, the host selectivity was thus in the order 4MA (68.9%) >> 3MA (14.1%) > 2MA (8.5%)  $\approx$  ANI (8.5%).

In all successful complexation experiments, the overall H:G was consistently 1:1, with the exception of the quaternary mixture, where this ratio was 1:2.

All relevant  $^1\text{H}$  NMR spectra and GC traces are provided in the SI (Figures S43–S46).

### 6.2.3 Assessment of the selectivity behaviour of **H1** in binary mixtures containing ANI, 2MA, 3MA and 4MA where the $G_A:G_B$ molar ratios were sequentially varied

The selectivity profiles that were obtained for **H1** by plotting Z for  $G_A$  (or  $G_B$ ) against X for  $G_A$  (or  $G_B$ ) after GC analyses of the crystals emanating from the binary solutions are provided in Figures 6.2a–c. (Once more, analogous experiments with **H2** were not possible.) Note that if these binary solutions did not contain 4MA, only apohost was recovered from the glass vials in every case and no selectivity profiles could be constructed in these instances. The averaged K values ( $K_{\text{ave}}$ ) for the three sets of binary experiments are summarised in Table 6.3.

From Figure 6.2a (4MA/ANI), it is clear that 4MA remained significantly preferred across the concentration range. This was true even at low concentrations (20%) of 4MA, where the recovered crystals then already contained 66.2% of this guest species. This particular experiment also furnished the highest selectivity coefficient ( $K = 6.8$ ). When the solution contained 40% 4MA, the so-formed crystals were observed to have 81.9% 4MA, while the 60:40 and 80:20 (4MA/ANI) mixtures produced crystals that were significantly enriched with 4MA (86.1 and 95.8%, respectively).  $K_{ave}$  for this set of experiments was 6.1 (Table 6.3) and, in general, the  $K$  values were too low for the efficient separations of such mixtures, as suggested by Nassimbeni et al.<sup>34</sup>

Figure 6.2b (4MA/2MA) shows that 4MA was, once more, the favoured guest solvent throughout. Solutions with 20, 50, 60 and 80% 4MA afforded crystals that contained 35.0, 89.3, 89.7 and 93.6% of this guest solvent. The highest  $K$  value that was calculated was 8.3 and this was in the binary solution that contained equal molar quantities of each guest species, while  $K_{ave}$  was 5.0 in this set of experiments. Once more, **H1** would not be able to effectively separate any of these mixtures.

Once again, Figure 6.2c (4MA/3MA) demonstrates that **H1** consistently selected for 4MA. The  $K$  values in these experiments ranged from a modest 1.9 to 6.7 and were calculated from experiments that had 4MA concentrations of 40 and 80%, respectively. The  $K_{ave}$  was, however, only 3.4. **H1** would, therefore, also not be able to effect the separation of these solutions.

Overall, the performance of **H1** was better in 4MA/ANI mixtures followed by 4MA/2MA and 4MA/3MA solutions, as observed from the  $K_{ave}$  values (6.1, 5.0 and 3.4%, Table 6.3). This was not entirely unexpected given the host selectivity order  $4MA \gg 3MA > 2MA \approx ANI$  as obtained from the equimolar experiments. Hence ANI and 2MA were not able to compete effectively with 4MA, whilst 3MA did offer some opposition. The  $K$  values from experiments in this work were always lower than 10, and so **H1** cannot be nominated as an ideal host candidate to successfully effect these anisole separations.

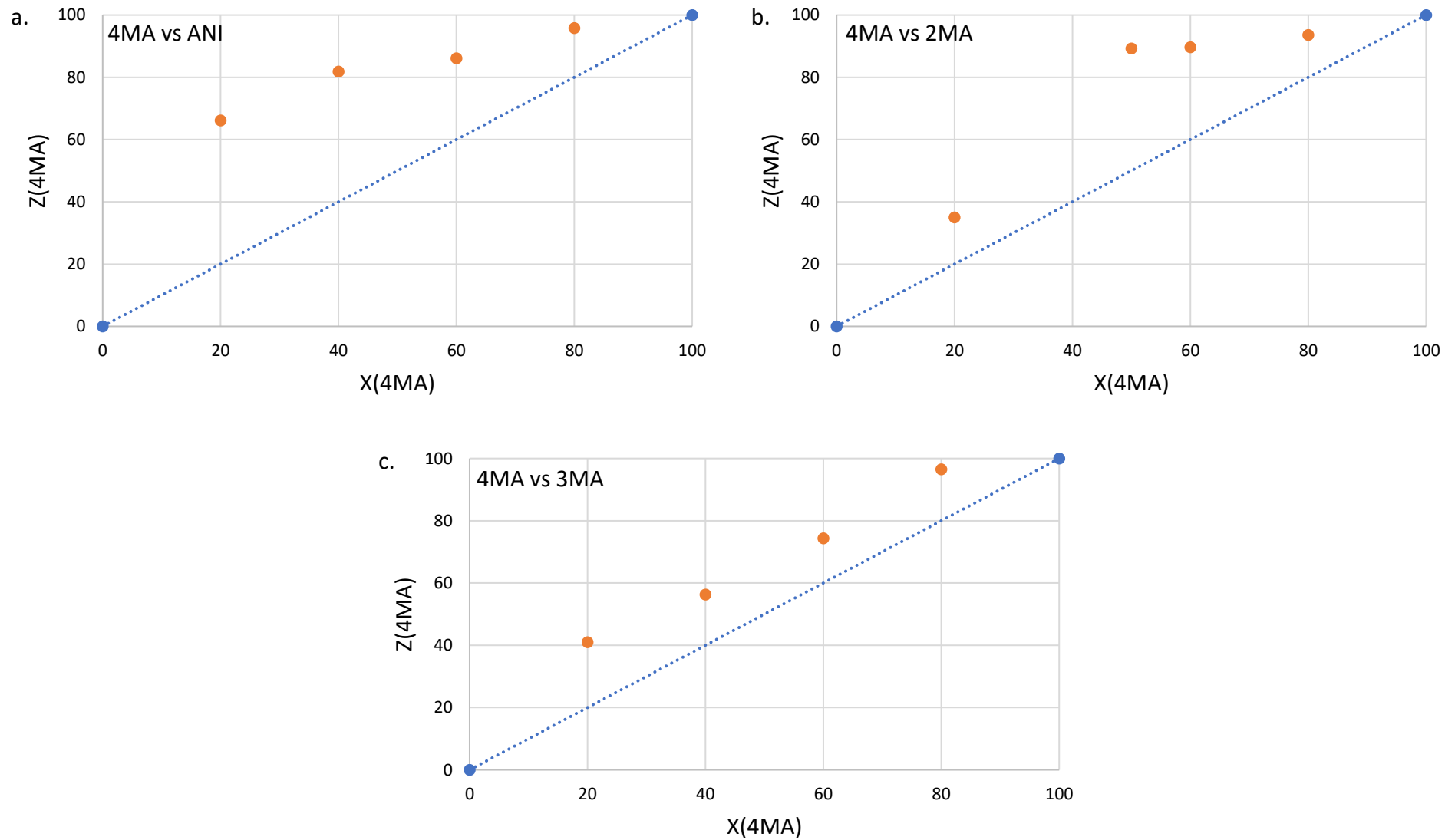


**Figure 6.2:** Selectivity profiles of **H1** in a) 4MA/ANI, b) 4MA/2MA and c) 4MA/3MA binary solutions



**Table 6.3:**  $K_{ave}$  values for the binary guest competition experiments with **H1** in the anisoles

Binary mixture	$K_{ave}$
4MA/ANI	6.1
4MA/2MA	5.0
4MA/3MA	3.4

The GC data that allowed for the construction of Figures 6.2a–c are provided in the SI (Figures S47–49).

#### 6.2.4 Single crystal X-ray diffraction experiments

Suitable crystals of the single solvent complexes were analysed by means of SCXRD experiments with the exception of 2(**H1**)·2MA, which was recovered as a fine powder. In **H1**·3MA and **H1**·4MA, the guest molecules were disordered around an inversion point, while there were two guest molecules in the unit cell of 2(**H2**)·3(ANI): one ANI was also disordered around an inversion point while the second ANI molecule showed no disorder whatsoever.

A summary of the applicable crystallographic data for these SCXRD experiments is provided in Table 6.4. All three of the complexes crystallized in the triclinic crystal system and space group  $P\bar{1}$ . Owing to the very similar unit cell dimensions for **H1**·3MA and **H1**·4MA, it could be concluded that these two complexes shared a common host packing. In 2(**H2**)·3(ANI), however, this packing was unique.

Host-guest unit cell and packing figures were prepared using Mercury software for each of the three complexes,<sup>111</sup> as well as void diagrams to observe the nature of the guest accommodation, whether in channels or discrete cages, by removing each guest from the packing calculation and analysing the spaces that remained with a probe of 1.2 Å diameter. These are provided in Figures 6.3a–c for **H1**·3MA, **H1**·4MA and 2(**H2**)·3(ANI), respectively. It is clear from the first two of these (Figures 6.3a and b) that the host packing in the complex containing 3MA and 4MA is indeed isostructural, and that both types of guest molecules were housed in wide open and infinite channels that were parallel to the a-axis. A visual inspection of the dimensions of these channels (feasible since host molecules are the same size in both figures) suggests that 4MA occupied channels that were ever so slightly less extensive compared with those in which 3MA was accommodated. In the 3(**H2**)·2(ANI) complex, ANI was also housed in channels, but these were multi-directional (along both the a- and c-axes, Figure 6.3c).

With the knowledge that the host packing in **H1**·3MA and **H1**·4MA was isostructural (and both enjoyed the same H:G ratios, 1:1, Table 6.1), it was deemed reasonable that one might expect 3MA and 4MA to compete effectively with one another for **H1** when present in mixtures. However, from Table 6.2, this was clearly not the case, and 4MA was overwhelmingly preferred in the binary equimolar mixture containing these two guests (84.4 %). The question therefore arose as to why this was the case, why did 3MA not compete successfully with 4MA for the spaces in crystals of the complex if the host packing was isostructural. Clearly, the host packing with 4MA must have offered advantages compared to packing with 3MA. We therefore considered the densities of the crystals of **H1**·3MA and **H1**·4MA (Table 6.4) and found that these differed somewhat (1.184 and 1.214 g·cm<sup>-1</sup>, correspondingly). This, in itself, is significant since the chemical formulae of the two complexes are identical (Table 6.4). Also notable are the unit cell void volumes upon removing the guest molecules from the packing calculations, which was 29.4% in the case of the 3MA-containing complex and only 25.1% for that with 4MA. Therefore, 3MA required more space for it to be included while 4MA used less space (as is expected given the more streamlined geometry of 4MA relative to 3MA). We therefore conclude that one of the reasons for the preference of **H1** for 4MA in 3MA/4MA mixtures was due to a more optimal (tighter) packing of the host molecules in the unit cell.

**Table 6.4:** Crystallographic data for the **H1·3MA**, **H1·4MA** and **2(H2)·3(ANI)**

	<b>H1·3MA</b>	<b>H1·4MA</b>	<b>2(H2)·3(ANI)</b>
Chemical formula	C <sub>44</sub> H <sub>36</sub> N <sub>2</sub> ·C <sub>8</sub> H <sub>10</sub> O	C <sub>44</sub> H <sub>36</sub> N <sub>2</sub> ·C <sub>8</sub> H <sub>10</sub> O	2(C <sub>44</sub> H <sub>40</sub> N <sub>2</sub> )·3(C <sub>7</sub> H <sub>8</sub> O)
Formula weight	714.91	714.91	1516.96
Crystal system	Triclinic	Triclinic	Triclinic
Space group	<i>P</i> $\bar{1}$	<i>P</i> $\bar{1}$	<i>P</i> $\bar{1}$
$\mu$ (Mo-K $\alpha$ )/mm <sup>-1</sup>	0.070	0.071	0.071
a/Å	8.8540(4)	8.7789(5)	12.3235(7)
b/Å	10.4874(5)	10.3493(6)	13.4341(8)
c/Å	11.4956(6)	11.4397(6)	13.8154(8)
alpha/°	96.485(2)	96.560 (2)	106.750(2)
beta/°	102.370(2)	102.110 (2)	93.267(2)
gamma/°	102.734(2)	102.726 (2)	102.939(2)
<i>V</i> /Å <sup>3</sup>	1002.53(9)	976.14(10)	2103.6(2)
Z	1	1	1
D(calc)/g·cm <sup>-1</sup>	1.184	1.214	1.198
F(000)	380	380	810
Temp./K	296	200	296
Restraints	136	60	68
Nref	4954	4815	10394
Npar	282	282	558
R	0.0478	0.0407	0.0437
wR2	0.1446	0.1114	0.1208
S	1.05	1.05	1.03
$\theta$ min–max/°	1.8, 28.3	1.8, 28.3	1.6, 28.3
Tot. data	35289	36097	73977
Unique data	4954	4816	10394
Observed data [ <i>I</i> > 2.0 sigma( <i>I</i> )]	4009	4183	8283
R <sub>int</sub>	0.020	0.019	0.017
Completeness	0.999	0.998	0.999
Min. resd. dens. (e/Å <sup>3</sup> )	–0.31	–0.20	–0.17
Max. resd. dens. (e/Å <sup>3</sup> )	0.30	0.32	0.28

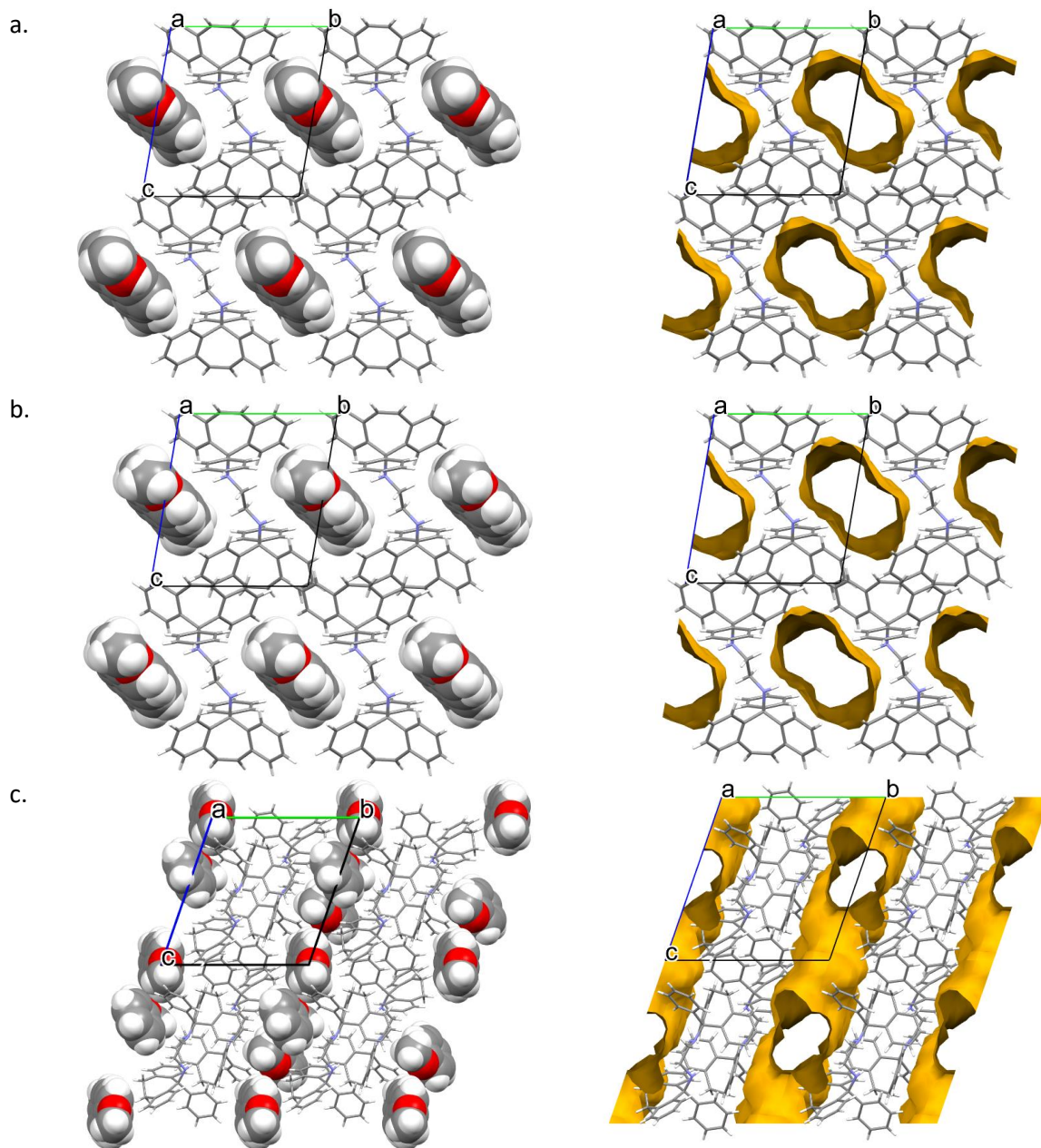


**Figure 6.3:** Unit cells (left) and void diagrams (right) for a. **H1**·3MA, b. **H1**·4MA and c. 2(**H2**)·3(ANI)

The non-covalent interactions in the two isostructural complexes (**H1**·3MA and **H1**·4MA) were subsequently compared. Each of the two complexes experienced one significant intermolecular (host) $\pi\cdots\pi$ (host) interaction between two aromatic moieties of the tricyclic fused ring systems (Figure 6.4) and one intermolecular (host)C–H $\cdots\pi$ (host) contact (Figure 6.5). These measured 3.645 (**H1**·3MA) and 3.636 Å (**H1**·4MA) (slippages were 0.833 and 0.822 Å, respectively), and 2.761 (**H1**·3MA) and 2.682 Å (**H1**·4MA) (H $\cdots\pi$ ) (with both corresponding C–H $\cdots\pi$  angles being 151°). These  $\pi\cdots\pi$  and C–H $\cdots\pi$  interactions in the latter complex were much shorter than in the former, and it is plausible that these shorter distances were responsible for the greater density of crystals of **H1**·4MA

compared with **H1**·3MA, thus facilitating a tighter packing between the host molecules in the 4MA-containing complex. These observations therefore explain the preferential behaviour of **H1** towards 4MA compared with 3MA. Furthermore, in **H1**·3MA were also observed four short intermolecular interactions, three of these between host and guest molecules, and one involving host molecules only. The first three interactions were of the (host)C–C⋯C–C (guest), (host)N–H⋯C–C(guest) and (host)C–H⋯H–C(guest) types, with distances and angles of 2.74 (118°), 2.89(2) (151.3(13)°) and 2.29 (156°) Å, respectively (Table 6.5). The fourth was a (host)C–H⋯H–C(host) close contact that measured 2.21 Å (121°). **H1**·4MA, on the other hand, experienced three short intermolecular contacts and none of them were between host and guest molecules (this complex was thus a true clathrate): these (host)C–H⋯H–C(host), (host)C–H⋯C–C(host) and (guest)C–H⋯H–C(guest) interactions had distances of 2.16 and 2.85 Å (119 and 139°) for the host⋯host interactions, and 2.37 Å (152°) in the case of the interaction between guest molecules. Finally, in both complexes, two intramolecular non-classical hydrogen bonds were also identified. These were of the (host)C–H⋯N(host) type, and measured 2.38 (**H1**) and 2.37 Å (**H2**) (with understandably small angles, 104°) (Table 6.6).

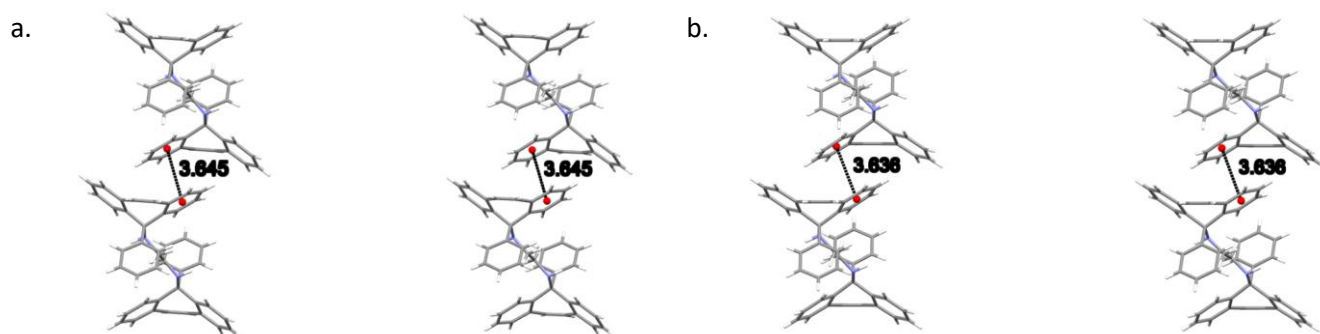


**Figure 6.4:** Stereoviews of the intermolecular (host) $\pi$ ⋯ $\pi$ (host) interactions in a. **H1**·3MA and b. **H1**·4MA

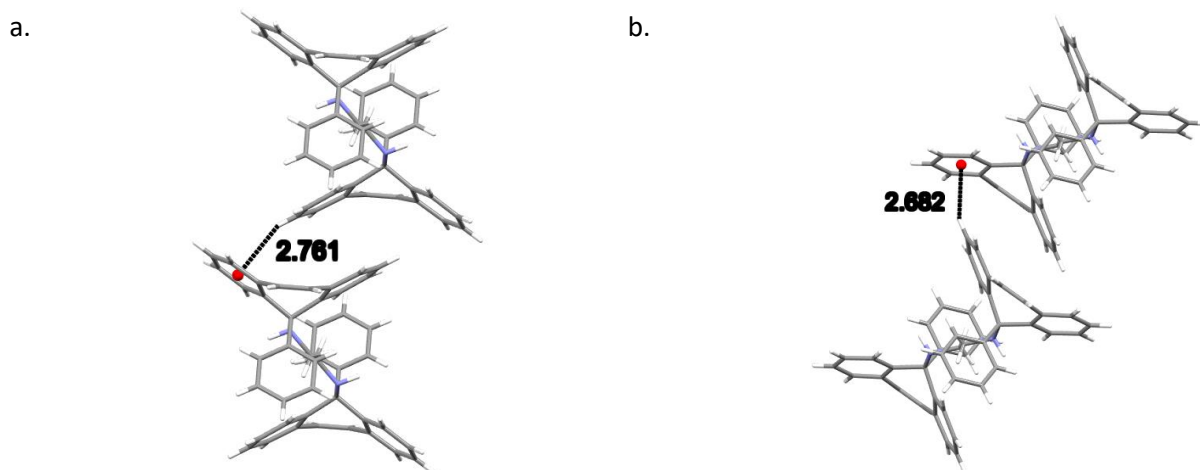


**Figure 6.5:** Intermolecular (host)C–H···π(host) interactions in the a. **H1·3MA** and b. **H1·4MA** complexes

**Table 6.5:** Characteristics of the intermolecular short contacts for complexes **H1·3MA**, **H1·4MA** and **3(H2)·2(ANI)<sup>a</sup>**

Interaction	<b>H1·3MA</b>	<b>H1·4MA</b>	<b>2(H2)·3(ANI)</b>
(host)C–H···H–C(host)	2.21 Å, 121°, <	2.16 Å, 119°, << 2.85 Å, 139°, <	None
(guest)C–H···H–C(guest)	None	2.37 Å, 152°, <	None
(host)C–H···C–C(host)	None	None	2.80 Å, 136°, < 2.87 Å, 157°, <
(host)C–C···C–C(host)	None	None	2.87 Å, 147°, <
(host)N–H···H–C(guest)	2.89(2) Å, 151.3(13)°, <	None	None
(host)C–C···H–C(guest)	2.74 Å, 118°, <	None	None
(host)C–H···H–C(guest)	2.29 Å, 156°, <	None	None
(host)C–H···O–C(guest)	None	None	2.66 Å, 138°, < (guest 1) 2.62 Å, 161°, < (guest 2)
(guest)C–H···O–C(guest)	None	None	2.68 Å, 129°, <

<sup>a</sup> < denotes contacts less than the sum of the van der Waals radii and << contacts less than this sum minus 0.2 Å

**Table 6.6:** Characteristics of the intramolecular short contacts for complexes **H1·3MA**, **H1·4MA** and **3(H2)·2(ANI)**

Interaction	<b>H1·3MA</b>	<b>H1·4MA</b>	<b>2(H2)·3(ANI)</b>
(host)C–H···N <sub>1</sub> (host)	2.38 Å, 104° 2.38 Å, 104°	2.37 Å, 104° 2.37 Å, 104°	2.34 Å, 104° 2.38 Å, 106°
(host)C–H···N <sub>2</sub> (host)	None	None	2.42 Å, 102°
(host)N <sub>2</sub> –H···N <sub>1</sub> (host)	None	None	2.41 Å, 103° 2.43 (1) Å, 113.8(11)°

The non-covalent C–H··· $\pi$  interactions present in the 2(**H2**)·3(ANI) complex are summarized in Table 6.7. Two intramolecular (host)C–H··· $\pi$ (host) (2.99, 2.79 Å and 127, 141°, an example of which is provided in Figure 9.6a) contacts, one intermolecular (host)C–H··· $\pi$ (host) (2.80 Å, 155°, Figure 6.6b) contact and one intermolecular (guest)C–H··· $\pi$ (host) (2.75 Å, 167°, Figure 6.6c) interaction were each identified. There were several other short intermolecular contacts as well, and these ranged between 2.62 and 2.87 Å (105–161°) (Table 6.5). Finally, both classical and non-classical intramolecular host···host hydrogen bonding interactions were also observed in this complex (Table 6.6), with distances between 2.34 and 2.43 Å (102–113.8(11)°).

**Table 6.7:** Characteristics of four C–H··· $\pi$  interactions in 2(**H2**)·3(ANI)

Interaction	H··· $\pi$ /Å	C–H··· $\pi$ /°
(host)C–H··· $\pi$ (host) <sup>a</sup>	2.99	127
(host)C–H··· $\pi$ (host) <sup>a</sup>	2.79	141
(host)C–H··· $\pi$ (host) <sup>b</sup>	2.80	155
(guest 1)C–H··· $\pi$ (host) <sup>b,c</sup>	2.75	167

<sup>a</sup> Intramolecular interaction

<sup>b</sup> Intermolecular interaction

<sup>c</sup> Guest 1 refers to one of the disordered guest components that was modelled.

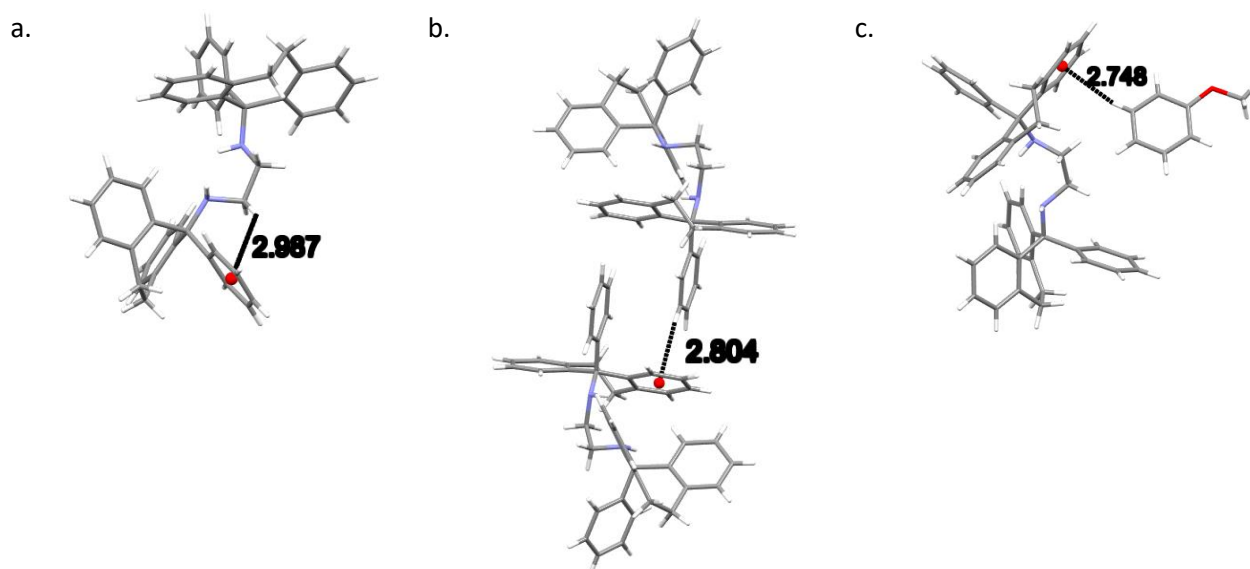


**Figure 6.6:** Depiction of a. one of the intramolecular (host)C–H··· $\pi$ (host), b. the only intermolecular (host)C–H··· $\pi$ (host) and c. the only intermolecular (guest)C–H··· $\pi$ (host) interactions in 2(**H2**)·3(ANI)

These SCXRD data have therefore demonstrated why 4MA was preferred by **H1** rather than 3MA (where higher crystal densities were noted in the 4MA-containing complex as a result of tighter packing which was facilitated by shorter intermolecular host···host contacts).

### 6.2.5 Thermal analysis

The thermogravimetric (TG), its derivative (DTG), and differential scanning calorimetric (DSC) traces are provided (overlaid) in Figures 6.7a–c (**H1**) and 6.8 (**H2**), while the more important data from these traces are summarized in Table 6.8.

**Table 6.8:** Thermal data for the 2(**H1**)·2MA, **H1**·3MA, **H1**·4MA and 2(**H2**)·3(ANI) complexes

Complex	T <sub>on</sub> /°C <sup>a</sup>	Calculated mass loss/%	Experimental mass loss/%
2( <b>H1</b> )·2MA	136.1	9.5	8.1
<b>H1</b> ·3MA	70.5	17.1	16.3
<b>H1</b> ·4MA	104.9	17.1	17.1
2( <b>H2</b> )·3(ANI)	<sup>b</sup>	21.4	14.2 <sup>b</sup>

<sup>a</sup> T<sub>on</sub> is the onset temperature for the guest release process and a measure of the thermal stability of the complex, and was estimated from the DTG/TG

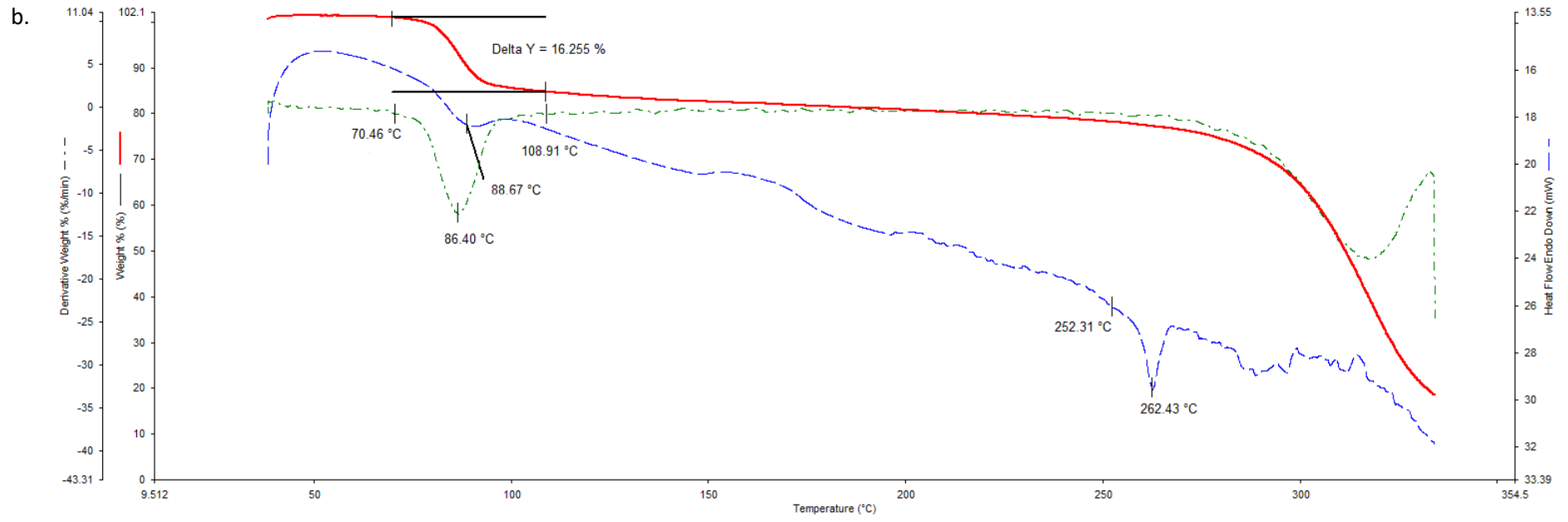
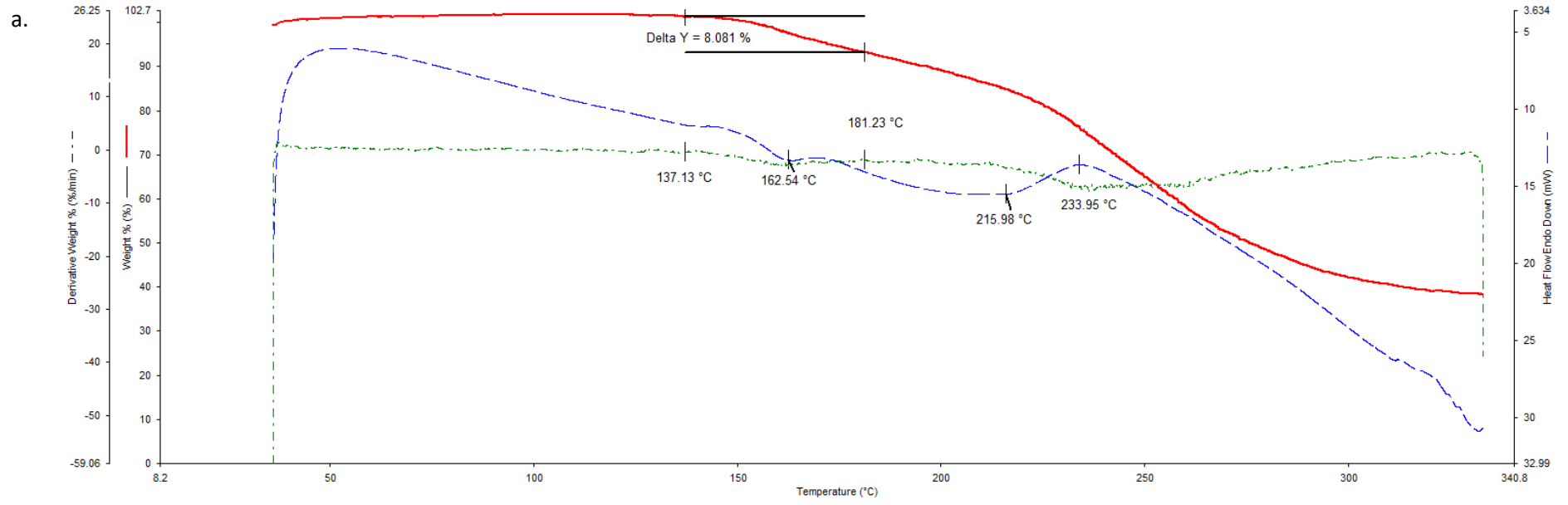
<sup>b</sup> Some guest escaped from the crystals during sample preparation

If one compares the onset temperatures for the guest release process (T<sub>on</sub>, which is a measure of relative thermal stability of complexes) for **H1**·3MA and **H1**·4MA (Figures 6.7a and b), it is clear that the latter inclusion compound is considerably more thermally stable than the former (T<sub>on</sub> 104.9 compared with 70.5 °C) (Table 6.8). This is in accordance with the observations made in both the guest/guest competition (where 4MA was significantly preferred over 3MA) and the SCXRD (where crystals of the 4-MA-containing complex possessed a higher density and shorter intermolecular host···host interactions than that containing 3MA) experiments. In both complexes, the guest release is via a single step, and expected and calculated mass loss measurements concurred closely (expected 17.1%, observed 16.3 and 17.1%, respectively). These guest release processes were then followed by the host melt endotherm which commenced at 251.1 and 252.3 °C, and which is in agreement with the literature (255 °C<sup>98</sup>). It is unfortunate that 2(**H1**)·2MA crystallized out as a powder and therefore that the reason for its high thermal stability (T<sub>on</sub> 136.1 °C) could not be established since a SCXRD experiment was not possible. However, it must be noted that the thermal trace for this complex was not unambiguous (Figure 6.7a): while the expected mass loss (9.5%) was



in reasonable agreement with that measured (8.1%), the guest release and host melt events are not obvious in this figure.

In the case of the 2(**H2**)·3(ANI) complex, the expected (21.4%) and measured (14.2%) mass losses differed significantly. It is proposed that some of the anisole guest escaped from its channels in the crystals of the complex during the preparation of the sample for thermal analysis, and so the mass loss measured was much lower than required for this 2:3 complex. Once more, the host melt endotherm is not obvious in this figure (the literature melting point of **H2** is between 186 and 187 °C<sup>98</sup>).



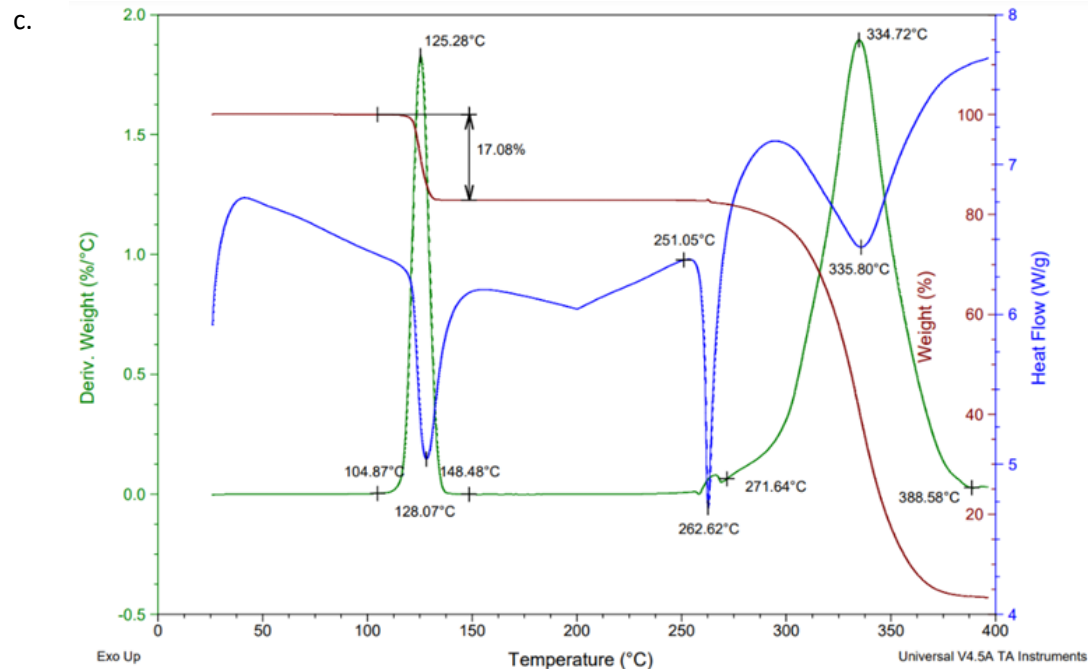


Figure 6.7: Overlaid TG, DTG and DSC traces for a. 2(H1)·2MA, b. H1·3MA and c. H1·4MA

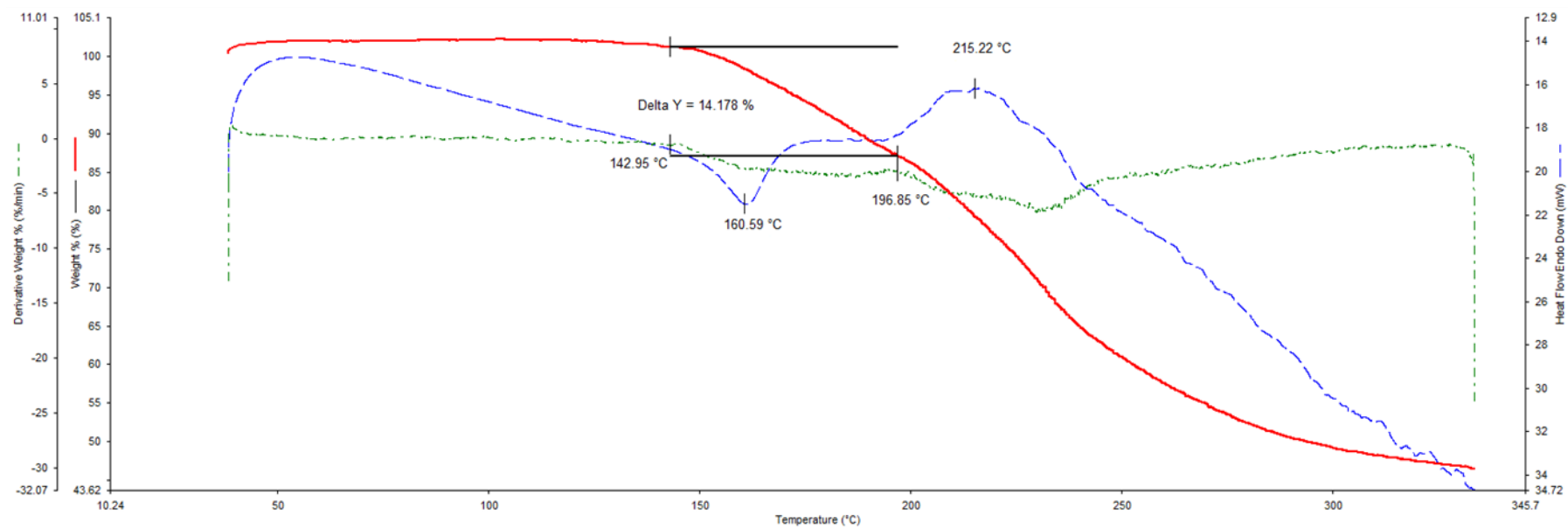


Figure 6.8: Overlaid TG, DTG and DSC traces for  $2(\text{H}_2) \cdot 3(\text{ANI})$

### 6.3 Conclusion

In this work, it was demonstrated that **H1** possessed a high affinity for 4MA in mixtures containing this guest, even though both 2MA and 3MA were also enclathrated in the single solvent recrystallization experiments: the H:G ratios were 2:1 (2MA) and 1:1 (both 3MA and 4MA). In the crystals from equimolar binary ANI/4MA, 2MA/4MA and 3MA/4MA solutions were measured between 84.4 and 91.7% 4MA. Remarkably, in the absence of 4MA, only apohost compound was recovered from the glass vessels. Selectivity profiles and their associate  $K_{ave}$  values in the 4MA/ANI, 4MA/2MA and 4MA/3MA solutions revealed that, while 4MA was consistently preferred across the concentration range,  $K_{ave}$  values (3.4–6.1) were not high enough to put **H1** forward as a suitable host candidate for these anisole separations. SCXRD experiments revealed the reasons for the affinity of **H1** for 4MA relative to 3MA: the intermolecular host···host C–H··· $\pi$  and  $\pi$ ··· $\pi$  interactions in the complex containing the preferred guest (4MA) were significantly shorter than in the complex with 3MA (note that no host···guest interactions were observed in **H1**·4MA, and this complex was therefore described as a true clathrate). This, in turn, led to a higher crystal density in **H1**·4MA (1.214 g·cm<sup>-3</sup>) compared with **H1**·3MA (1.184 g·cm<sup>-3</sup>) despite their identical chemical formulae, and implies that the complex with 4MA experiences a tighter and more stabilized host packing. This was confirmed by thermal analyses: the onset temperature for the guest release process of **H1**·4MA (104.9 °C) was much higher than for **H1**·3MA (70.5 °C). Both guest compounds, however, were observed to reside in wide open channels. Unfortunately, the 2MA-containing complex crystallized out as a powder and SCXRD analyses could not be employed in order to understand the guest retention mode in the crystals. This complex, however, experienced a high  $T_{on}$ , 136.1 °C, despite 2MA being significantly less preferred by **H1** than 4MA ( $T_{on}$  = 104.9 °C). Finally, the thermal traces for 2(**H1**)·2MA were not unambiguous and the host melt endotherm could not be clearly discerned on the DSC trace.

Unfortunately, **H2** only complexed with ANI, and no guest/guest competition experiments could be carried out owing to the very slow (months) recrystallization process of **H2** from these mixed guests (if crystallization occurred at all). However, ANI was observed to be held in the crystals of the complex by means of a number of short contacts by SCXRD experiments.

Despite this, the complex stability remained low since some guest escaped from the crystals at ambient conditions during sample preparation for thermal analysis.

## 7. Final remarks

This dissertation reports on the potential of two host compounds, *N,N'*-bis(5-phenyl-5-dibenzo[*a,d*]cycloheptenyl)ethylenediamine (**H1**) and *N,N'*-bis(5-phenyl-10,11-dihydro-5-dibenzo[*a,d*]cycloheptenyl)ethylenediamine (**H2**), to separate the constituents of three guest series, the xylene isomers and ethylbenzene, pyridine and its methylated isomers, and anisole with its methyl derivatives.

The synthesis of these host compounds was achieved by means of three reaction steps, namely a Grignard addition reaction of PhMgBr on the corresponding tricyclic fused aromatic ketones to afford the two alcohols, which were converted into perchlorate salts with perchloric acid, and then treated with ethylenediamine to furnish the host products **H1** and **H2**.

In the Xy/EB guest series, **H1** only formed a complex with *p*-Xy, while **H2** solely included *o*-Xy, in the single solvent experiments; all other experiments afforded apohost alone. The H:G ratios of both complexes was 1:1. Recrystallization experiments from equimolar mixed guests that did not have *p*-Xy (for **H1**) and *o*-Xy (**H2**) present also afforded only apohost compound. Experiments in the binary equimolar mixtures showed **H1** to have an overwhelming preference for *p*-Xy when the other guest solvents present were *m*-Xy, *o*-Xy or EB (87.2–88.7%); **H2**, on the other hand, favoured *o*-Xy when the other guest solvents were *p*-Xy and EB (91.3 and 88.1%, respectively). However, when *m*-Xy was present, the host (**H2**) selectivity declined (73.1%). The ternary mixtures with **H1** that did not form apohost revealed that the selectivity for *p*-Xy remained above 80% in all cases, while the quaternary solution afforded a mix complex that contained 76.7% *p*-Xy. **H2**, on the other hand, displayed much lower selectivities in the equimolar ternary mixtures and also in the quaternary solution (69.1–83.7 and 61.4%, respectively); the selectivity of **H1** for *p*-Xy was thus greater than that of **H2** for *o*-Xy. Constructed selectivity profiles largely concurred with the equimolar guest/guest competition experiments. The SCXRD analyses demonstrated that in the **H1**·*p*-Xy complex, the guest species was housed in wide open channels and was considered a true clathrate (as there were no non-covalent contacts between host and guest molecules), while *o*-Xy in **H2**·

*o*-Xy was housed in near discrete cavities and experienced interactions with the host molecule. These observations from the SCXRD data were further explained by thermoanalytical experiments, where **H1**·*p*-Xy was unstable at ambient conditions owing to the wide-open channels that the guests were housed in and the absence of any interactions between host and guest. **H2**·*o*-Xy, however, was stable at room temperature and  $T_{on}$  was 69.7 °C: this was as a result of the guest molecules residing in near-discrete cavities and the presence of host···guest interactions. Finally, it was concluded that both host compounds possessed the ability to effect the separations of a number of these C<sub>8</sub>H<sub>10</sub> isomeric mixtures.

In PYR/MP mixtures, **H2** was a much more selective host compound compared with **H1**: the former host compound formed complexes with only PYR and 4MP, while the latter enclathrated all four guests from this series. H:G ratios varied. **H1** possessed an affinity for 2MP, more usually, while PYR was favoured by **H2** in the equimolar experiments. Selectivity profiles suggested that **H1** has the ability to separate 2MP/PYR mixtures when the amount of 2MP present is 40%;  $K$  was calculated to be 11.8 in this experiment. **H2**, however, demonstrated remarkable affinities for PYR in PYR/2MP and PYR/3MP solutions even in mixtures containing low concentrations of PYR.  $K$  values were exceedingly high in these experiments (with  $K_{ave}$  of 76.9 and 17.2, respectively), and so **H2** is able to separate these mixtures effectively. SCXRD experiments demonstrated that shorter classical hydrogen bonding contacts were present in both **H1**·2(2MP) and **H2**·2(PYR) between host and guest molecules, shorter than in the other complexes, and thus explained the affinities of the two host compounds for 2MP and PYR, respectively. Thermal analyses showed that these two complexes were also more thermally stable, with  $T_{on}$  values of 63.2 and 76.5 °C for these complexes with **H1** and **H2**, respectively.

In ANI/MA mixtures, **H2** required a long period of time to crystallize, and so the behaviour of this host compound in such mixtures could not be compared with **H1**. Furthermore, this host compound (**H2**) was therefore also deemed an unsuitable candidate for such separations in a practical sense. However, **H2** was able to form a 2:3 complex with ANI, while gels remained in the glass vessels when the other three solvents were employed. A SCXRD experiment on this complex showed that a number of short contacts were present between host and host,



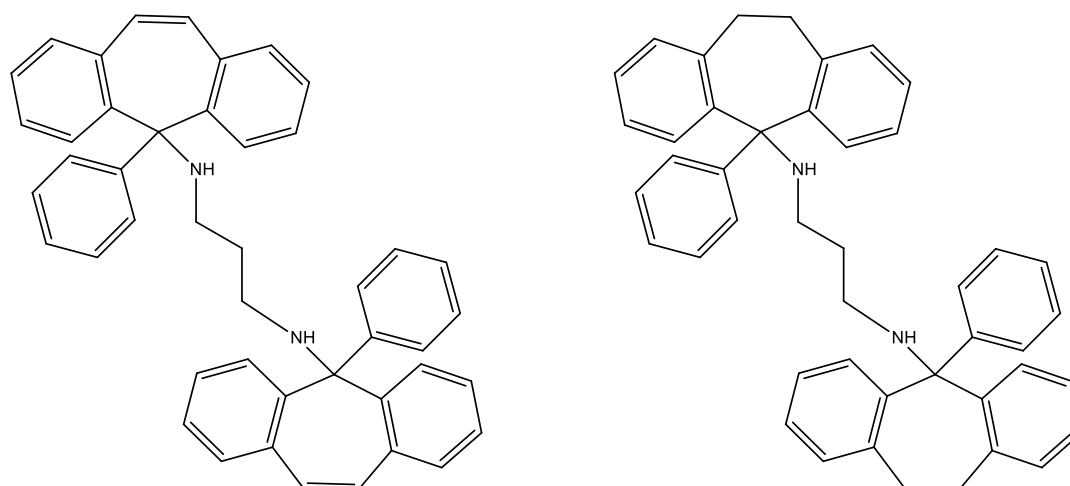
and host and guest, molecules. Thermal analyses demonstrated that the complex was not stable at ambient conditions. **H1**, on the other hand, formed inclusion complexes with 2MA, 3MA and 4MA (with H:G ratios of 2:1, 1:1 and 1:1, respectively). Surprisingly, even though the host compound included three of the four guest solvents, complexation was only successful in the guest/guest competition experiments when 4MA was present; in its absence, only apohost was recovered. In the binary equimolar ANI/4MA, 2MA/4MA and 3MA/4MA mixtures, the crystals that formed contained between 84.4 and 91.7% 4MA. Selectivity profiles suggested however, due to the low  $K$  values calculated ( $K_{ave}$  3.4–6.1), that **H1** was not suitable for separating these anisole/methylanisole mixtures. The preference of **H1** for 4MA in mixed solvents compared to 3MA was explained by SCXRD experiments: **H1**·4MA had significantly shorter host···host C–H··· $\pi$  and  $\pi$ ··· $\pi$  interactions. However, the **H1**·4MA complex was a true clathrate (there were no host···guest interactions at all). **H1**·4MA also had a higher crystal density ( $1.214 \text{ g} \cdot \text{cm}^{-3}$ ) compared to that of **H1**·3MA ( $1.184 \text{ g} \cdot \text{cm}^{-3}$ ) despite having identical chemical formulae, which showed that 4MA experienced tighter and more stabilized host packing. Thermal analyses also confirmed this, as the  $T_{on}$  for 4MA was much higher ( $104.9 \text{ }^\circ\text{C}$ ) compared to that of 3MA ( $70.5 \text{ }^\circ\text{C}$ ). No SCXRD analysis could be carried out on the complex of **H1** with 2MA due to poor crystal quality; however, this complex had the highest  $T_{on}$  ( $136.1 \text{ }^\circ\text{C}$ ) even though 2MA was not the most preferred guest solvent.

## 8. Future work

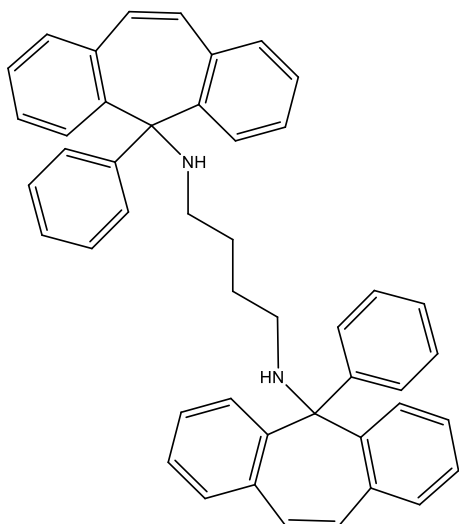
In this work, only three guest series were employed (Xy/EB, PYR/MP and ANI/MA). There are many more isomeric aromatic guest solvents that may be investigated that are extremely challenging to separate on an industrial scale by distillations/crystallizations. Some of these are the nitrotoluenes, toluidines, bromoanisoles, cresols, and dihydroxybenzenes, to mention only a few.

Since it was not possible to obtain a crystal structure of **H1**, this host compound, in powder form, will be analysed by means of synchrotron experiments, in order to observe the geometry of this host compound in the absence of guest. This can then be compared with the results from computational calculations.

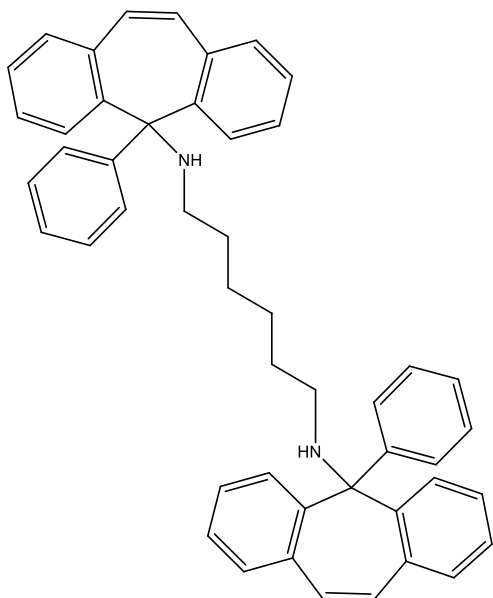
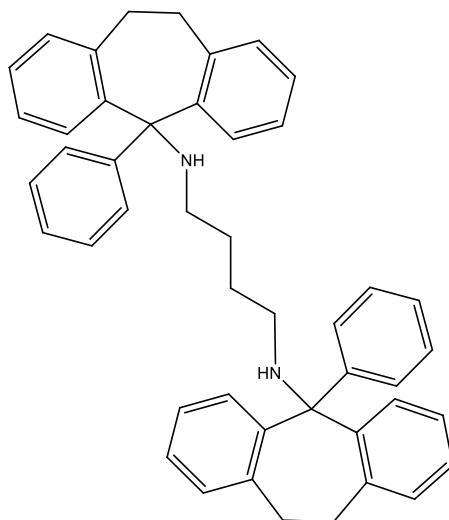
Both of these host compounds can be further modified to afford 18 new potential host compounds. The structures of these are provided in Figure 8.1, and are as a result of changing the nature of the linkers between the tricyclic fused systems. (The names of these linkers are provided beneath the structures.)



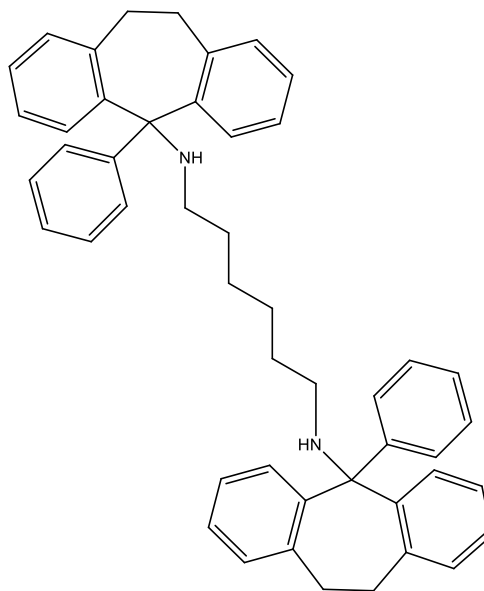
1,3-Diaminopropane

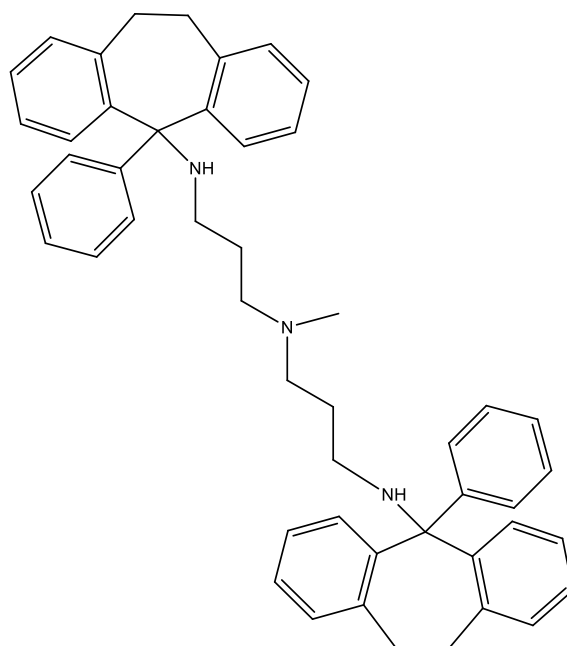
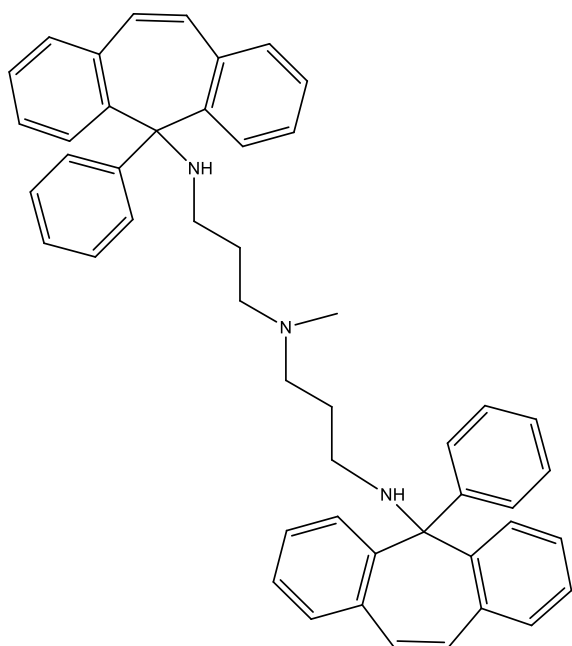


1,4-Diaminobutane

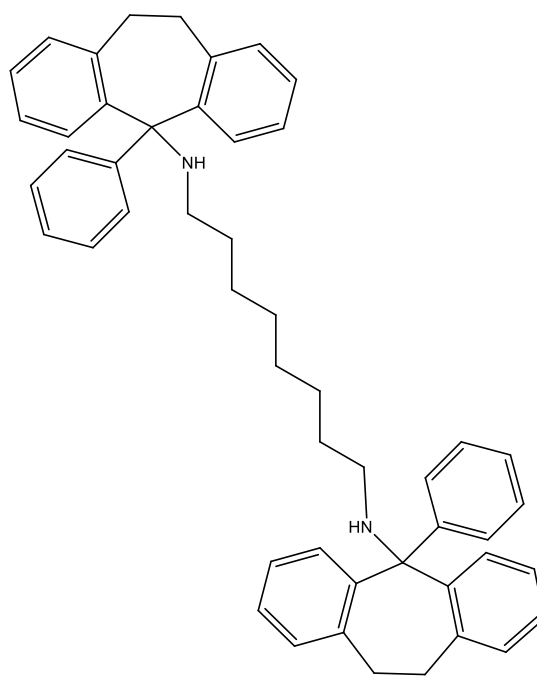
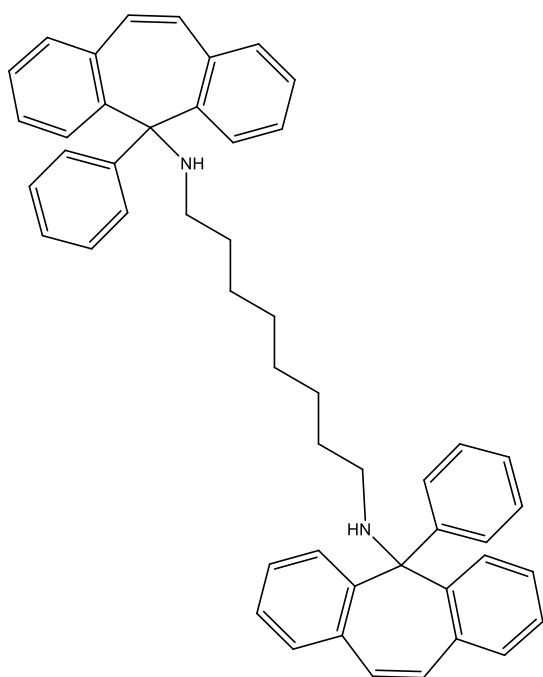


1,6-Diaminohexane

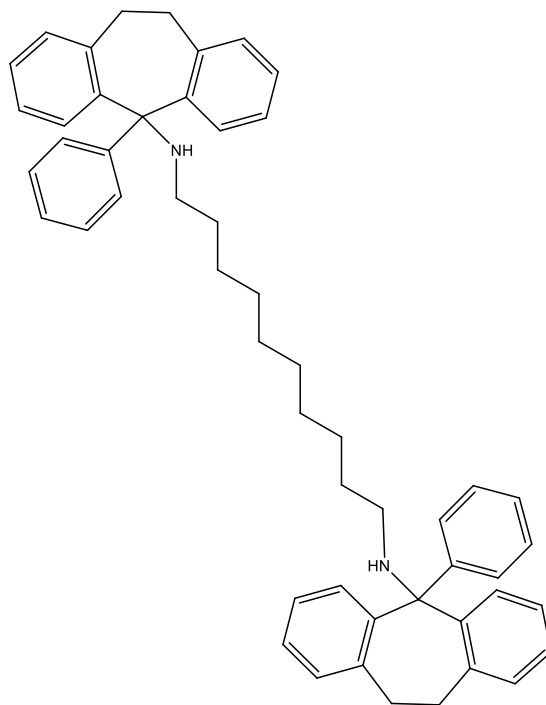
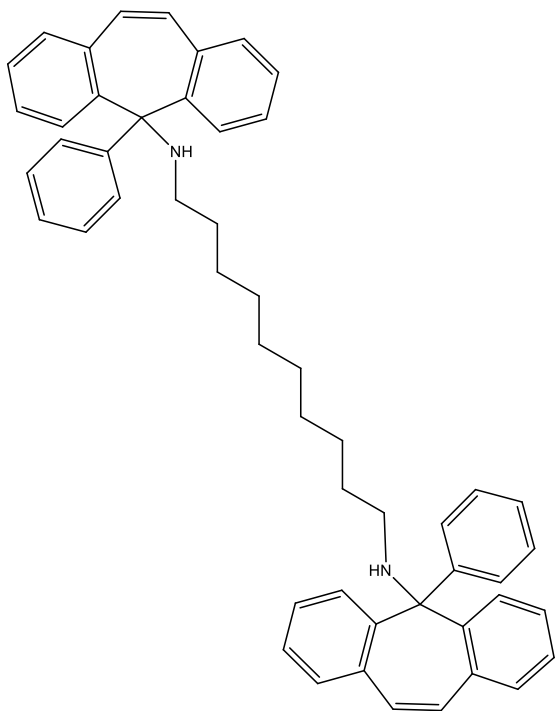




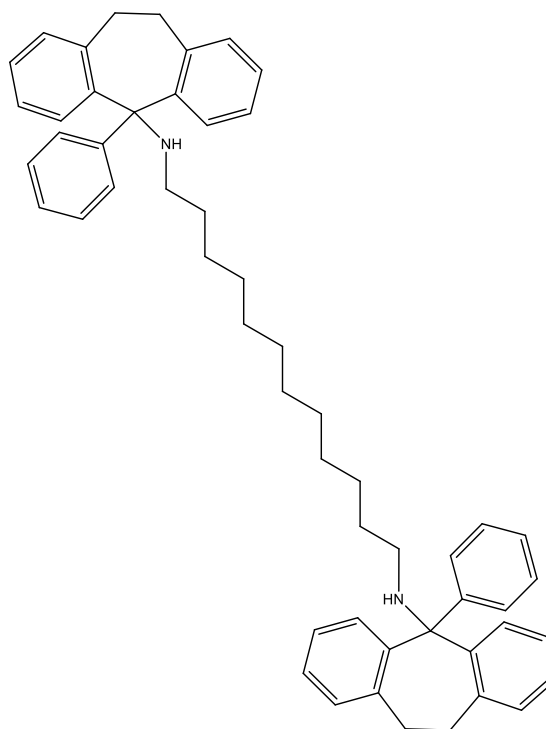
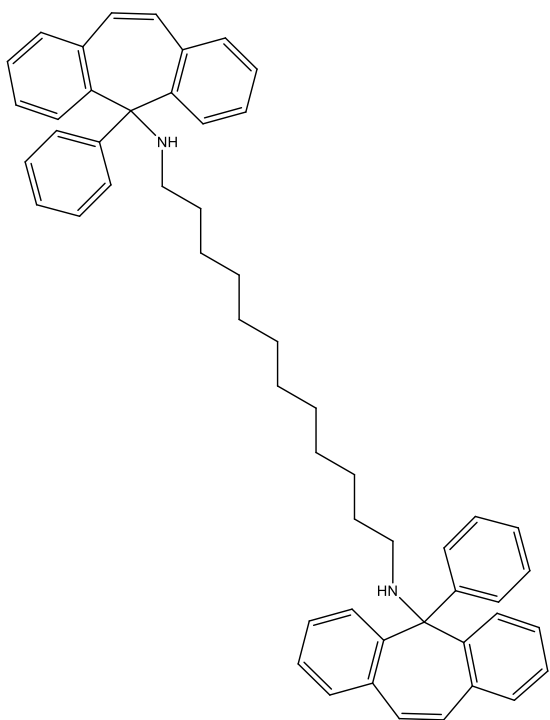
3,3'-Diamino-*N*-methyldipropylamine



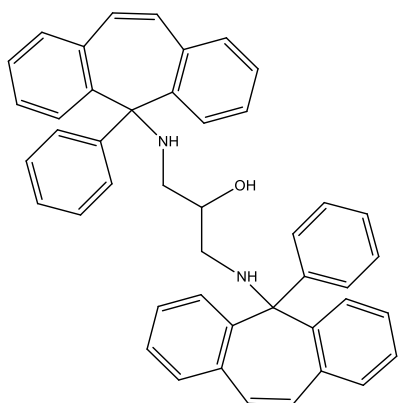
1,8-Diaminooctane



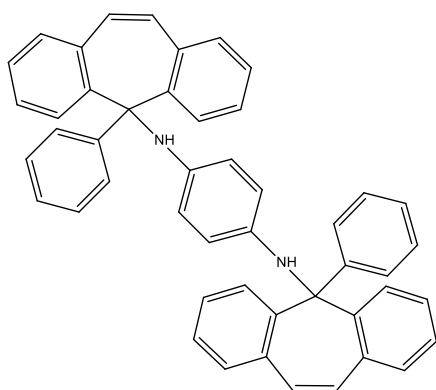
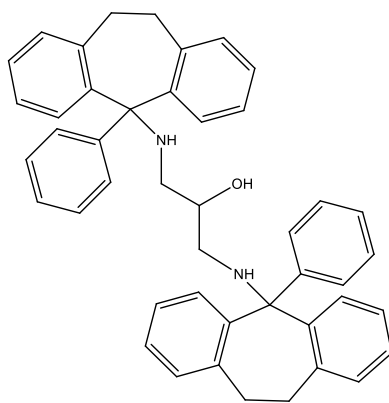
1,10-Diaminododecane



1,12-Diaminododecane



1,3-Diamino-2-propanol



1,4-Benzenediamine

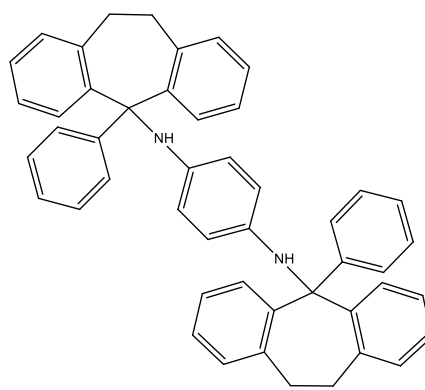


**Figure 8.1:** The structures of potential novel future host compounds

These proposed host compounds may display different and complementary selectivity behaviours in isomeric mixtures.

## References

1. Lehn, J.-M. Supramolecular Chemistry—Scope and Perspectives Molecules, Supermolecules, and Molecular Devices (Nobel Lecture). *Angew. Chem. Int. Ed. Engl.* **1988**, *27* (1), 89–112.
2. Steed, J. W.; Atwood, J. L. *Supramolecular Chemistry*, 2nd ed.; John Wiley & Sons: Chichester, West Sussex, **2022**.
3. *Comprehensive Supramolecular Chemistry II.*; Atwood, J. L., Gokel, G. W., Barbour, L. J., Eds.; Elsevier: Amsterdam, Netherlands, **2017**; Vol. 1.
4. Cram, D. J. Preorganization - from Solvents to Spherands. *Angew. Chem. Int. Ed. Engl.* **1986**, *25* (12), 1039–1057.
5. Vincenti, M. Special Feature: Perspective. Host-Guest Chemistry in the Mass Spectrometer. *J. Mass Spectrom.* **1995**, *30* (7), 925–939.
6. Dorfling, S. *Assessment of the host potential of TETROL [(+)-(2R,3R)-1,1,4,4-tetraphenylbutane-1,2,3,4-tetraol] for the separation of isomers and related compounds*; Nelson Mandela University: Port Elizabeth, **2017**.
7. Wenz, G. An Overview of Host-Guest Chemistry and Its Application to Nonsteroidal Anti-Inflammatory Drugs. *Clin. Drug Investig.* **2000**, *19* (Supplement 2), 21–25.
8. Wittenberg, J. B.; Isaacs, L. *Complementarity and Preorganization. Supramolecular Chemistry*; John Wiley & Sons, Ltd: Chichester, UK, **2012**.
9. Atwood, J. L.; Steed, J. W. *Encyclopaedia of Supramolecular Chemistry*; M. Dekker: New York, **2004**.
10. Carey, J. Affinity, Specificity, and Cooperativity of DNA Binding by Bacterial Gene Regulatory Proteins. *Int. J. Mol. Sci.* **2022**, *23*, 562–577.
11. Piper, J. W.; Swerlick, R. A.; Zhu, C. Determining Force Dependence of Two-Dimensional Receptor-Ligand Binding Affinity by Centrifugation. *Biophys. J.* **1998**, *74* (1), 492–513.
12. Barton, B.; McClelland, C. W.; Taljaard, B. The Synthesis of Novel Enclathration Compounds: Bis(9-Amino-9-Aryl-9H-Thioxanthenes) and Investigations of Their Host–Guest Inclusion Potential. *S. Afr. J. Chem.* **2002**, *55*, 144–148.

13. Barton, B.; Caira, M. R.; Hosten, E. C.; McClelland, C. W.; Weitz, S. Clathrates of TETROL: Further Aspects of the Selective Inclusion of Methylcyclohexanones in Their Energetically Unfavorable Axial Methyl Conformations. *J. Org. Chem.* **2015**, *80* (14), 7184–7192.
14. Barton, B.; Dorfling, S.-L.; Hosten, E. C. Cyclohexanone-Driven Discriminatory Behavior Change of Host Compound (+)-(2R,3R)-TETROL for Isomeric Methylcyclohexanone Guests. *Cryst. Growth Des.* **2017**, *17* (12), 6725–6732.
15. de Jager, L.; Barton, B.; Hosten, E. C. A Comparison of the Behaviour of Two Closely Related Xanthenyl-Derived Host Compounds in the Presence of Vaporous Dihaloalkanes. *J. Incl. Phenom. Macrocycl. Chem.* **2018**, *92* (1–2), 181–194.
16. Schneider, H.-J. *Applications of Supramolecular Chemistry*; Schneider, H.-J., Ed.; CRC Press: London, England, **2012**.
17. Arunan, E.; Desiraju, G. R.; Klein, R. A.; Sadlej, J.; Scheiner, S.; Alkorta, I.; Clary, D. C.; Crabtree, R. H.; Dannenberg, J. J.; Hobza, P.; Kjaergaard, H. G.; Legon, A. C.; Mennucci, B.; Nesbitt, D. J. Definition of the Hydrogen Bond (IUPAC Recommendations 2011). *Pure Appl. Chem.* **2011**, *83* (8), 1637–1641.
18. Kubik, S. *Supramolecular Chemistry: From Concepts to Applications*, 1st ed.; De Gruyter: Berlin, Germany, **2021**.
19. Riley, K. E.; Hobza, P. On the Importance and Origin of Aromatic Interactions in Chemistry and Biodisciplines. *Acc. Chem. Res.* **2013**, *46* (4), 927–936.
20. Beer, P.; Barendt, T.; Lim, J. *Supramolecular Chemistry: Fundamentals and Applications*, 2nd ed.; Oxford University Press: London, England, **2022**.
21. Nishio, M.; Umezawa, Y.; Fantini, J.; Weiss, M. S.; Chakrabarti, P. CH- $\pi$  Hydrogen Bonds in Biological Macromolecules. *Phys. Chem. Chem. Phys.* **2014**, *16* (25), 12648–12683.
22. Sippel, K. H.; Quioco, F. A. Ion-Dipole Interactions and Their Functions in Proteins: Ion-Dipoles in Nature. *Protein Sci.* **2015**, *24* (7), 1040–1046.
23. Bhalla, V. *Supramolecular Chemistry: From Molecule to Molecular Machines*. *Reson.* **2018**, *23* (3), 277–290.
24. Yang, X.; Yuan, D.; Hou, J.; Sedgwick, A. C.; Xu, S.; James, T. D.; Wang, L. Organic/Inorganic Supramolecular Nano-Systems Based on Host/Guest Interactions. *Coord. Chem. Rev.* **2021**, *428*, 213609–213623.
25. Ma, X.; Zhao, Y. Biomedical Applications of Supramolecular Systems Based on Host–Guest Interactions. *Chem. Rev.* **2014**, *115* (15), 7794–7839.



26. Guo, D.-S.; Liu, Y. Supramolecular Chemistry of *p*-Sulfonatocalix[n]arenes and Its Biological Applications. *Acc. Chem. Res.* **2014**, *47* (7), 1925–1934.
27. Perret, F.; Lazar, A. N.; Coleman, A. W. Biochemistry of the *para*-Sulfonatocalix[n]arenes. *Chem. Commun.* **2006**, 2425–2438
28. Perret, F.; Coleman, A. W. Biochemistry of Anionic Calix[n]arenes. *Chem. Commun.* **2011**, *47*, 7303–7319.
29. Atwood, J. L.; Barbour, L. J.; Hardie, M. J.; Raston, C. L. Metal Sulfonatocalix[4,5]arene Complexes: Bilayers, Capsules, Spheres, Tubular Arrays and Beyond. *Coord. Chem. Rev.* **2001**, *222*, 3–32.
30. McMurry, J. *Fundamentals of Organic Chemistry*, Seventh.; Brooks Cole, **2010**.
31. Barton, B.; Senekal, U.; Hosten, E. C. Comparing the Host Behaviour of Roof-Shaped Compounds *trans*-9,10-Dihydro-9,10-Ethanoanthracene-11,12-Dicarboxylic Acid and Its Dimethyl Ester in the Presence of Mixtures of Xylene and Ethylbenzene Guests. *CrystEngComm* **2021**, *23* (25), 4560–4572.
32. Quainoo, T.; Lavan, S. N.; Liu, Z.-F. Van Der Waals Density Functional Study of Hydrocarbon Adsorption and Separation in Metal–Organic Frameworks without Open Metal Sites. *J. Mater. Res.* **2022**, *37* (1), 334–345.
33. Barton, B.; Jooste, D. V.; Hosten, E. C. *Trans-N,N'*-Bis(9-Phenyl-9-Xanthenyl)Cyclohexane-1,2-Diamine and Its Thioxanthenyl Derivative as Potential Host Compounds for the Separation of Anilines through Host–guest Chemistry Principles. *J. Incl. Phenom. Macrocycl. Chem.* **2020**, *97* (3–4), 159–174.
34. Sykes, N. M.; Su, H.; Weber, E.; Bourne, S. A.; Nassimbeni, L. R. Selective Enclathration of Methyl- and Dimethylpiperidines by Fluorenol Hosts. *Cryst. Growth Des.* **2017**, *17* (2), 819–826.
35. Chaves Lima, R.; Bieseki, L.; Melguizo, P. V.; Pergher, S. B. C. *Environmentally Friendly Zeolites: Synthesis and Source Materials*, 1st ed.; Springer Nature: Cham, Switzerland, **2020**.
36. *Molecular Sieves: Principles of Synthesis and Identification*; Szostak, R., Ed.; Kluwer Academic: Dordrecht, Netherlands, **1988**.
37. Rasouli, M.; Yaghobi, N.; Allahgholipour, F.; Atashi, H. *para*-Xylene Adsorption Separation Process Using Nano-Zeolite Ba-X. *Chem. Eng. Res. Des.* **2014**, *92* (6), 1192–1199.

38. Molaei Dehkordi, A.; Khademi, M. Adsorption of Xylene Isomers on Na-BETA Zeolite: Equilibrium in Batch Adsorber. *Microporous Mesoporous Mater.* **2013**, *172*, 136–140.
39. Eddaoudi, M.; Moler, D. B.; Li, H. L.; Chen, B. L.; Reineke, T. M.; O’Keeffe, M.; Yaghi, O. M. Modular Chemistry: Secondary Building Units as a Basis for the Design of Highly Porous and Robust Metal-Organic Carboxylate Frameworks. *Acc. Chem. Res.* **2001**, *34*, 319–330.
40. Li, H.; Eddaoudi, M.; O’Keeffe, M.; Yaghi, O. M. Design and Synthesis of an Exceptionally Stable and Highly Porous Metal-Organic Framework. *Nature* **1999**, *402* (6759), 276–279.
41. Ferey, G. Hybrid Porous Solids: Past, Present, Future. *Chem. Soc. Rev.* **2008**, *37*, 191–214.
42. Gee, J. A.; Zhang, K.; Bhattacharyya, S.; Bentley, J.; Rungta, M.; Abichandani, J. S.; Sholl, D. S.; Nair, S. Computational Identification and Experimental Evaluation of Metal–Organic Frameworks for Xylene Enrichment. *J. Phys. Chem. C* **2016**, *120* (22), 12075–12082.
43. Huang, W.; Jiang, J.; Wu, D.; Xu, J.; Xue, B.; Kirillov, A. M. A Highly Stable Nanotubular MOF Rotator for Selective Adsorption of Benzene and Separation of Xylene Isomers. *Inorganic Chemistry* **2015**, *54* (22), 10524–10526.
44. Salvatierra, D.; Díez, C.; Jaime, C. Host/Guest Interactions and NMR Spectroscopy. A Computer Program for Association Constant Determination. *J. Incl. Phenom. Mol. Recognit. Chem.* **1997**, *27* (3), 215–231.
45. Cragg, P. J. *Supramolecular Chemistry: From Biological Inspiration to Biomedical Applications*. Springer Netherlands, **2010**.
46. Brittain, H. *Analytical Profiles of Drug Substances and Excipients*; Elsevier, **1993**.
47. Barton, B.; de Jager, L.; Hosten, E. C. Host Behavior of *N,N'*-Bis(9-Phenyl-9-Thioxanthanyl)Ethylendiamine in the Presence of Aromatic and Aliphatic Five-Membered Heterocyclic Guests: Selectivity Correlations with Hirshfeld Surface Analyses. *Cryst. Growth Des.* **2019**, *19* (2), 1268–1281.
48. Berlin, H. U. Z. Investigation of Polymers with Differential Scanning Calorimetry. *Adv. Lab DSC Investig. Polym.* **2009**, 1–17.
49. JoVE Science Education Database. Inorganic Chemistry. Single Crystal and Powder X-ray Diffraction. JoVE, Cambridge, MA, **2022**.
50. Gokel, G. W.; Leevy, W. M.; Weber, M. E. Crown Ethers: Sensors for Ions and Molecular Scaffolds for Materials and Biological Models. *Chem. Rev.* **2004**, *104* (5), 2723–2750.
51. Pedersen, C. J. The Discovery of Crown Ethers. *Science* **1988**, *241* (4865), 536–540.

52. Hiraoka, M.; Pedersen, C. J. *Crown Ethers and Analogous Compounds : [to the Memory of Charles J. Pedersen 1904-1989]*. Elsevier, Amsterdam, **1992**.
53. Zhang, M.; Yan, X.; Huang, F.; Niu, Z.; Gibson, H. W. Stimuli-Responsive Host–Guest Systems Based on the Recognition of Cryptands by Organic Guests. *Acc. Chem. Res.* **2014**, *47* (7), 1995–2005.
54. Kang, S. O.; Llinares, J. M.; Day, V. W.; Bowman-James, K. Cryptand-like Anion Receptors. *Chem. Soc. Rev.* **2010**, *39* (10), 3980–4003.
55. García-López, V.; Liu, D.; Tour, J. M. Light-Activated Organic Molecular Motors and Their Applications. *Chem. Rev.* **2020**, *120* (1), 79–124.
56. Cram, D. J. The Design of Molecular Hosts, Guests, and Their Complexes (Nobel Lecture). *Angew. Chem. Int. Ed. Engl.* **1988**, *27* (8), 1009–1020.
57. Lindoy, L. F.; Park, K.-M.; Sung Lee, S. *Cryptands and Spherands. Supramolecular Chemistry*; John Wiley & Sons, Ltd: Chichester, UK, **2012**.
58. Bryant, J. A.; Helgeson, R. C.; Knobler, C. B.; DeGrandpre, M. P.; Cram, D. J. Host-Guest Complexation. 53. Functional Groups Preorganized in Hemispherands for Binding Alkali Metal and Ammonium Cations. *J. Org. Chem.* **1990**, *55* (15), 4622–4634.
59. Villiers, A., Sur la fermentation de la fécule par l’action du ferment ´ butyrique. *Compt. Rend. Acad. Sci.* **1891**, *112*, 536–538.
60. Stick, R.; Williams, S. *Carbohydrates: The Essential Molecules of Life*, 2nd ed.; Elsevier Science, **2008**.
61. Nasir, A.; Si, H.; Kaur, A. Cyclodextrins: an excipient tool in drug delivery. *Int. Res. J. Pharm.* **2012**, *3* (4), 44–50.
62. Linde, G. A.; Laverde, A., Jr; Colauto, N. B. Changes to Taste Perception in the Food Industry: Use of Cyclodextrins. *In Handbook of Behavior, Food and Nutrition*; Springer New York: New York, NY, **2011**, 99–118.
63. Baeyer, A. Ueber Die Verbindungen Der Aldehyde Mit Den Phenolen Und Aromatischen Kohlenwasserstoffen. *Ber. Dtsch. Chem. Ges.* **1872**, *5* (2), 1094–1100.
64. Zinke, A.; Ziegler, E. Zur Kenntnis Des Härtungsprozesses von Phenol-Formaldehyd-Harzen, X. Mitteilung. *Ber. Dtsch. Chem. Ges. (A and B Series)* **1944**, *77* (3–4), 264–272.
65. Niederl, J. B.; Vogel, H. J. Aldehyde—Resorcinol Condensations<sup>1</sup>. *J. Am. Chem. Soc.* **1940**, *62* (9), 2512–2514.

66. *Calixarenes: A Versatile Class of Macrocyclic Compounds*, 1991st ed.; Vicens, J., Böhmer, V., Eds.; Springer: Dordrecht, Netherlands, **2012**.
67. Gutsche, C. D.; Dhawan, B.; No, K. H.; Muthukrishnan, R. Calixarenes. 4. The Synthesis, Characterization, and Properties of the Calixarenes from p-Tert-Butylphenol. *J. Am. Chem. Soc.* **1981**, *103* (13), 3782–3792.
68. Dhawan, B.; Chen, S. I.; Gutsche, C. D. Calixarenes, 19.† Studies of the formation of calixarenes via condensation of p-alkylphenols and formaldehyde. *Makromol. Chem.* **1987**, *188* (5), 921–950.
69. Hogberg, A. G. S. Stereoselective synthesis and NMR study of two 1,8,15,22-tetraphenyl (14) metacyclophan-3,5,10,12,17,19,24,26-octols. *J. Am. Chem. Soc.* **1980**, *102*, 6046–6050.
70. Hoegberg, A. G. S. Two Stereoisomeric Macrocyclic Resorcinol-Acetaldehyde Condensation Products. *J. Org. Chem.* **1980**, *45* (22), 4498–4500.
71. Cram, D. J.; Karch, S.; Kim, Y. H.; Baczynskyj, L.; Marti, K.; Sampson, R. M.; Kallemeyn, G. W. Host-Guest Complexation. 47. Carcerands and Carcaplexes, the First Closed Molecular Container Compounds. *J. Am. Chem. Soc.* **1988**, *110* (8), 2554–2560.
72. Cram, D. J.; Tanner, M. E.; Knobler, C. B. Host-Guest Complexation. 58. Guest Release and Capture by Hemicarcerands Introduces the Phenomenon of Constrictive Binding. *J. Am. Chem. Soc.* **1991**, *113* (20), 7717–7727.
73. *Advances in Diverse Industrial Applications of Nanocomposites*; Reddy, B., Ed.; InTech, **2011**.
74. Warmuth, R. Carcerands and Hemicarcerands. *Supramolecular Chemistry*; John Wiley & Sons, Ltd: Chichester, UK, **2012**.
75. Timmerman, P.; Boerrigter, H.; Verboom, W.; Hummel, G. J.; Harkema, S.; Reinhoudt, D. N. Proximally Functionalized Cavitands and Synthesis of a Flexible Hemicarcerand. *J Incl Phenom Macrocycl Chem.* **1994**, *19*, 167–191.
76. Legrand, S.; *Stereoselectivity and regioselectivity in organic chemistry: novel systems and applications*. University of Kalmar, **2006**.
77. Goldberg, I.; Stein, Z.; Weber, E.; Dörpinghaus, N.; Franken, S. Exploring the Inclusion Properties of New Clathrate Hosts Derived from Tartaric Acid. X-Ray Structural Characterization of the Free Ligands and Their Selective Interaction Modes with Alkylamine Guests. *J. Chem. Soc., Perkin Trans. 2* **1990**, *6*, 953–963.

78. Seebach, D.; Beck, A. K.; Heckel, A. TADDOLs, Their Derivatives, and TADDOL Analogues: Versatile Chiral Auxiliaries. *Angew. Chem. Int. Ed Engl.* **2001**, *40* (1), 92–138.
79. Tanaka, K.; Honke, S.; Urbanczyk-Lipkowska, Z.; Toda, F. New Chiral Hosts Derived from Dimeric Tartaric Acid: Efficient Optical Resolution of Aliphatic Alcohols by Inclusion Complexation. *European J. Org. Chem.* **2000**, *18*, 3171–3176.
80. Barton, B.; de Jager, L.; Dorfling, S.-L.; Hosten, E. C.; McClelland, C. W.; Pohl, P. L. Host Behaviour of Related Compounds, TETROL and DMT, in the Presence of Two Different Classes of Aromatic Guest Compounds. *Tetrahedron* **2018**, *74* (36), 4754–4760.
81. Weber, E.; Hens, T.; Gallardo, O.; Csöreg, I. Roof-Shaped Hydroxy Hosts: Synthesis, Complex Formation and X-Ray Crystal Structures of Inclusion Compounds with EtOH, Nitroethane and Benzene. *J. Chem. Soc., Perkin Trans. 2* **1996**, *4*, 737–745.
82. Weber, E.; Dörpinghaus, N.; Csöreg, I. Versatile and Convenient Lattice Hosts Derived from Singly Bridged Triarylmethane Frameworks, X-Ray Crystal Structures of Three Inclusion Compounds. *J. Chem. Soc., Perkin Trans. 2* **1990**, *12*, 2167–2177.
83. Barton, B.; Caira, M. R.; de Jager, L.; Hosten, E. C. *N,N'*-Bis(9-Phenyl-9-Thioxanthanyl)Ethylenediamine: Highly Selective Host Behavior in the Presence of Xylene and Ethylbenzene Guest Mixtures. *Cryst. Growth Des.* **2017**, *17* (12), 6660–6667.
84. Bengen, F.; Schlenk, W., Jr. Über neuartige Additionsverbindungen des Harnstoffs. *Experientia* **1949**, *5* (5), 200–200.
85. Harris, K. D. M. Meldola Lecture: Understanding the Properties of Urea and Thiourea Inclusion Compounds. *Chem. Soc. Rev.* **1997**, *26* (4), 279–289.
86. Hermann, C.; Lenne, H. Die Struktur der hexagonalen Thioharnstoff-Einschlußverbindungen. *Naturwissenschaften* **1952**, *10*, 234–235.
87. Lenné, H.-U. Röntgenographische Strukturuntersuchungen Hexagonaler Einschlußverbindungen Des Thioharnstoffs. *Acta Crystallogr.* **1954**, *7* (1), 1–15.
88. Maris, T.; Henson, M. J.; Heyes, S. J.; Prout, K. Investigations of the Phase Transitions in Thiourea Inclusion Compounds with Cycloheptane, Cyclooctane, and Cyclooctanone. *Chem. Mater.* **2001**, *13* (8), 2483–2492.
89. Barton, B.; Betz, B.; Caira, M.R.; Hosten, E.C.; McClelland, C.W.; Pohl, P.L.; Taljaard, B. Clathrates of novel ethylenediamine derivatives: thermal, X-ray crystallographic and conformational analysis of inclusion complexes of *N,N'*-bis(5-phenyl-5-

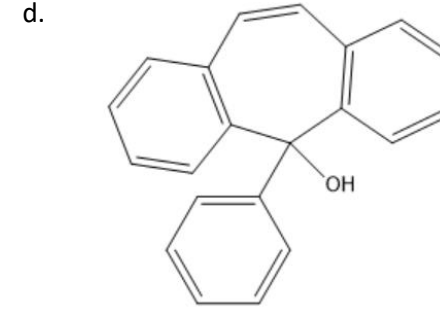
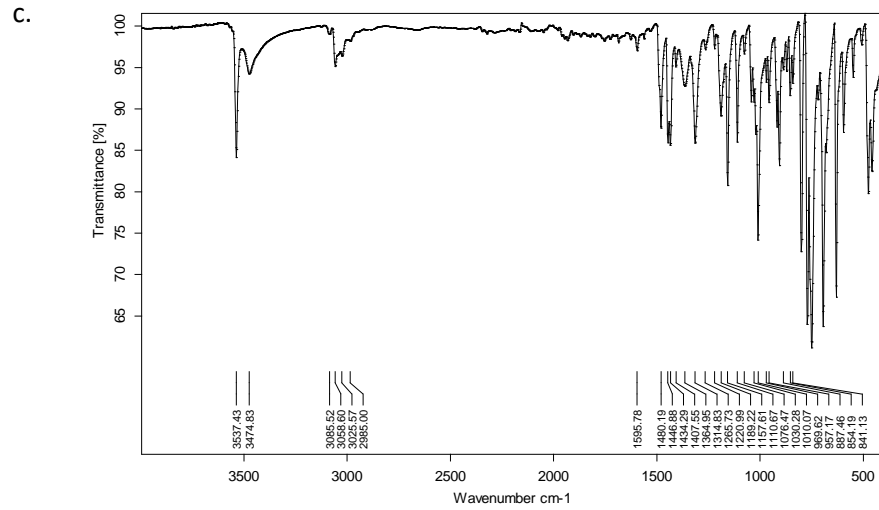
- dibenzo[a,d]cycloheptenyl)ethylenediamine and its 10,11-dihydro analogue. *Tetrahedron* **2016**, *72*, 7536–7551.
90. Barton, B.; Trollip, D. B.; Hosten, E. C. Selected Tricyclic Fused Systems: Host Behavior in the Presence of Mixed Xylenes and Ethylbenzene. *Cryst. Growth Des.* **2022**, *22* (11), 6726–6734.
91. Bruker, A. APEX2, SADABS and SAINT; Bruker AXS Inc.: Madison (WI), USA, **2010**.
92. Sheldrick, G. M. Crystal structure refinement with SHELXL. *Acta Crystallogr.* **2015**, C71, 3–8.
93. Hübschle, C. B.; Sheldrick, G. M.; Dittrich, B. ShelXle: a Qt graphical user interface for SHELXL. *J. Appl. Crystallogr.* **2011**, *44*, 1281–1284.
94. Bruker, U. APEX3 v2019.1-0, SAINT V8.40A; Bruker AXS Inc.: Madison (WI), USA, **2019**.
95. Krause, L.; Herbst-Irmer, R.; Sheldrick, G.M.; Stalke, D. Comparison of silver and molybdenum microfocus X-ray sources for single-crystal structure determination. *J. Appl. Crystallogr.* **2015**, *48*, 3–10.
96. Sheldrick, G. M. A short history of SHELX. *Acta Crystallogr.* **2008**, A64, 112–122.
97. Barbour, L. J. X-Seed—A software tool for supramolecular crystallography. *J. Supramol. Chem.* **2001**, *1*, 189–191.
98. Barton, B.; Betz, R.; Caira, M. R.; Hosten, E. C.; McClelland, C. W.; Pohl, P. L.; Taljaard, B. (deceased). Clathrates of novel ethylenediamine derivatives: thermal, X-ray crystallographic and conformational analysis of inclusion complexes of *N,N'*-bis(5-phenyl-5-dibenzo[a,d]cycloheptenyl)ethylenediamine and its 10,11-dihydro analogue. *Tetrahedron*, **2016**, *72*, 7536–7551.
99. Weber, E.; Dorpinghaus, N.; Csöregi, I. Versatile and convenient lattice hosts derived from singly bridged triarylmethane frameworks, X-ray crystal structures of three inclusion compounds. *J. Chem. Soc., Perkin Trans. 2* **1990**, 2167–2177.
100. Pivovar, A. M.; Holman, K. T.; Ward, M. D. Shape-Selective Separation of Molecular Isomers with Tunable Hydrogen-Bonded Host Frameworks. *Chem. Mater.* **2001**, *13* (9), 3018–3031.
101. Spartan' 10 V1.1.0. **2010**. Wavefunction. Inc., Irvine.
102. Yang, Y.; Bai, P.; Guo, X. Separation of Xylene Isomers: A Review of Recent Advances in Materials. *Ind. Eng. Chem. Res.* **2017**, *56* (50), 14725–14753.

103. Zhang, G.; Ding, Y.; Hashem, A.; Fakim, A.; Khashab, N.M. Xylene Isomer Separations by Intrinsically Porous Molecular Materials. *Cell Reports Phys. Sci.* **2021**, *2* (6), 100470–100489.
104. Mohameed, H. A.; Jdayil, B. A.; Takrouri, K. Separation of *para*-Xylene from Xylene Mixture via Crystallization. *Chem. Eng. Process.* **2007**, *46* (1), 25–36.
105. Shi, Q.; Gonçalves, J. C.; Ferreira, A. F. P.; Rodrigues, A. E. A Review of Advances in Production and Separation of Xylene Isomers. *Chem. Eng. Process.* **2021**, *169*, 108603–108618.
106. Santacesaria, E.; Morbidelli, M.; Servida, A.; Storti, G.; Carra, S. Separation of Xylenes on Y Zeolites. 2. Breakthrough Curves and Their Interpretation. *Ind. Eng. Chem. Process Des. Dev.* **1982**, *21* (3), 446–451.
107. Jin, Z.; Zhao, H.-Y.; Zhao, X.-J.; Fang, Q.-R.; Long, J. R.; Zhu, G.-S. A Novel Microporous MOF with the Capability of Selective Adsorption of Xylenes. *Chem. Commun.* **2010**, *46* (45), 8612–8614.
108. Rodrigues, A. *Simulated Moving Bed Technology: Principles, Design and Process Applications*; Butterworth-Heinemann: Woburn, MA, **2015**.
109. Su, D.; Maksimova, N. I.; Mestl, G.; Kuznetsov, V. L.; Keller, V.; Schlögl, R.; Keller, N. Oxidative Dehydrogenation of Ethylbenzene to Styrene over Ultra-Dispersed Diamond and Onion-like Carbon. *Carbon* **2007**, *45* (11), 2145–2151.
110. Tossavainen, A. Styrene Use and Occupational Exposure in the Plastics Industry. *Scand. J. Work Environ. Health* **1978**, *4* Suppl 2, 7–13.
111. Macrae, C. F.; Sovago, I.; Cottrell, S. J.; Galek, P. T. A.; McCabe, P.; Pidcock, E.; Platings, M.; Shields, G. P.; Stevens, J. S.; Towler, M.; Wood, P. A. Mercury 4.0: from Visualization to Analysis. Design and prediction. *J. Appl. Crystallogr.* **2020**, *53*, 226–235.
112. Weber, E.; Czugler, M. Functional Group Assisted Clathrate Formation — Scissor-like and Roof-shaped Host Molecules. *Top. Curr. Chem.* **1988**, *149*, 45–135.
113. Tanaka, K.; Hori, K.; Tsuyuhara, S.; Motoki, S.; Shide, S.; Arakawa, R.; Caira, M.R. Role of Halogen Bonding in Clathrate Formation of Tetra- and Hexasalicylides Derived from Halogenated Salicylic Acids. *Tetrahedron* **2013**, *69*, 1120–1127.
114. Altaf, A.A.; Shahzad, A.; Gul, Z.; Rasool, N.; Badshah, A.; Lal, B.; Khan, E. A Review on the Medicinal Importance of Pyridine Derivatives. *J. drug des. med. chem.* **2015**, *1* (1), 1–11.

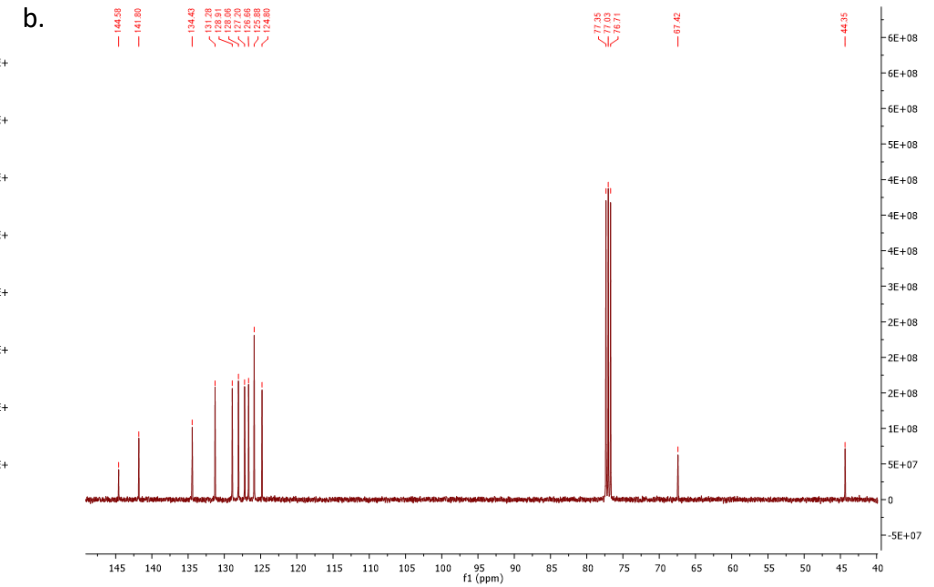
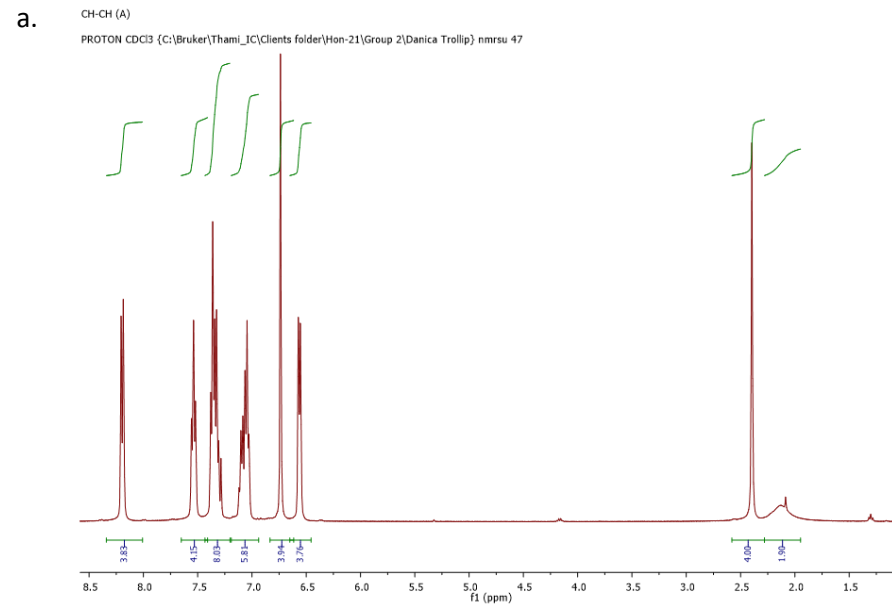
115. Barton, B.; Caira, M. R.; Jooste, D. V.; Hosten, E. C. Investigation of the Separation Potential of Xanthenyl- and Thioxanthenyl-Based Host Compounds for Pyridine and Isomeric Picoline Mixtures. *J. Incl. Phenom. Macrocycl. Chem.* **2020**, *98* (3–4), 223–235.
116. Grigor'eva, N. G.; Filippova, N. A.; Tselyutina, M. I.; Kutepov, B. I. Synthesis of Pyridine and Methylpyridines over Zeolite Catalysts. *Appl. Petrochem. Res.* **2015**, *5* (2), 99–104.
117. Barton, B.; Caira, M. R.; Jooste, D. V.; Hosten, E. C. Alternative Purification Protocols of Mixed Pyridines in the Presence of Trans-N,N'-Bis(9-Phenyl-9-Xanthenyl)Cyclohexane-1,4-Diamine. *J. Incl. Phenom. Macrocycl. Chem.* **2021**, *99* (3–4), 235–243.
118. Senekal, U.; Barton, B.; Hosten, E. C. Inclusion Ability and Selectivity of Ethylenediamine Derivatives for Pyridine in the Presence of Methylpyridine Isomers. *J. Incl. Phenom. Macrocycl. Chem.* **2020**, *96* (3–4), 251–262.
119. Cullinane, N. M.; Chard, S. J.; Meatyard, R. The Preparation of Methylpyridines by Catalytic Methods. *J. Soc. Chem. Ind.* **1948**, *67* (4), 142–143.
120. Coulson, E. A.; Jones, J. I. Studies in Coal Tar Bases. I. Separation of  $\beta$ - and  $\gamma$  Picolines and 2:6-Lutidine. *J. Soc. Chem. Ind.* **1946**, *65* (6), 169–175.
121. PubChem. Anisole. Nih.gov. <https://pubchem.ncbi.nlm.nih.gov/compound/Anisole> (accessed 2022-11-18).
122. Dang, D.; Wang, Z.; Lin, W.; Song, W. Synthesis of anisole by vapor phase methylation of phenol with methanol over catalysts supported on activated alumina. *Chin. J. Catal.* **2016**, *37*, 720–726.
123. Wu, Y.; Huang, Y.; Huang, H.; Muhammad, Y.; Huang, Z.; Winarta, J.; Zhang, Y.; Nie, S.; Zhao, Z.; Mu, B. Porous Fe@C Composites Derived from Silkworm Excrement for Effective Separation of Anisole Compounds. *ACS Omega* **2019**, *4* (25), 21204–21213.
124. Balsama, S.; Beltrame, P.; Beltrame, P. L.; Carniti, P.; Forni, L.; Zuretti, G. Alkylation of phenol with methanol over zeolites. *Appl. Catal.* **1984**, *13*, 161–170.
125. Huang, F.; Li, L.; Guan, M.; Hong, Z.; Miao, L.; Zhao, G.; Zhu, Z. A Review of the Process on Vapor Phase Methylation of Phenol with Methanol. *Catal. Letters* **2022**.
126. Barton, B.; Caira, M. R.; Senekal, U.; Hosten, E. C. Selectivity Considerations of the Roof-Shaped Host Compound Trans- $\alpha,\alpha',A',A'$ -Tetrakis(4-Chlorophenyl)-9,10-Dihydro-9,10-Ethanoanthracene-11,12-Dimethanol in Mixed Anisoles. *Cryst. Growth Des.* **2022**, *22* (11), 6818–6826.

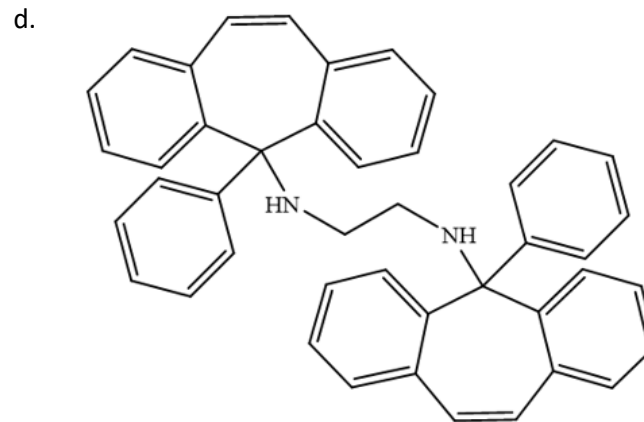
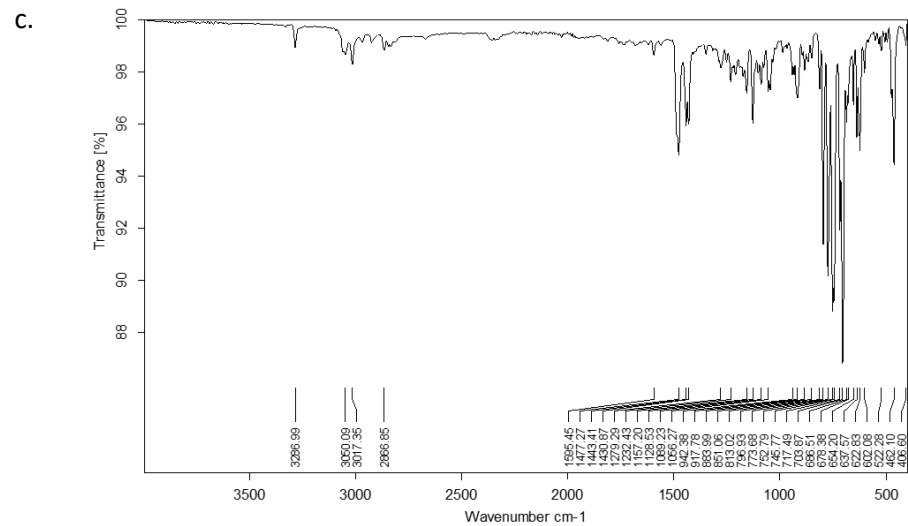




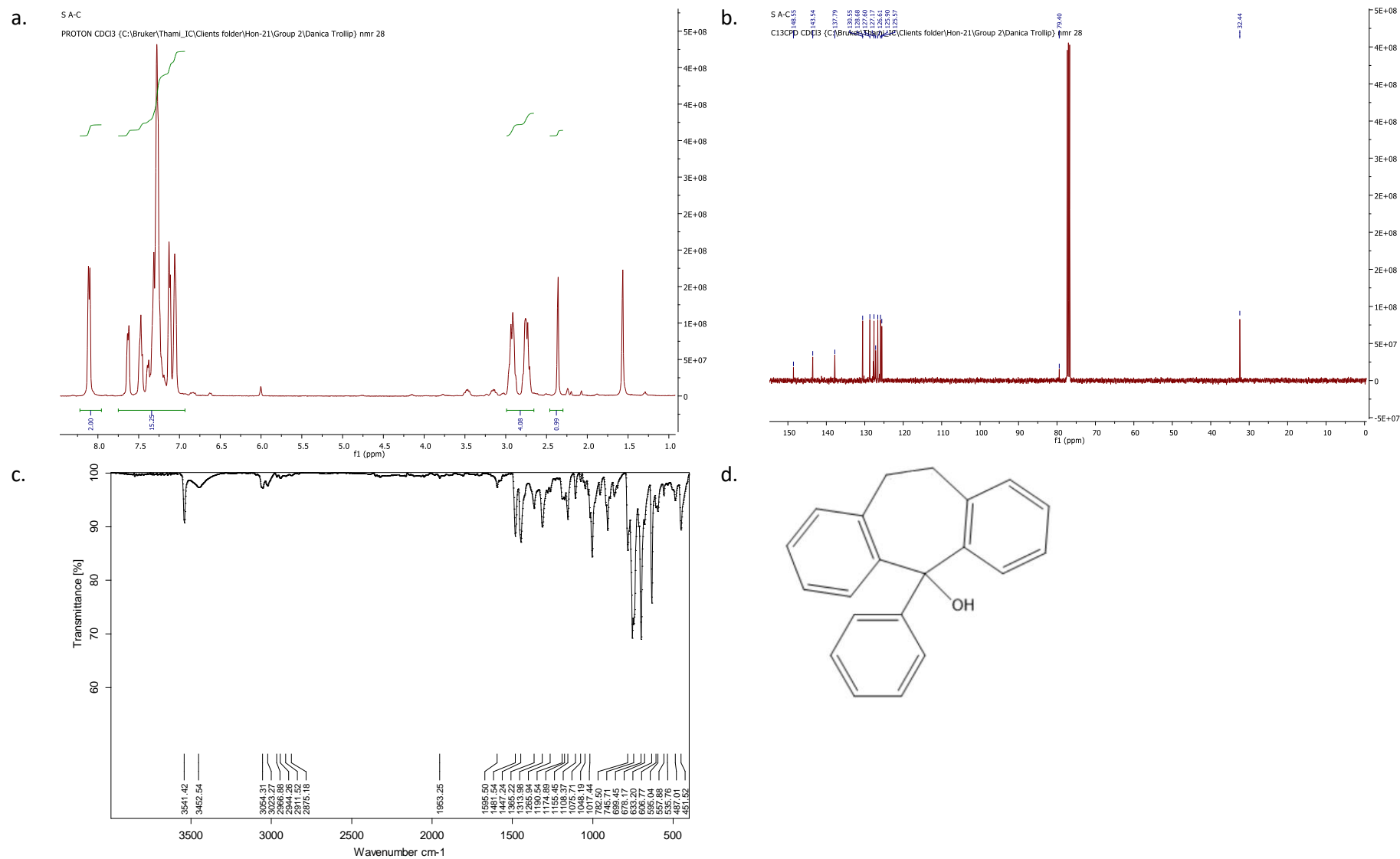


**Figure S1:** a.  $^1\text{H-NMR}$ , b.  $^{13}\text{C-NMR}$ , c. IR spectrum and d. structure of 5-Hydroxy-5-phenyldibenzo[a,d]cycloheptene

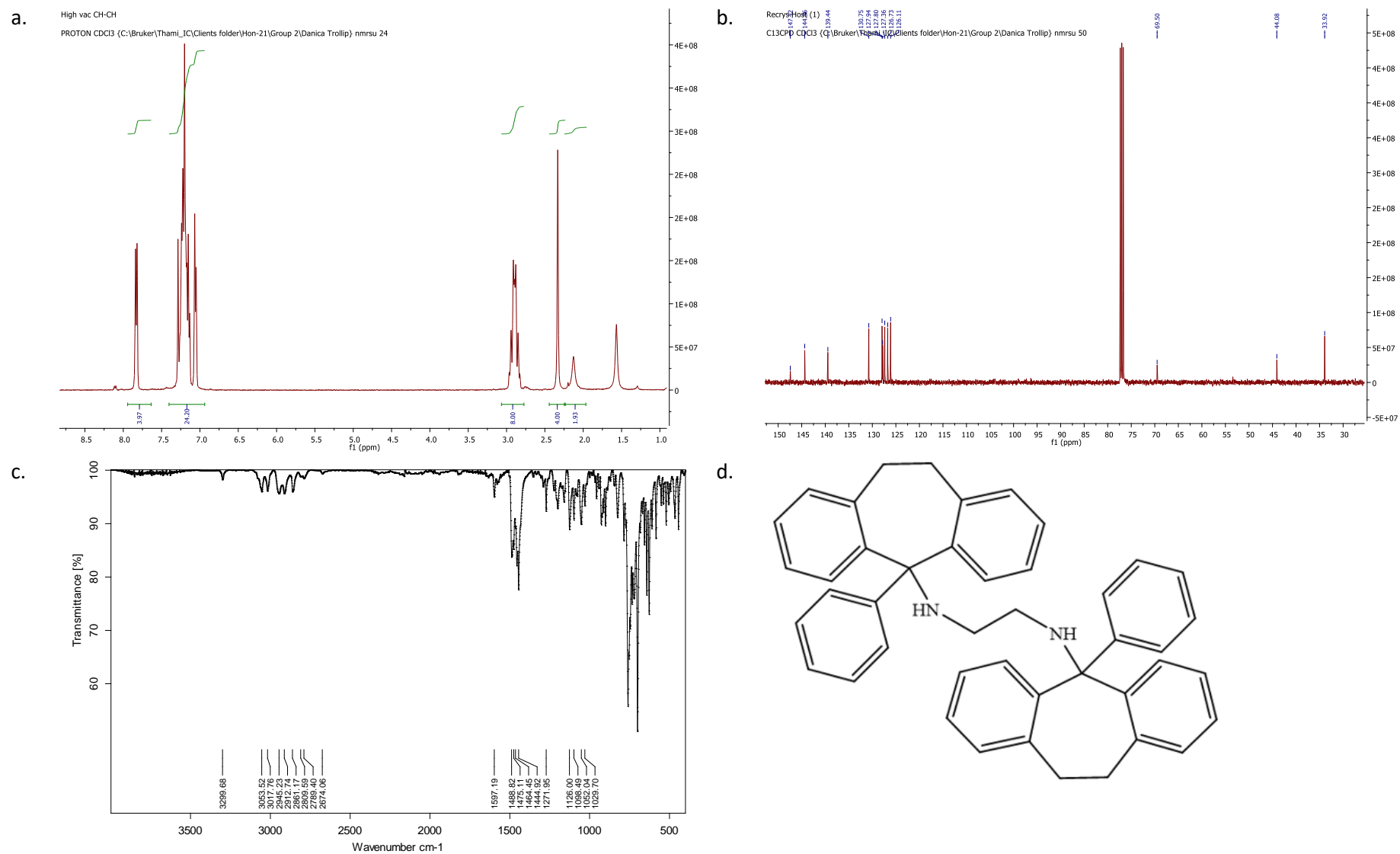




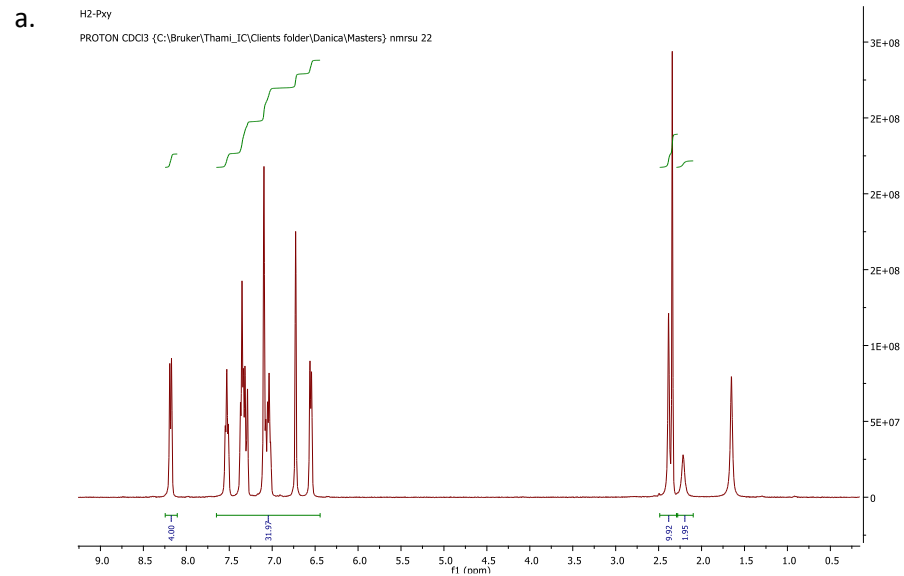
**Figure S2:** a. <sup>1</sup>H-NMR, b. <sup>13</sup>C-NMR, c. IR spectrum and d. structure of *N,N'*-bis(5-phenyl-5-dibenzo[*a,d*]cycloheptenyl)-ethylenediamine (**H1**)

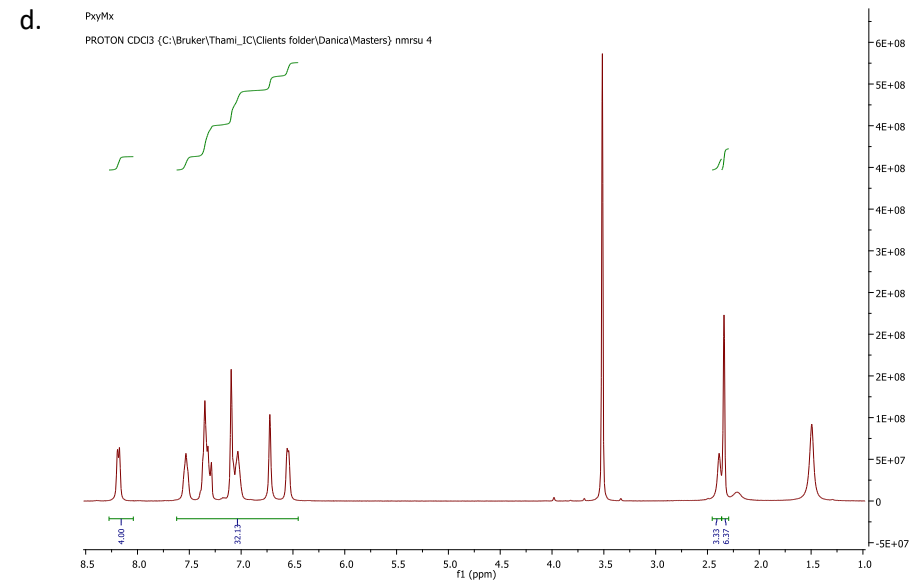
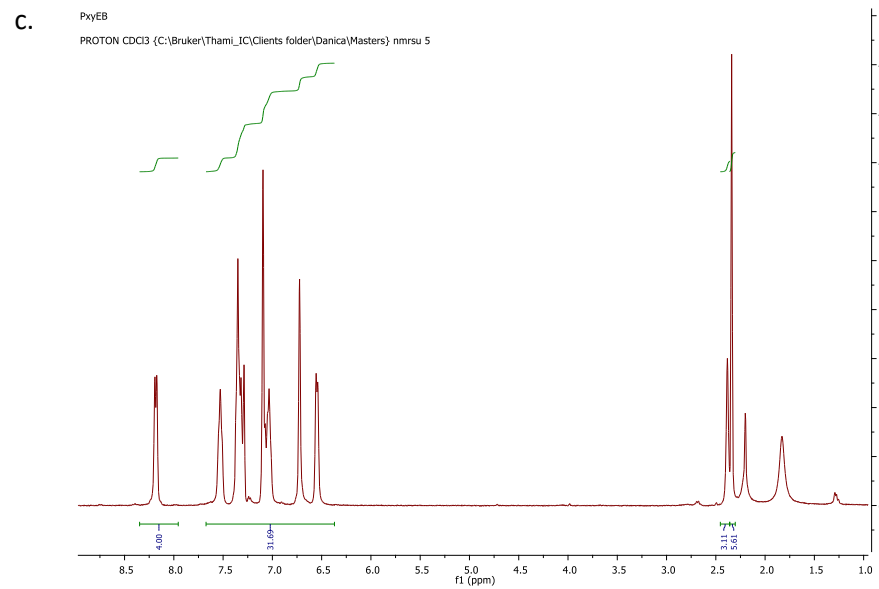
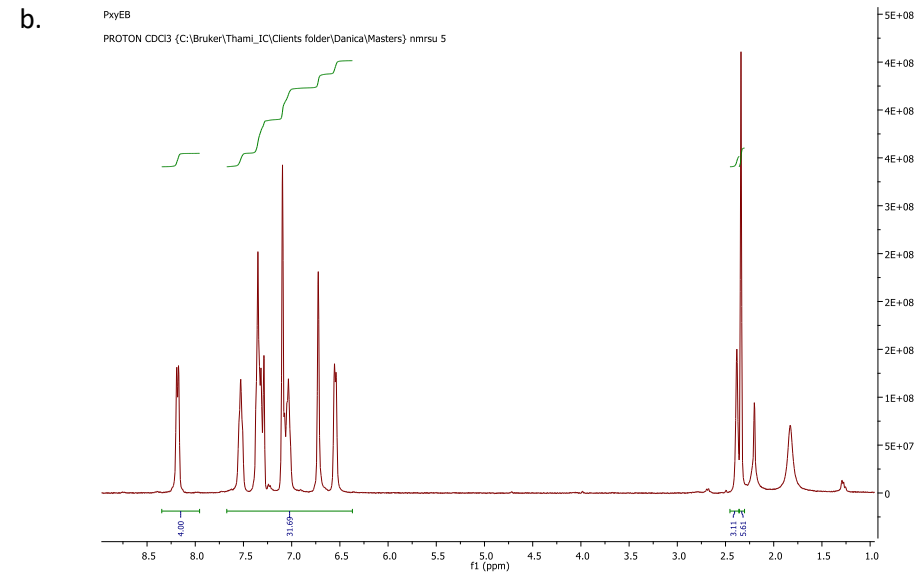
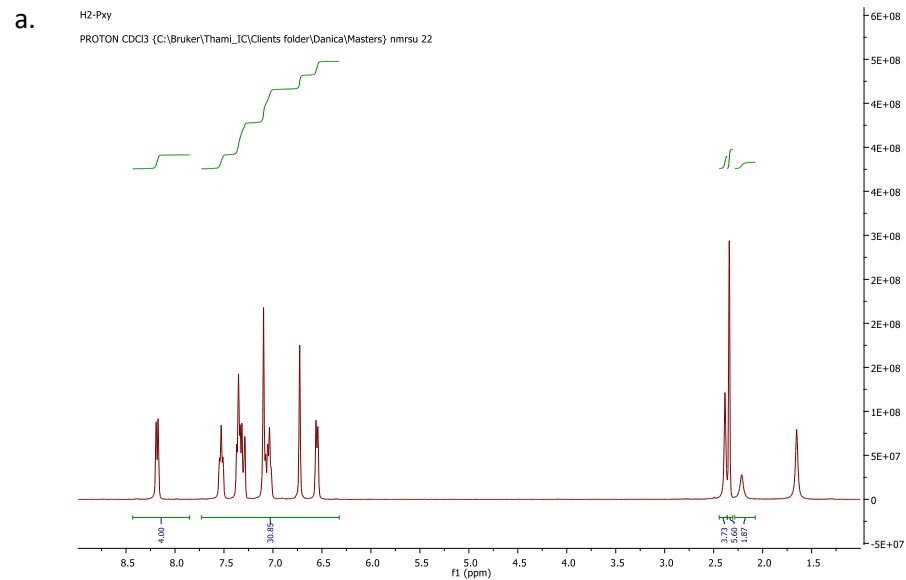


**Figure S3:** a. <sup>1</sup>H-NMR, b. <sup>13</sup>C-NMR, c. IR spectrum and d. structure of 5-Hydroxy-5-phenyl-10,11-dihydrodibenzo[a,d]cycloheptene



**Figure S4:** a. <sup>1</sup>H-NMR, b. <sup>13</sup>C-NMR, c. IR spectrum and d. structure of *N,N'*-Bis(5-phenyl-10,11-dihydro-5-dibenzo[*a,d*]cycloheptenyl) ethylenediamine (**H2**)





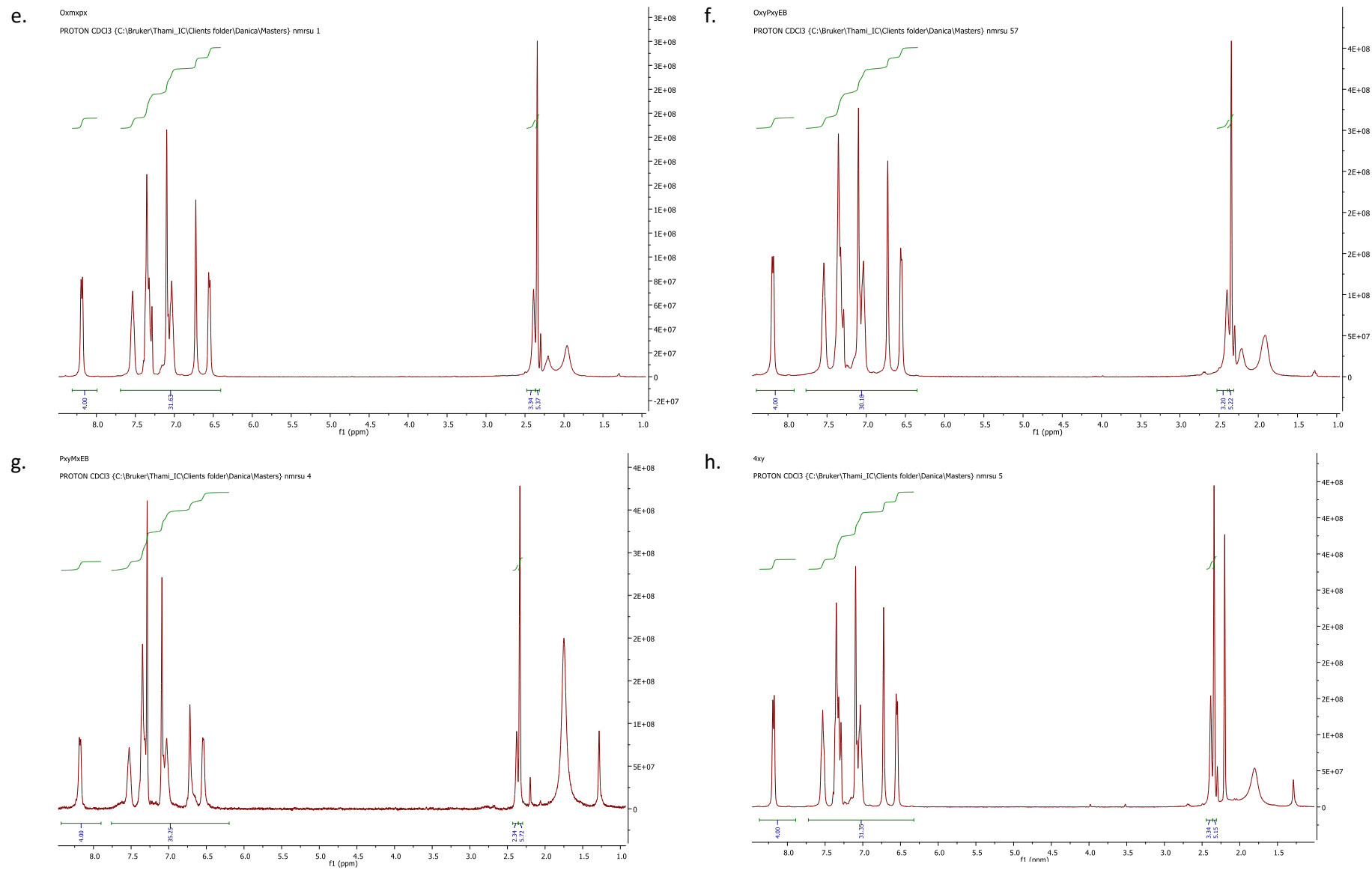
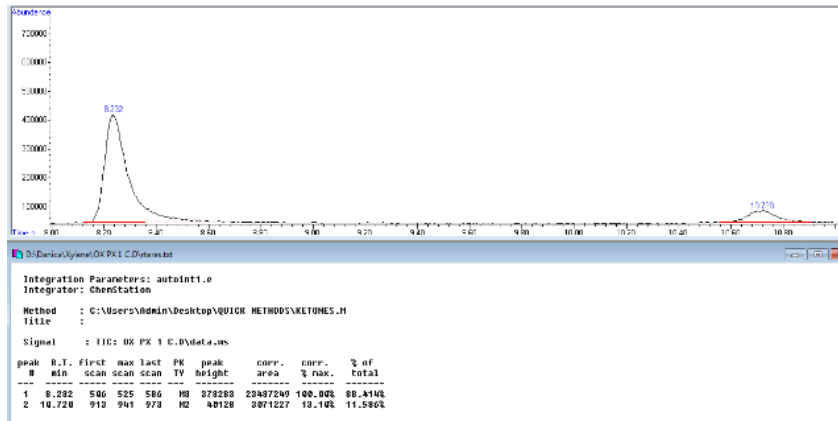


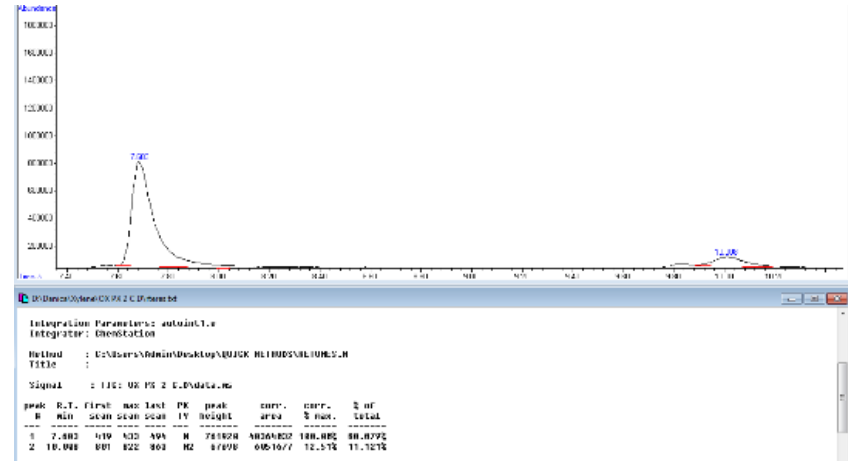
Figure S6: H1 with a. *p*-Xy, b. *o*-Xy/*p*-Xy, c. *p*-Xy/EB, d. *p*-Xy/*m*-Xy, e. *o*-Xy/*m*-Xy/*p*-Xy, f. *o*-Xy/*p*-Xy/EB, g. *p*-Xy/*m*-Xy/EB and h. all 4 Xy/EB



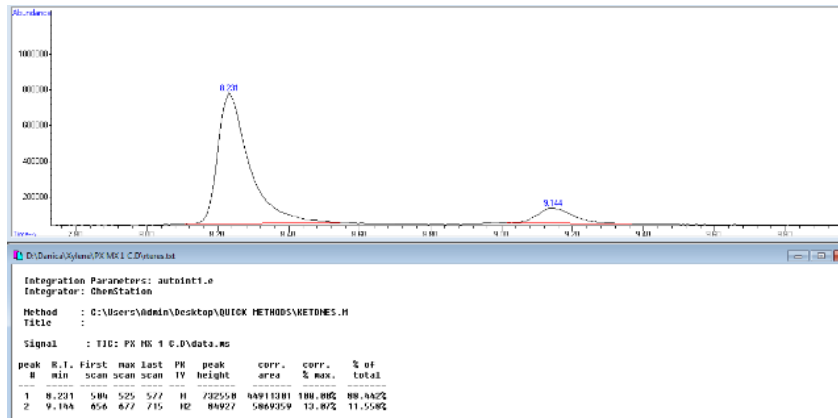
a.



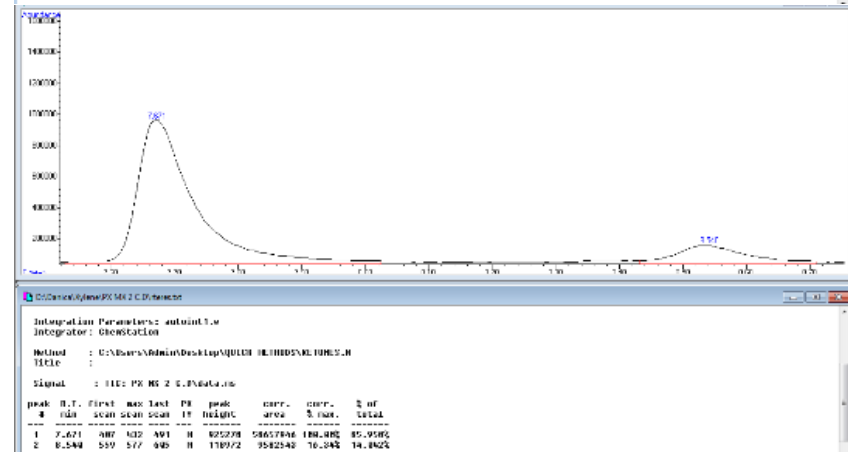
b.



c.



d.



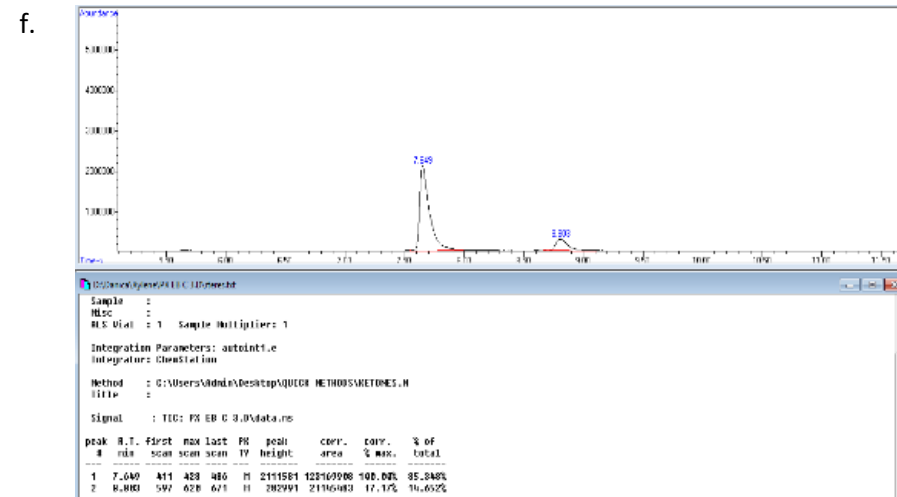
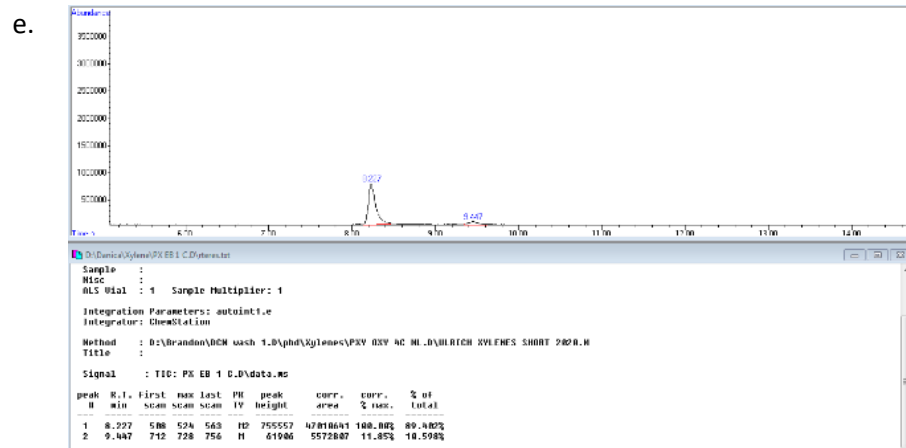
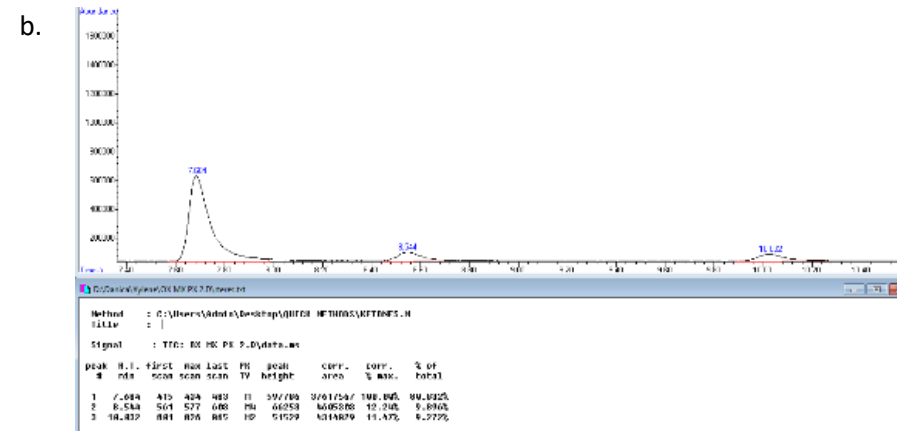
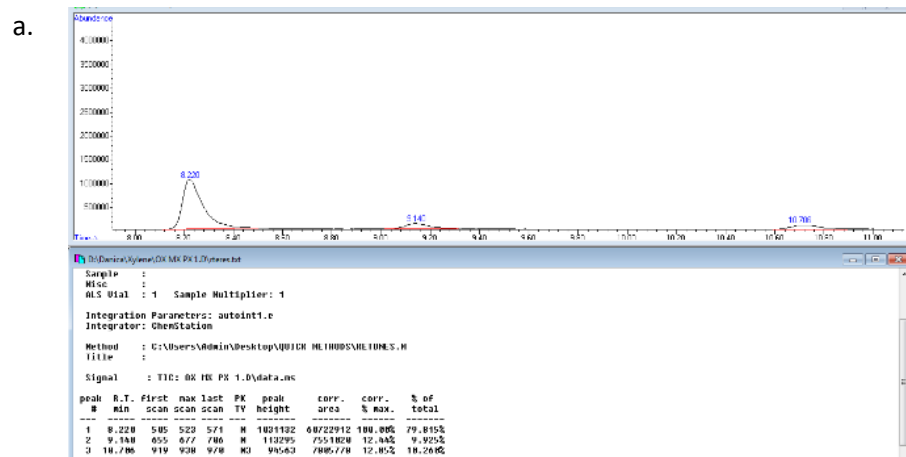


Figure S7: Host compound H1 with the duplicate crystal data for *p*-Xy/*o*-Xy in a. and b., for *p*-Xy/*m*-Xy in c. and d., and for *p*-Xy/EB in e. and f.



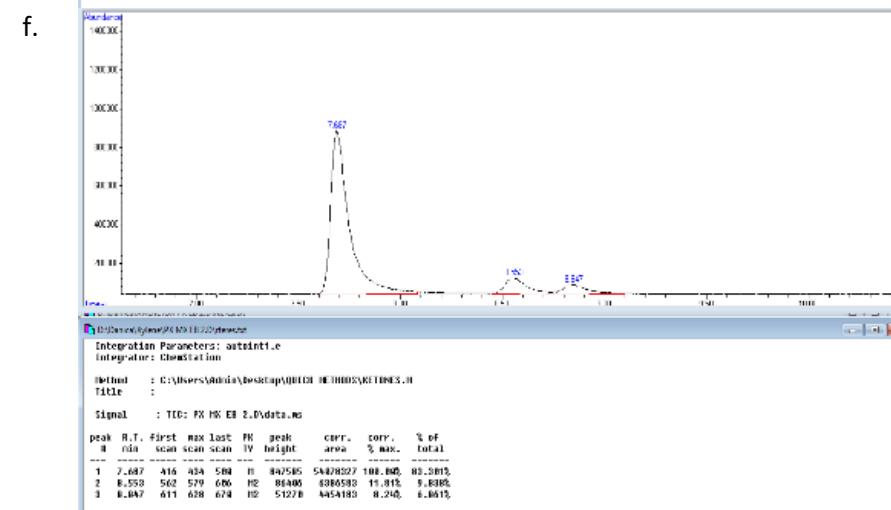
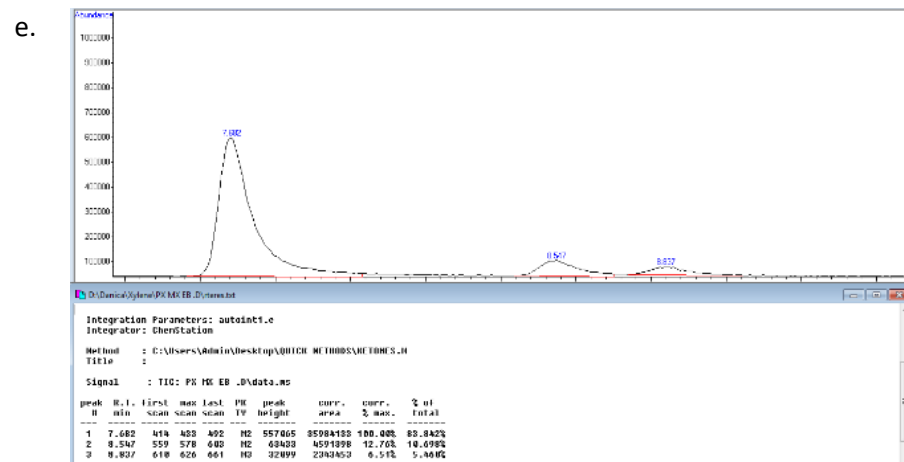
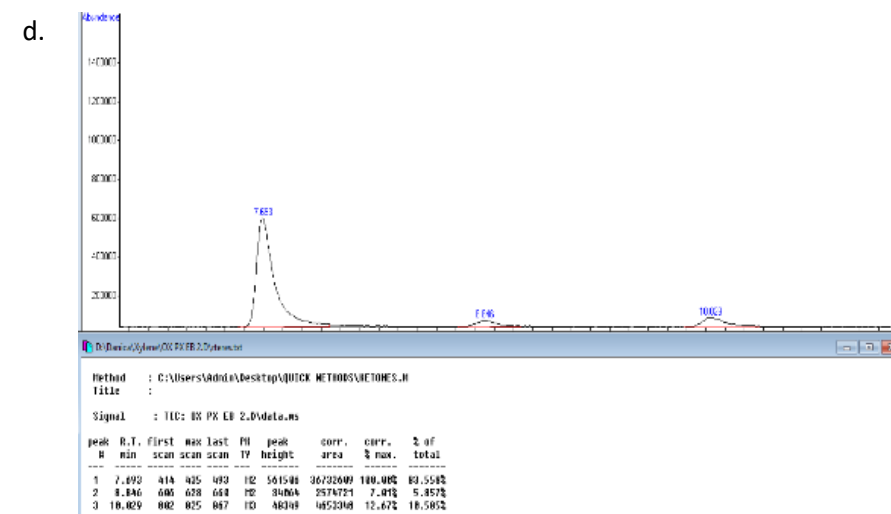
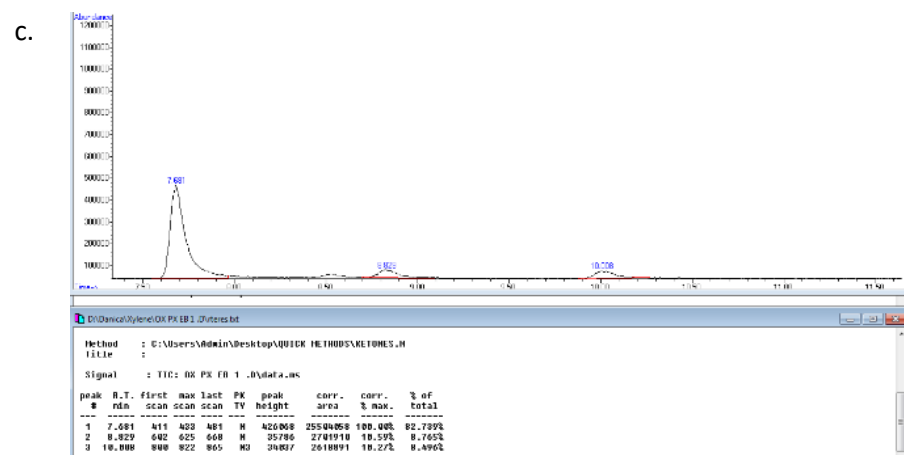


Figure S8: Host compound H1 crystal data with p-Xy-o-Xy-EB in a. and b., with p-Xy-o-Xy-m-Xy in c. and d., and with p-Xy-m-Xy-EB in e. and f.

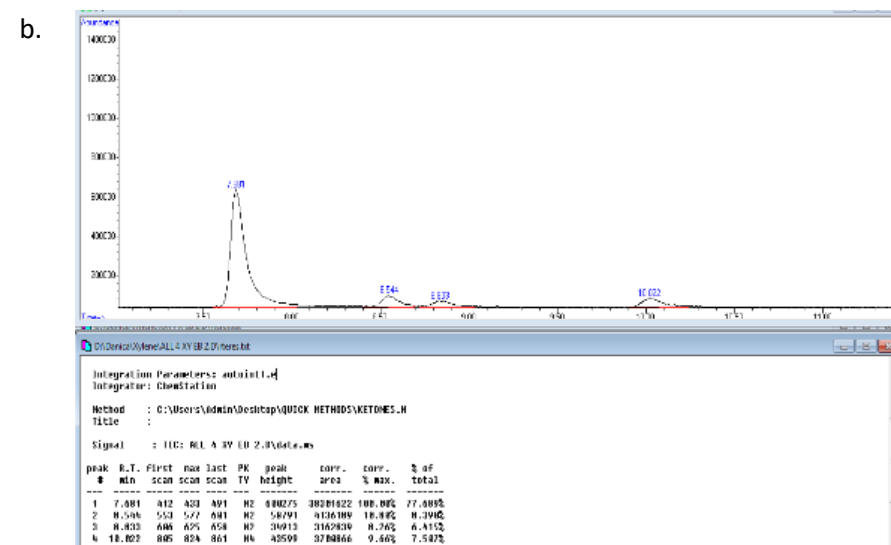
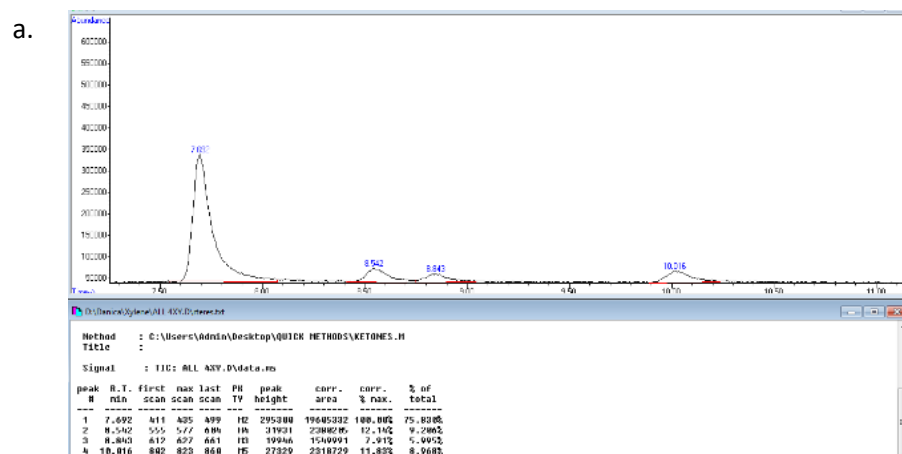
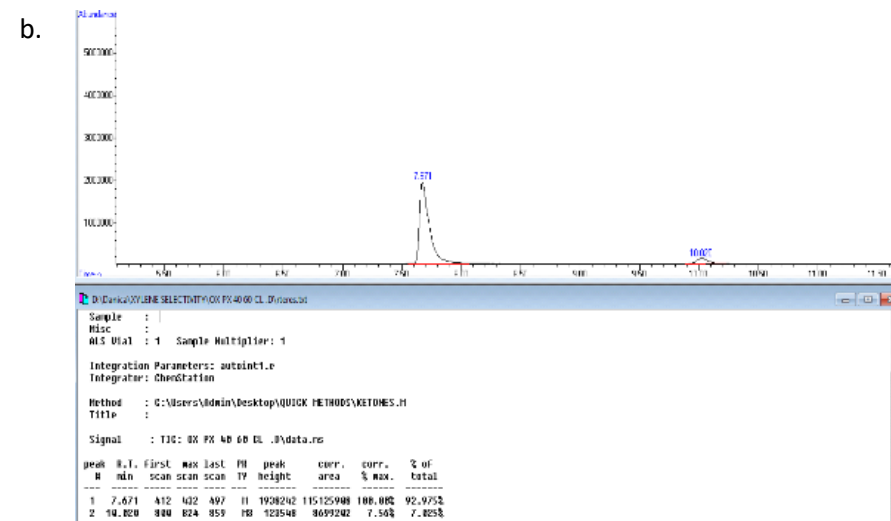
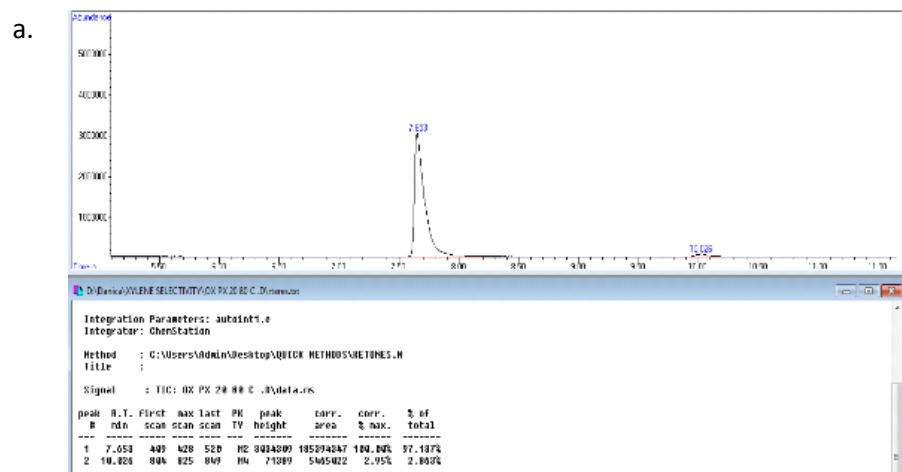


Figure S9: Host compound H1 crystal data with all 4 xylene isomers and ethylbenzene in a. and b.



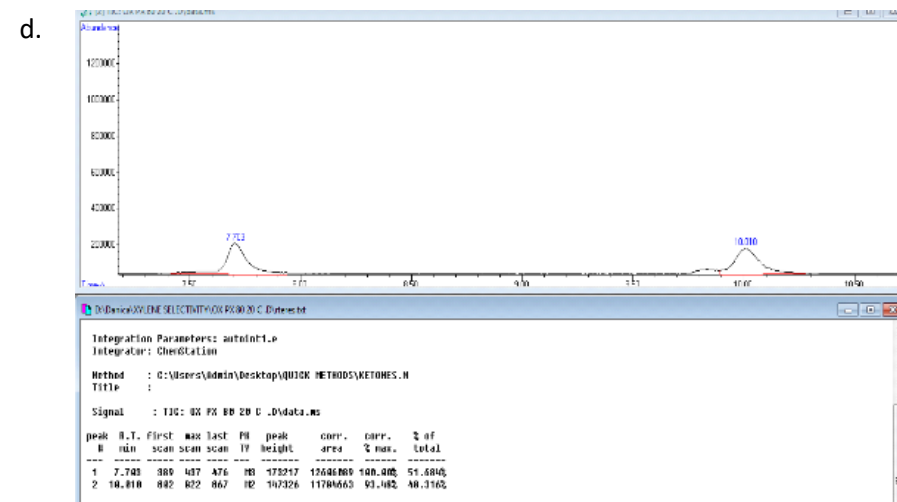
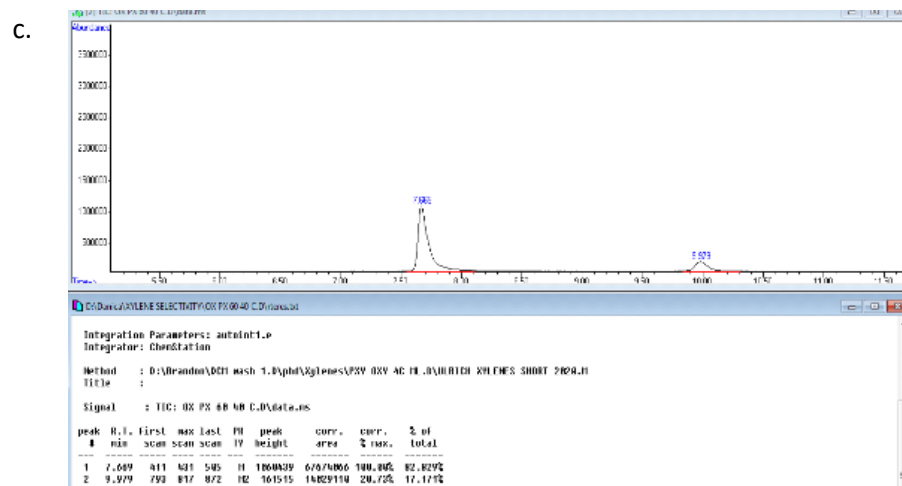
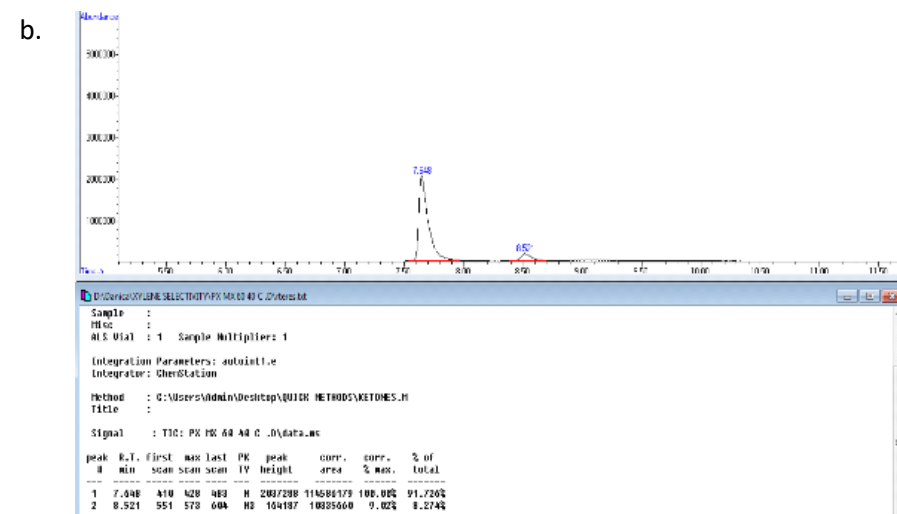
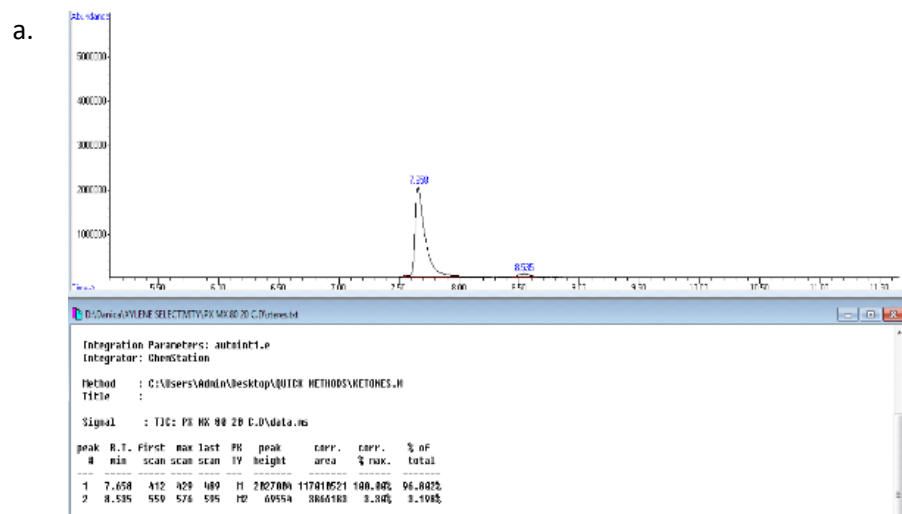


Figure S10: Host compound H1 for the selectivity profile *p*-Xy/*o*-Xy for the crystals with a. 80 20, b. 60 40, c. 40 60, and d. 20 80 concentrations



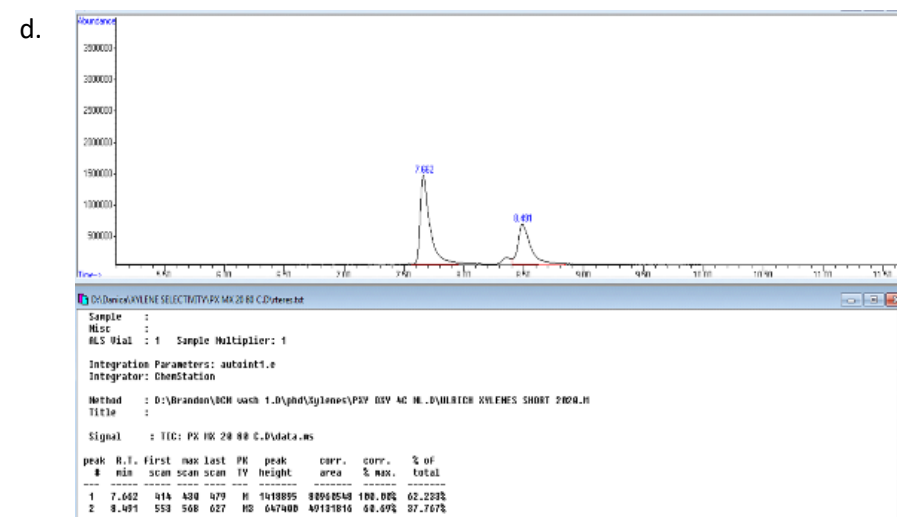
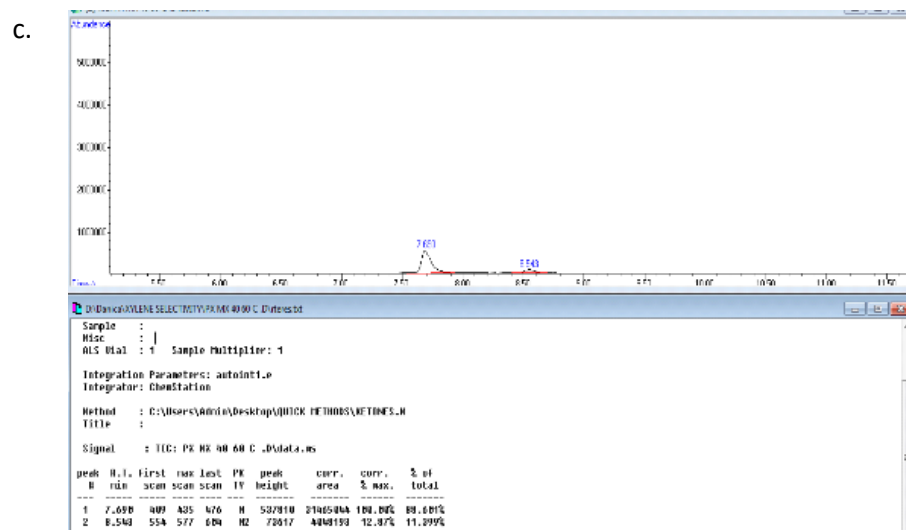
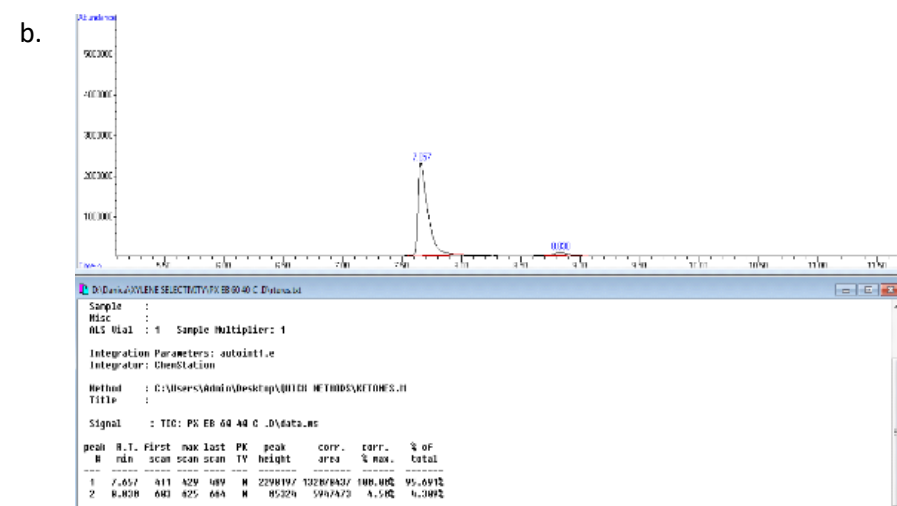
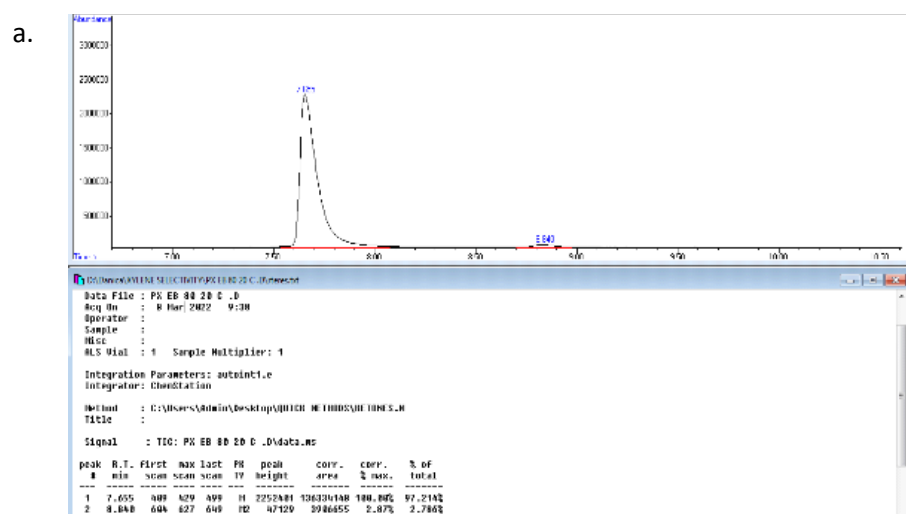


Figure S11: Host compound H1 for the selectivity profile *p*-Xy/*m*-Xy for the crystals with a. 80 20, b. 60 40, c. 40 60, and d. 20 80 concentrations



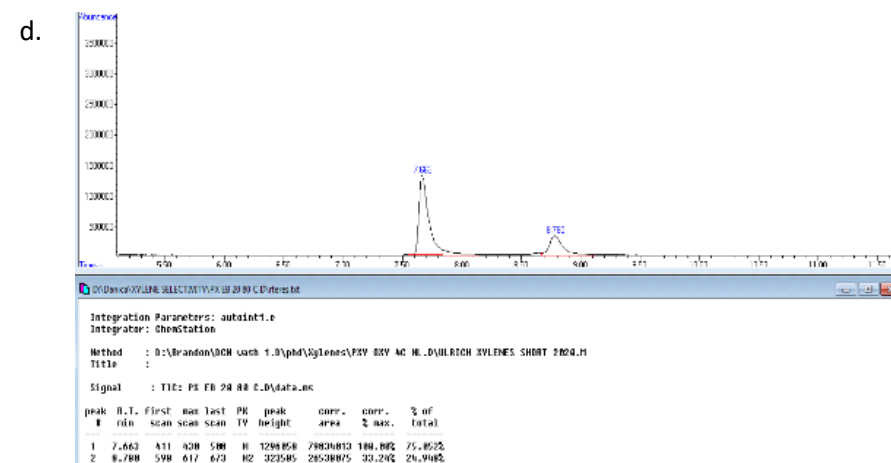
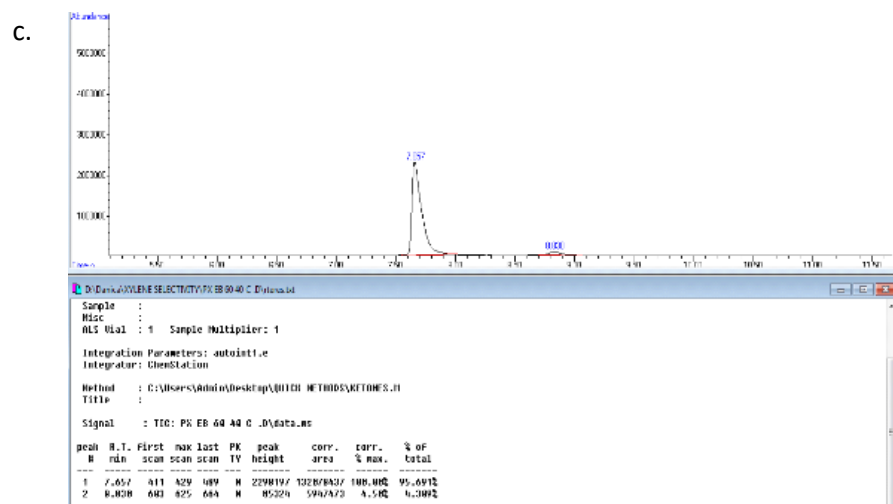


Figure S12: Host compound H1 for the selectivity profile *p*-Xy/EB for the crystals with a. 80 20, b. 60 40, c. 40 60, and d. 20 80 concentrations

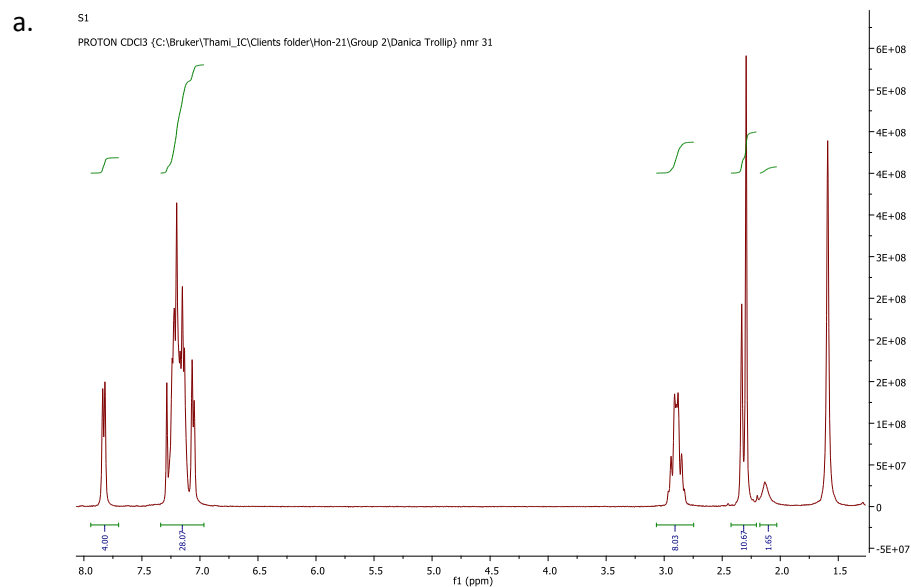
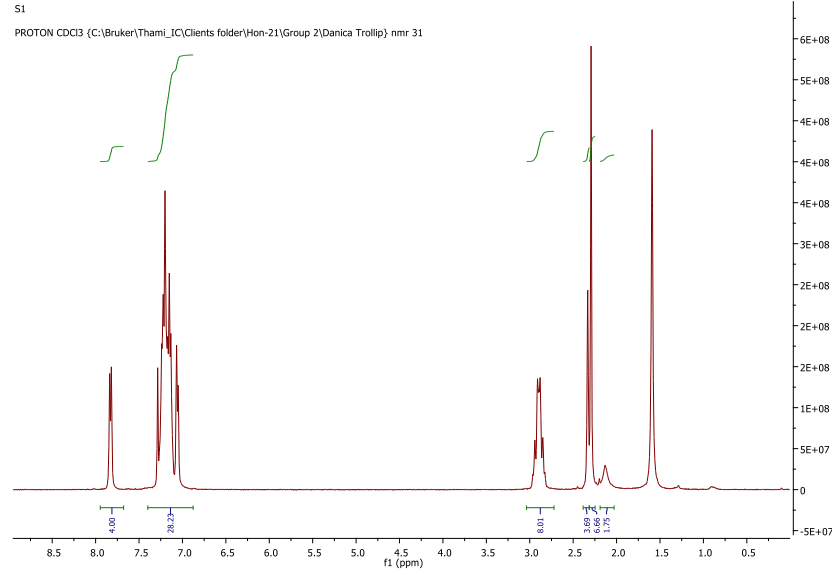


Figure S13: Host compound H2 single solvent experiment with a. *o*-Xy

a.

S1

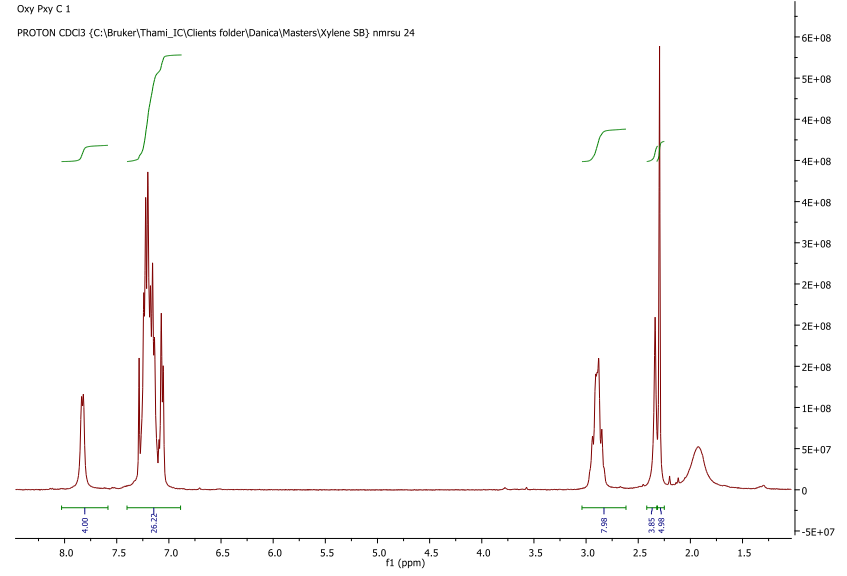
PROTON CDCl3 (C:\Bruker\Tham1\_IC\Clients folder\Hon-21\Group 2\Danica Trollip) nmr 31



b.

Oxy Pxy C 1

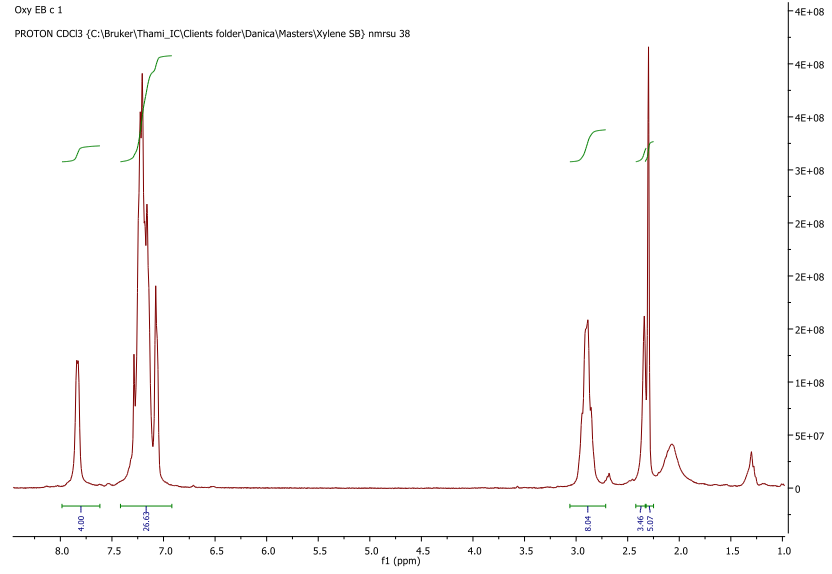
PROTON CDCl3 (C:\Bruker\Tham1\_IC\Clients folder\Danica\Masters\Xylene SB) nmrsu 24



c.

Oxy EB c 1

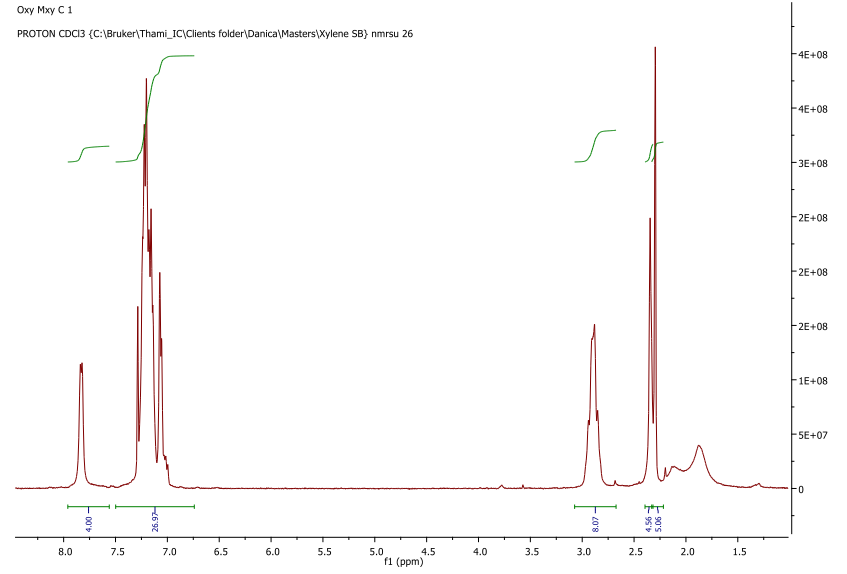
PROTON CDCl3 (C:\Bruker\Tham1\_IC\Clients folder\Danica\Masters\Xylene SB) nmrsu 38



d.

Oxy Mxy C 1

PROTON CDCl3 (C:\Bruker\Tham1\_IC\Clients folder\Danica\Masters\Xylene SB) nmrsu 26





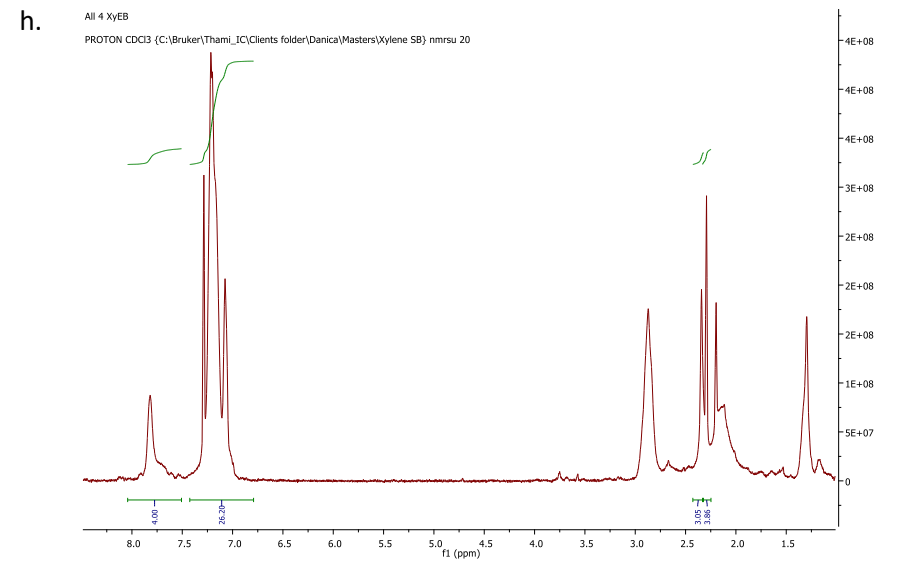
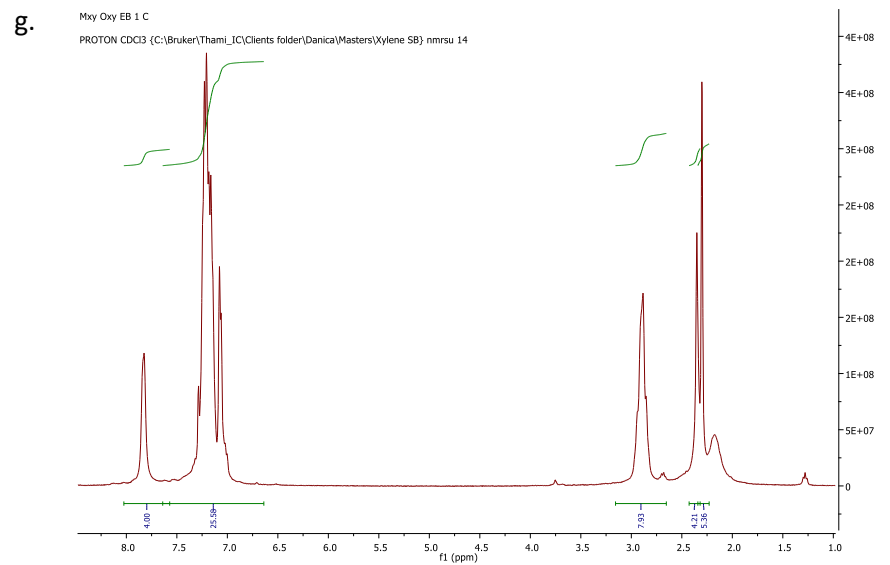
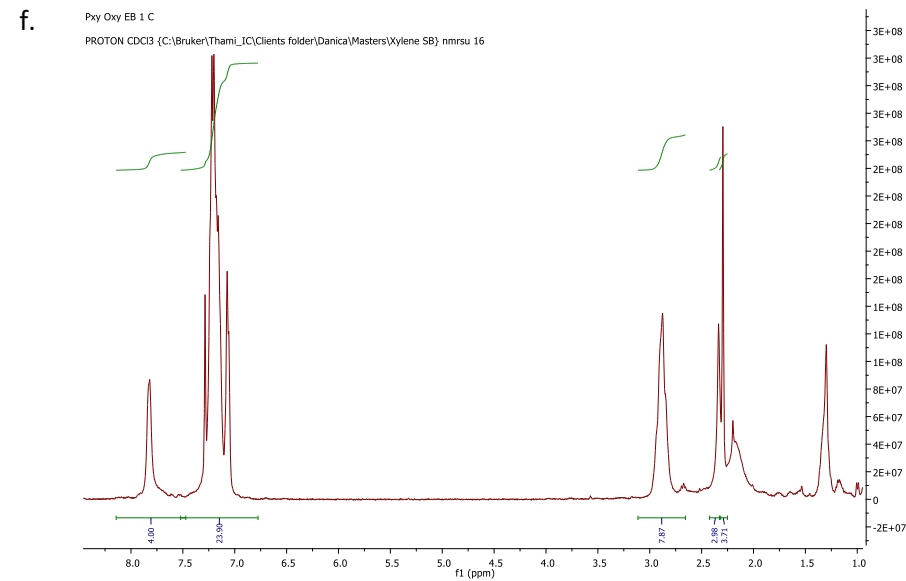
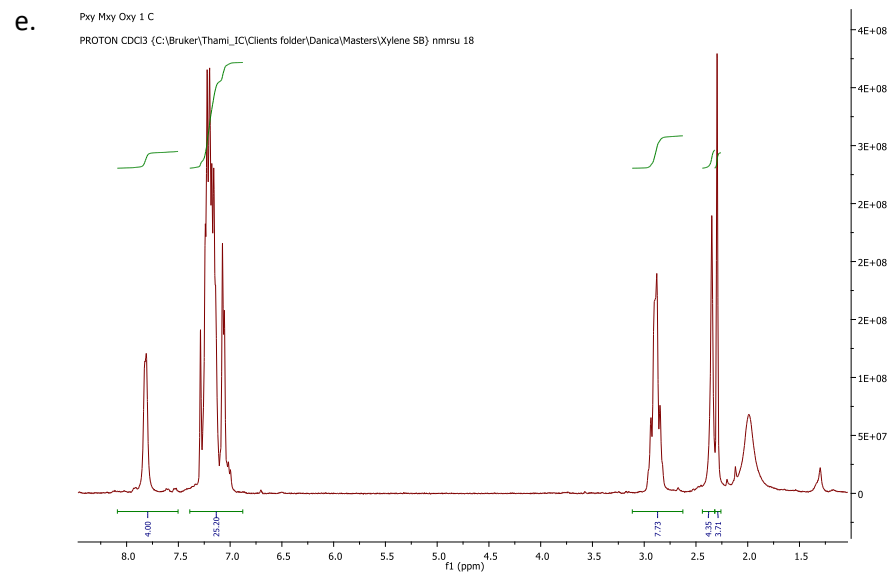
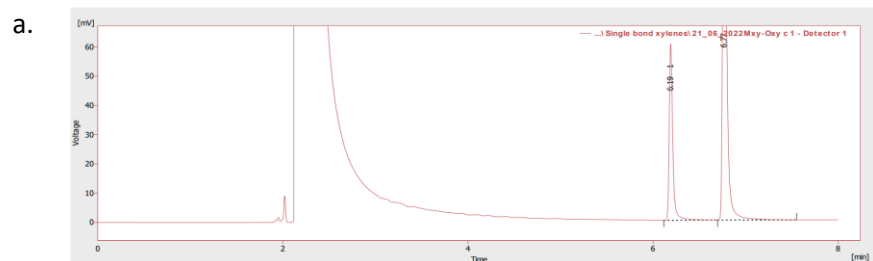
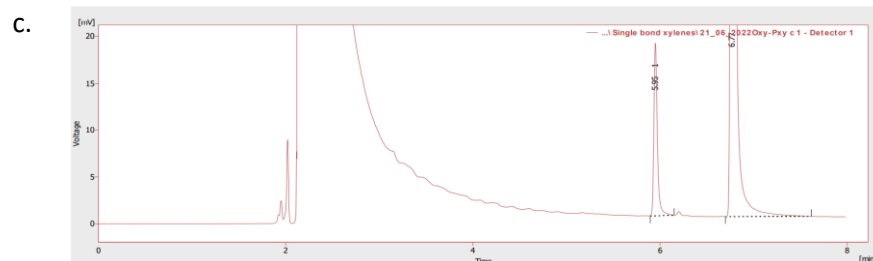


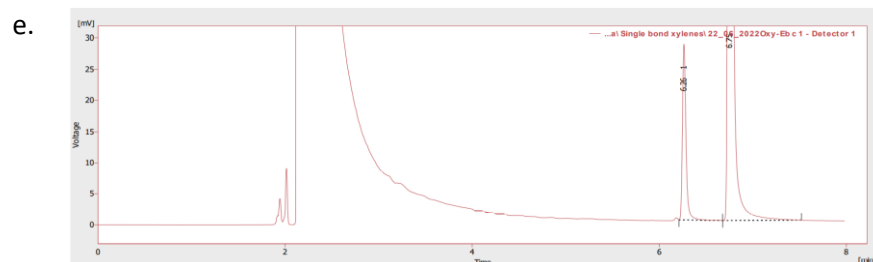
Figure S14: H2 with a. o-Xy, b. o-Xy/p-Xy, c. o-Xy/EB, d. o-Xy/m-Xy, e. o-Xy/m-Xy/p-Xy, f. o-Xy/p-Xy/EB, g. o-Xy/m-Xy/EB and h. all 4 Xy/EB



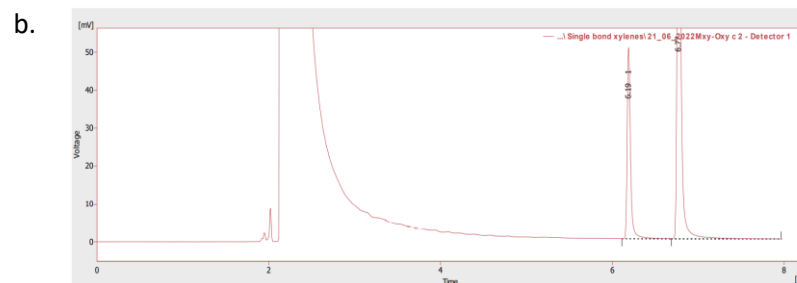
	Reten. Time [min]	Area [mV.s]	Height [mV]	Area [%]	Height [%]	W05 [min]	Compound Name
1	6.190	161.540	60.339	26.4	29.2	0.04	
2	6.768	450.133	145.963	73.6	70.8	0.04	
	Total	611.673	206.302	100.0	100.0		



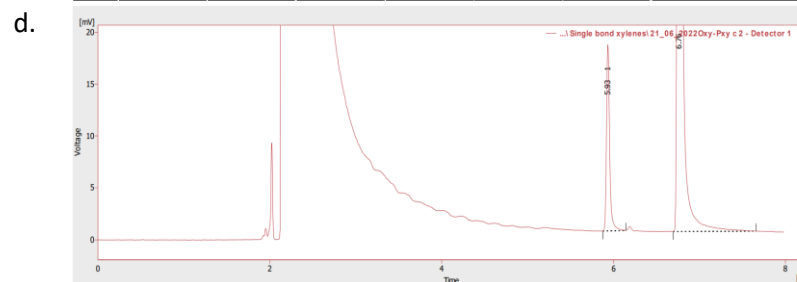
	Reten. Time [min]	Area [mV.s]	Height [mV]	Area [%]	Height [%]	W05 [min]	Compound Name
1	5.950	47.017	18.412	9.1	10.8	0.04	
2	6.770	471.290	151.563	90.9	89.2	0.05	
	Total	518.307	169.975	100.0	100.0		



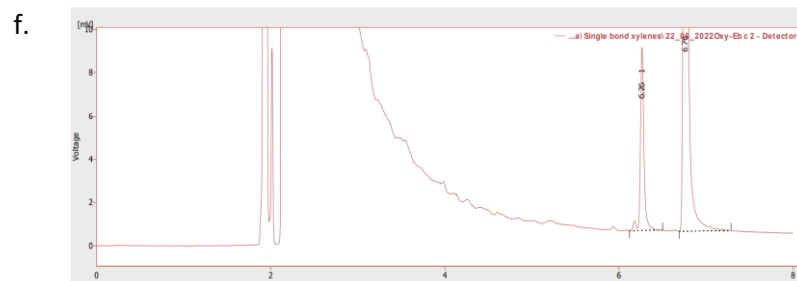
	Reten. Time [min]	Area [mV.s]	Height [mV]	Area [%]	Height [%]	W05 [min]	Compound Name
1	6.263	74.567	28.179	10.9	12.7	0.04	
2	6.752	606.732	194.125	89.1	87.3	0.05	
	Total	681.299	222.305	100.0	100.0		



	Reten. Time [min]	Area [mV.s]	Height [mV]	Area [%]	Height [%]	W05 [min]	Compound Name
1	6.188	138.500	50.428	26.3	28.5	0.04	
2	6.770	388.014	126.748	73.7	71.5	0.04	
	Total	526.514	177.177	100.0	100.0		



	Reten. Time [min]	Area [mV.s]	Height [mV]	Area [%]	Height [%]	W05 [min]	Compound Name
1	5.933	45.449	17.991	8.3	9.8	0.04	
2	6.762	504.543	165.626	91.7	90.2	0.04	
	Total	549.993	183.618	100.0	100.0		



	Reten. Time [min]	Area [mV.s]	Height [mV]	Area [%]	Height [%]	W05 [min]	Compound Name
1	6.265	23.953	8.456	13.0	13.5	0.04	
2	6.762	160.290	54.124	87.0	86.5	0.04	
	Total	184.244	62.581	100.0	100.0		

Figure S15: Host compound H2 with the duplicate crystal data for *o*-Xy/*m*-Xy in a. and b., for *o*-Xy/*p*-Xy in c. and d., and for *o*-Xy/EB in e. and f.

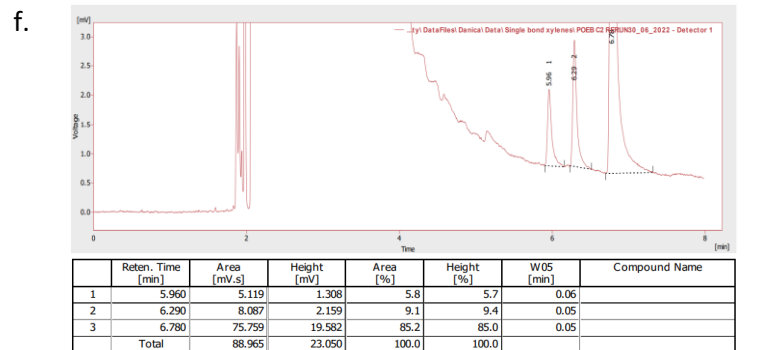
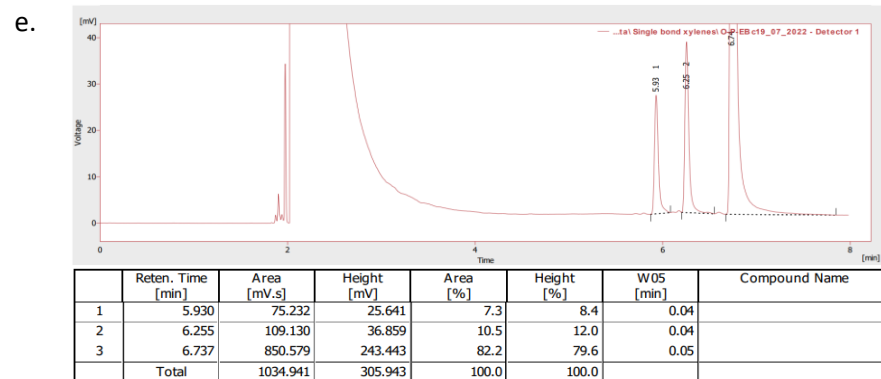
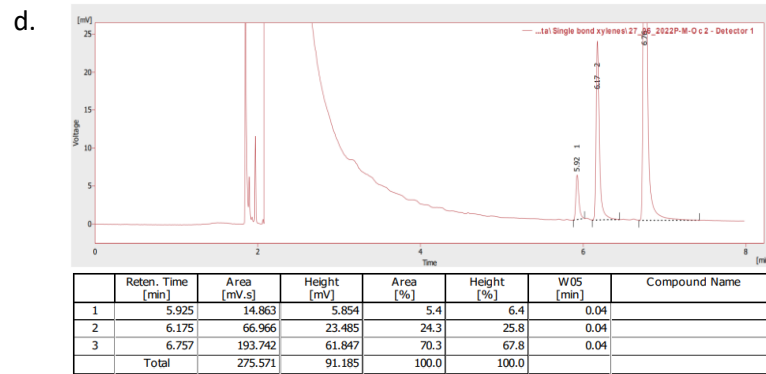
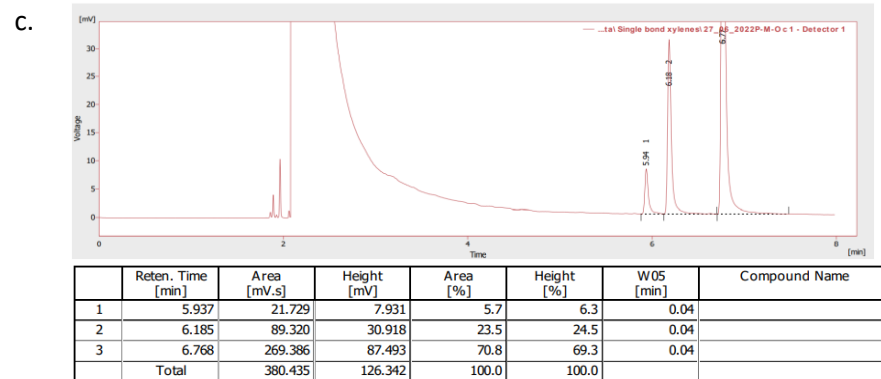
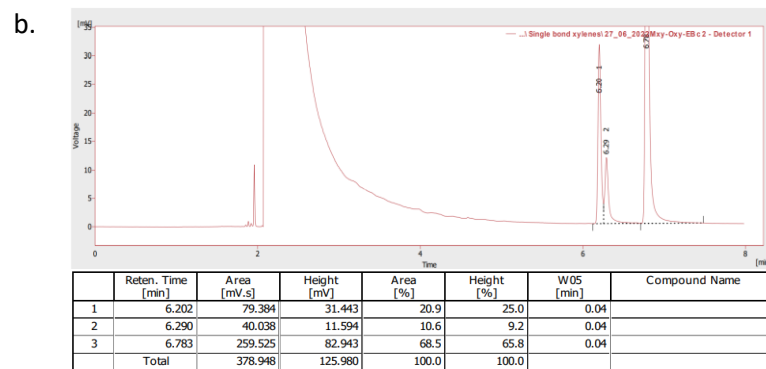
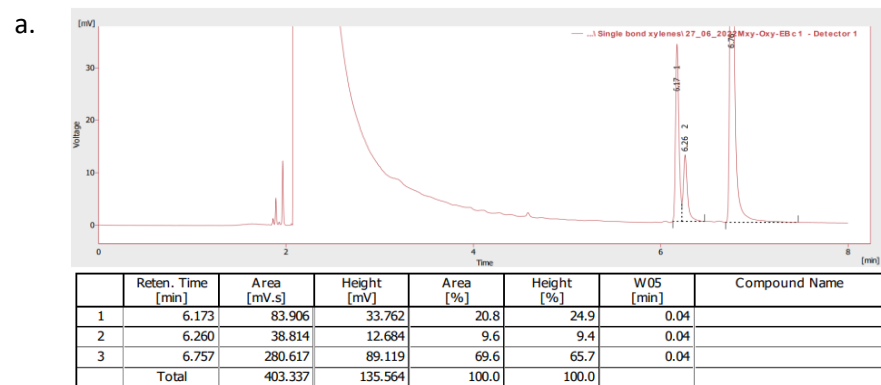


Figure S16: Host compound H2 crystal data with *o*-Xy-*m*-Xy-EB in a. and b., with *p*-Xy-*o*-Xy-*m*-Xy in c. and d., and with *o*-Xy-*p*-Xy-EB in e. and f.

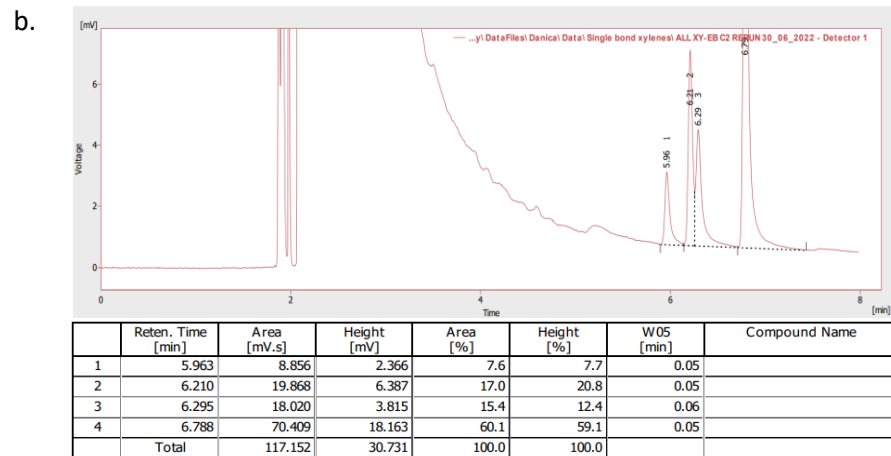
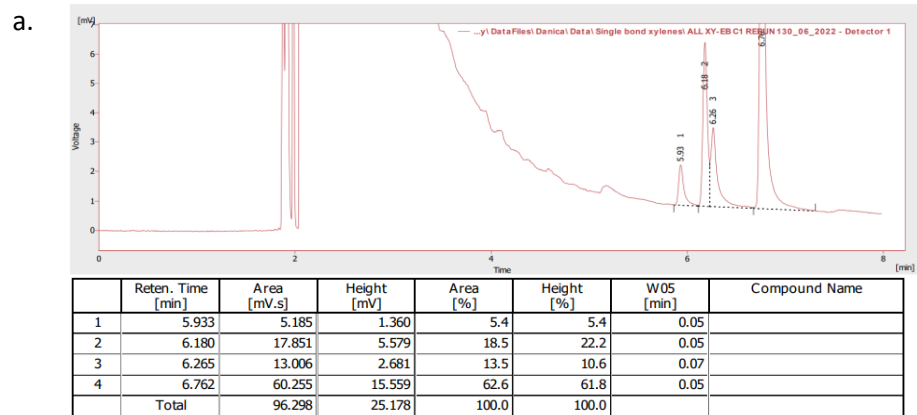
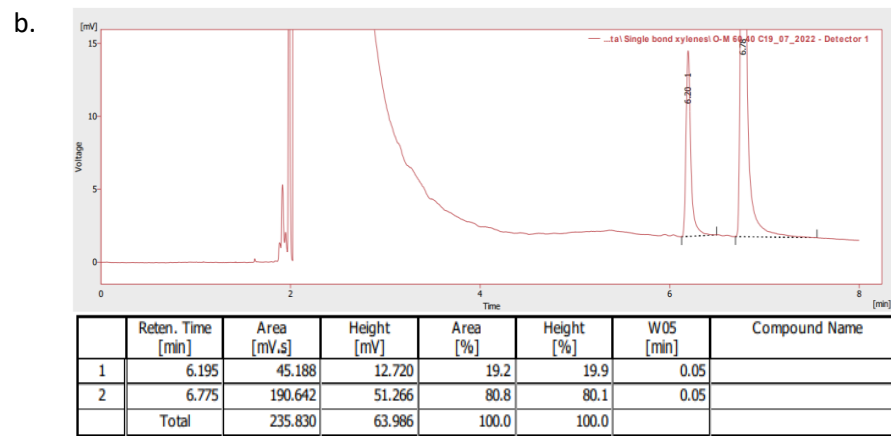
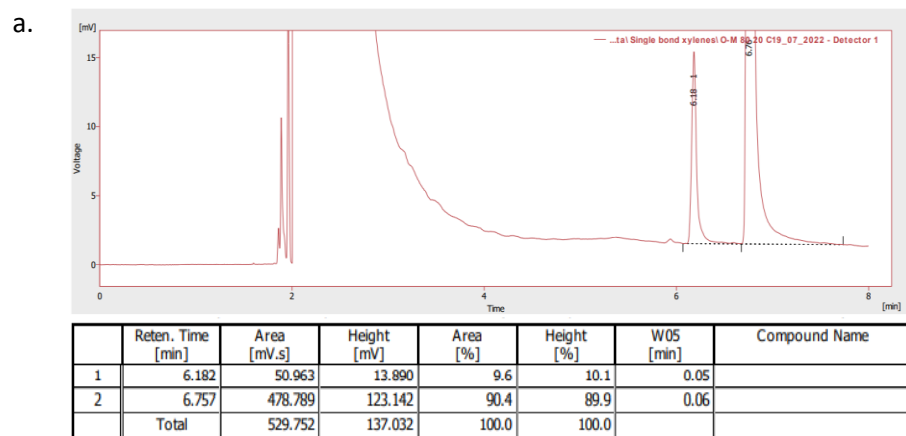


Figure S17: Host compound H2 crystal data with all 4 xylene isomers and ethylbenzene in a. and b.



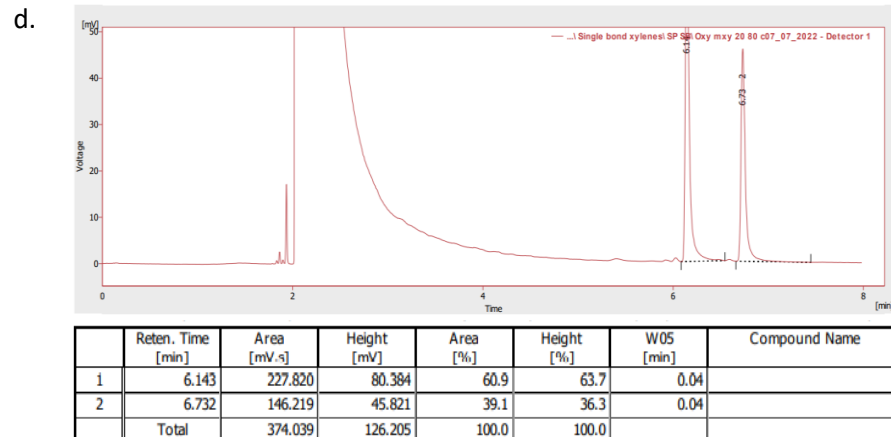
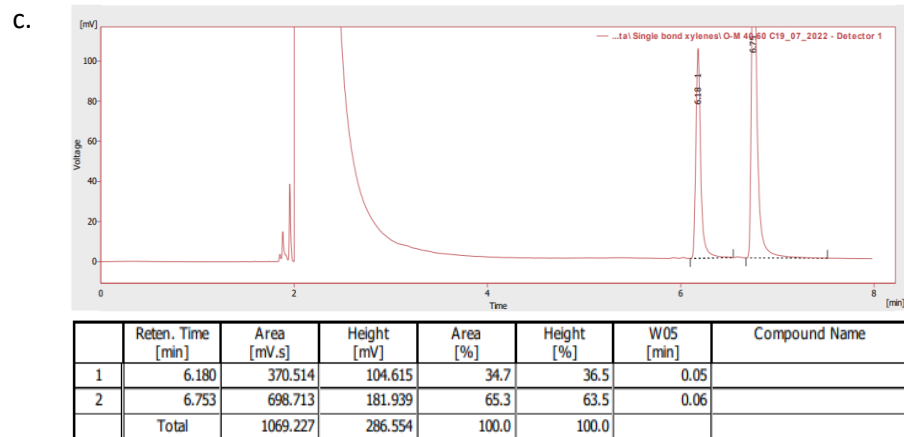
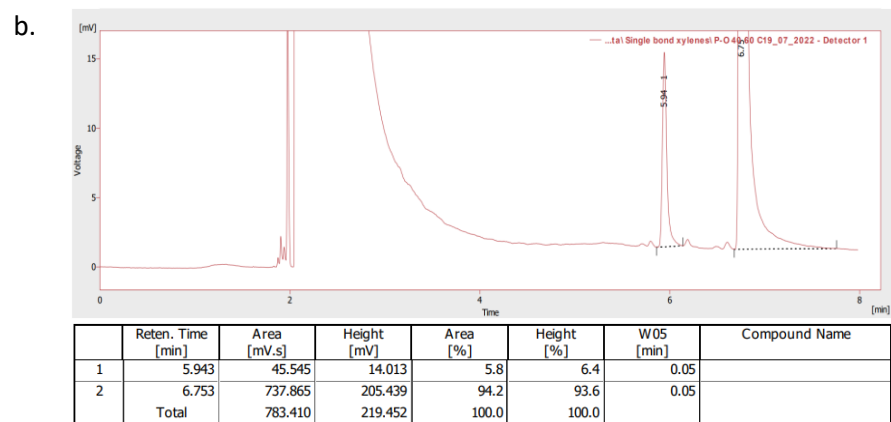
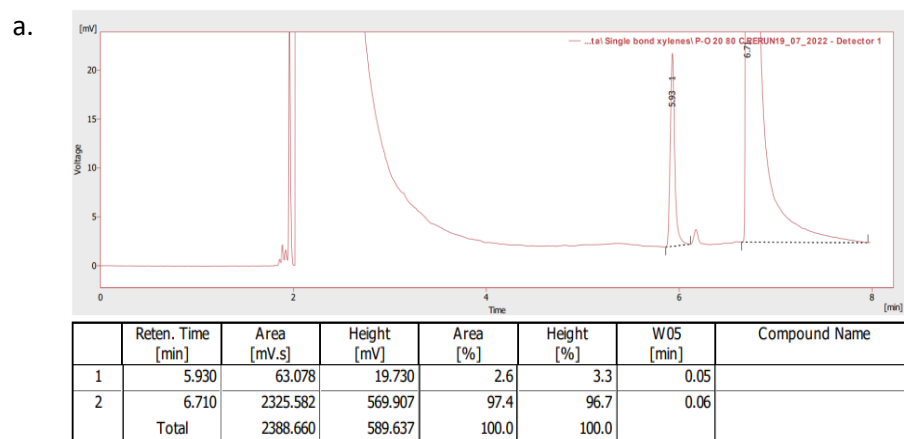
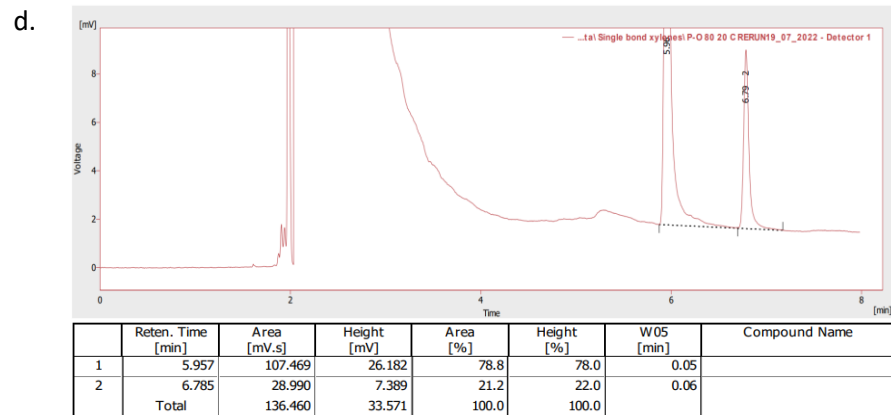
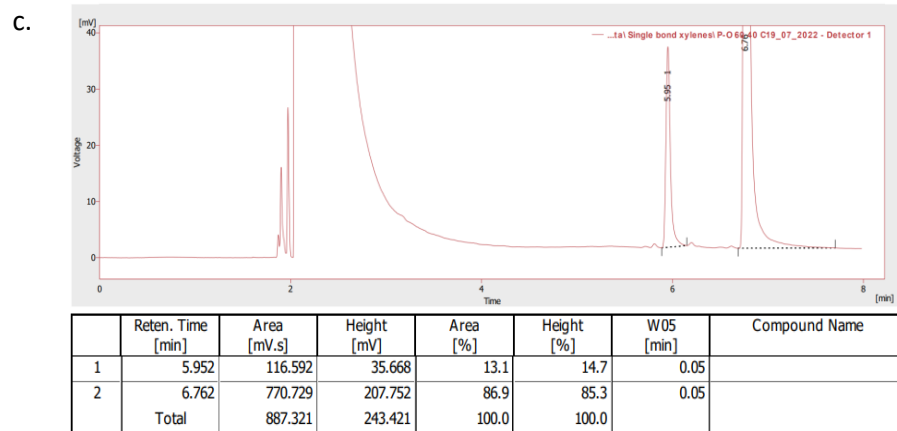
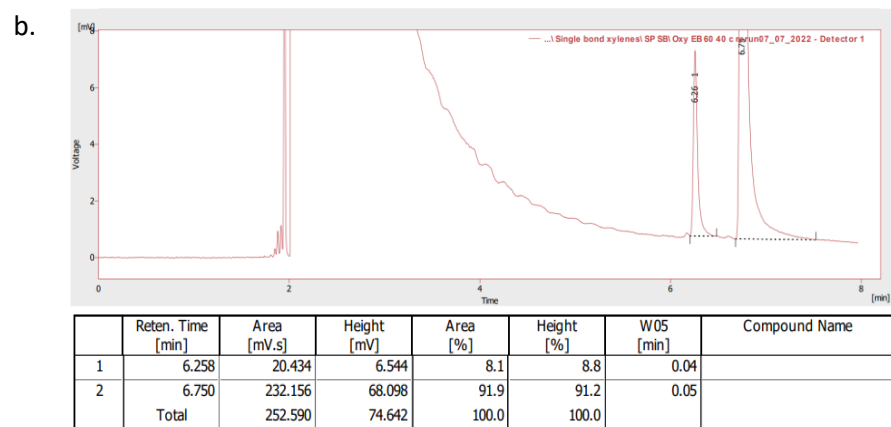
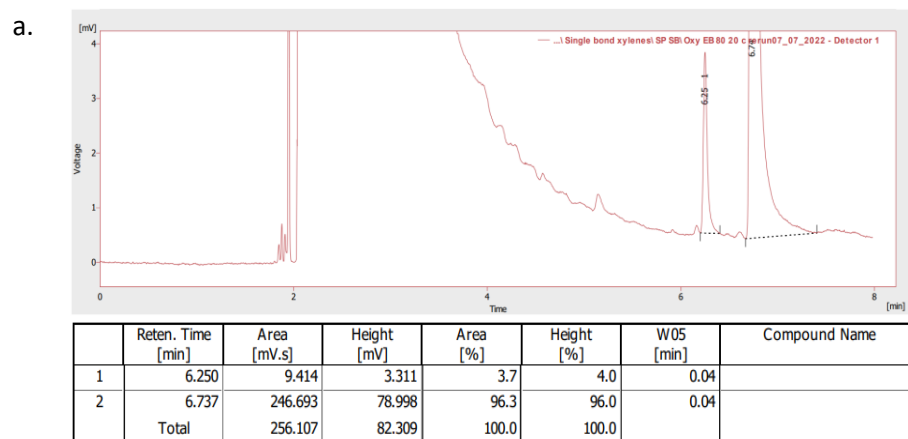


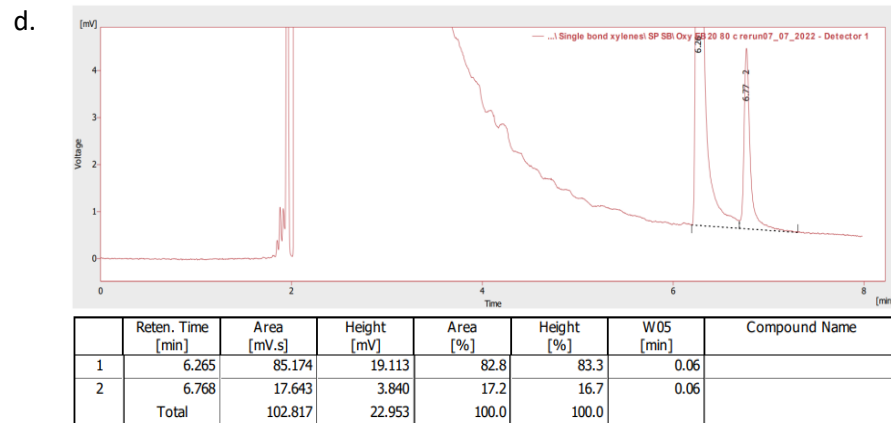
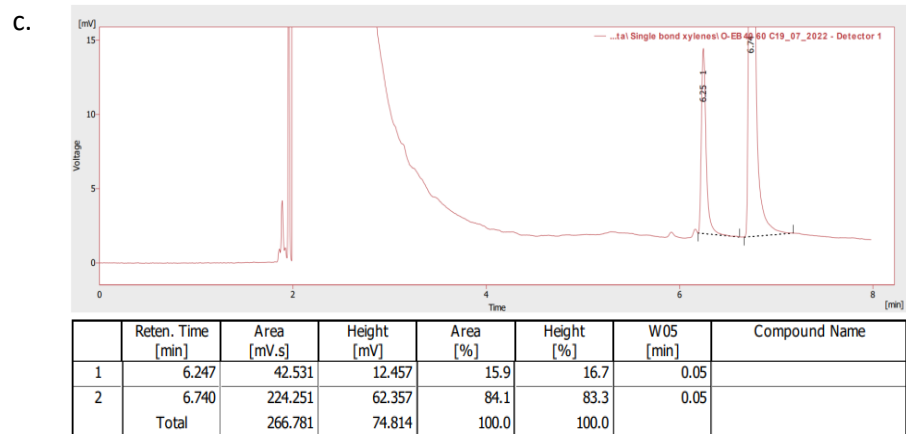
Figure S18: Host compound H2 for the selectivity profile *o*-Xy/*m*-Xy for the crystals with a. 80 20, b. 60 40, c. 40 60, and d. 20 80 concentrations



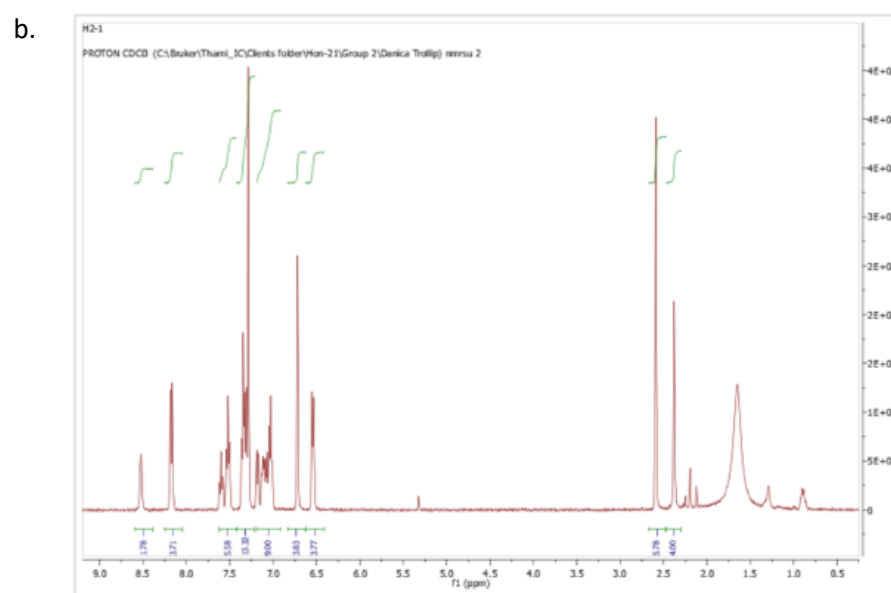
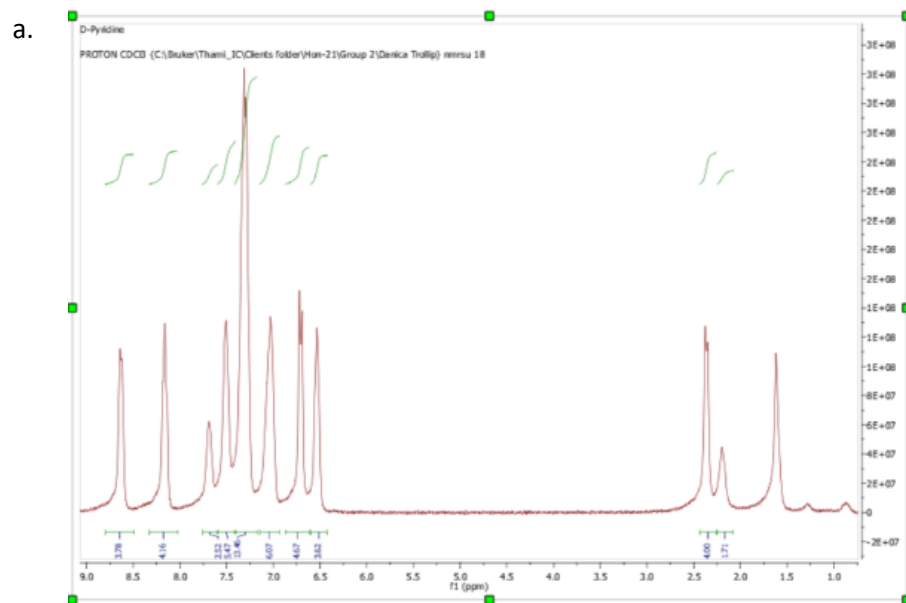


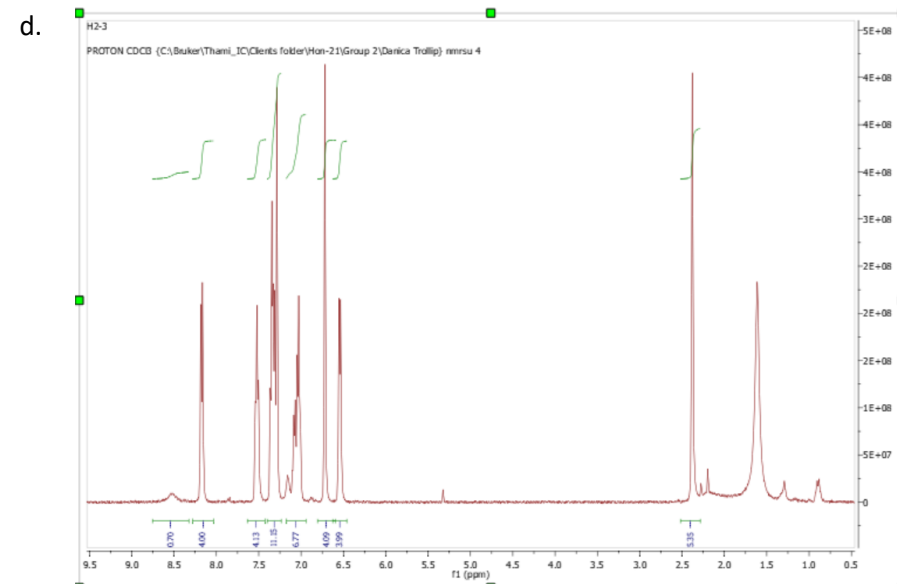
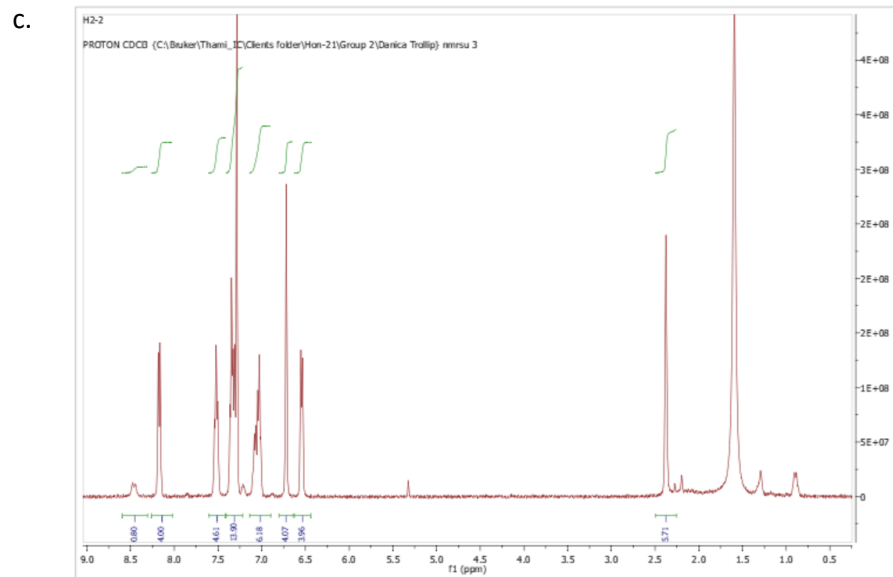
**Figure S19:** Host compound H2 for the selectivity profile *o*-Xy/*p*-Xy for the crystals with a. 80 20, b. 60 40, c. 40 60, and d. 20 80 concentrations





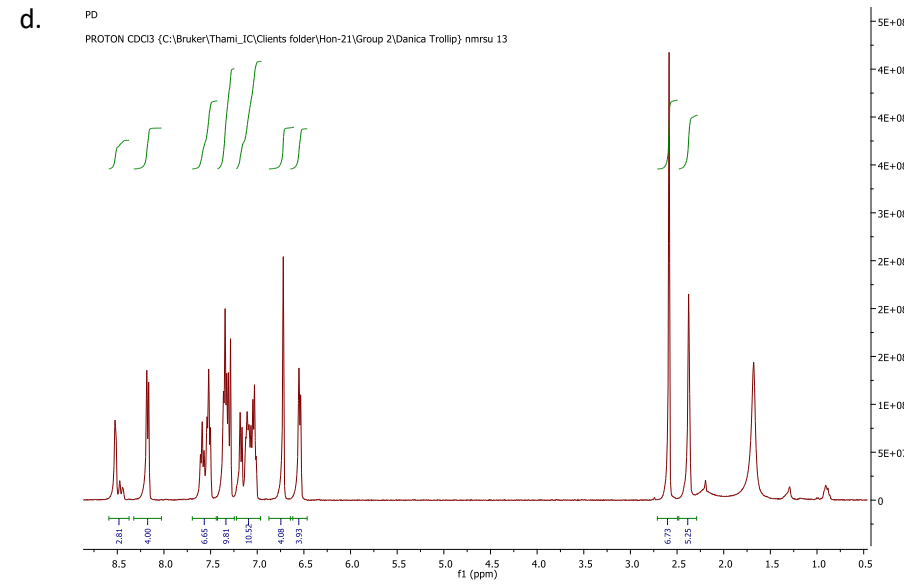
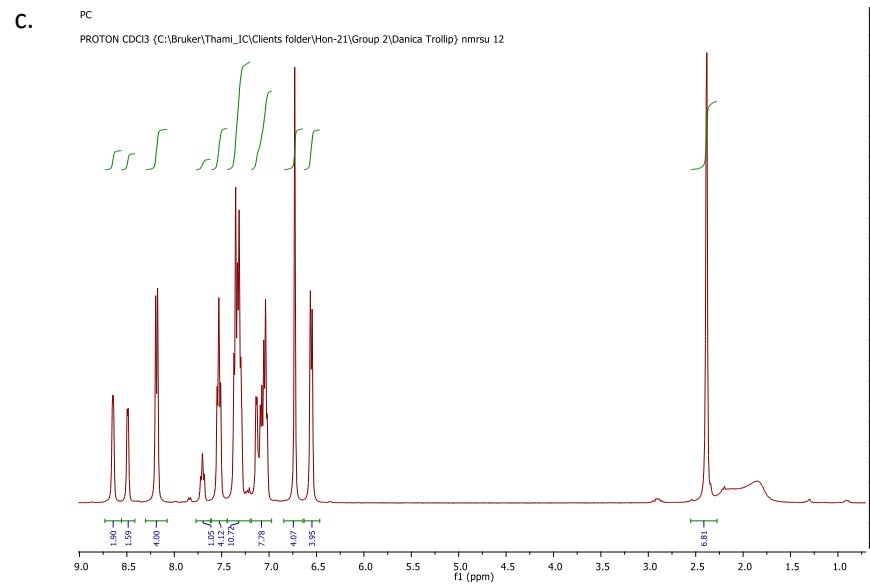
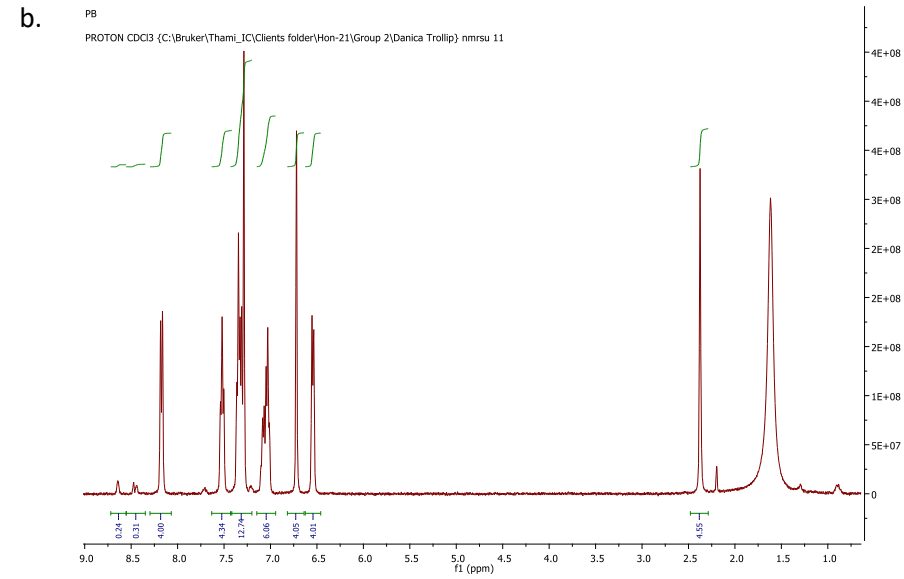
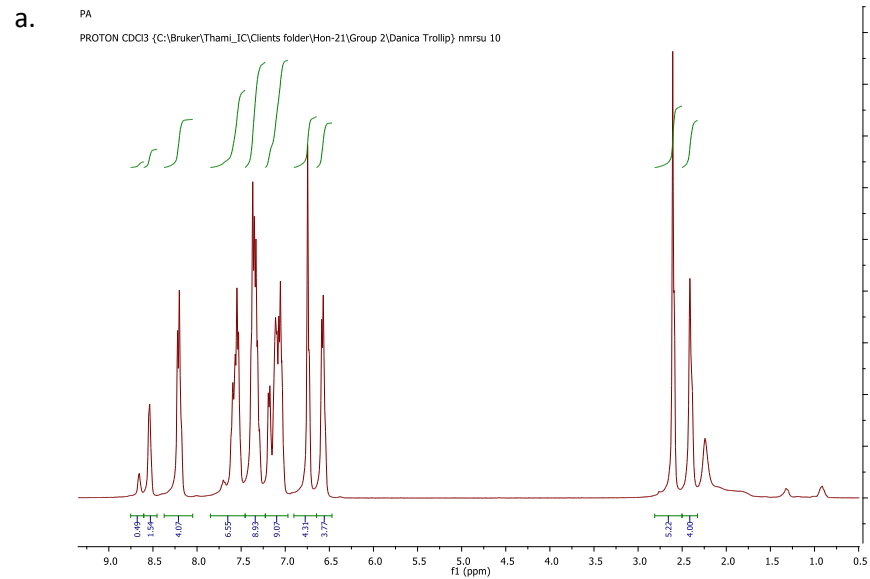
**Figure S20:** Host compound **H2** for the selectivity profile *o*-Xy/EB for the crystals with a. 80 20, b. 60 40, c. 40 60, and d. 20 80 concentrations

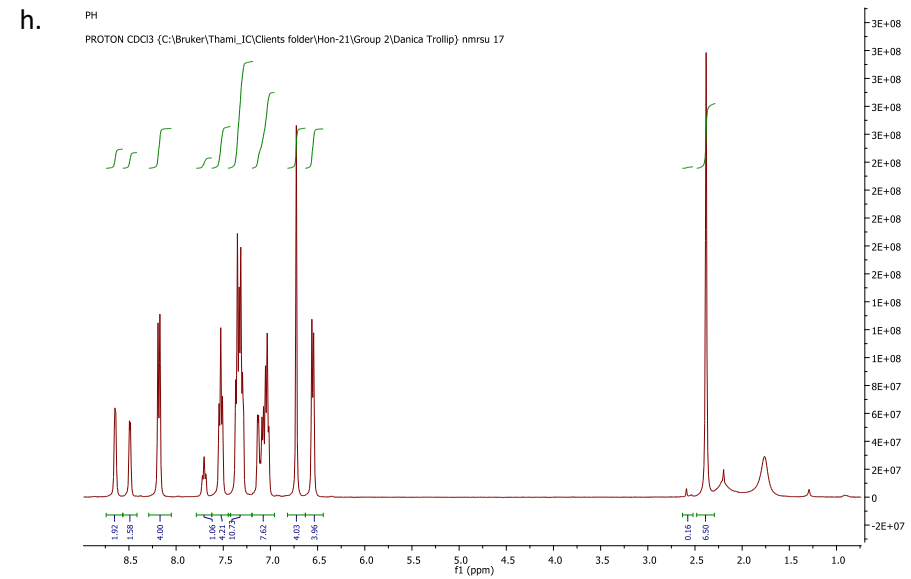
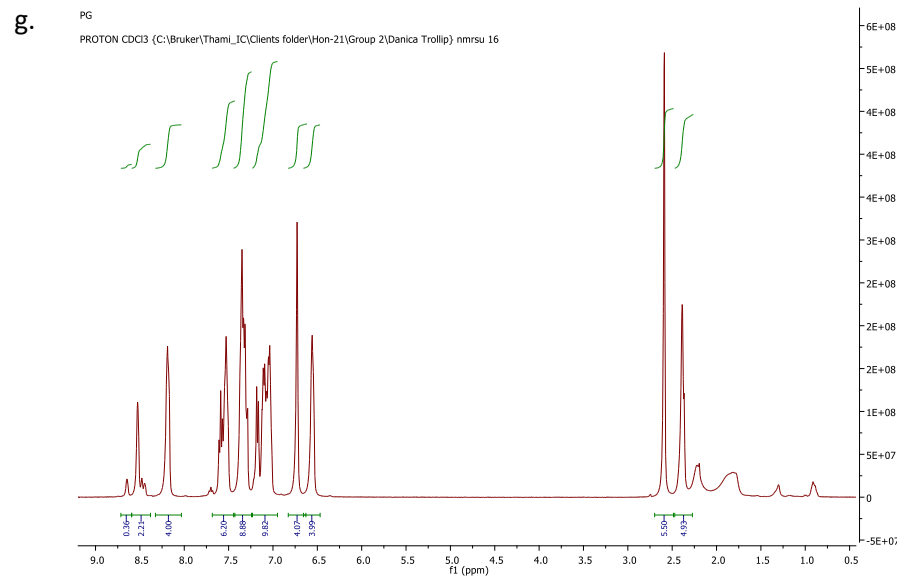
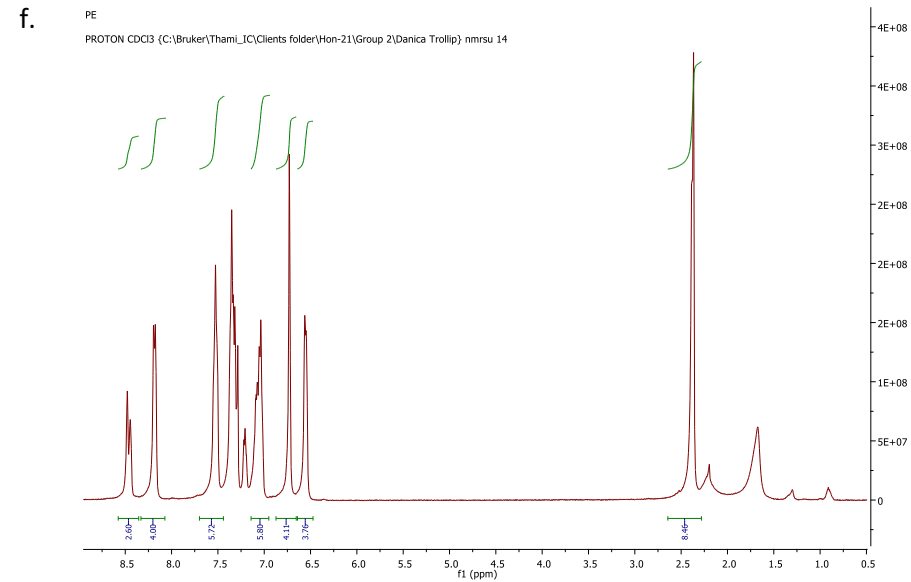
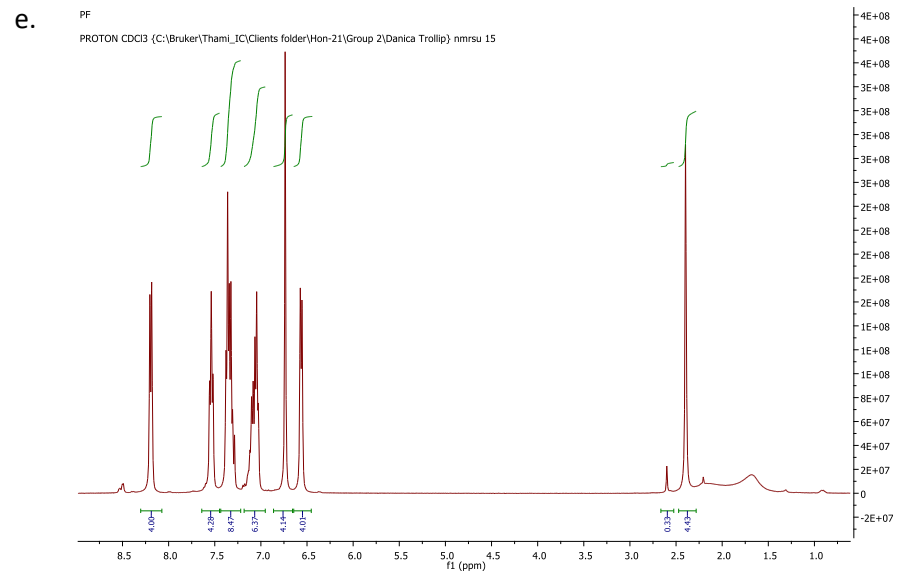




**Figure S21:** Host compound **H1** single solvent experiments with a. PYR, b. 2MP, c. 3MP and d. 4MP







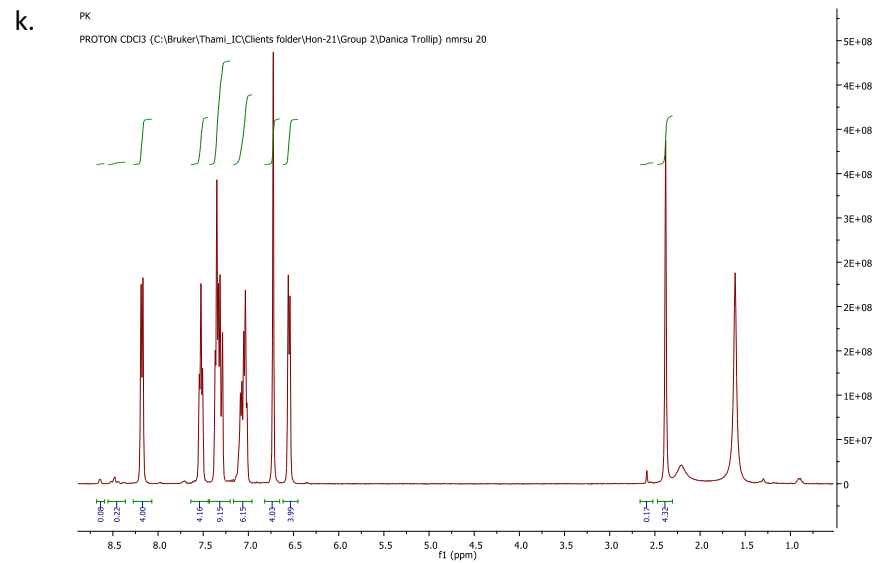
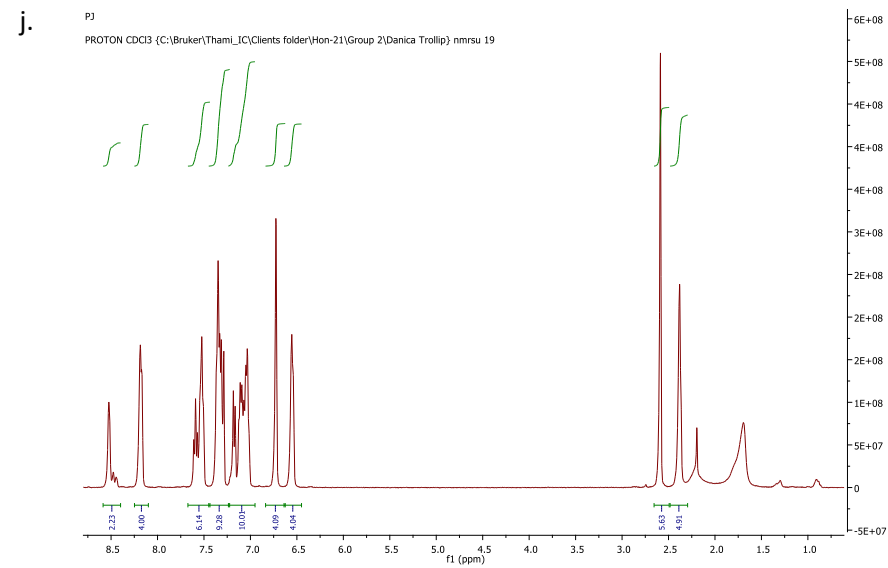
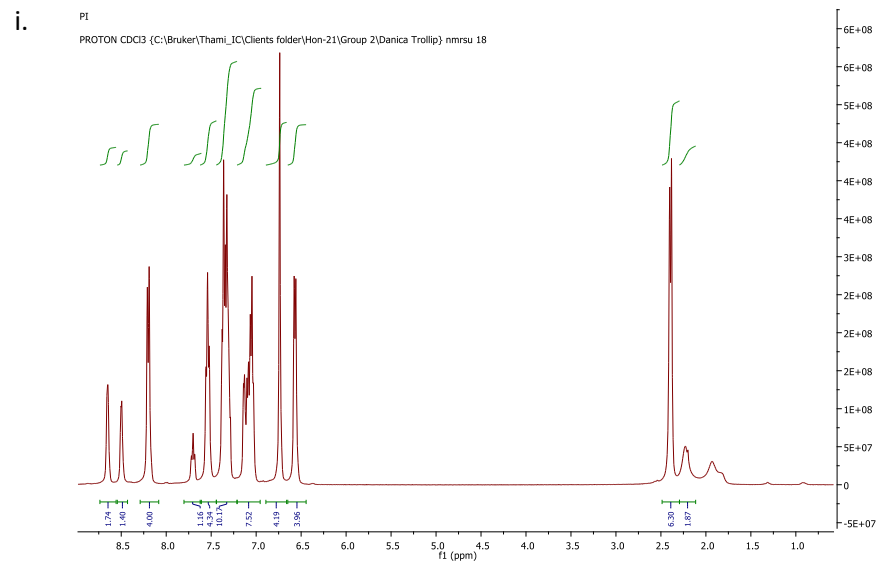
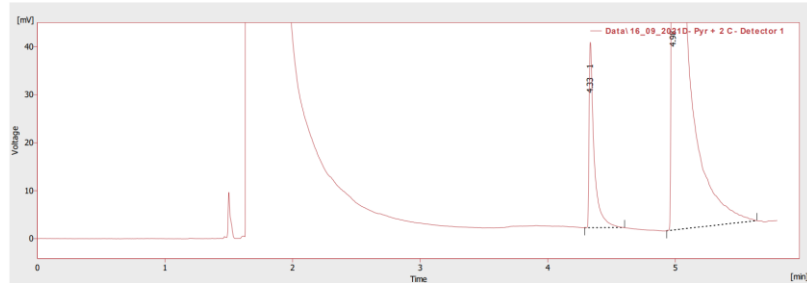


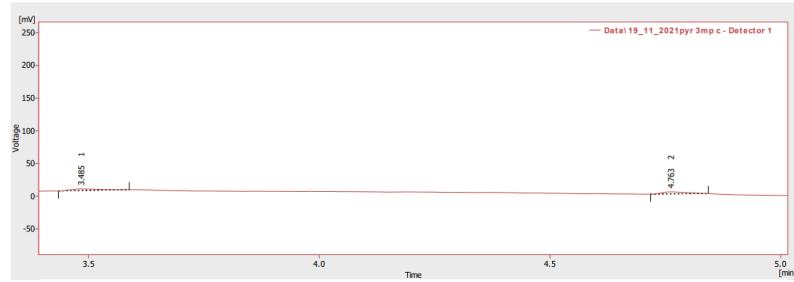
**Figure S22:**  $^1\text{H}$  with a. PYR/2MP, b. PYR/3MP, c. PYR/4MP, d. 2MP/3MP, e. 2MP/4MP, f. 3MP/4MP, g. PYR/2MP/3MP, h. PYR/2MP/4MP, i. PYR/3MP/4MP, j. 2MP/3MP/4MP, and k. all 4 PYR/MP's

a.



	Reten. Time [min]	Area [mV.s]	Height [mV]	Area [%]	Height [%]	W05 [min]	Compound Name
1	4.333	105.953	38.620	8.8	16.0	0.04	
2	4.983	1102.428	202.173	91.2	84.0	0.06	
	Total	1208.381	240.793	100.0	100.0		

c.



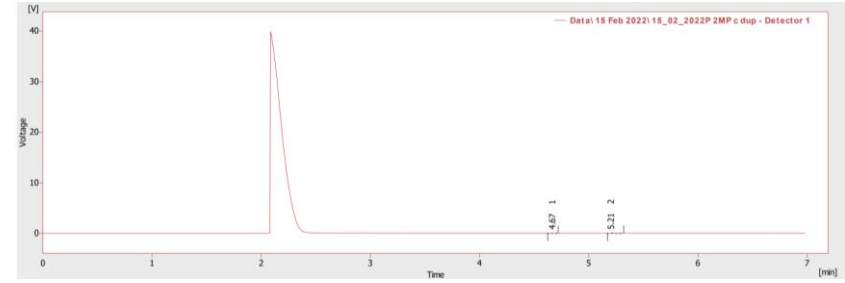
	Reten. Time [min]	Area [mV.s]	Height [mV]	Area [%]	Height [%]	W05 [min]	Compound Name
1	3.485	10.995	2.578	47.2	44.6	0.13	
2	4.763	12.299	3.206	52.8	55.4	0.07	
	Total	23.295	5.783	100.0	100.0		

e.



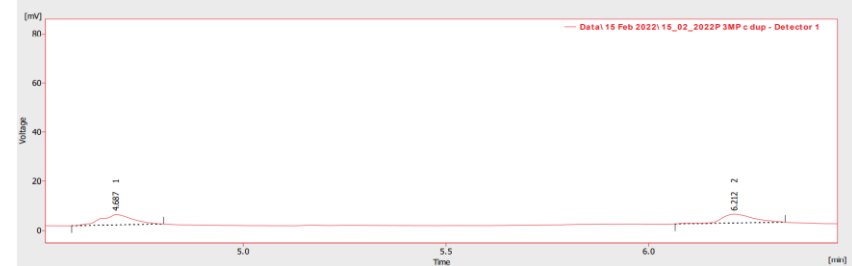
	Reten. Time [min]	Area [mV.s]	Height [mV]	Area [%]	Height [%]	W05 [min]	Compound Name
1	4.698	28.133	7.797	41.0	49.7	0.06	
2	6.380	40.560	7.889	59.0	50.3	0.09	
	Total	68.693	15.686	100.0	100.0		

b.



	Reten. Time [min]	Area [mV.s]	Height [mV]	Area [%]	Height [%]	W05 [min]	Compound Name
1	4.670	18.357	7.248	8.8	11.0	0.04	
2	5.207	190.932	58.795	91.2	89.0	0.05	
	Total	209.289	66.043	100.0	100.0		

d.



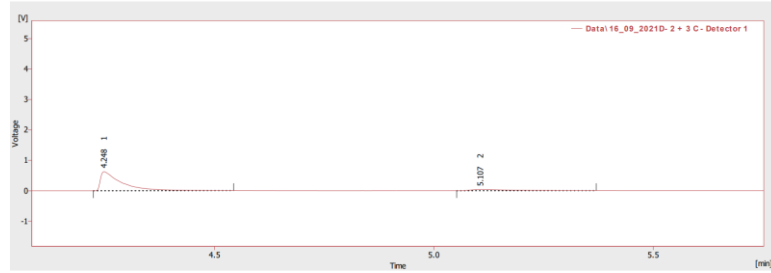
	Reten. Time [min]	Area [mV.s]	Height [mV]	Area [%]	Height [%]	W05 [min]	Compound Name
1	4.687	22.874	4.229	53.7	54.2	0.09	
2	6.212	19.694	3.574	46.3	45.8	0.08	
	Total	42.568	7.803	100.0	100.0		

f.



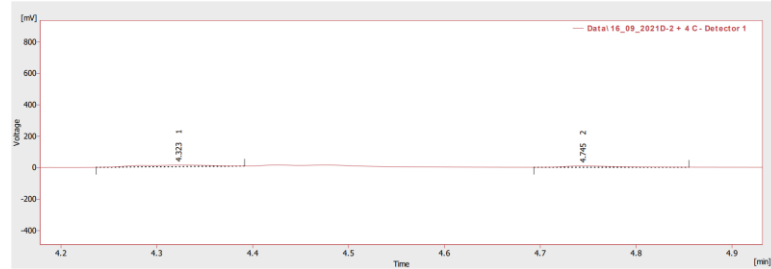
	Reten. Time [min]	Area [mV.s]	Height [mV]	Area [%]	Height [%]	W05 [min]	Compound Name
1	4.565	42.572	11.120	45.2	50.7	0.06	
2	6.157	51.662	10.820	54.8	49.3	0.07	
	Total	94.234	21.940	100.0	100.0		

g.



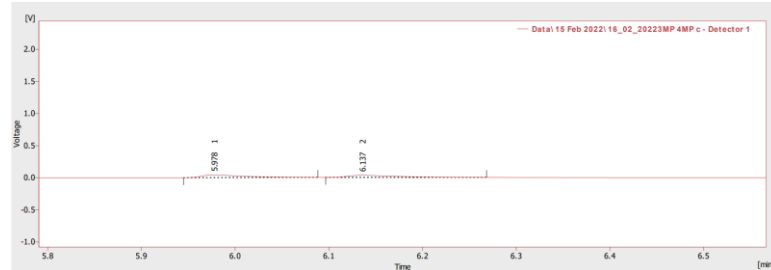
	Reten. Time [min]	Area [mV.s]	Height [mV]	Area [%]	Height [%]	W05 [min]	Compound Name
1	4.248	2086.201	624.760	89.6	94.4	0.04	
2	5.107	242.709	36.943	10.4	5.6	0.09	
Total		2328.911	661.704	100.0	100.0		

i.



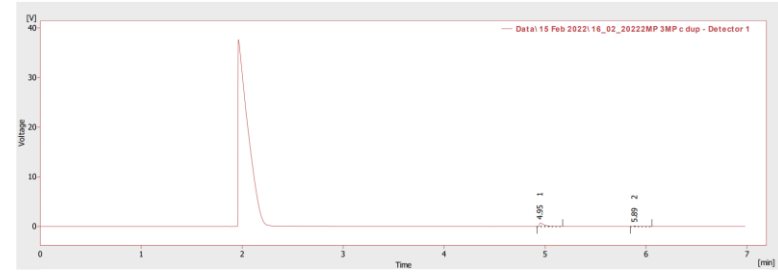
	Reten. Time [min]	Area [mV.s]	Height [mV]	Area [%]	Height [%]	W05 [min]	Compound Name
1	4.323	52.245	9.944	63.2	53.8	0.10	
2	4.745	30.400	8.532	36.8	46.2	0.06	
Total		82.645	18.476	100.0	100.0		

k.



	Reten. Time [min]	Area [mV.s]	Height [mV]	Area [%]	Height [%]	W05 [min]	Compound Name
1	5.978	137.129	42.215	52.6	55.9	0.05	
2	6.137	123.805	33.276	47.4	44.1	0.06	
Total		260.934	75.491	100.0	100.0		

h.



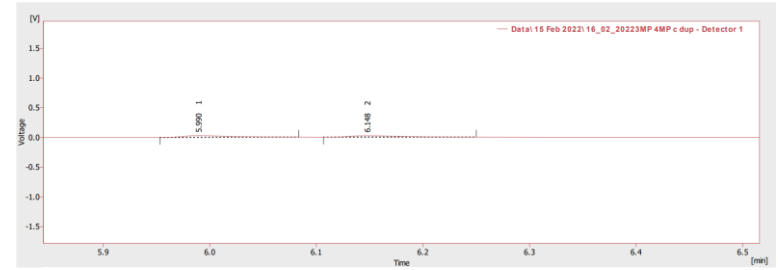
	Reten. Time [min]	Area [mV.s]	Height [mV]	Area [%]	Height [%]	W05 [min]	Compound Name
1	4.952	2341.457	682.771	88.0	89.4	0.05	
2	5.887	319.590	81.182	12.0	10.6	0.06	
Total		2661.047	763.953	100.0	100.0		

j.



	Reten. Time [min]	Area [mV.s]	Height [mV]	Area [%]	Height [%]	W05 [min]	Compound Name
1	5.115	26.586	6.606	63.8	66.1	0.06	
2	6.175	15.059	3.394	36.2	33.9	0.08	
Total		41.645	9.999	100.0	100.0		

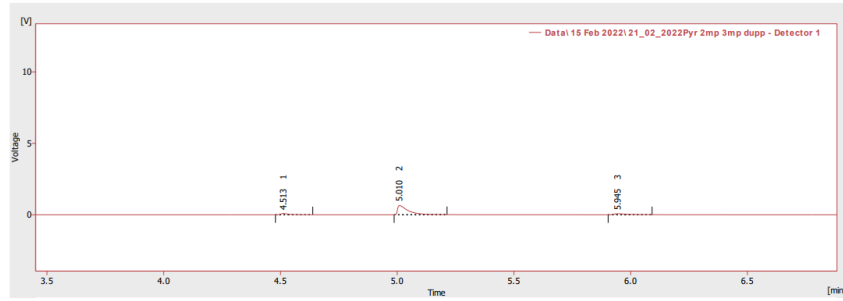
l.



	Reten. Time [min]	Area [mV.s]	Height [mV]	Area [%]	Height [%]	W05 [min]	Compound Name
1	5.990	88.416	28.040	52.2	55.6	0.05	
2	6.148	80.891	22.425	47.8	44.4	0.06	
Total		169.308	50.464	100.0	100.0		

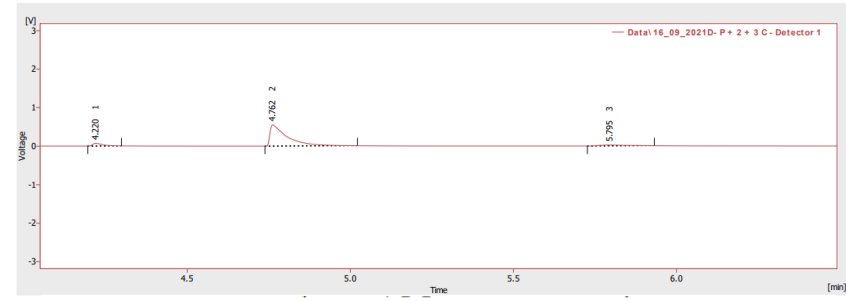
**Figure S23:** Host compound H1 with the duplicate crystal data for PYR/2MP in a. and b., for PYR/3MP in c. and d., for PYR/4MP in e. and f., for 2MP/3MP in g. and h., for 2MP/4MP in i. and j., and for 3MP/4MP in k. and l.

a.



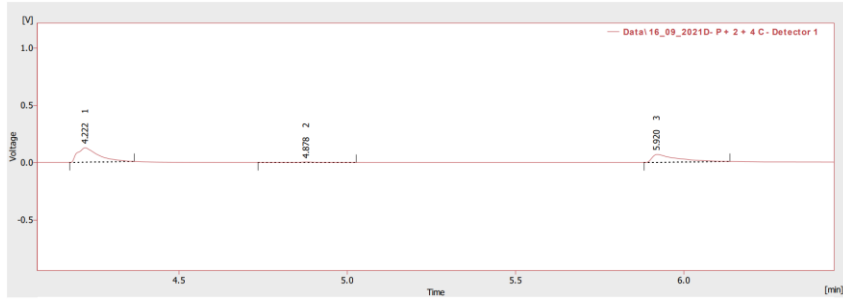
	Reten. Time [min]	Area [mV.s]	Height [mV]	Area [%]	Height [%]	W05 [min]	Compound Name
1	4.513	207.362	89.660	8.3	11.1	0.03	
2	5.010	2017.566	648.044	80.9	80.2	0.04	
3	5.945	269.724	70.497	10.8	8.7	0.06	
	Total	2494.653	808.201	100.0	100.0		

b.



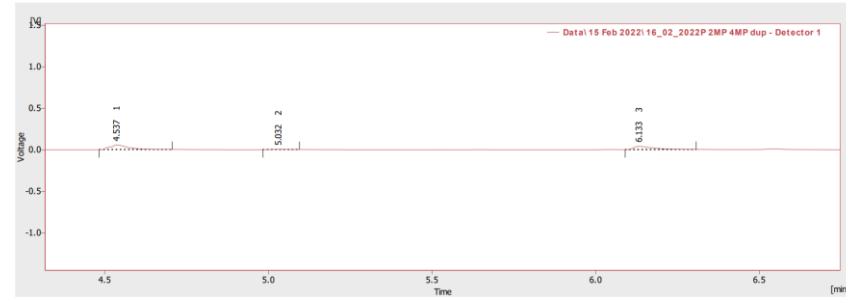
	Reten. Time [min]	Area [mV.s]	Height [mV]	Area [%]	Height [%]	W05 [min]	Compound Name
1	4.220	148.914	69.151	6.4	10.8	0.03	
2	4.762	2042.215	549.900	87.8	85.6	0.05	
3	5.795	135.440	23.455	5.8	3.7	0.11	
	Total	2326.568	642.507	100.0	100.0		

c.



	Reten. Time [min]	Area [mV.s]	Height [mV]	Area [%]	Height [%]	W05 [min]	Compound Name
1	4.222	545.106	125.566	59.0	63.3	0.07	
2	4.878	17.435	4.247	1.9	2.1	0.05	
3	5.920	362.022	68.696	39.2	34.6	0.08	
	Total	924.563	198.509	100.0	100.0		

d.



	Reten. Time [min]	Area [mV.s]	Height [mV]	Area [%]	Height [%]	W05 [min]	Compound Name
1	4.537	216.654	56.020	54.6	56.7	0.06	
2	5.032	10.292	3.693	2.6	3.7	0.05	
3	6.133	169.771	39.051	42.8	39.5	0.06	
	Total	396.718	98.764	100.0	100.0		

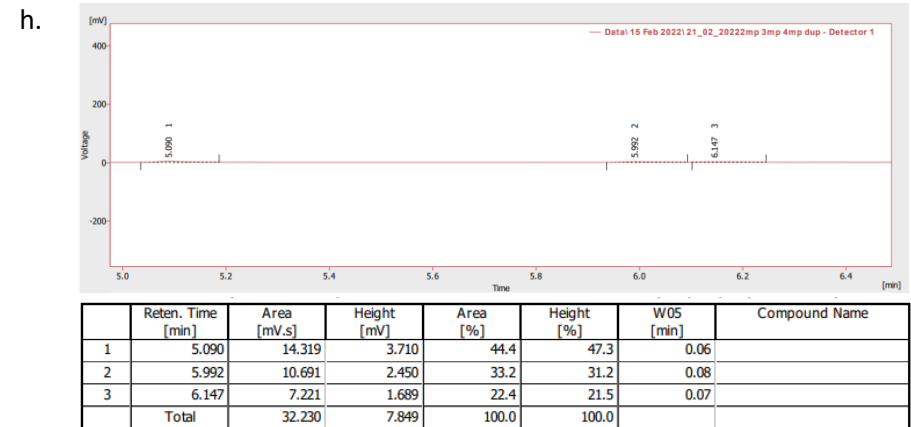
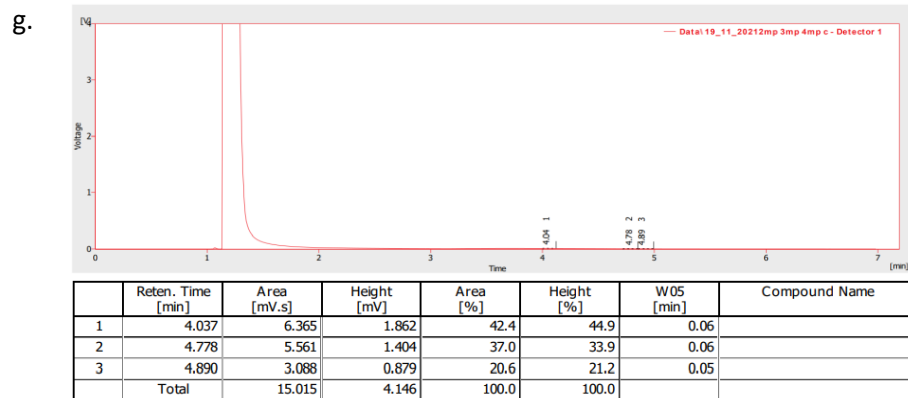
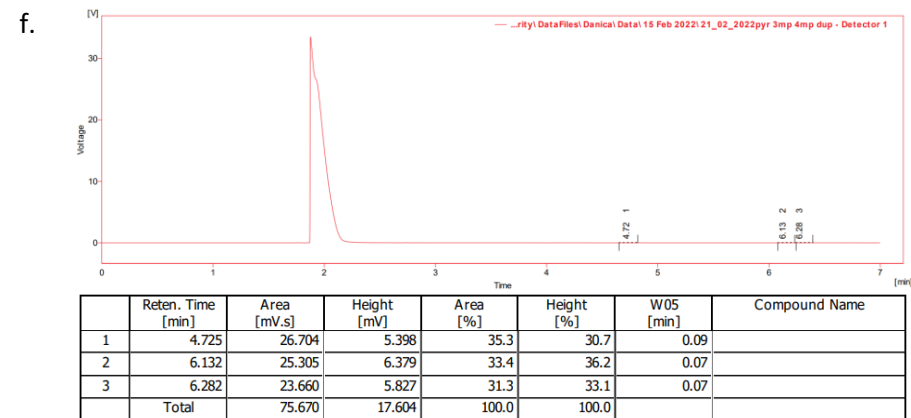
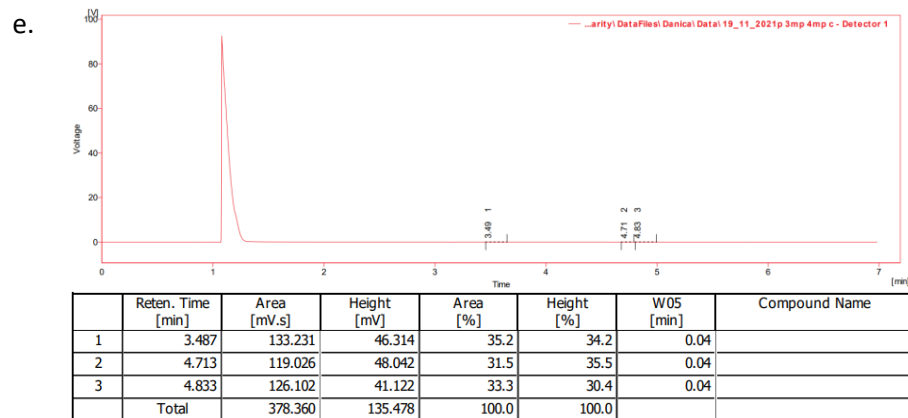


**Figure S24:** Host compound **H1** crystal data with PYR/2MP/3MP in a. and b., with PYR/2MP/4MP in c. and d., with PYR/3MP/4MP in e. and f., and with 2MP/3MP/4MP in g. and h.

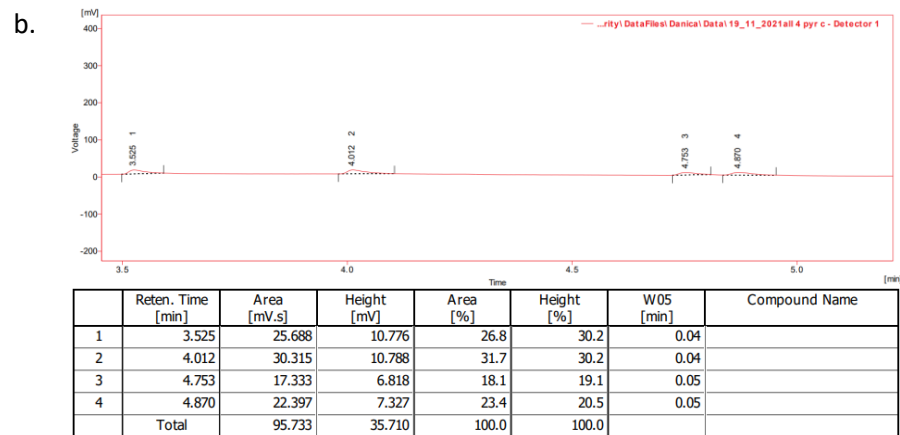
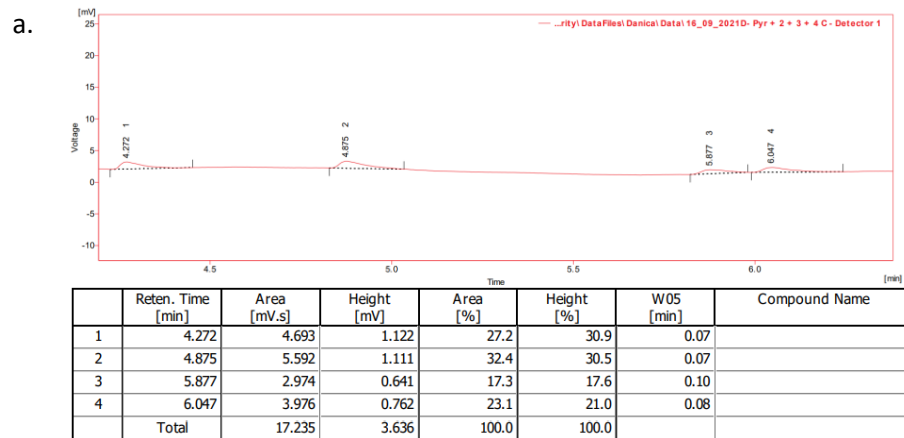
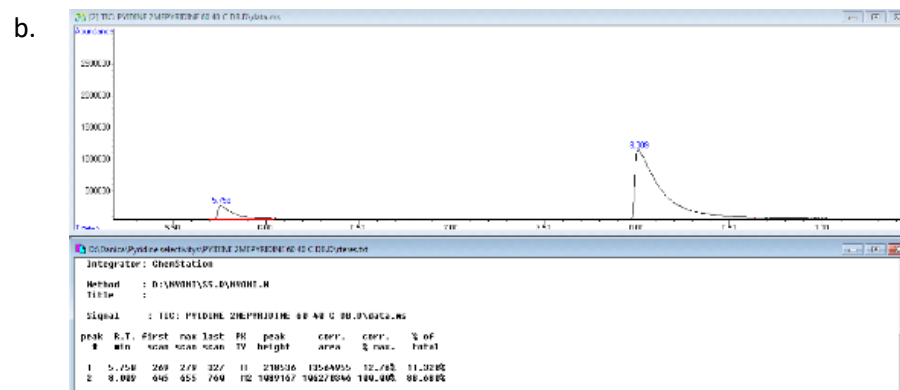
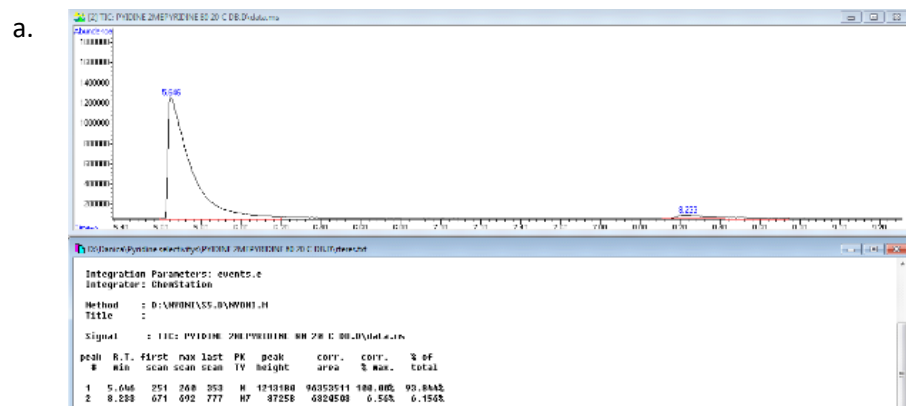


Figure S25: Host compound H1 crystal data with all 4 PYR/MP's in a. and b.





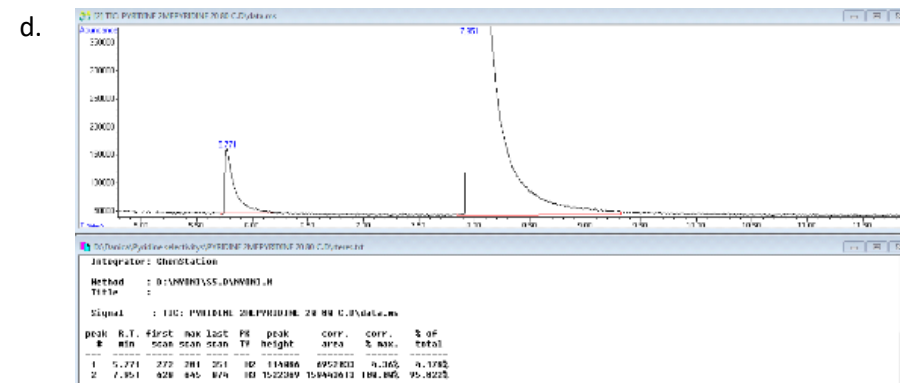
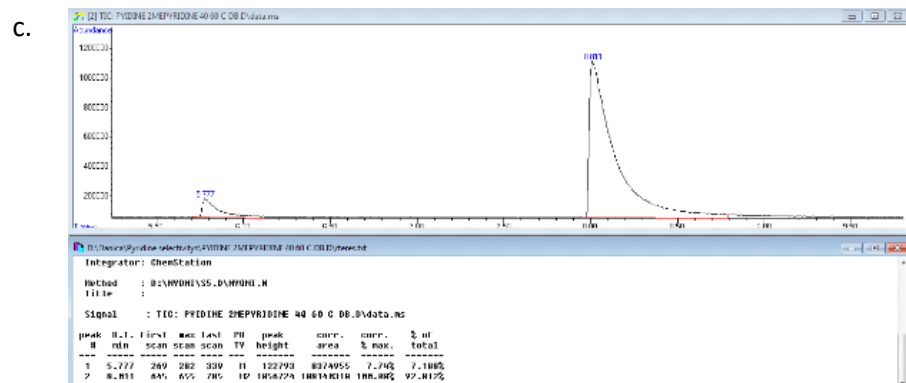
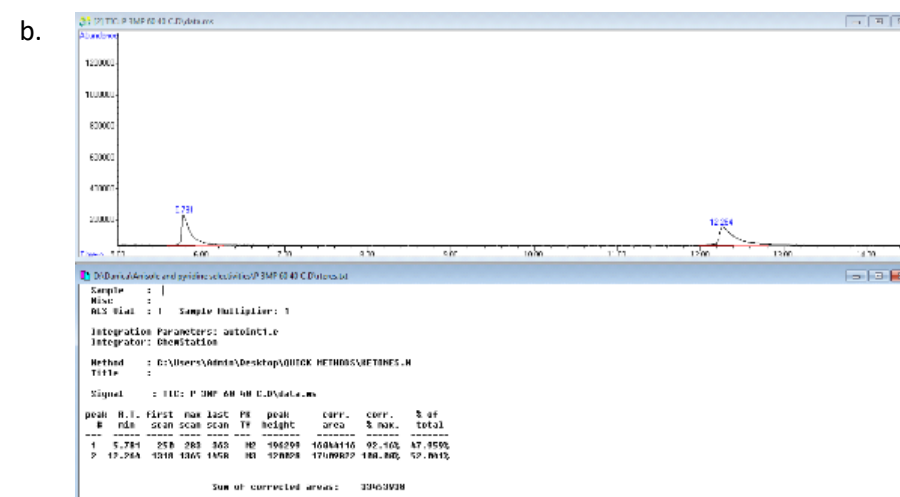
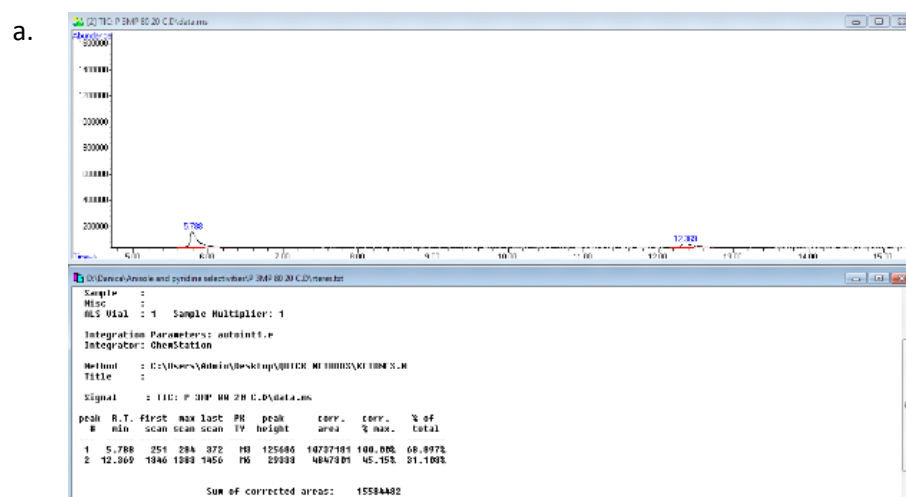


Figure S26: Host compound H1 for the selectivity profile PYR/2MP for the crystals with a. 80 20, b. 60 40, c. 40 60, and d. 20 80 concentrations



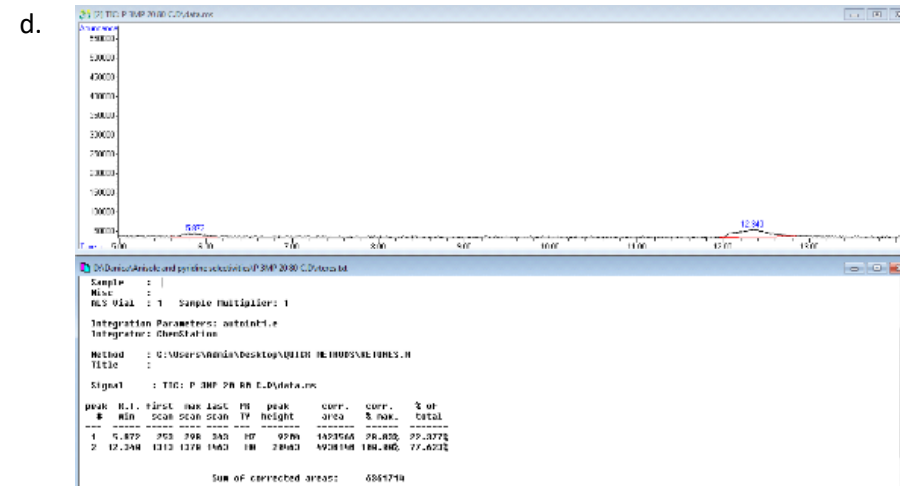
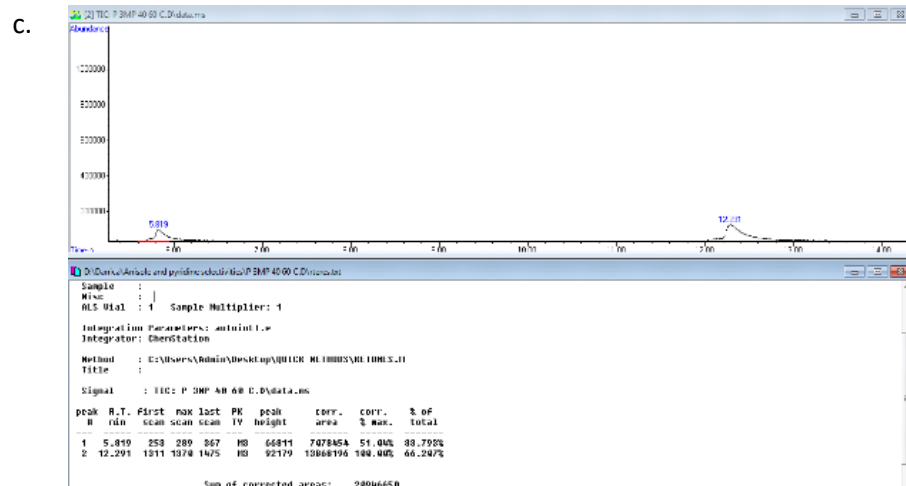
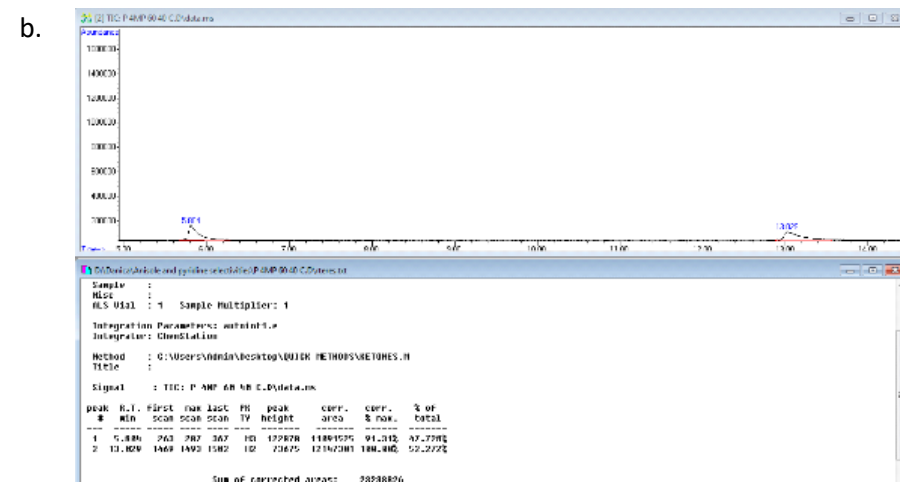
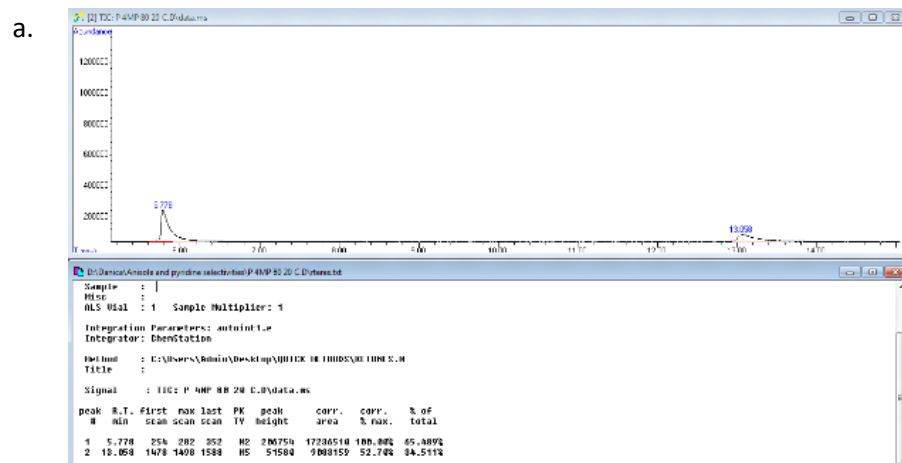


Figure S27: Host compound H1 for the selectivity profile PYR/3MP for the crystals with a. 80 20, b. 60 40, c. 40 60, and d. 20 80 concentrations



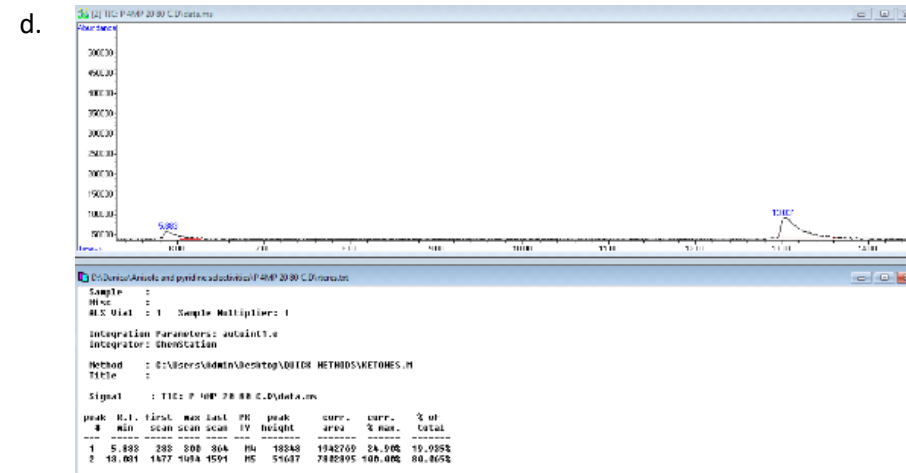
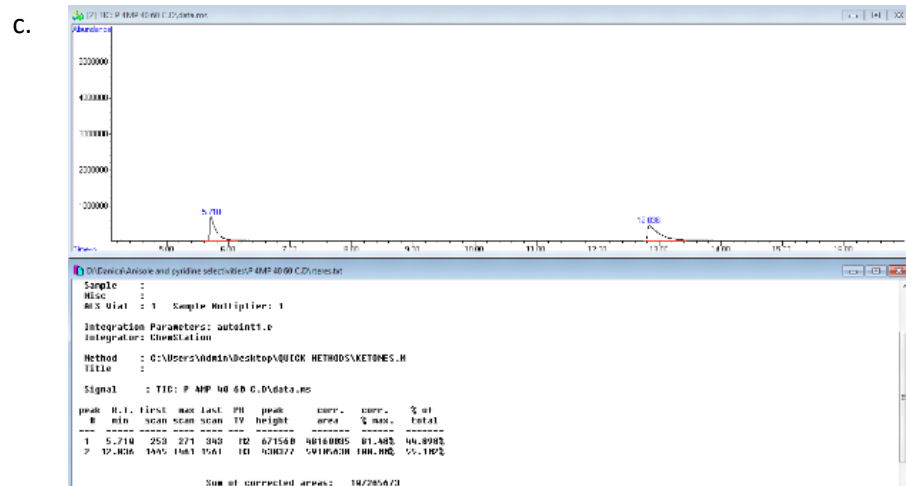
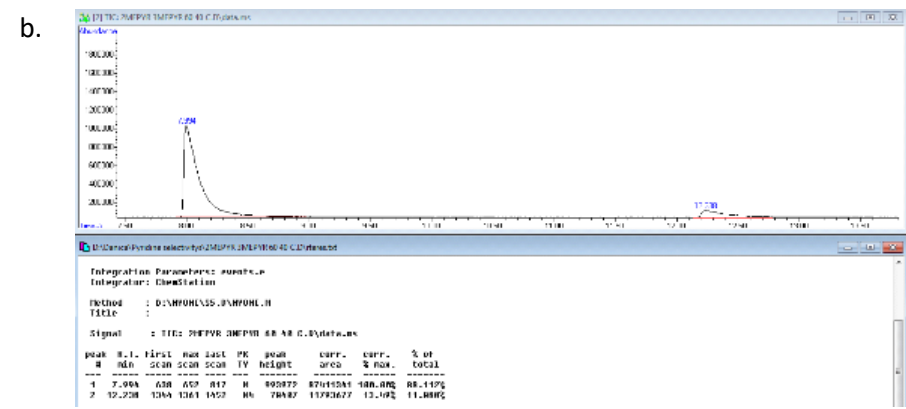
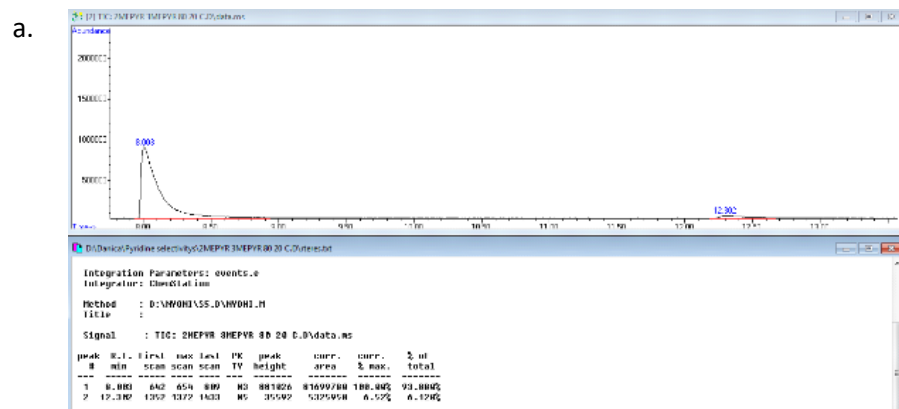


Figure S28: Host compound H1 for the selectivity profile PYR/4MP for the crystals with a. 80 20, b. 60 40, c. 40 60, and d. 20 80 concentrations



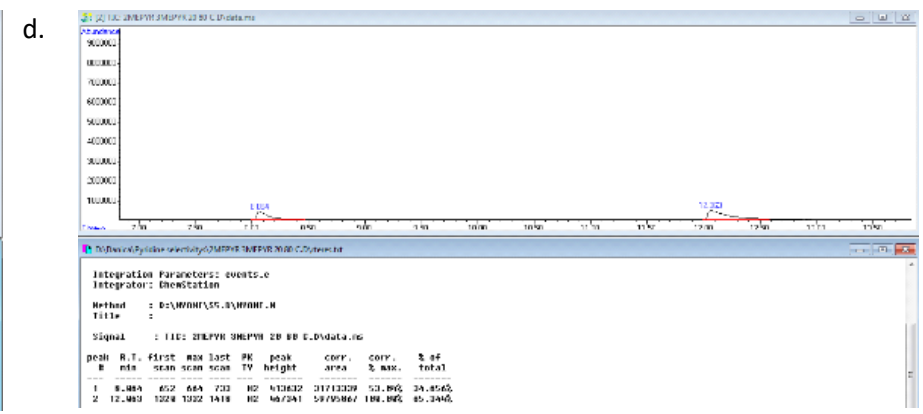
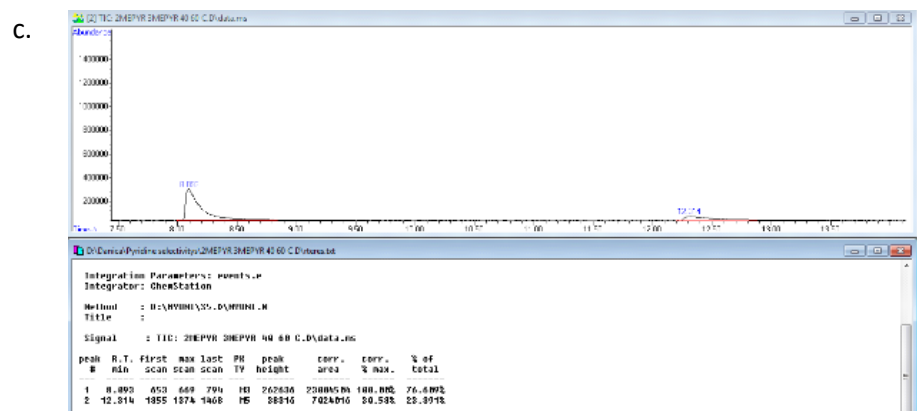
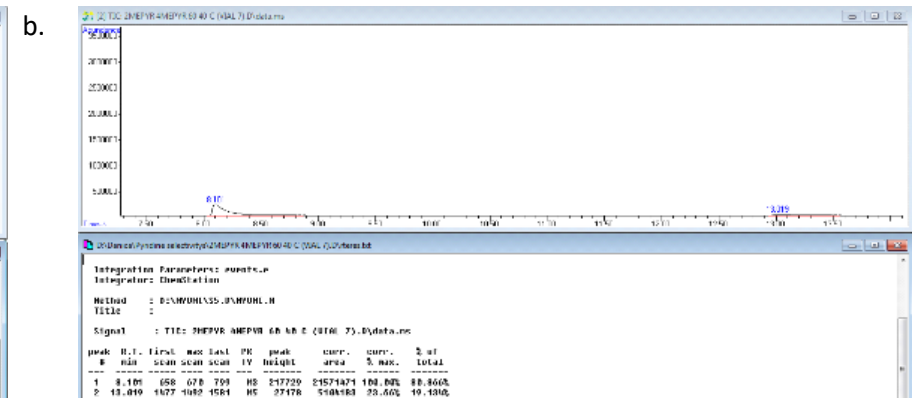
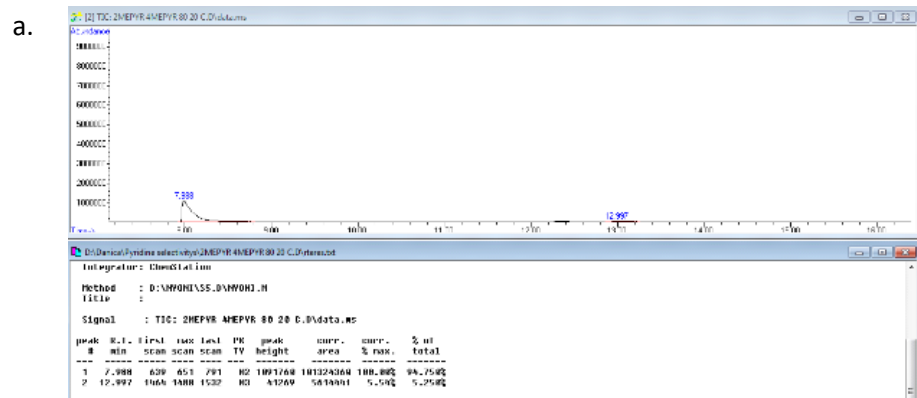


Figure S29: Host compound H1 for the selectivity profile 2MP/3MP for the crystals with a. 80 20, b. 60 40, c. 40 60, and d. 20 80 concentrations



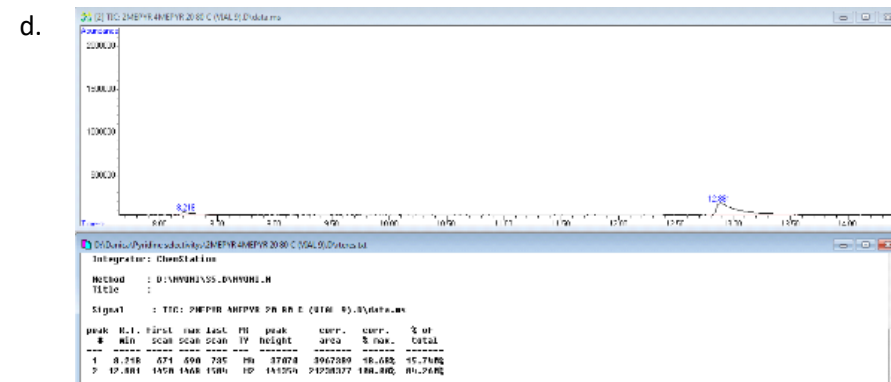
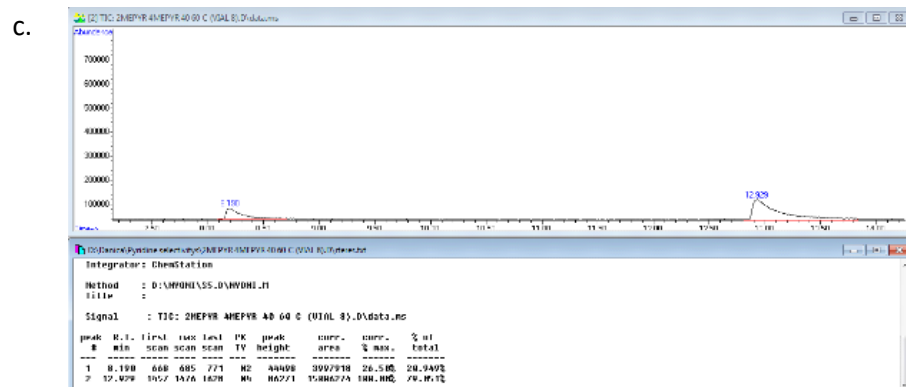
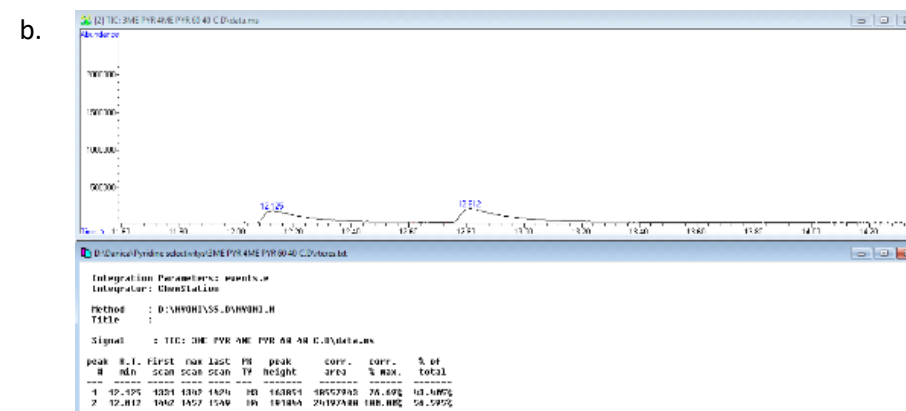
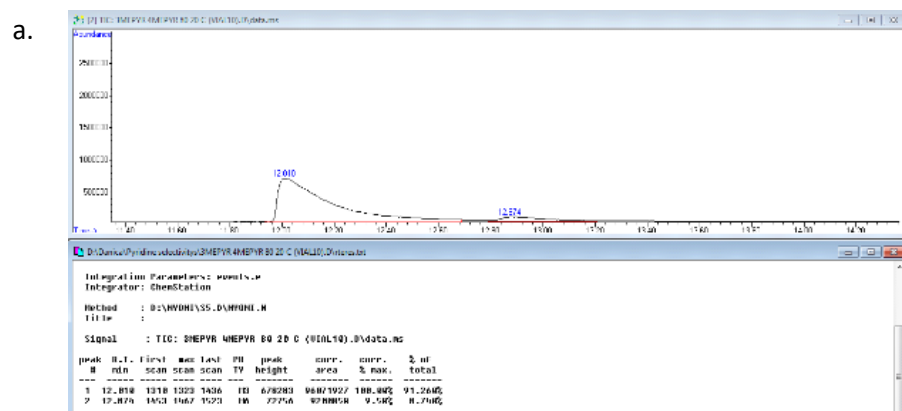


Figure S30: Host compound H1 for the selectivity profile 2MP/4MP for the crystals with a. 80 20, b. 60 40, c. 40 60, and d. 20 80 concentrations



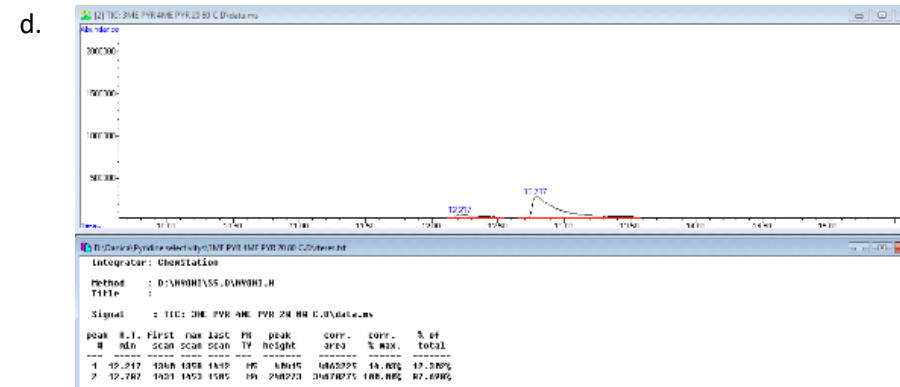
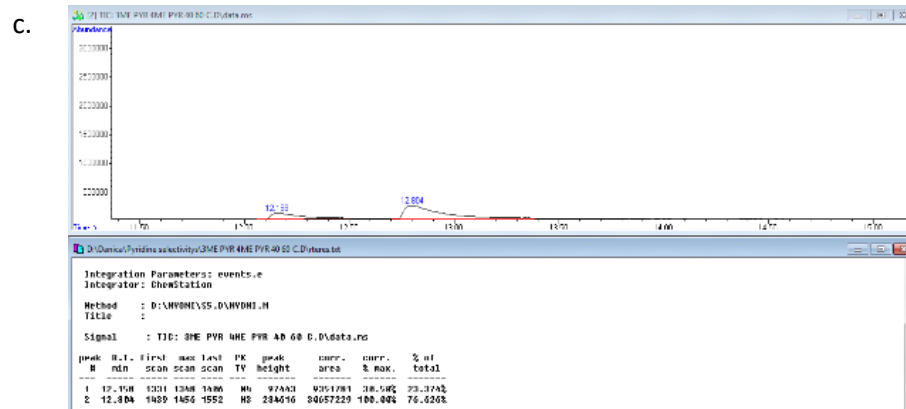


Figure S31: Host compound H1 for the selectivity profile 3MP/4MP for the crystals with a. 80 20, b. 60 40, c. 40 60, and d. 20 80 concentrations

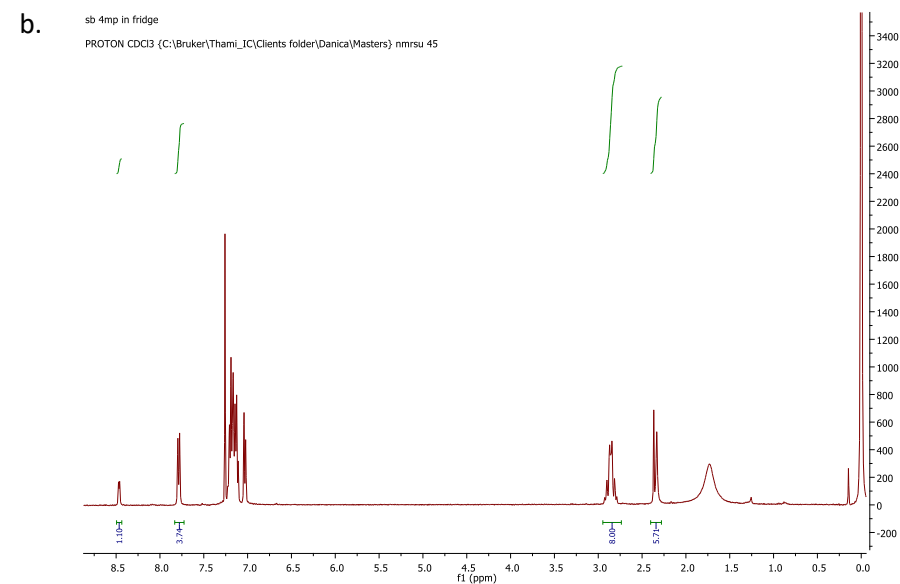
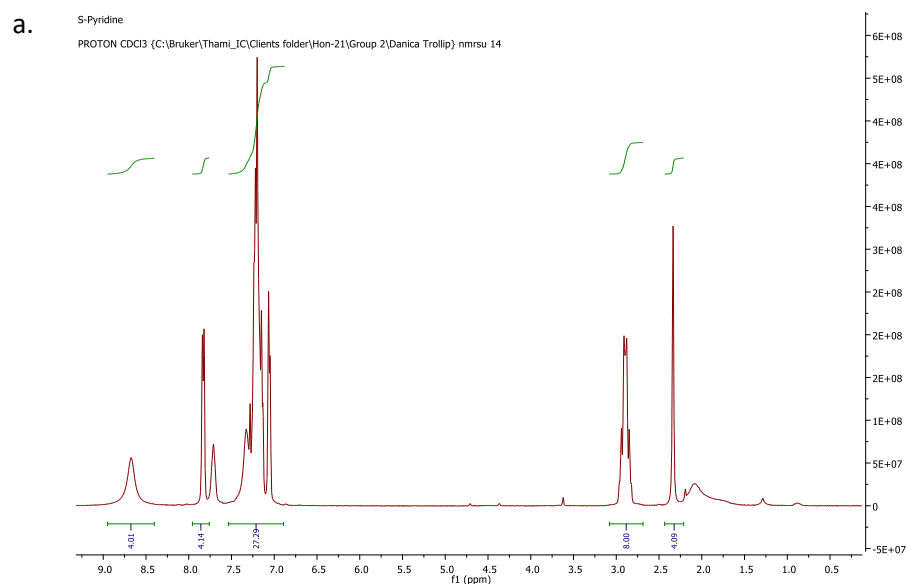
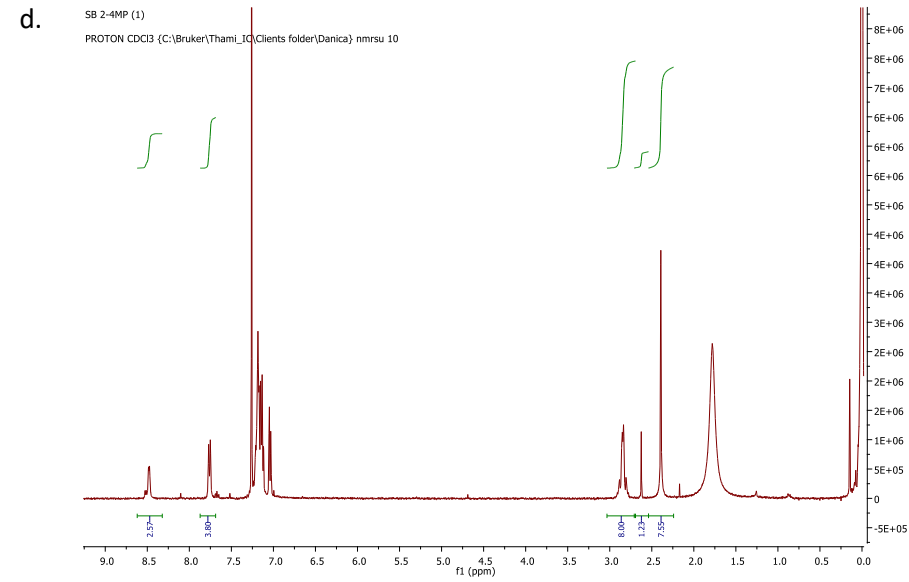
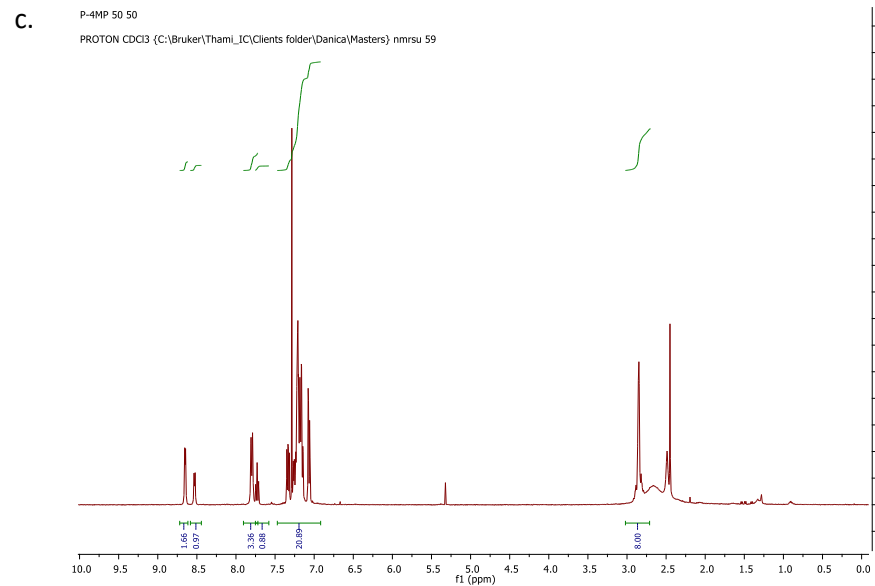
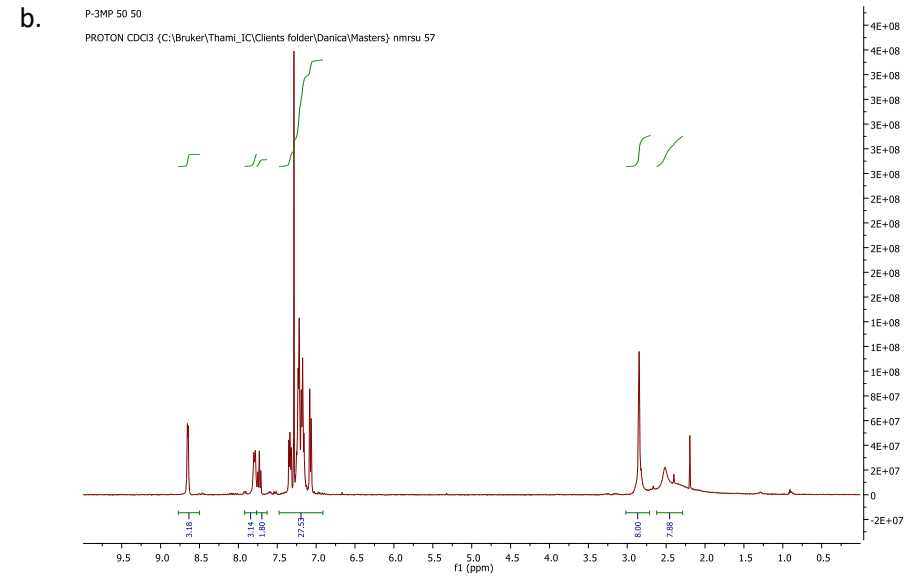
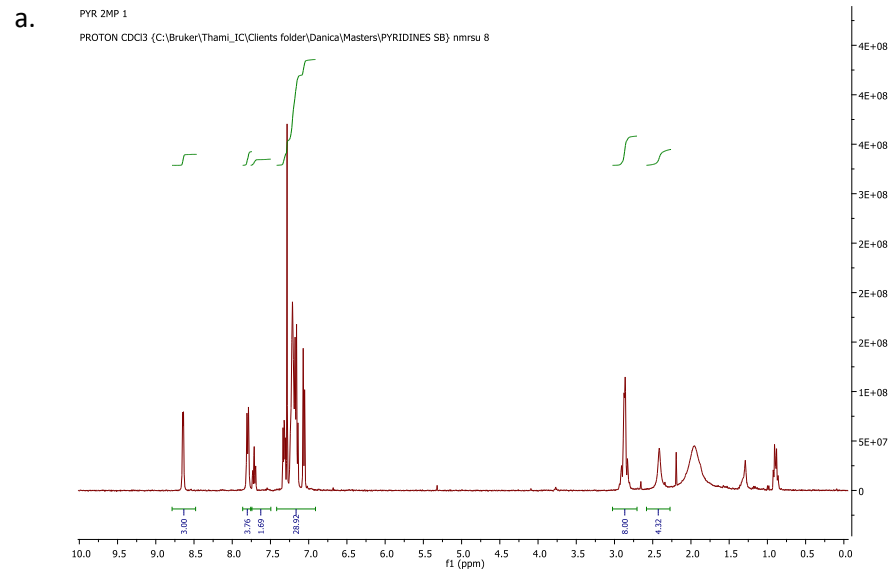
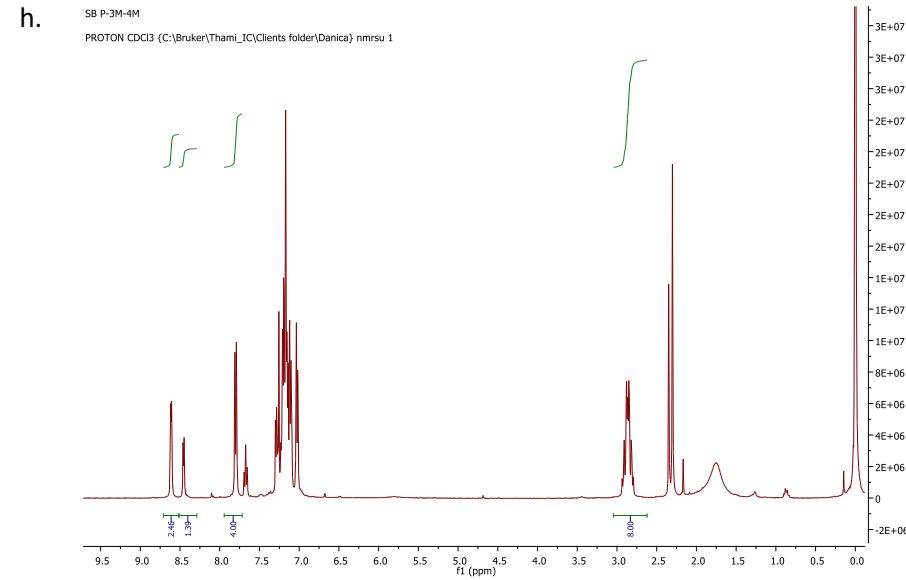
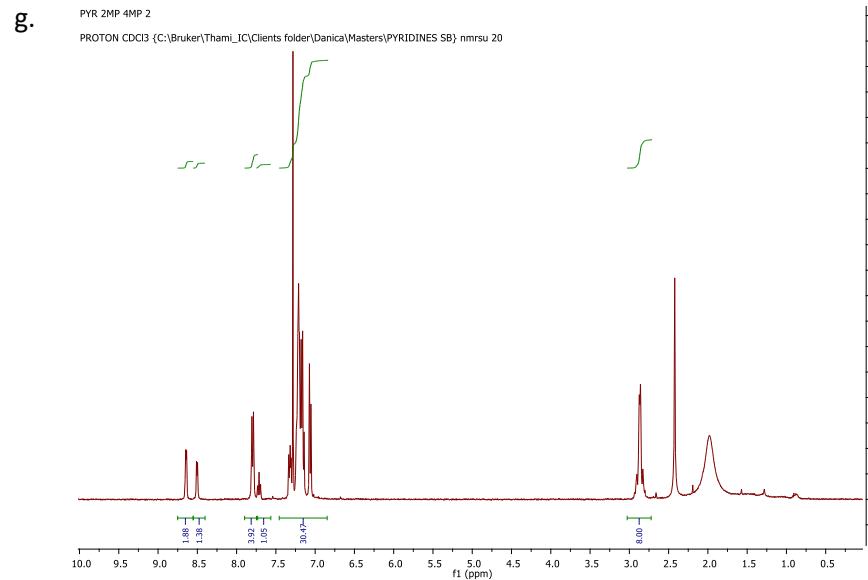
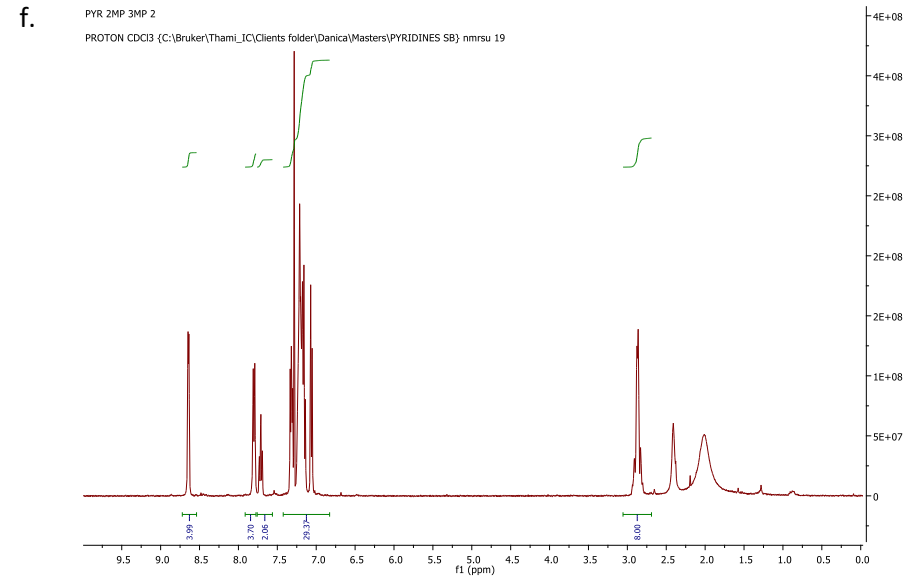
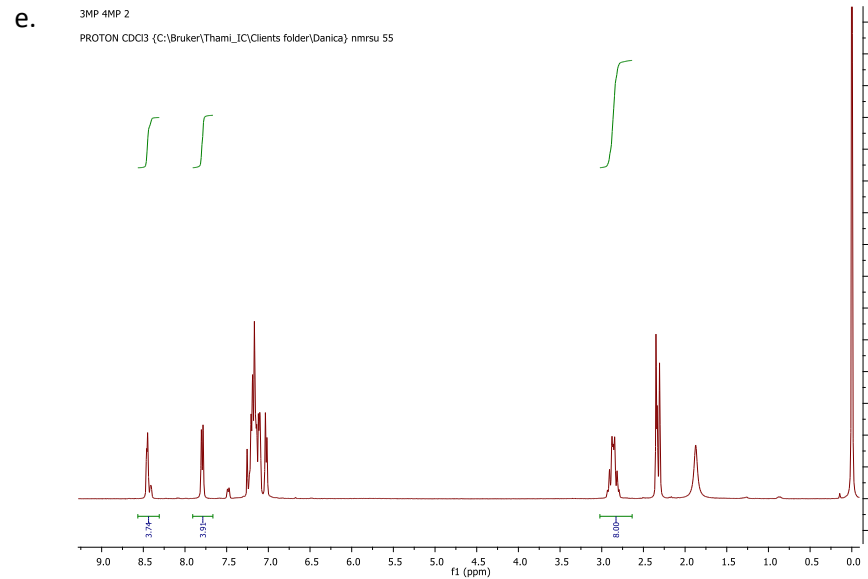
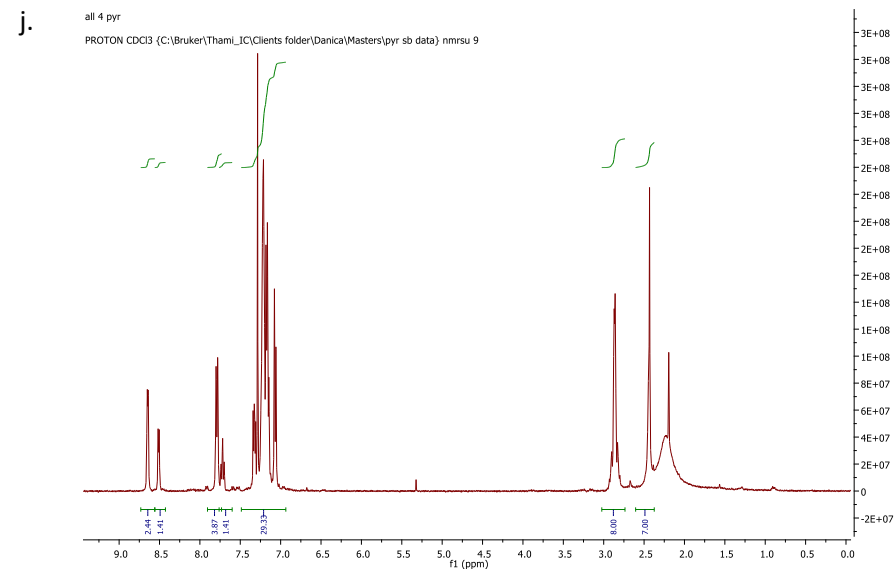
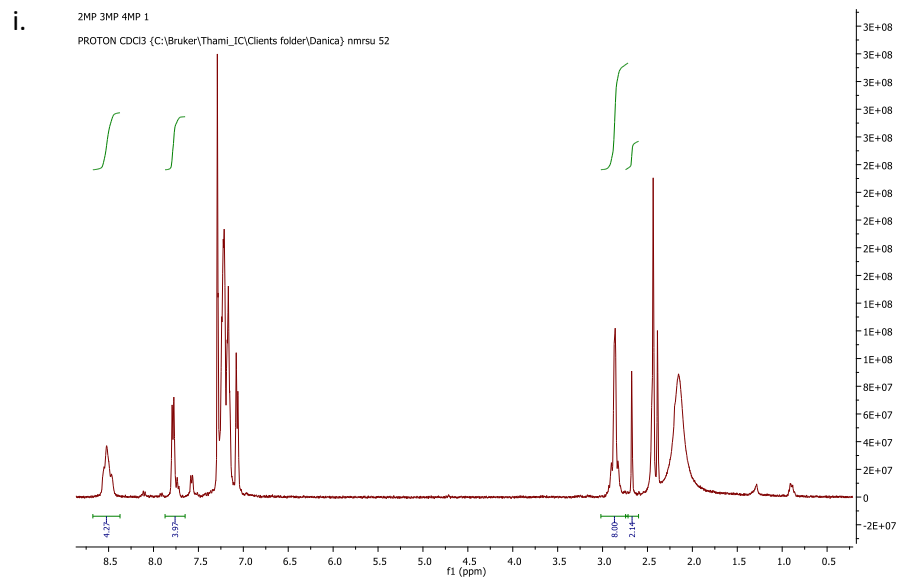


Figure S32: Host compound H2 single solvent experiments with a. PYR and b. 4MP

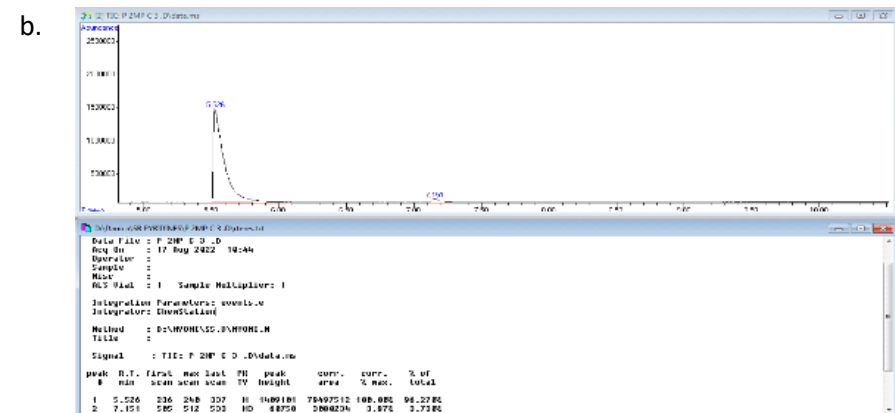
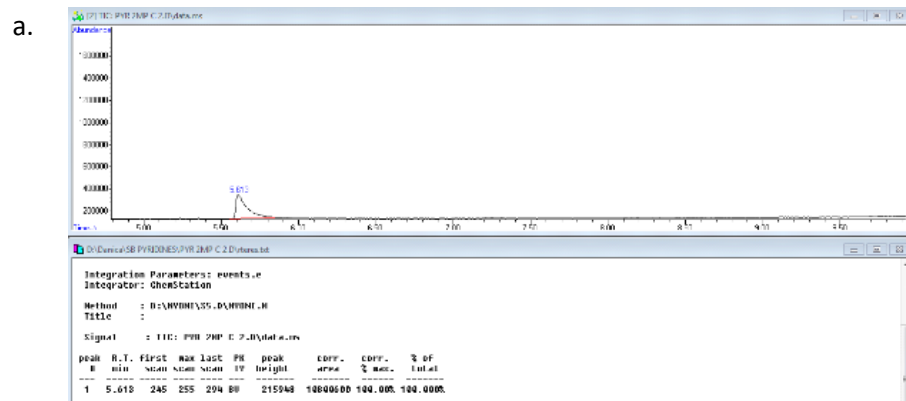




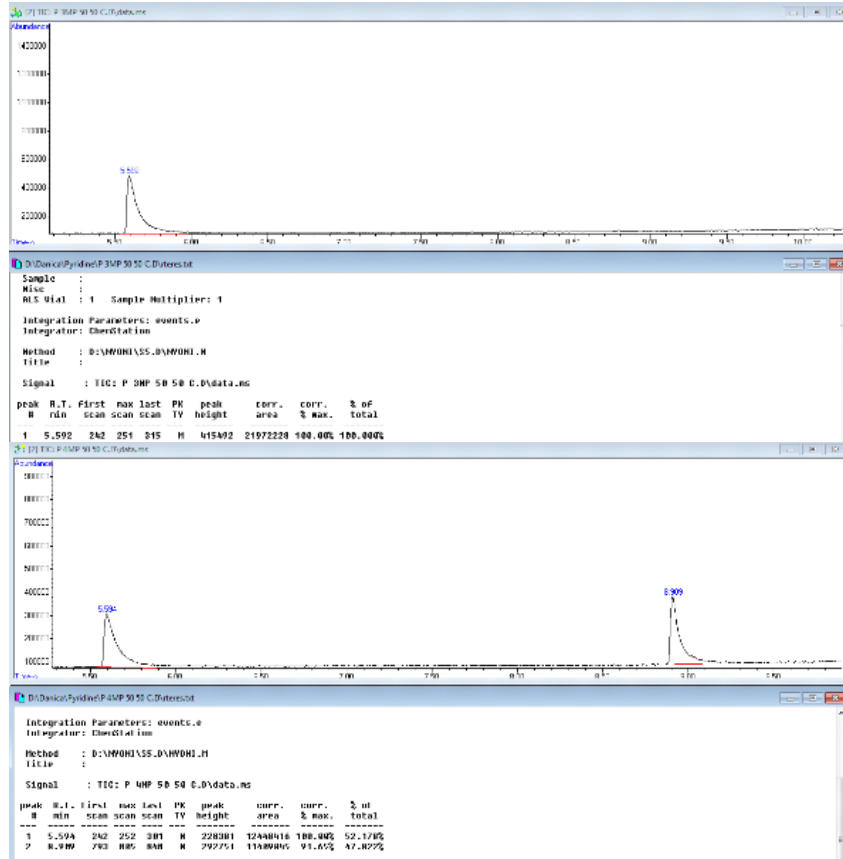




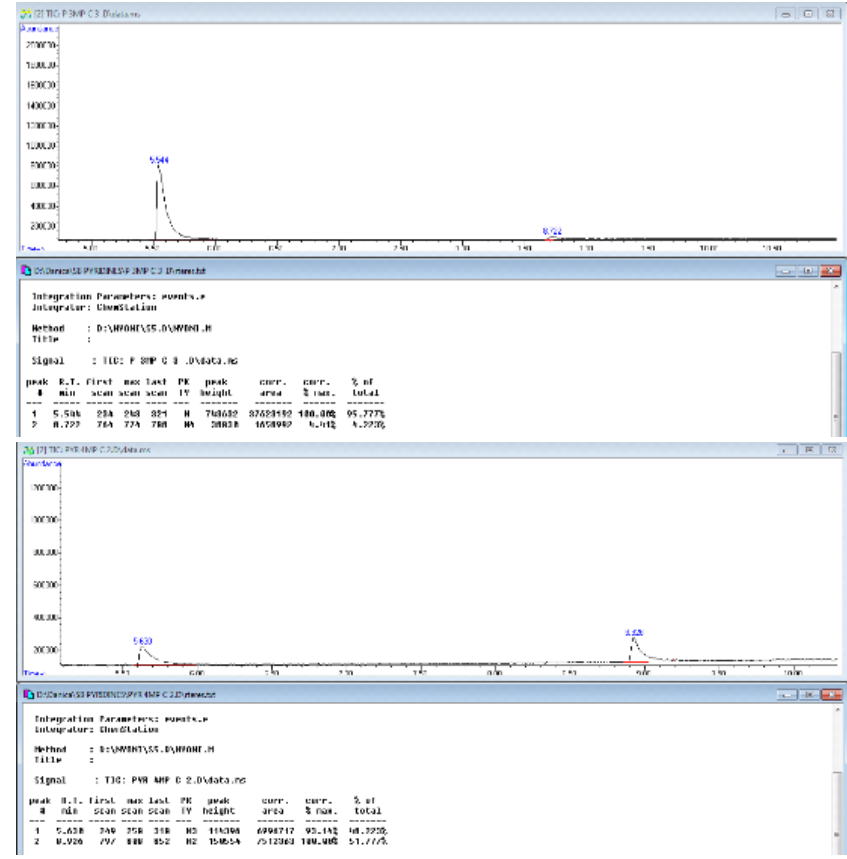
**Figure S33: H2** with a. PYR/2MP, b. PYR/3MP, c. PYR/4MP, d. 2MP/4MP, e. 3MP/4MP, f. PYR/2MP/3MP, g. PYR/2MP/4MP, h. PYR/3MP/4MP, i. 2MP/3MP/4MP, and j. all 4 PYR/MP's



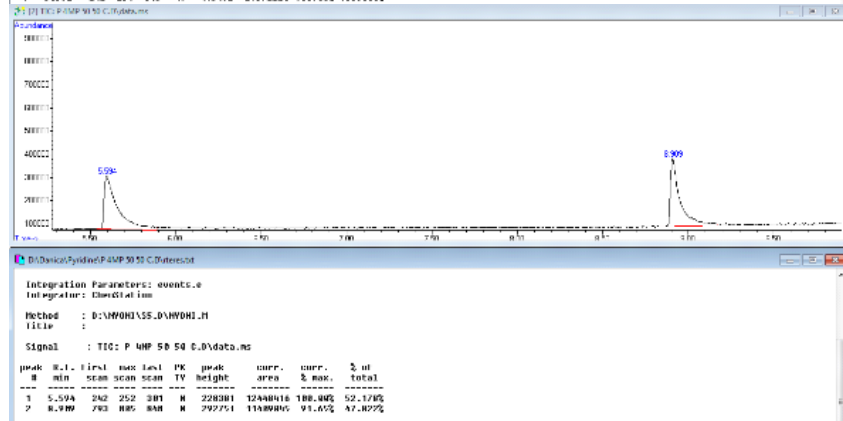
c.



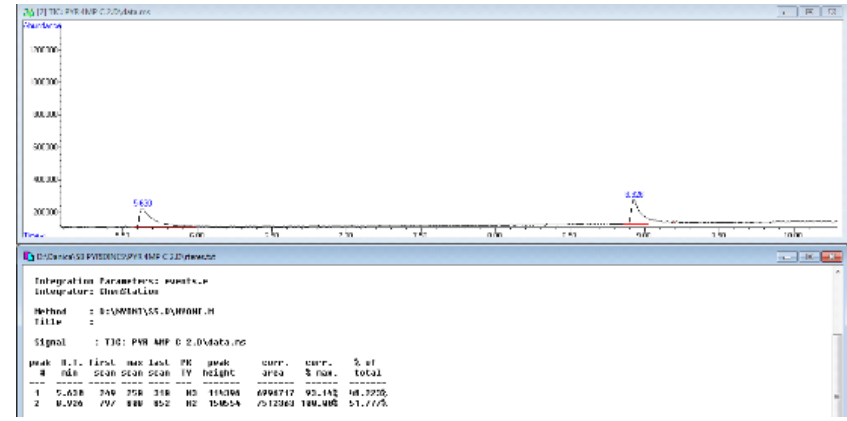
d.

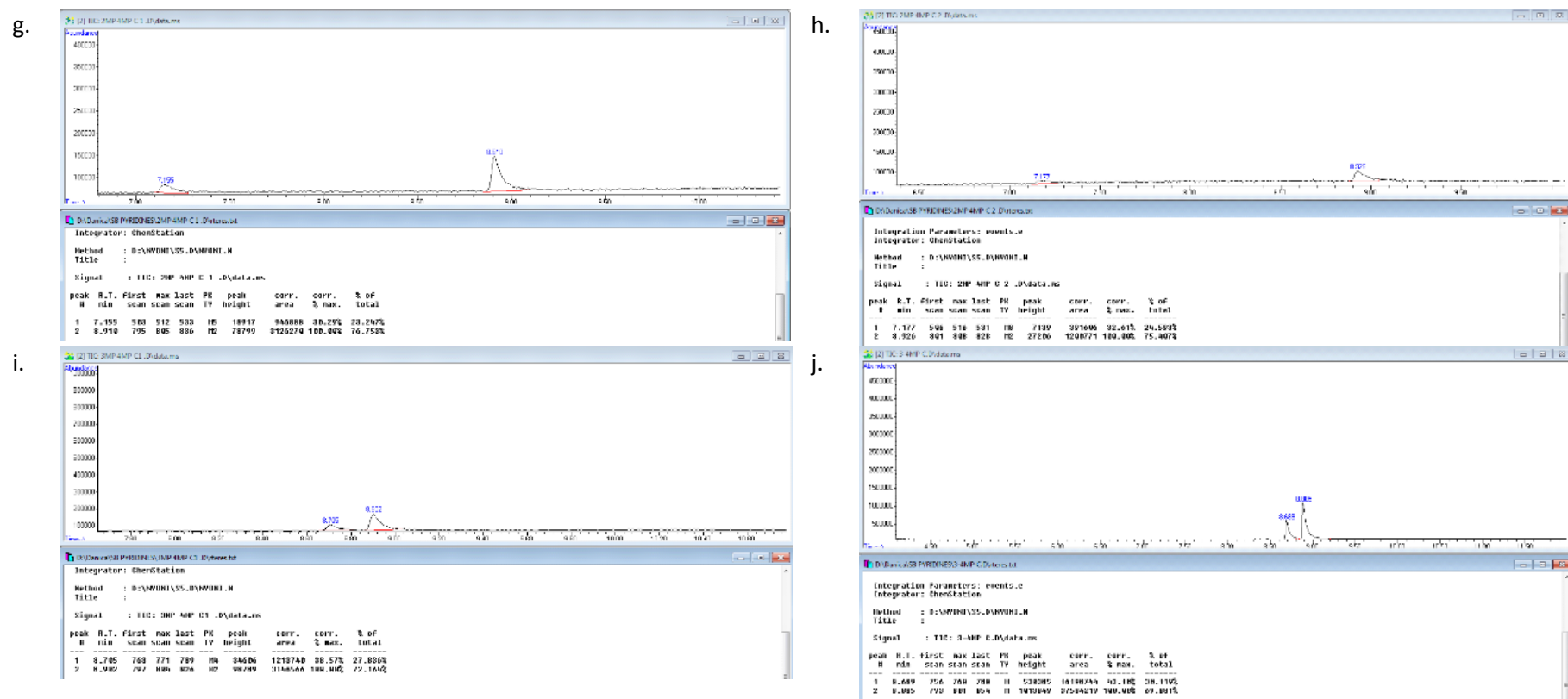


e.

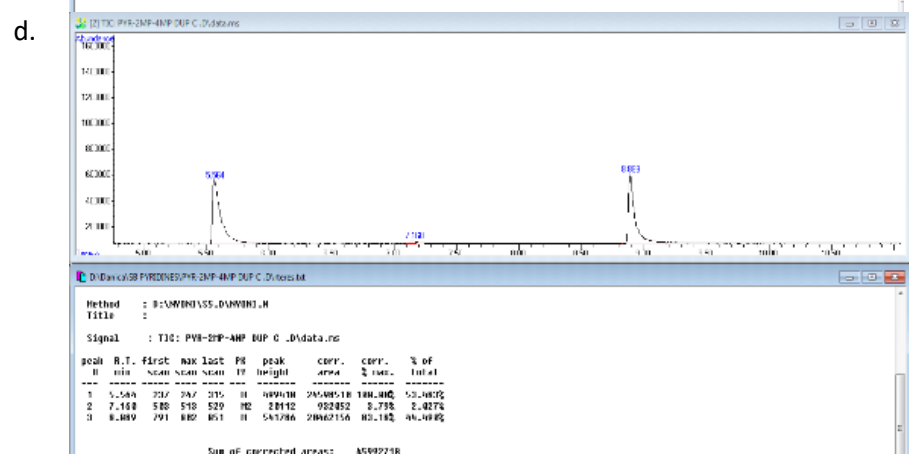
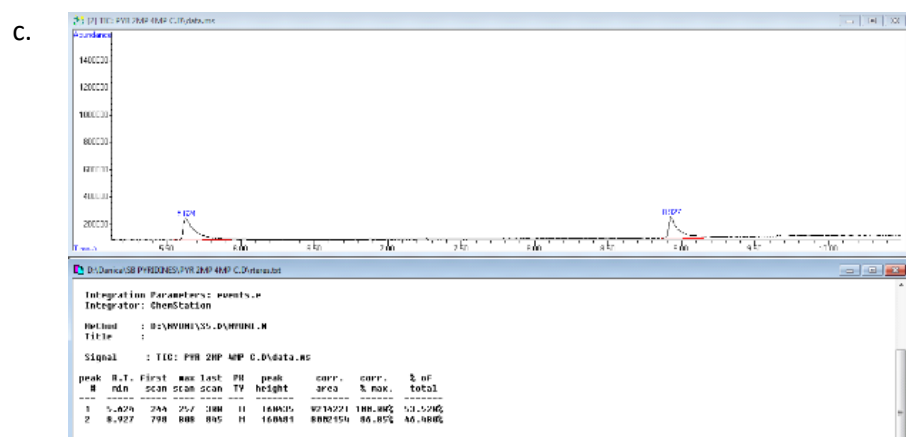
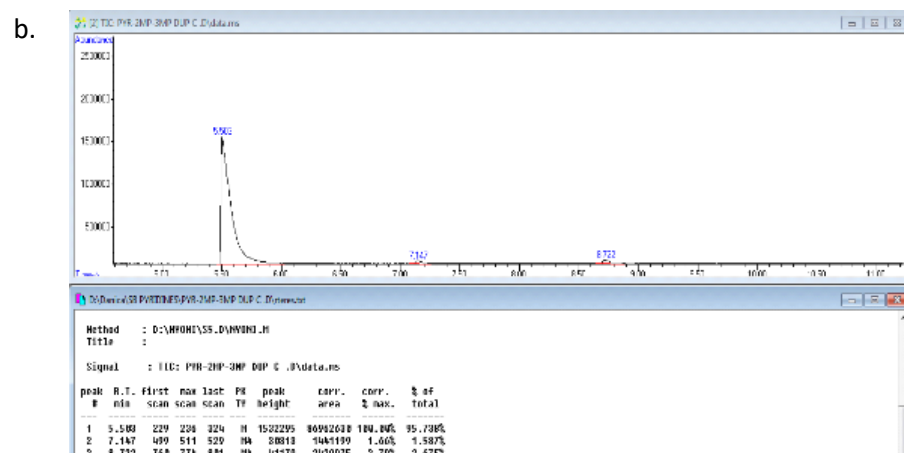
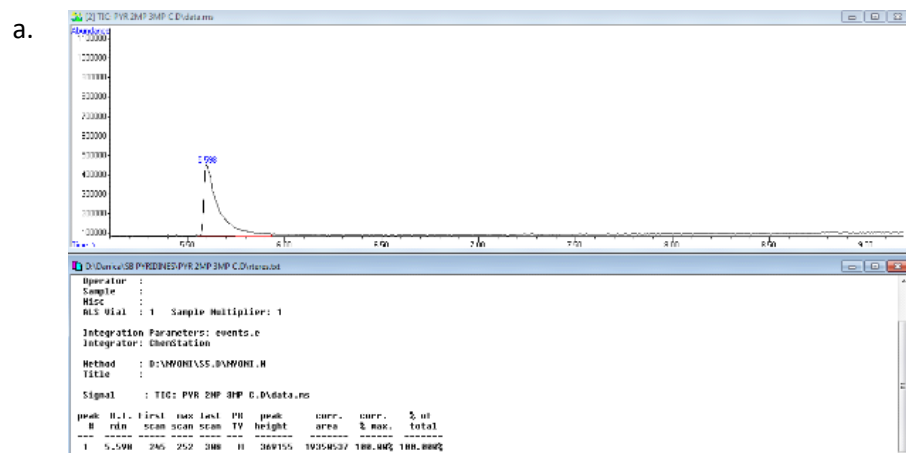


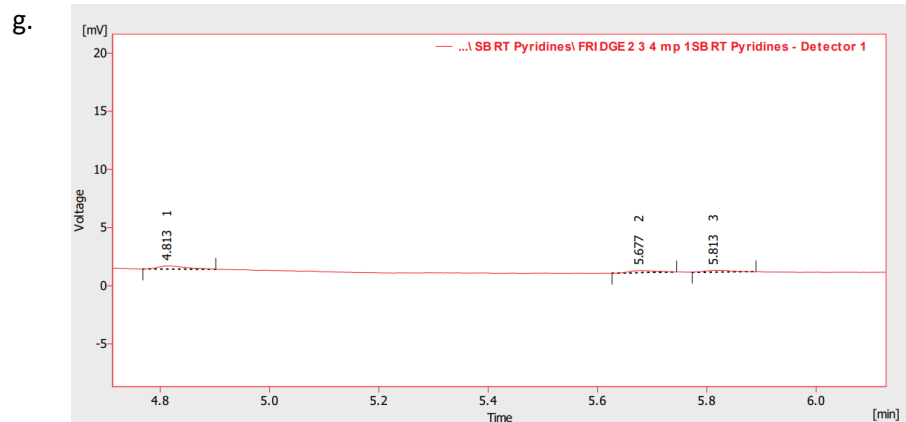
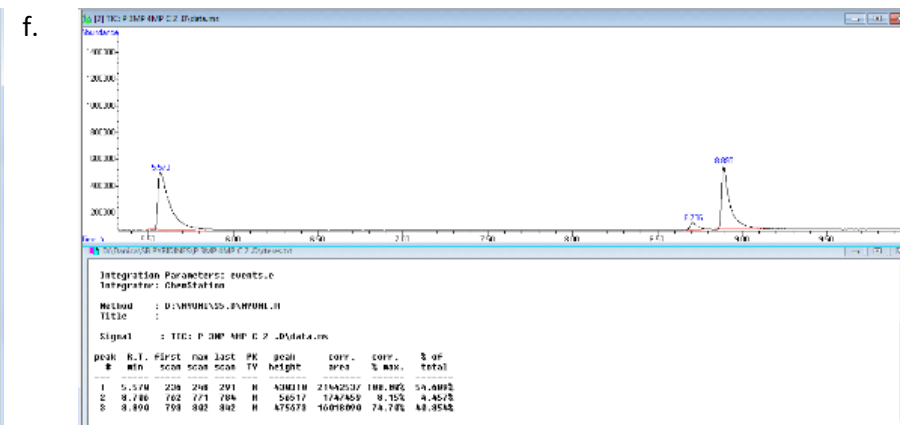
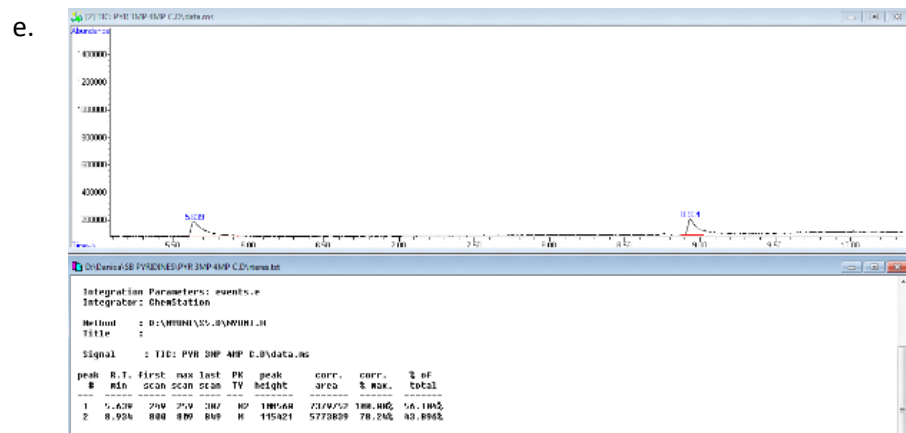
f.



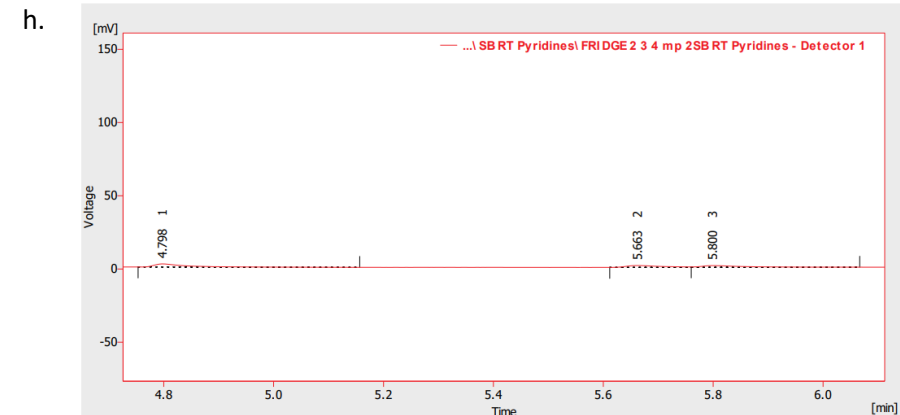


**Figure S34:** Host compound **H2** with the duplicate crystal data for PYR/2MP in a. and b., for PYR/3MP in c. and d., for PYR/4MP in e. and f., for 2MP/4MP in g. and h., and for 3MP/4MP in i. and j.





	Reten. Time [min]	Area [mV.s]	Height [mV]	Area [%]	Height [%]	W05 [min]	Compound Name
1	4.813	0.960	0.268	46.2	44.9	0.05	
2	5.677	0.609	0.179	29.3	29.9	0.07	
3	5.813	0.509	0.150	24.5	25.1	0.06	
Total		2.077	0.598	100.0	100.0		



	Reten. Time [min]	Area [mV.s]	Height [mV]	Area [%]	Height [%]	W05 [min]	Compound Name
1	4.798	9.235	2.139	43.2	46.7	0.05	
2	5.663	5.704	1.274	26.7	27.8	0.07	
3	5.800	6.435	1.172	30.1	25.6	0.07	
Total		21.374	4.585	100.0	100.0		

**Figure S35:** Host compound **H2** crystal data with PYR/2MP/3MP in a. and b., with PYR/2MP/4MP in c. and d., with PYR/3MP/4MP in e. and f., and with 2MP/3MP/4MP in g. and h.

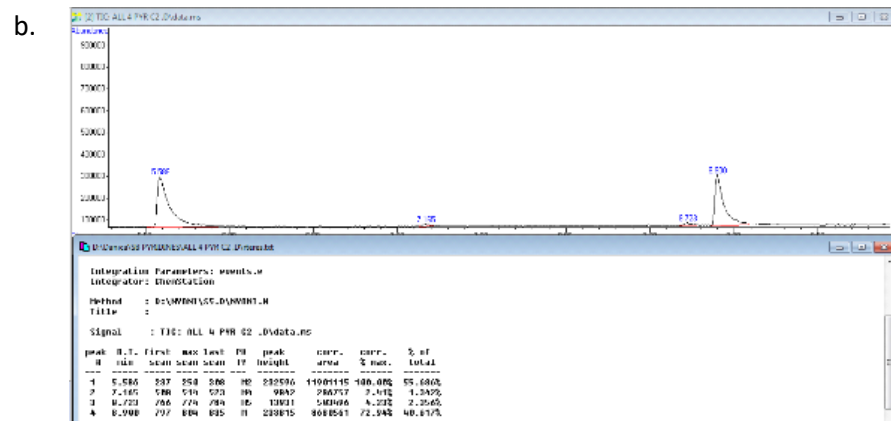
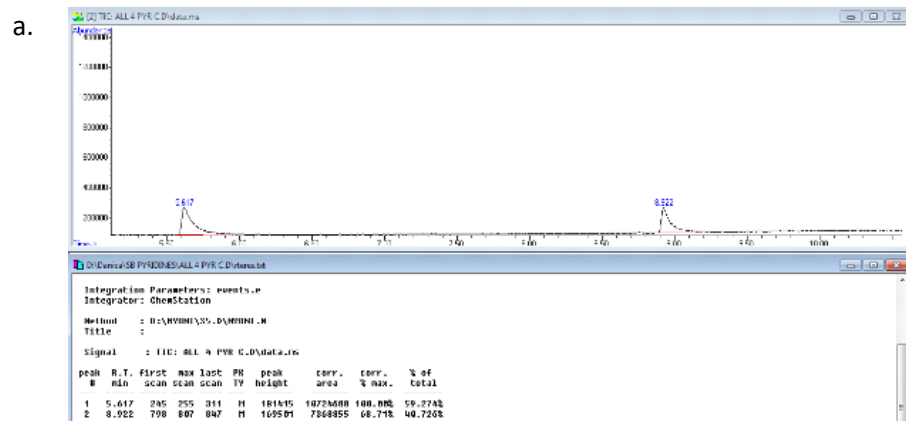
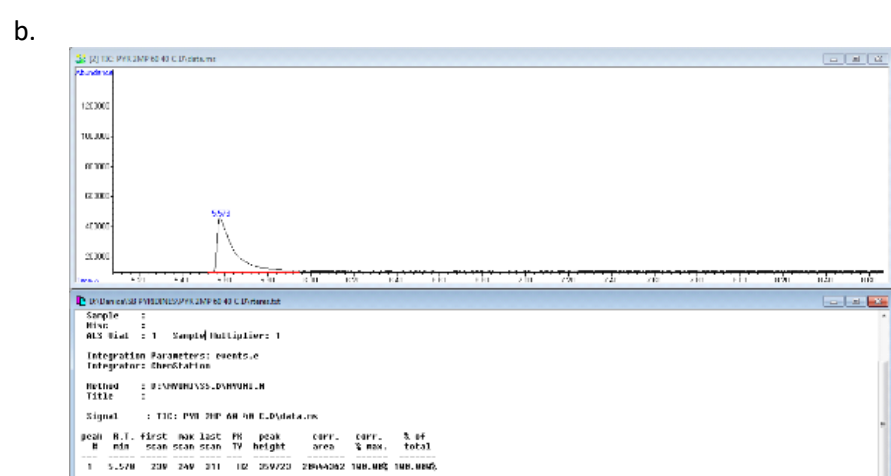
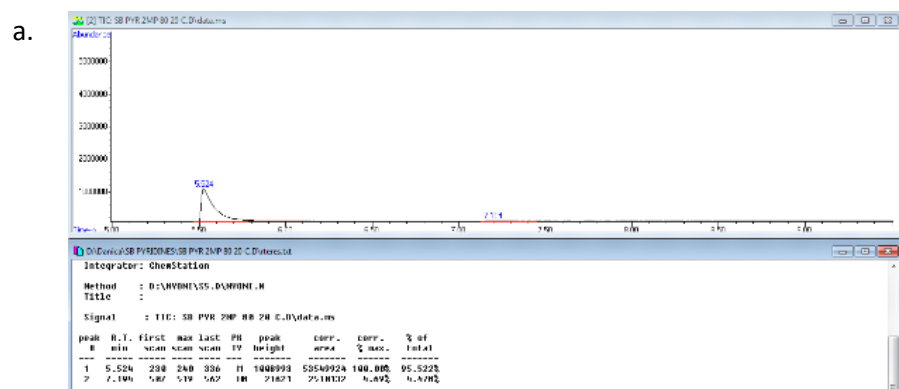


Figure S36: Host compound H2 crystal data with all 4 PYR/MP's in a. and b.



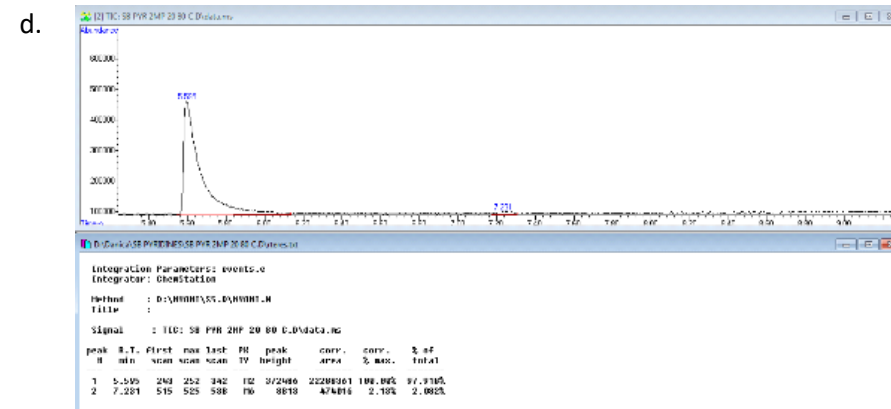
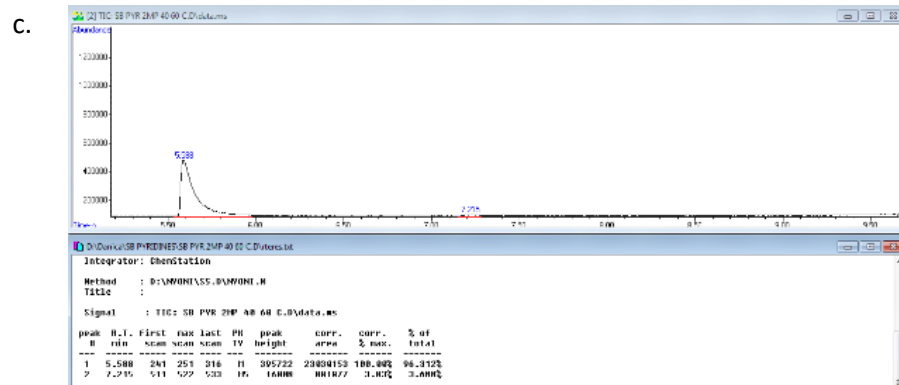
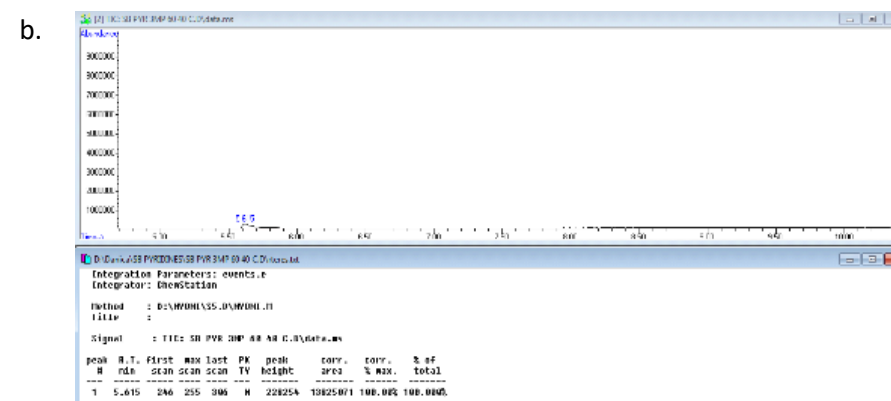
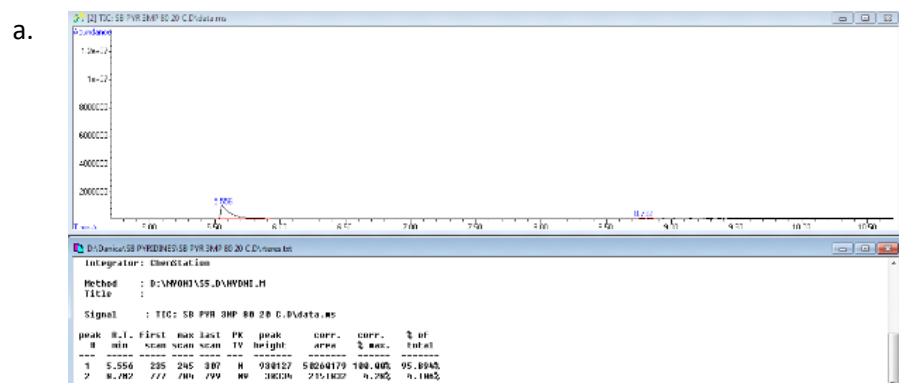


Figure S37: Host compound H2 for the selectivity profile PYR/2MP for the crystals with a. 80 20, b. 60 40, c. 40 60, and d. 20 80 concentrations



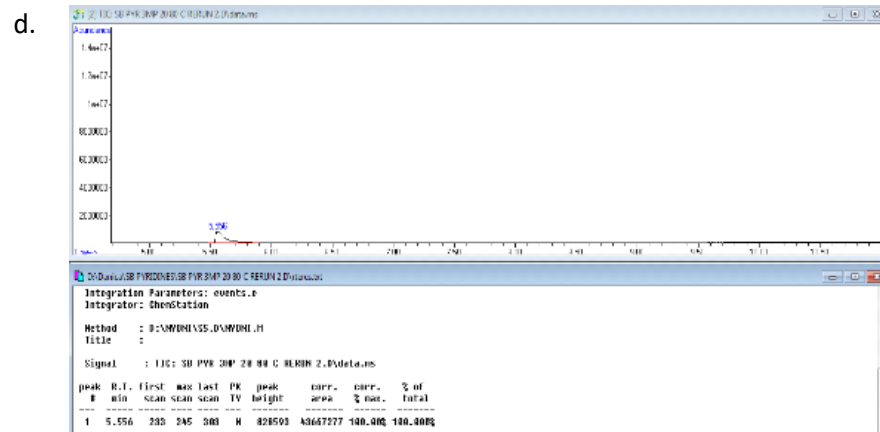
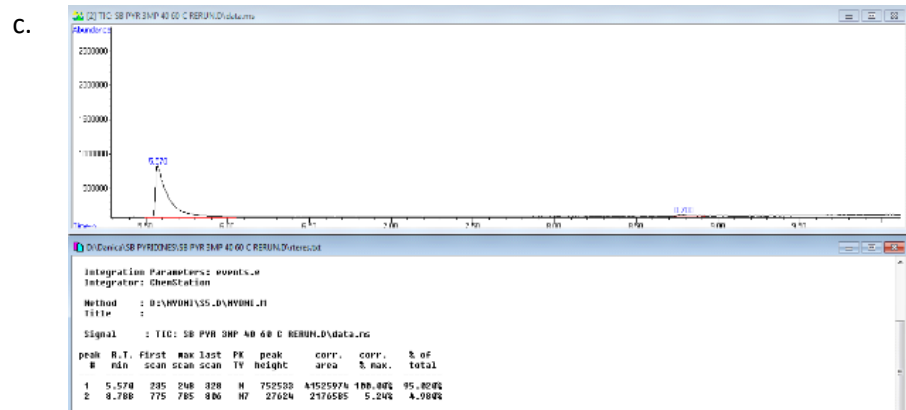
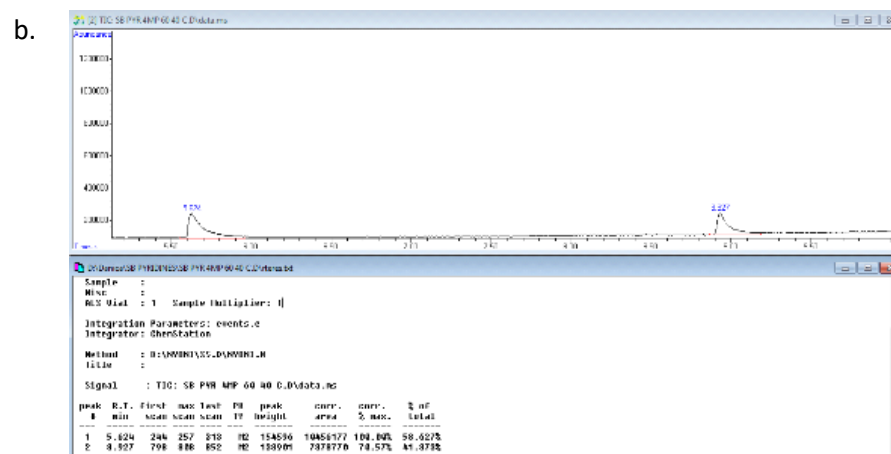
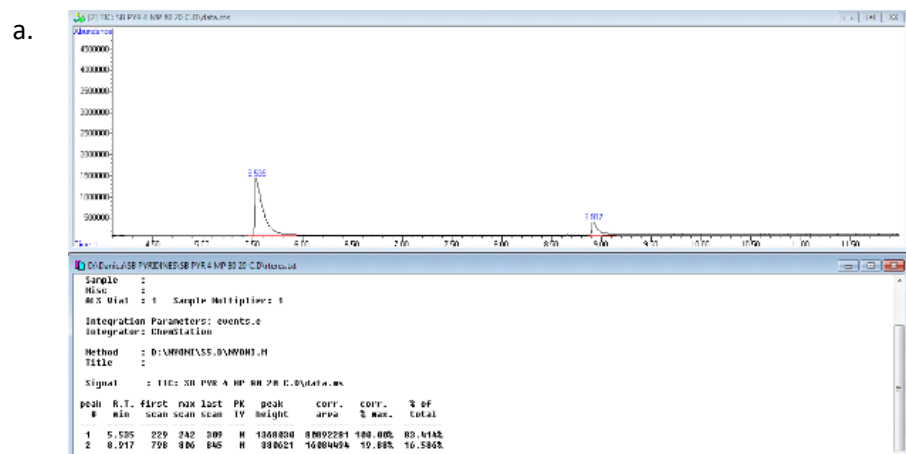


Figure S38: Host compound H2 for the selectivity profile PYR/3MP for the crystals with a. 80 20, b. 60 40, c. 40 60, and d. 20 80 concentrations





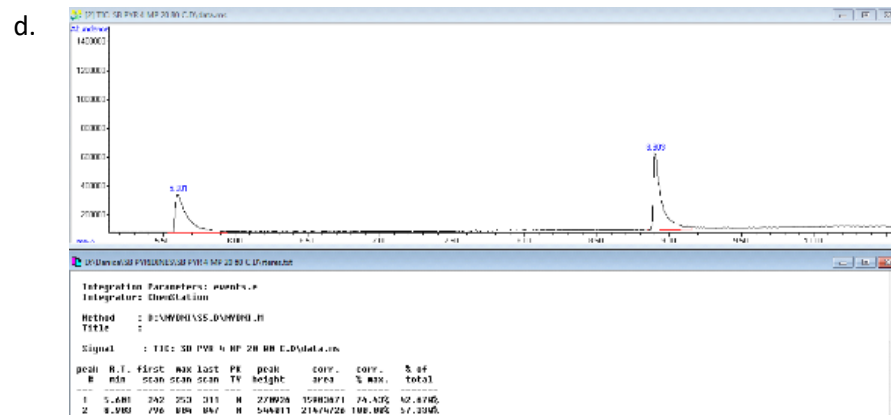
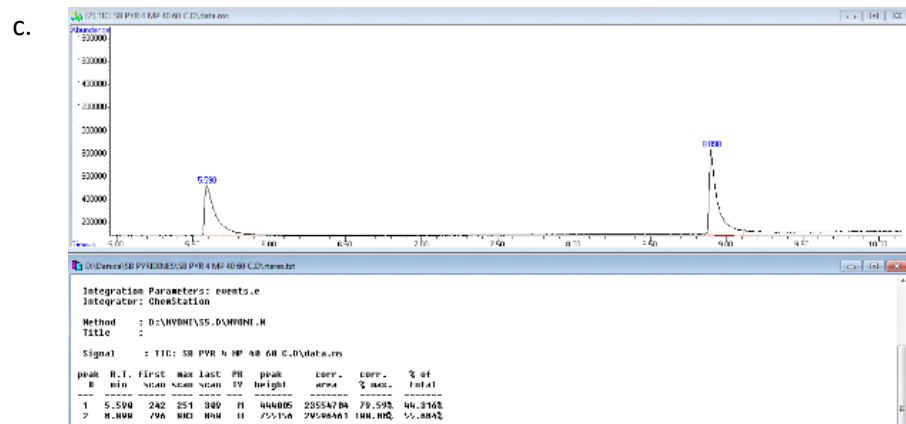
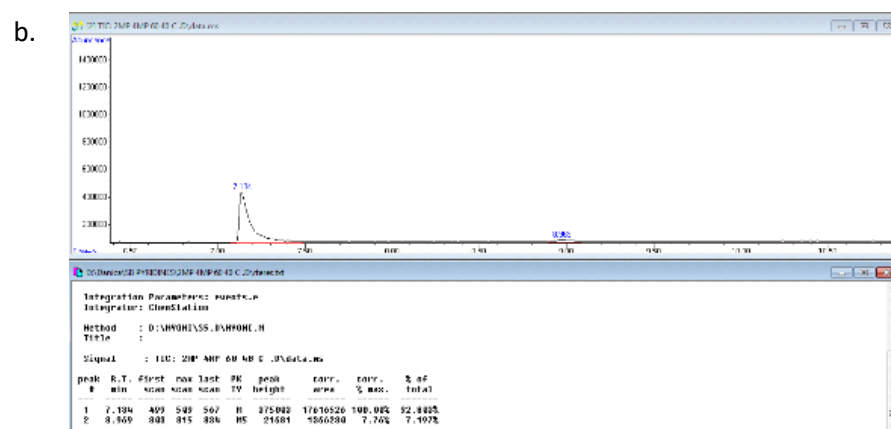
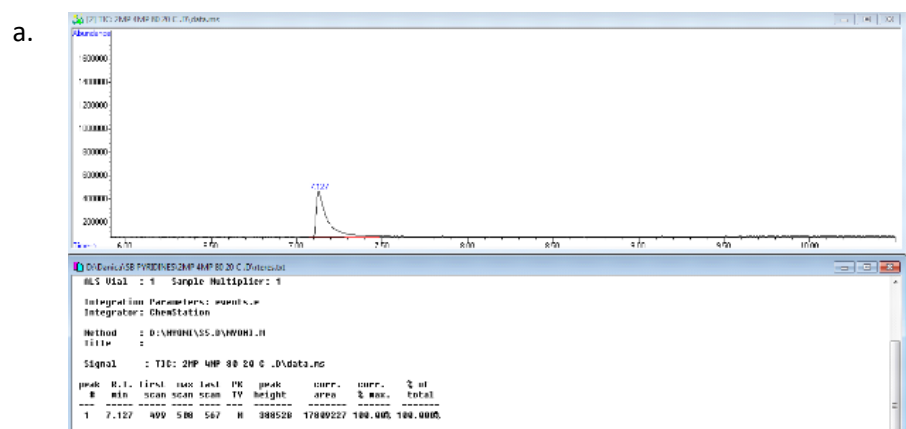


Figure S39: Host compound H2 for the selectivity profile PYR/4MP for the crystals with a. 80 20, b. 60 40, c. 40 60, and d. 20 80 concentrations



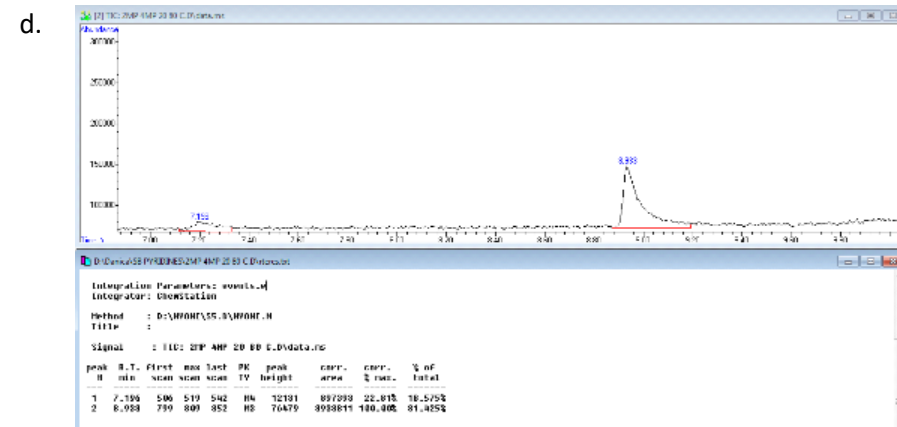
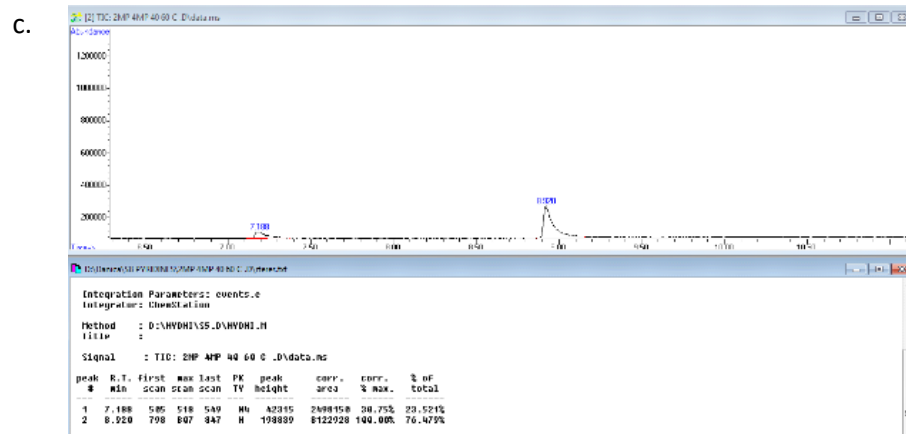
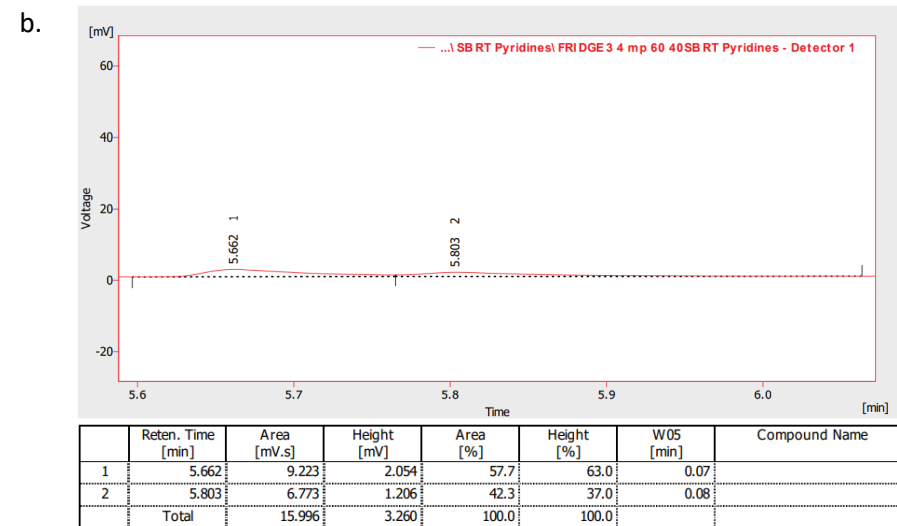
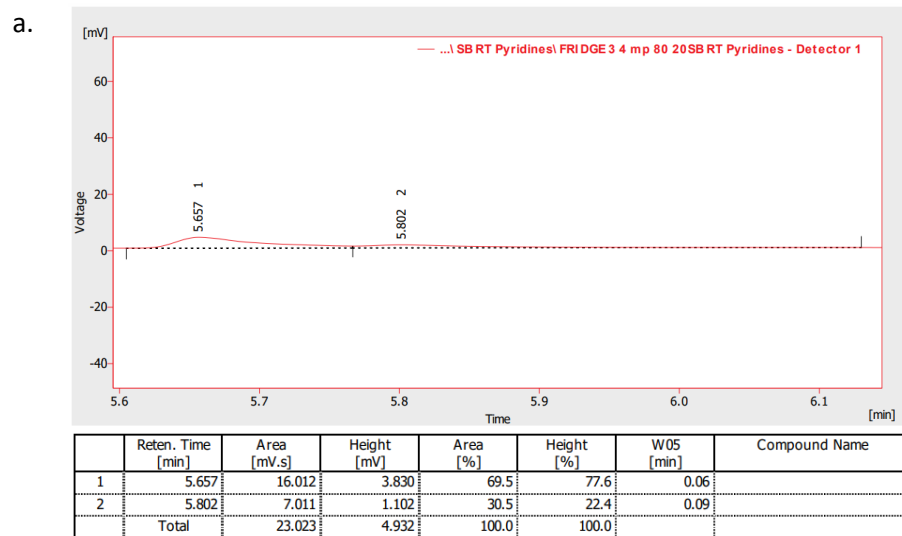
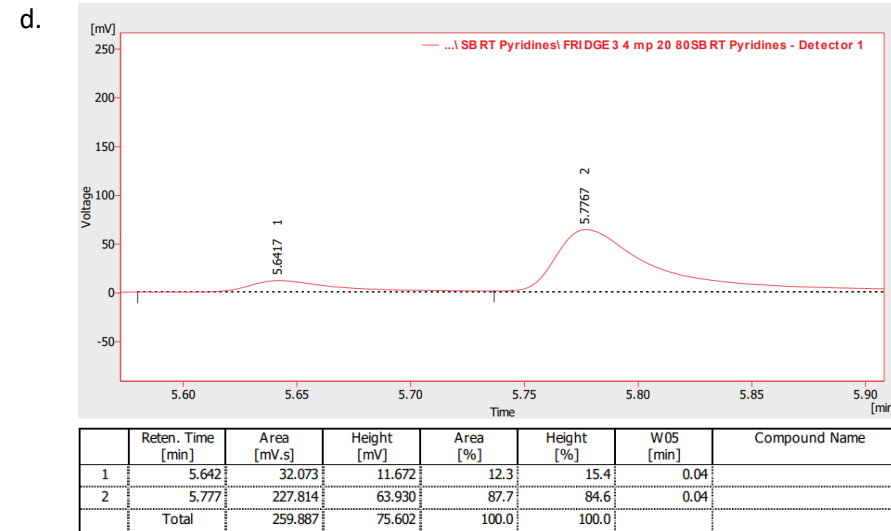
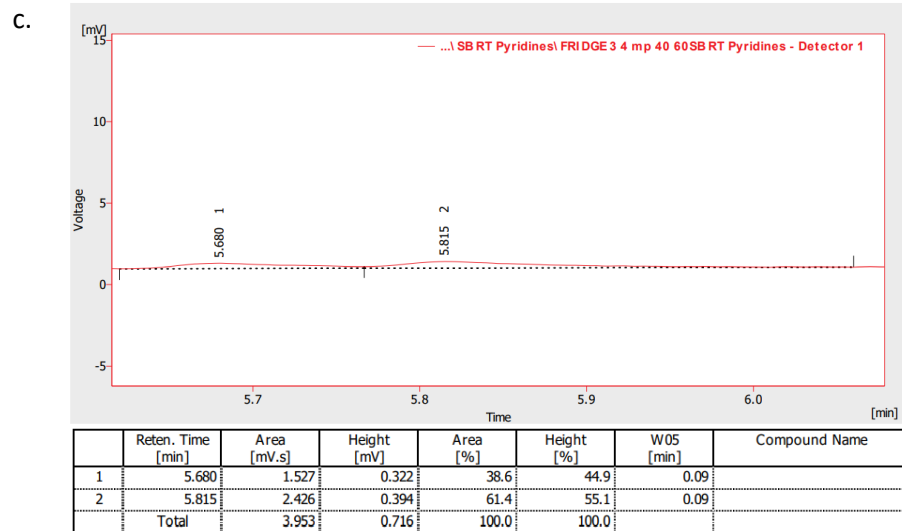
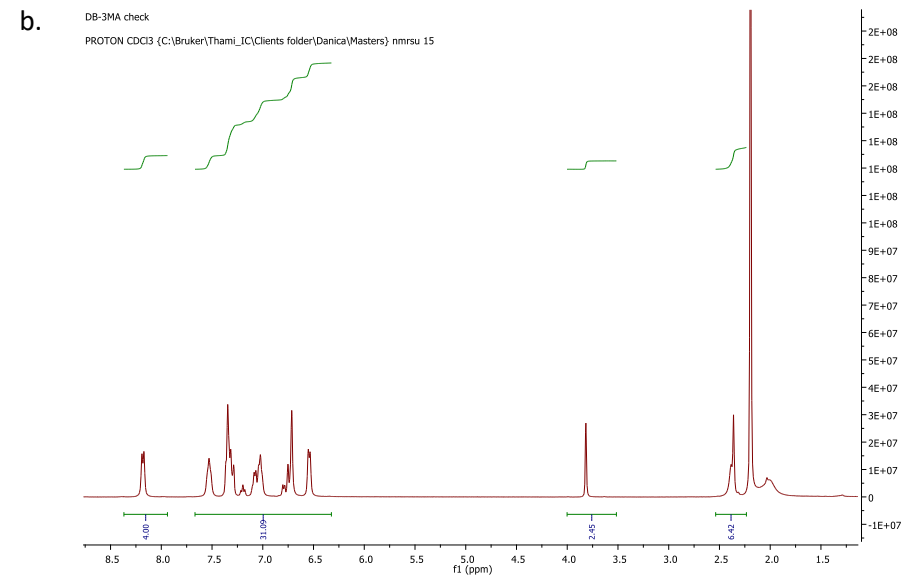
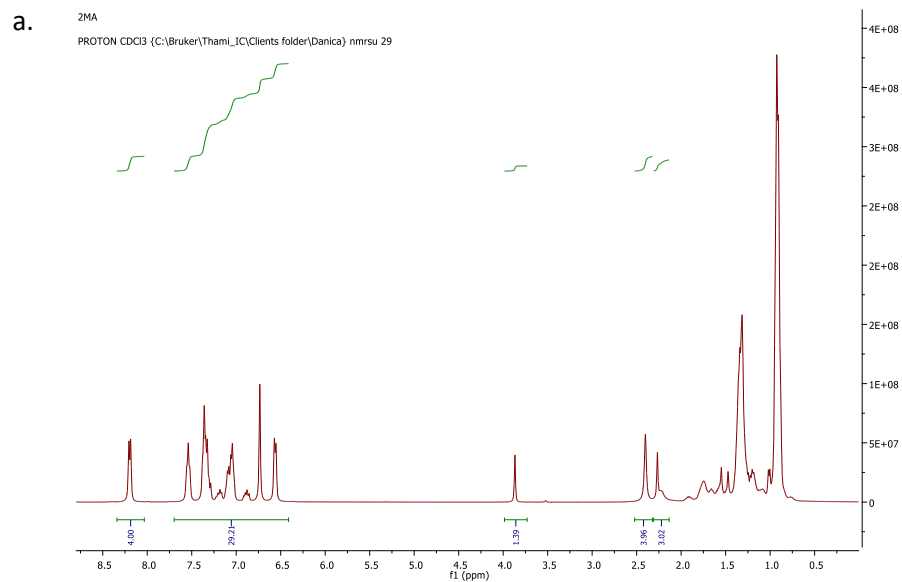


Figure S40: Host compound H2 for the selectivity profile 2MP/4MP for the crystals with a. 80 20, b. 60 40, c. 40 60, and d. 20 80 concentrations

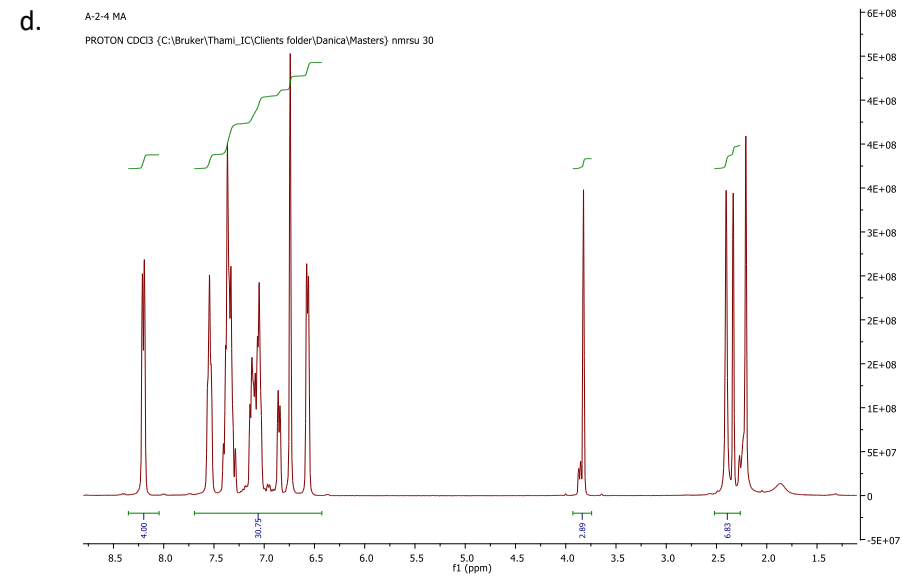
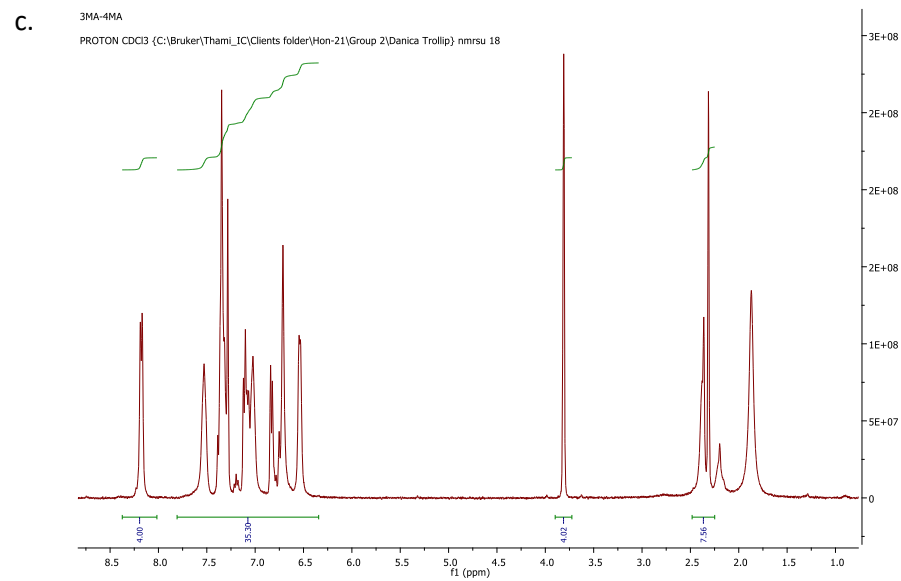
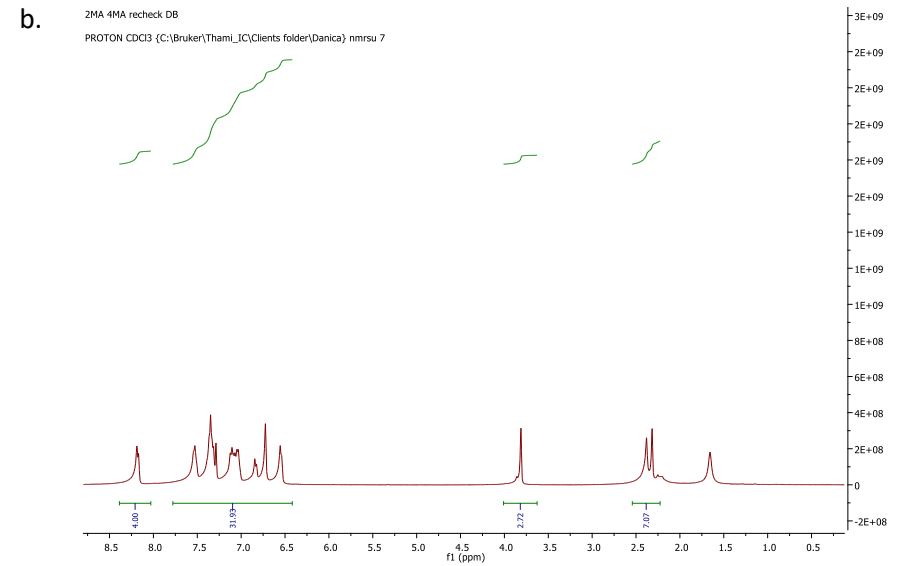
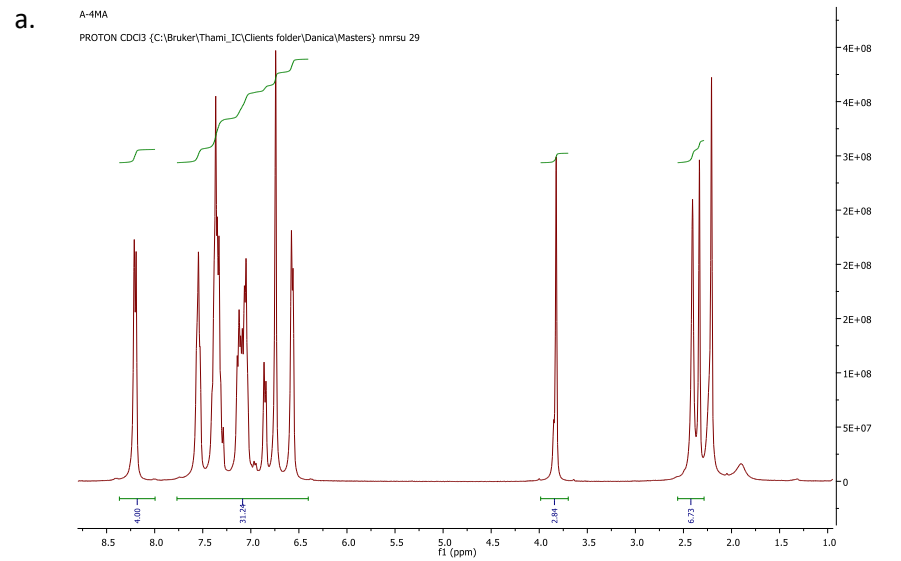




**Figure S41:** Host compound H2 for the selectivity profile 3MP/4MP for the crystals with a. 80 20, b. 60 40, c. 40 60, and d. 20 80 concentrations







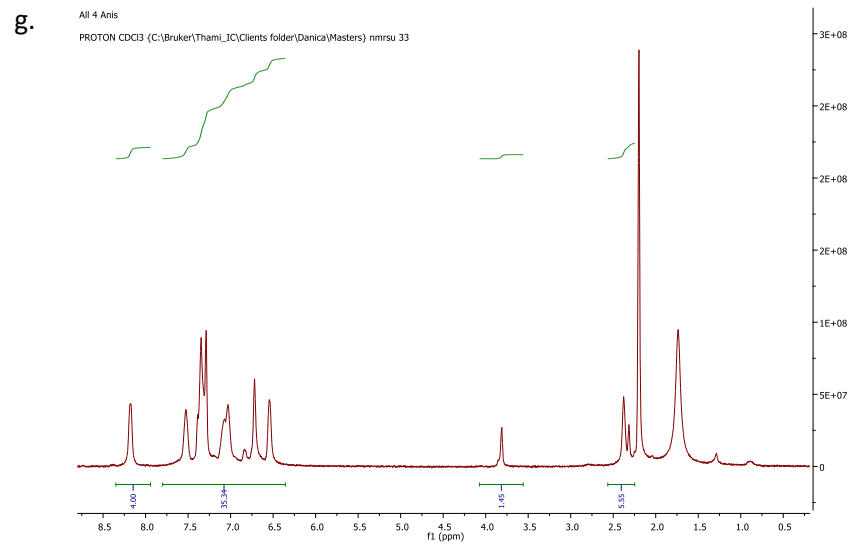
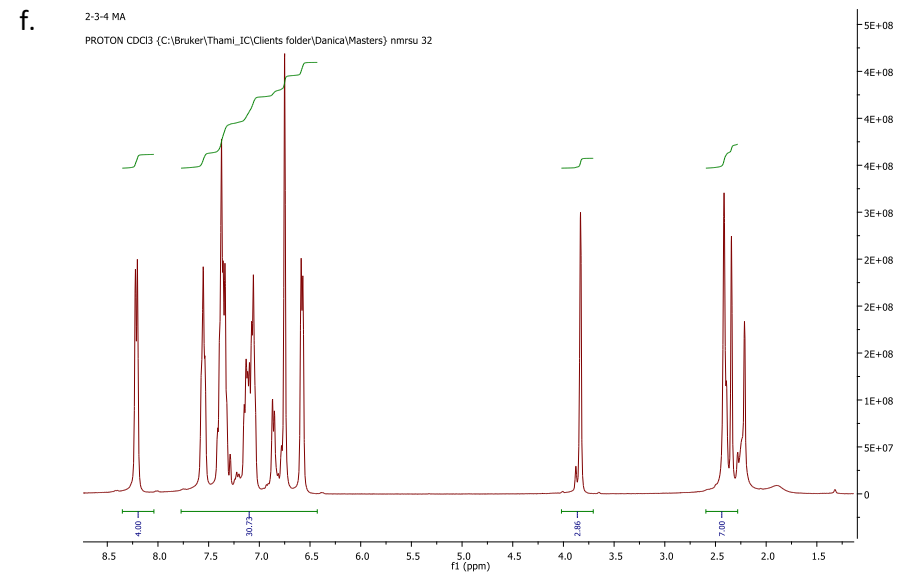
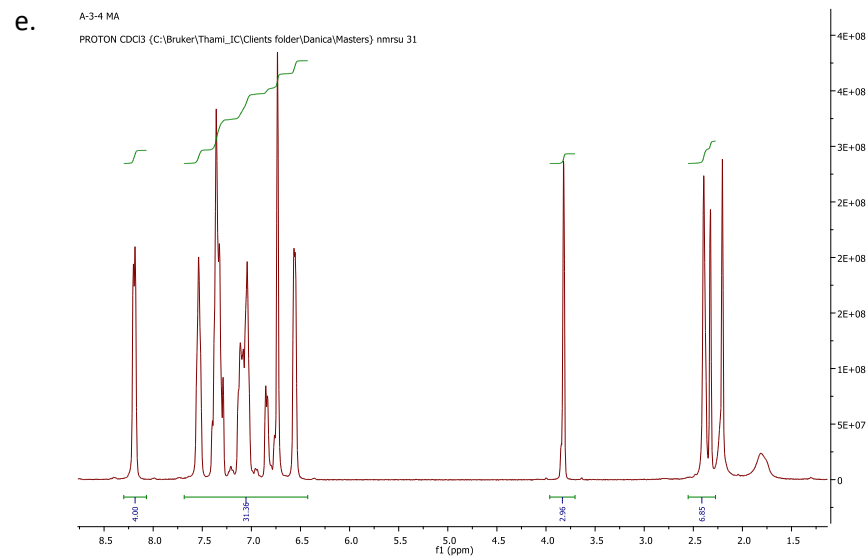


Figure S43:  $^1\text{H}$  with a. ANI/4MA, b. 2MA/3MA c. 3MA/4MA, d. A/2MA/4MA, e. a/3MA/4MA, f. 2MA/3MA/4MA, g. all 4 ANI/MA's

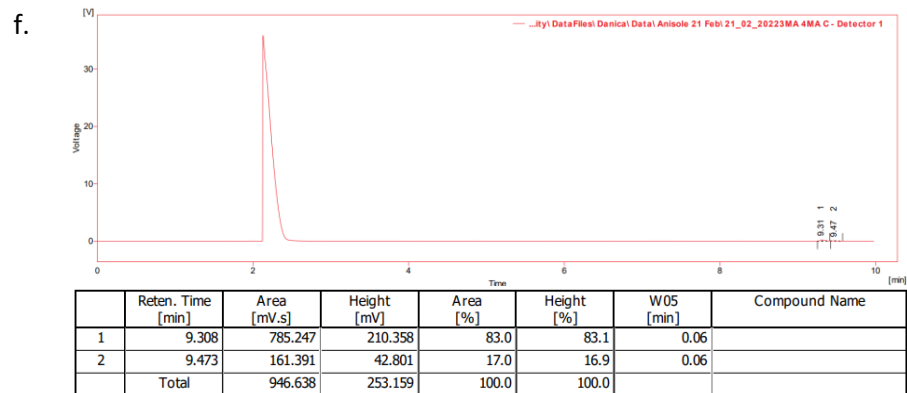
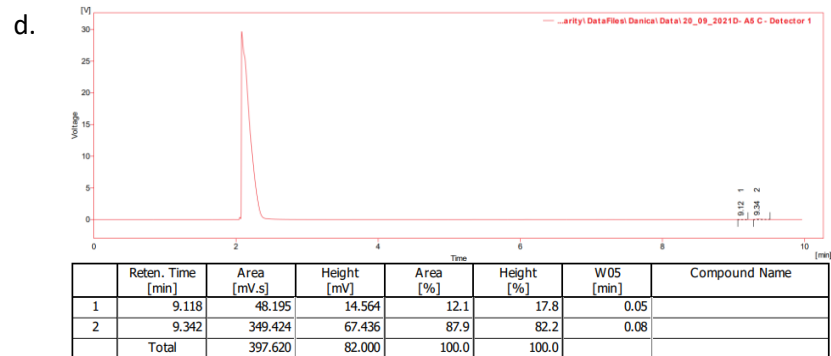
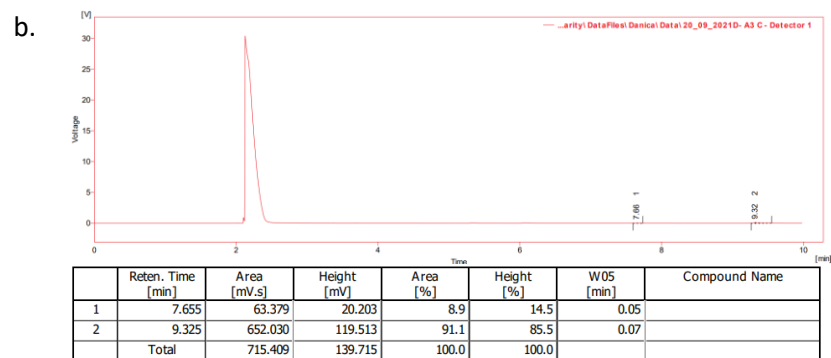
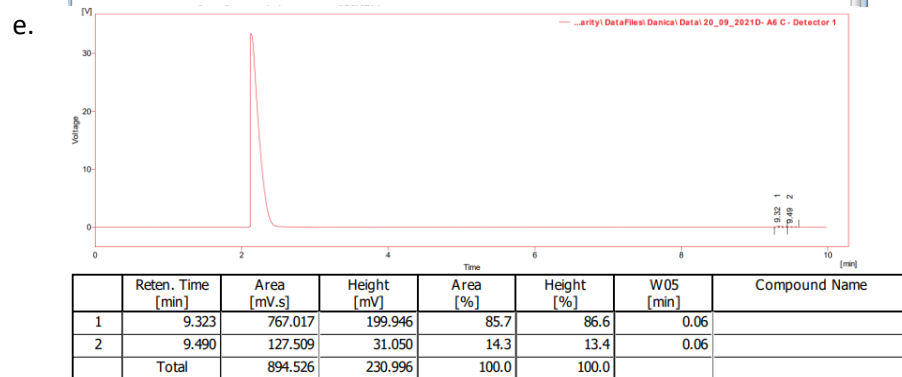
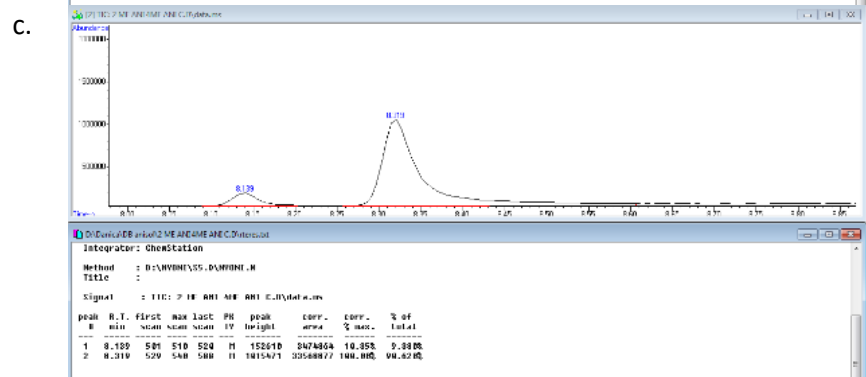
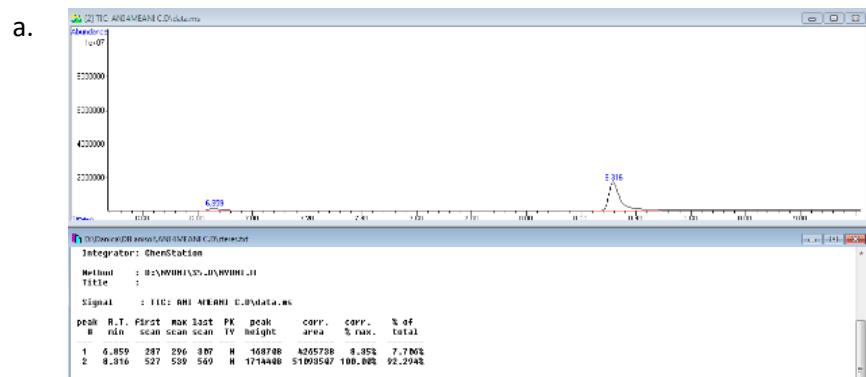
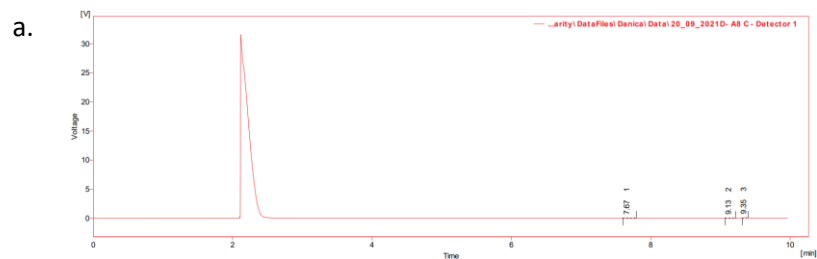
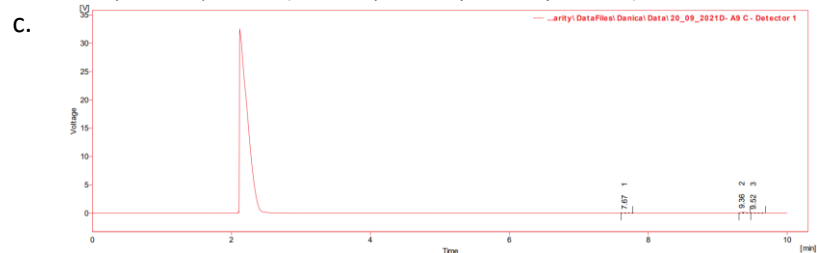


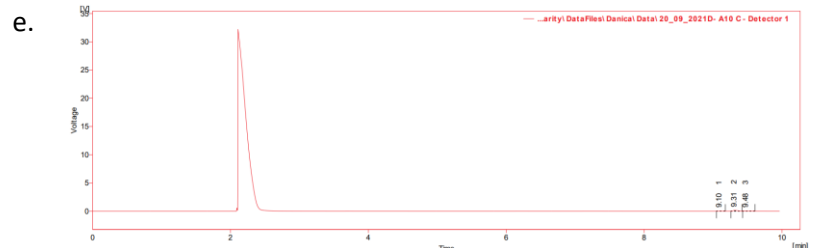
Figure S44: Host compound H1 with the duplicate crystal data for ANI/4MA in a. and b., for 2MA/4MA in c. and d., and for 3MA/4MA in e. and f.



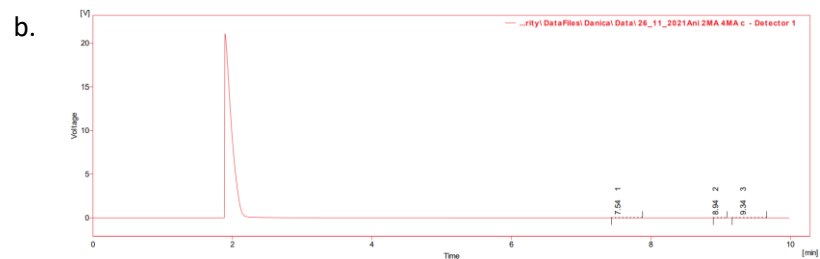
	Reten. Time [min]	Area [mV.s]	Height [mV]	Area [%]	Height [%]	W05 [min]	Compound Name
1	7.668	66.885	16.488	21.6	16.7	0.07	
2	9.127	51.659	15.739	16.7	15.9	0.05	
3	9.345	190.892	66.622	61.7	67.4	0.06	
Total		309.435	98.849	100.0	100.0		



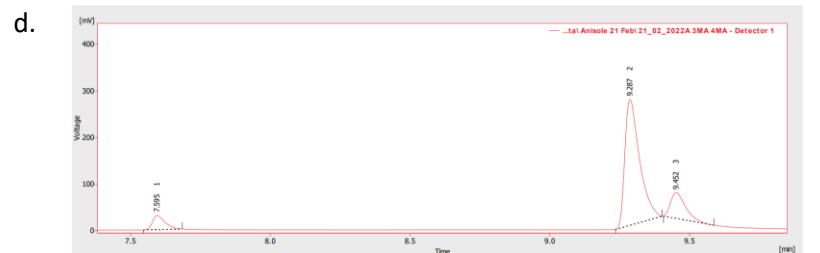
	Reten. Time [min]	Area [mV.s]	Height [mV]	Area [%]	Height [%]	W05 [min]	Compound Name
1	7.668	115.605	28.745	11.4	11.0	0.07	
2	9.357	742.044	198.221	73.3	75.5	0.06	
3	9.523	154.057	35.441	15.2	13.5	0.06	
Total		1011.706	262.407	100.0	100.0		



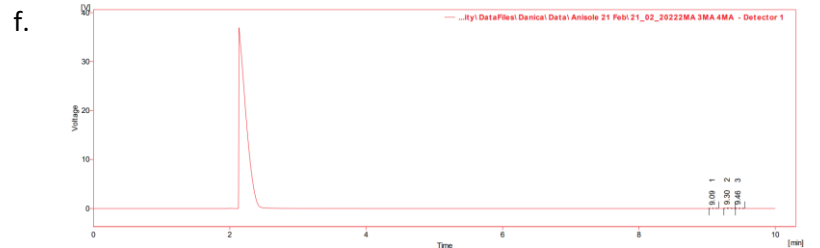
	Reten. Time [min]	Area [mV.s]	Height [mV]	Area [%]	Height [%]	W05 [min]	Compound Name
1	9.098	86.753	28.830	11.3	14.3	0.05	
2	9.315	554.541	143.788	72.4	71.1	0.06	
3	9.482	125.150	29.535	16.3	14.6	0.06	
Total		766.444	202.154	100.0	100.0		



	Reten. Time [min]	Area [mV.s]	Height [mV]	Area [%]	Height [%]	W05 [min]	Compound Name
1	7.538	0.821	0.065	16.4	16.2	0.10	
2	8.940	0.641	0.103	12.8	25.5	0.08	
3	9.335	3.550	0.235	70.8	58.2	0.24	
Total		5.013	0.403	100.0	100.0		



	Reten. Time [min]	Area [mV.s]	Height [mV]	Area [%]	Height [%]	W05 [min]	Compound Name
1	7.595	93.992	30.678	7.3	8.6	0.05	
2	9.287	988.444	269.881	76.7	75.9	0.06	
3	9.452	206.676	55.117	16.0	15.5	0.06	
Total		1289.113	355.676	100.0	100.0		



	Reten. Time [min]	Area [mV.s]	Height [mV]	Area [%]	Height [%]	W05 [min]	Compound Name
1	9.087	30.466	9.556	7.0	8.0	0.05	
2	9.303	347.273	93.047	79.4	78.0	0.06	
3	9.462	59.591	16.697	13.6	14.0	0.06	
Total		437.331	119.300	100.0	100.0		

**Figure S45:** Host compound **H1** with the duplicate crystal data for ANI/2MA/4MA in a. and b., for ANI/3MA/4MA in c. and d., and for 2MA/3MA/4MA in e. and f.



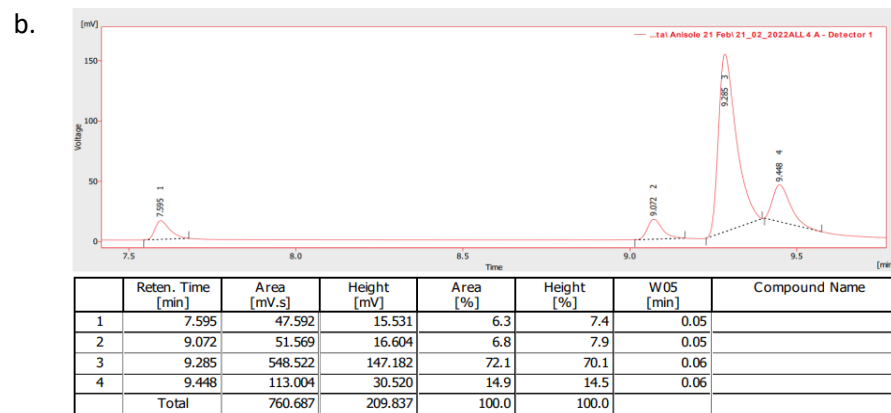
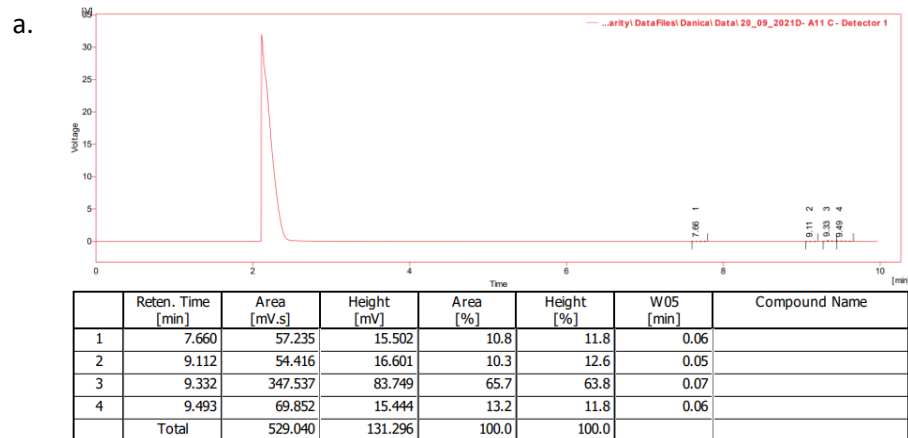
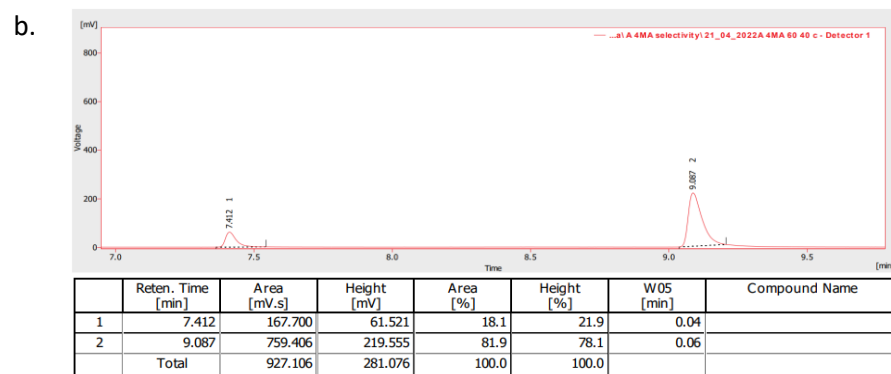
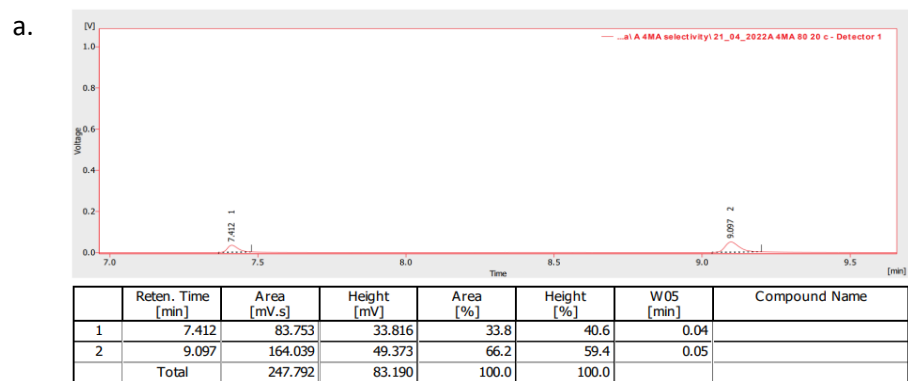


Figure S46: Host compound H1 with the duplicate crystal data for all 4 ANI/MA's in a. and b.



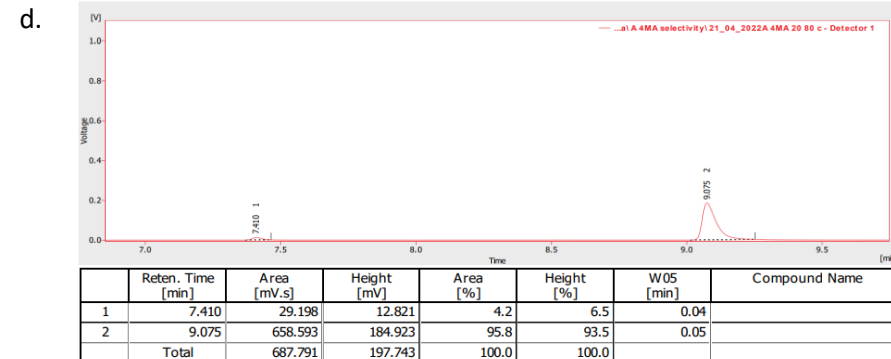
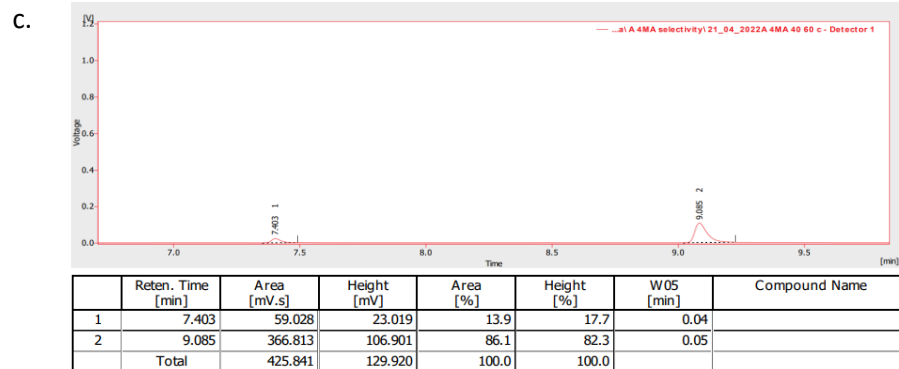
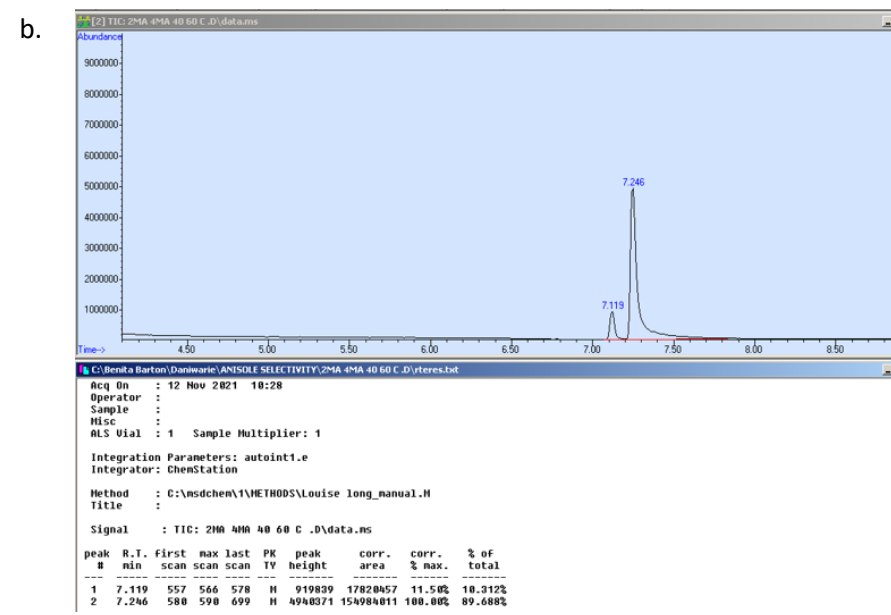
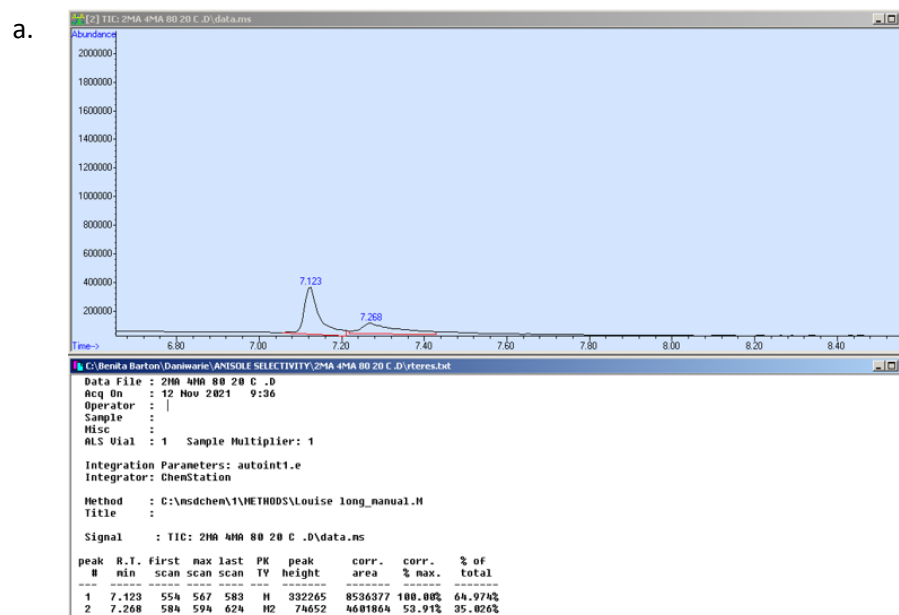


Figure S47: Host compound H1 for the selectivity profile A/4MA for the crystals with a. 80 20, b. 60 40, c. 40 60, and d. 20 80 concentrations



c.

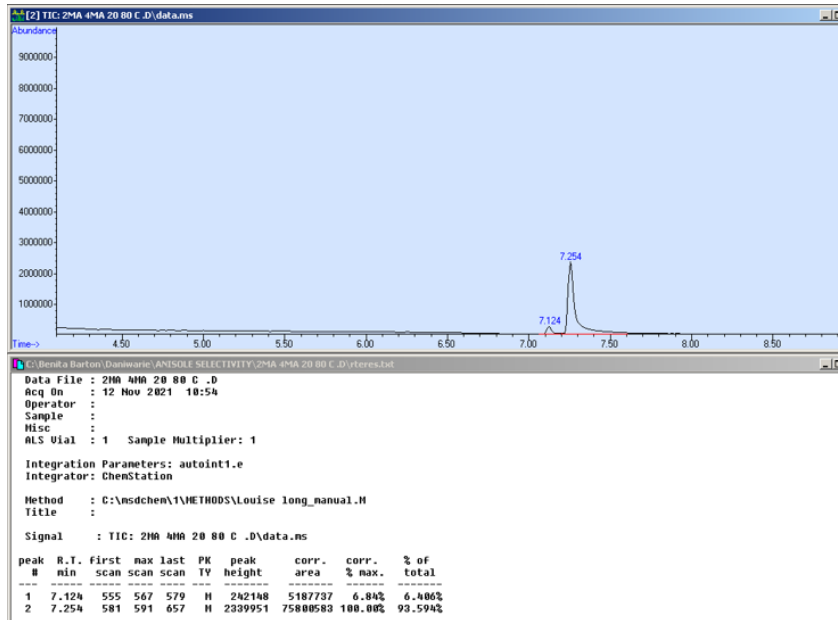
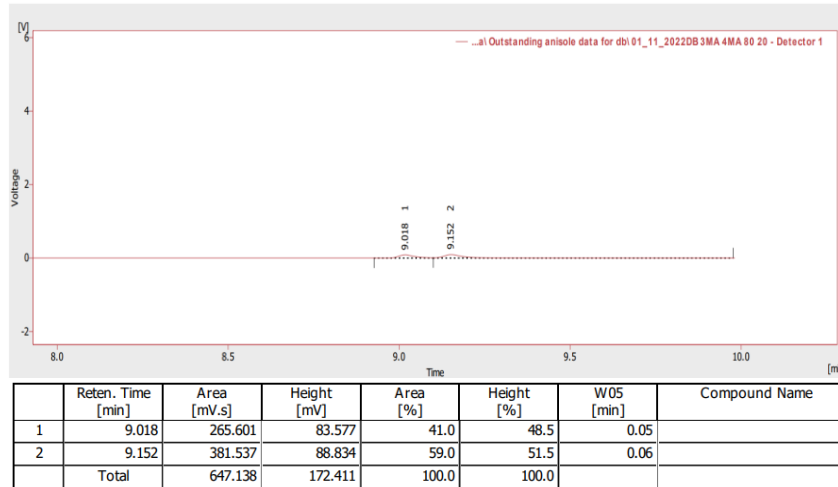
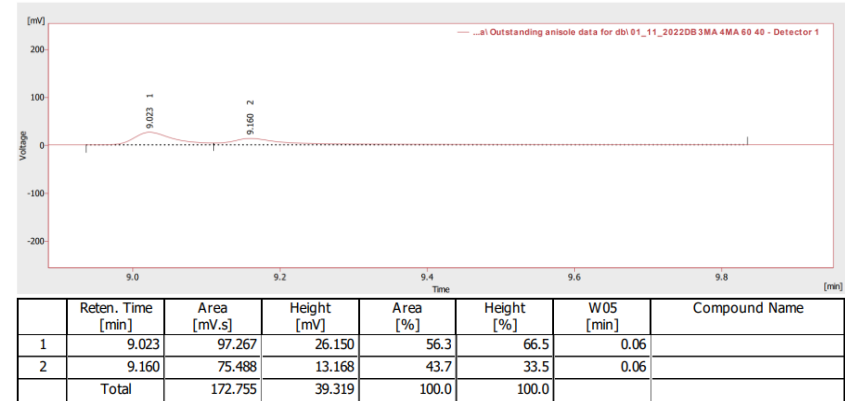


Figure S48: Host compound H1 for the selectivity profile 2MA/4MA for the crystals with a. 80 20, b. 40 60, and c. 20 80 concentrations

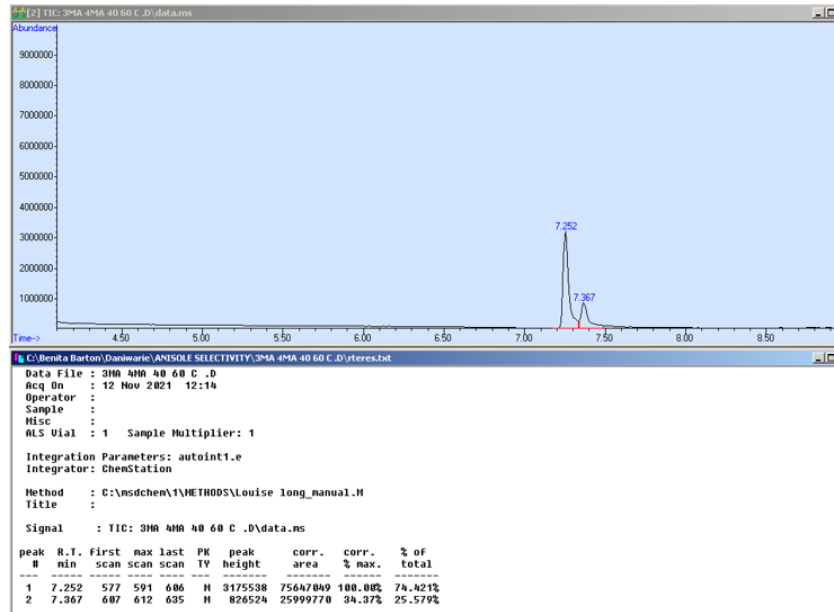
a.



b.



c.



d.

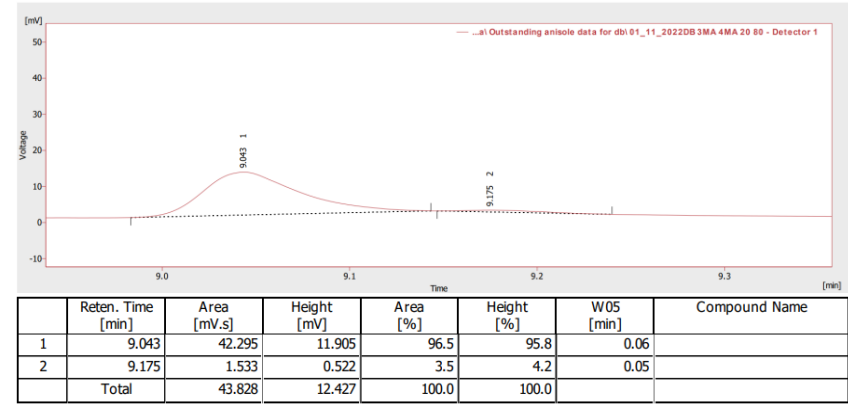


Figure S49: Host compound H1 for the selectivity profile 3MA/4MA for the crystals with a. 80 20, b. 60 40, c. 40 60, and d. 20 80 concentrations

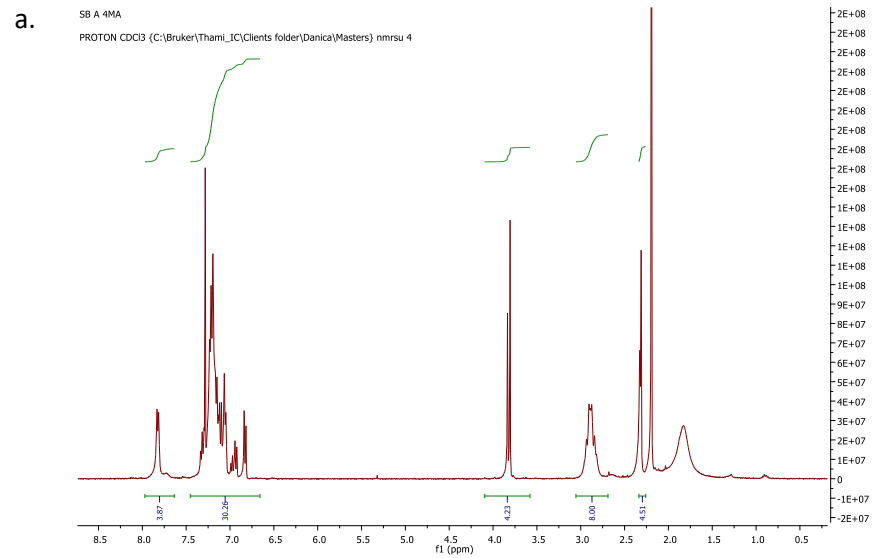


Figure S50: Host compound H2 single solvent experiments with a. ANI